In vitro und *in vivo* Tumoreigenschaften eines kleinzelligen Ovarialkarzinoms vom hyperkalzämischen Typ und mögliche therapeutische Ansätze

Von der Naturwissenschaftlichen Fakultät
der Gottfried Wilhelm Leibniz Universität Hannover
zur Erlangung des Grades

Doktorin der Naturwissenschaften

(Dr. rer. nat.)

genehmigte Dissertation
von

Dipl.-Biochem. Anna-Kathrin Otte
geboren am 02.12.1982, in Bremen

2015

Referent:	Prof. Dr. rer. nat. Ralf Hass
Korreferent:	Prof. Dr. rer. nat. Walter Müller
Korreferent:	Prof. Dr. rer. nat. Frank Entschladen
Tag der Promotion:	11.12.2015

Und sie bewegt sich doch!

(Galileo Galilei 1564 – 1642)

Zusammenfassung

Das kleinzellige Ovarialkarzinom vom hyperkalzämischen Typ (SCCOHT) repräsentiert einen sehr seltenen und aggressiven Tumortyp des Ovarialkarzinoms, welcher vornehmlich bei jungen Frauen im fortpflanzungsfähigen Alter auftritt. Diese Tumorerkrankung geht einher mit einer schlechten Prognose und bei 2/3 der Patientinnen entwickelt sich eine pathologisch erhöhte Kalziumkonzentration im Serum (Hyperkalzämie). Dank der Tatsache, dass seit kurzem zwei Zelllinien dieses Krankheitstyps etabliert wurden (SCCOHT-1 und BIN-67), ergibt sich nun die Möglichkeit für *in vitro* und *in vivo* Studien.

Bei diesen Untersuchungen stellte sich heraus, dass durch eine Erhöhung der Kalzium-konzentration im Kulturmedium auf ein hyperkalzämisches Niveau eine signifikante Wachstumshemmung beobachtet werden konnte. Dieser Einfluss auf die Proliferation war begleitet von einer Aktivierung der p44/42 MAPK und einer gesteigerten Produktion an Prostaglandin E2.

Mit Hilfe weiterer *in vitro* Versuche wurde die Chemosensitivität der SCCOHT Zellen ausgetestet. Hierbei zeigte sich, dass die Zellen gegenüber Epothilone, Methotrexat und Topotecan sensitiv waren, aber gegenüber Platin-Präparaten eine Resistenz zeigten. Das Chemotherapeutikum mit dem höchsten Potenzial in dieser Untersuchung war Epothilon B. Mit zunehmender Versuchsdauer konnte eine Akkumulation der G_1- und G_2-Phase, gefolgt von einem Anstieg der Anzahl toter Zellen im Zellzyklus beobachtet werden. Ebenfalls konnte ein Anstieg der Ser15 Phosphorylierung von P53 nach Epothilon B Behandlung der SCCOHT-1 Zellen beobachtet werden. Nach xenogener Tumorinduktion in NODscid Mäusen konnten die Ergebnisse aus dem Tierversuch die *in vitro* erhobenen Daten bestätigten. Eine verstärkte Zytotoxizität *in vitro* und *in vivo* konnte darüber hinaus durch den synchronen Einsatz von Epothilon B und exogenem Kalzium beobachtet werden.

Durch eine sekretorische Untersuchung von SCCOHT-1 zeigte sich, dass die Zellen auch eine Reihe von Zytokine und Wachstumsfaktoren konstitutiv produzieren, darunter unter anderem der Hepatozyten Wachstumsfaktor (HGF). HGF ist der Ligand für den Rezeptor c-Met und immunhistochemische Untersuchung von 15 SCCOHT-Tumoren zeigten eine heterogene c-Met Verteilung von 0-80%. In den untersuchten Zelllinien konnten bei SCCOHT-1 41 % und bei BIN-67 6,5 % c-Met Expression beobachtet werden, was auf einen autokrinen

Stimulationsmechanismus über das gleichzeitig freigesetzte HGF schließen ließ. Folgende weitere Gemeinsamkeiten konnten zwischen diesen beiden Zelllinien beobachtet werden: sie exprimieren kein BRG-1 (*SMARCA4* Mutation) und EpCAM, dafür aber CD90. Im kompletten Gegensatz dazu exprimieren die Zelllinien der ovarialen Adenokarzinome (SK-OV-3 und NIH:OVCAR-3) BRG-1 und EpCAM, dafür aber kein CD90.

Durch die Stimulation des c-Met Rezeptors von SCCOHT-1 mit HGF konnte eine Phosphorylierung von c-Met (Tyr 1349) und infolge weiterer Signalweiterleitung ebenfalls die Phosphorylierung von Thr202/Tyr204 der p44/42 MAPK beobachtet werden. Diese durch HGF vermittelte Signalkaskade konnte durch die Verwendung des Tyrosinkinase Inhibitors Foretinib unterbrochen werden, was auch zu einer Akkumulation der G_2-Phase im Zellzyklus und einem Anstieg der Apoptose führte. Im Tierversuch konnte die wachstumsinhibierende Wirkung von Foretinib bestätigt werden und es konnte eine 5- bis 10-fach reduzierte SCCOHT Tumorgröße im Vergleich zu den Kontrolltumoren festgestellt werden. Zusätzlich zeigte sich bei den Foretinib behandelten Mäusen eine signifikant reduzierte Vaskularisierung der Tumore und deren Tumormikromilieus. Mit Hilfe einer durch c-Met siRNA vermittelten Herunterregulation konnte ein direkter Zusammenhang zwischen der verminderten c-Met Expression und der verlangsamten Proliferation bestätigt werden.

Schlagwörter: SCCOHT, Epothilon B, Foretinib

Abstract / Summary

The small cell carcinoma of the ovary hypercalcemic type (SCCOHT) represents a rare and aggressive form of ovarian tumors. This tumorigenic disease is associated with poor prognosis and predominantly affects young women during reproductive age. Two thirds of the patients develop a pathologically increased serum calcium concentration (hypercalcemia). Two cell lines (SCCOHT-1 and BIN-67) of this tumor entity have been established recently providing cellular models to perform *in vitro* and *in vivo* experiments.

Exposure of SCCOHT-1 cells to hypercalcemic-like conditions demonstrated a progressively reduced proliferation rate. These calcium-mediated antiproliferative effects were accompanied by the activation of p44/42 MAPK and an increased production of prostaglandin E2.

Moreover, chemosensitivity of SCCOHT-1 cells was tested by several *in vitro* approaches. The cells displayed sensitivity for certain epothilones, methotrexate and topotecan whereas little if any cytotoxicity was observed with platin-based compounds. In particular, epothilone B demonstrated the maximal cytotoxic effects in SCCOHT-1 cells. In addition, a significant G_1 and G_2 cell cycle accumulation with subsequent cell death in subG_1 phase was observed during epothilone B incubation. Moreover, an increased Ser15 phosphorylation of P53 became detectable following epothilone treatment. These *in vitro* data were confirmed *in vivo* after induction of SCCOHT xenograft tumors in NODscid mice. The concomitant use of epothilone B and exogenously-added calcium displayed synergistic cytotoxicity *in vitro* and *in vivo*.

Furthermore, screening of constitutive chemokine and growth factor production by SCCOHT-1 cells revealed a significant production of hepatocyte growth factor (HGF). Whereas HGF represents the ligand for c-Met receptor, immunohistochemistry of c-Met expression in SCCOHT tumors demonstrated a heterogeneous distribution between undetectable levels and 80 %. Here, SCCOHT-1 cells exhibited 41 % and BIN-67 cells 6.5 % of c-Met expression. Further characterization of SCCOHT-1 and BIN-67 cells showed an absence of BRG-1 protein (due to a *SMARCA4* mutation), strong expression of CD90 and undetectable EpCAM levels which was in contrast to the ovarian adenocarcinoma cell lines (SK-OV-3 and NIH:OVCAR-3) displaying completely opposite expression patterns for these three markers.

HGF stimulation of SCCOHT-1 cells was associated with c-Met phosphorylation at Tyr 1349 and a downstream Thr202/Tyr204 phosphorylation of p44/42 MAP kinase. This HGF-induced signaling cascade was abolished by the c-Met inhibitor foretinib. Cell cycle analysis after foretinib treatment demonstrated enhanced G_2 accumulation and increasing apoptosis. Animal experiment in SCCOHT-induced tumors in mice could confirm the antiproliferative effects of foretinib demonstrating a 5- to 10-fold reduced tumor size in comparison to untreated control tumors. Furthermore, foretinib-treated tumors revealed a significantly reduced vascularization within the SCCOHT tumor microenvironment. The important role of c-Met activation for the proliferative capacity of SCCOHT-1 cells and appropriate *in vivo* tumor growth could be substantiated by specific experimental approaches using c-Met siRNA-mediated protein knock down.

keywords: SCCOHT, epothilone B, foretinib

Inhaltsverzeichnis

Abkürzungsverzeichnis

5'-FU	**5'-F**luor**u**racil
A2780	Ovarialkarzinom Zelllinie
ACTH	**A**drenoc**o**rticot**r**opes **H**ormon
AKT	Synonym: Protein Kinase B; Serin-Threonin-Kinase
ALK	**A**naplastische **L**ymphom**k**inase
AML	**a**kute **m**yeloische **L**eukämie
Ara-C	**C**ytosin-**Ara**binosid
Arg (R)	**Arg**inin
ATP	**A**denosin**tri**p**h**osphat
BAD	„**B**CL-2 **a**ntagonist oft the cell **d**eath“; Proapoptotischer Faktor
BCL2	„**B-c**ell **l**ymphoma **2**“; Proteinfamilie mit anti- und proapoptotischen Mitgliedern
BID	„**B**H3 **i**nteracting-domain **d**eath agonist“
BIN-67	SCCOHT - Zelllinie
BRAF	„**B-Raf** proto-oncogene, serine/threonine kinase“ bzw. „v-raf murine sarcoma viral oncogene homolog B1“
BRCA1	„**br**east **ca**ncer **1**, early onset „
BRCA2	„**br**east **ca**ncer **2**, early onset“
BRG-1	„ATP-dependent helicase SMARCA4“; Protein
c-CBL	„**c**asitas **B**-linage **l**ymphoma“, E3 ubiquitin-protein ligase
c-KIT	„V-kit Hardy-Zuckerman 4 feline sarcoma viral oncogene homolog“; Synonym: CD117, KIT
c-MET	„mesenchymal epithelial transition factor“; Hepatozyten-Wachstumsfaktor Rezeptor
CA125	„cancer antigen 125“; Tumormarker
cAMP	**z**yklisches **A**denosin**m**ono**p**hosphat
CD15	„fucosyltransferase 4“; Synonym: FUT4
CD29	„Integrin, subunit beta 1“; Fibronectin Rezeptor
CD326	„**ep**ithelial **c**ell **a**dhesion **m**olecule“; Synonym: EpCAM
CD44	cell-surface glycoprotein
CD90	„Thy-1 cell surface antigen“
COX-1	„**cy**clo**ox**ygenase-**1**“

COX-2	„**c**yclo**ox**ygenase-**2**“
CRK	„v-**crk** avin sarcoma virus CT10 oncogene homolog“
CRKL	„v-**crk** avin sarcoma virus CT10 oncogene homolog-**l**ike“
DAG	**D**i**a**cyl**g**lycerol
DHFR	„**di**h**f**olate **r**eductase“; **D**i**h**ydro**f**olat**r**eduktase
DNA/DNS	„**d**eoxyribo**n**ucleic **a**cid“; **D**esoxyribo**n**uklein**s**äure
EGFR	„**e**pidermal **g**rowth **f**actor **r**eceptor“; Synonym: HER1
EMA	„**e**pithelial **m**embran **a**ntigen“; Synonym: MUC1, CD227
EOS	epitheliale Ovarialtumor
EP1	Prostaglandin E Rezeptor 1
EP2	Prostaglandin E Rezeptor 2
EP3	Prostaglandin E Rezeptor 3
EP4	Prostaglandin E Rezeptor 4
Epo A	**Epo**thilon **A**
Epo B	**Epo**thilon **B**
ERBB2	„**erb-b2** receptor tyrosine kinase 2“; Synonym: HER2
FAS	„**Fas** cell surface death receptor“; Zelltodrezeptor, Synonym: CD95
FdUMP	**F**luoro**d**esoxy**u**ridin**m**ono**p**hosphat
FdUTP	**F**luoro**d**esoxy**u**ridin**tri**p**h**osphat
FGF	„**f**ibroblast **g**rowth **f**actor“; Fibroblasten-Wachstumsfaktoren
FGFR1	„**f**ibroblast **g**rowth **f**actor **r**eceptor **1**“
FIGO	**F**ederation **I**nternationale de **G**ynécologie et d`**O**bstétrique
Flt-3	„Fms-related tyrosine kinase 3“; Synonym: CD135
FUTP	**F**luoro**u**ridin**tri**p**h**osphat
GAB1	„**G**RB2 **a**ssociated-**b**inding **p**rotein **1**“
GDP	**G**uanosin**di**p**h**osphat
GRB2	„**g**rowth-**f**actor **r**eceptor-**b**ound protein **2**“
GSK1363089	Foretinib
GTP	**G**uanosin**tri**p**h**osphat
H/E	**H**ämatoxylin-**E**osin
HGF/SF	„**h**epatocyte **g**rowth/**s**catter **f**actor“; Hepatozyten-Wachstumsfaktor
HGFA	**„HGF a**ctivator“; Hepatozyten-Wachstums-Aktivatorfaktor
HSP 27	„**h**eat **s**hock **p**rotein **27**“; Hitzeschockprotein 27
IC50	mittlere **i**nhibitorische **K**onzentration

ICRAC	„**c**alcium **r**elease-**a**ctivated **c**alcium channels“
IHC	**I**mmun**h**isto**c**hemie
IL8	**I**nter**l**eukin **8**; Synonym: CXCL8 CXC-Motiv-Chemokin 8
INI1	„**in**tegrase **i**nteractor **1**“ bzw. „SWI/SNF related, matrix associated, actin dependent regulator of chromatin, bubfamily b, member 1 (SMARCB1)“
IP3	**I**nositol**trip**hosphat
IP3R	**I**nositol**trip**hosphat **R**ezeptor
JNK	„c-**J**un **N**-terminal **k**inases“; c-Jun Amino-Kinase
KIT	„KIT proto-oncogene receptor tyrosine kinase“; Synonym: CD117, c-Kit
KRAS	„Kirsten rat sarcoma viral oncogene homolog“
MAPK	„**M**itogen **a**ctivated **p**rotein **k**inases“; Mitogen-aktivierte Proteinkinase
MDA-MB 231	Brustkrebszelllinie
MDM2	„MDM2 proto-oncogene, E3 ubiquitin-protein ligase“
MPSC	„**m**icro**p**apillary **s**erous **c**arcinoma“; mikropapilläres seröses Karzinom
MRTO	„**m**alignant **r**habdoid **t**umor of the **o**vary“
mTORC2	„**m**ammalian **t**arget **o**f **r**apamycin **c**omplex **2**“
MTX	Methotrexat
NIH:OVCAR-3	ovariale Adenokarzinom-Zelllinie
NOD	„**n**on-**o**bese **d**iabetic“; Nicht-fettleibig-diabetisch
NSCLC	„**n**on-**s**mall **c**ell **l**ung **c**arcinoma“; nichtkleinzelligen Bronchialkarzinomen
NSCSCC	„**n**on-**s**mall **c**ell **s**mall **c**ell **c**arcinoma“
ORAI1	„calcium release-activated calcium channel protein 1“
OS-1	SCCOHT Zelllinie
p	Phosphorylierung
P38	Isoform von MAPK (11-14) gehört zur Familie der MAPK
P53	Tumor **P**rotein **53**
panCK	**Z**yto**k**eratin (1 ,2 , 3, 4, 5, 6, 7, 8, 10, 14, 15, 16, 19)
PAVEP	Abkürzung für Chemoterapeutika-Kombination: Cisplatin, Adriamycin, Vepeside, Cyklophosphamid

PDGF	„**p**latelet-**d**erived **g**rowth **f**actor“; Blutplätchen Wachstumsfaktor
PDGFRα	„**p**latelet-**d**erived **g**rowth **f**actor **r**eceptor, **a**lpha polypeptide“; Synonym: PDGFR2
PDGFRβ	„**p**latelet-**d**erived **g**rowth **f**actor **r**eceptor, **b**eta polypeptide“; Synonym PDGFR1
PDK1	„**p**hosphoinositide **d**epending **k**inase **1**“; Synonym: PDPK1
PF-02341066	Crizotinib
PGE2	**P**rost**g**landin **E2**
Pgp9.5	„ubiquitin carboxy-terminal hydrolase L1“; Synonym: UCH-L1
PH	„**P**leckstrin **h**omology domain“; Plextrin-homologe Domäne
PHA 665752	c-Met Inhibitor
PI3K	„**p**hosphatidyl**i**nositol **3**-**k**inase“; Phosphoinositol-3-Kinase
PIP2	„**p**hosphatidyl**i**nositol (4,5)-**bisp**hosphate“
PIP3	„**p**hosphat**i**dylinositol (3,4,5)-**trip**hosphate“
PKB	**P**rotein **K**inase **B**
PKC	**P**rotein **K**inase **C**
PLA2	**P**hospho**l**ipase **A2**
PLC-γ1	**P**hospho**l**ipase **C- γ1**
PTB	„**p**hospho**t**yrosine-**b**inding domain“; Phosphotyrosin-bindender Bereich
PTH	„**p**ara**t**hyroid **h**ormone“; Parathormon
PTHrP	„**p**ara**t**hyroid **h**ormone-**r**elated **p**rotein“; Parathormon-related Protein
PTP	„**p**rotein **t**yrosine **p**hosphatases“
RAF	„v-raf murine sarcoma viral oncogene homolog B1“; MAP-Kinase-Kinase-Kinase
RAS-GAP	„**R**as **G**TPase **a**ctivating **p**rotein, Ras p21 protein activator 1“
RNA/RNS	„**r**ibo**n**ucleic **a**cid“; **R**ibo**n**uklein**s**äure
RON	„macrophage-stimulating protein receptor/ **R**ecepteur d'**O**rigine **N**antais“; Synonym: MST1R
ROS1	„**ROS** proto-oncogene **1**, receptor tyrosine kinase“
RTK	**R**ezeptor **T**yrosink**i**nase
SCCOHT	„**s**mall **c**ell **c**arcinoma of the **o**vary **h**ypercalcemic **t**ype“; kleinzelliges Ovarialkarzinom vom hyperkalzämischen Typ
SCCOHT-1	SCCOHT Zelllinie

SCCOPT	„**s**mall-**c**ell **c**arcinoma of the **o**vary, **p**ulmonary **t**ype“
scid	„**s**evere **c**ombined **i**mmuno**d**eficiency“; **s**chwerer **k**ombinierter **I**mmun**d**efekt
SD	„**s**tandard **d**eviation“; Standardabweichung
Ser (S)	**Se**rin
SH2	„**S**rc **h**omology **2**“
SHC	„Src-homology-2 -domain-containing tansforming protein“; Adaptor-Protein
SHIP-2	„**S**rc **h**omology 2 domain-containing 5’ **i**nositol **p**hosphatase“
SHP2	„**S**rc **h**omology 2 domain-containing **p**hosphatase-**2**“
SK-OV-3	ovariale Adenokarzinom-Zelllinie
SMARCB1	„**S**WI/SNF-related **m**atrix-associated **a**ctin-dependent **r**egulator of **c**hromatin subfamily **B** member **1**“; Protein: INI1
SMARCA4	„**S**WI/SNF related, **m**atrix associated, **a**ctin dependent **r**egulator of **c**hromatin, subfamily **A**, member **4**“; Protein: BRG1
SOS	„Ras guanine nucleotide exchange factor **s**on-**o**f-**s**even“
STAT-3	„**s**ignal **t**ransducer and **a**ctivator of **t**ranscription **3**“
STIM-1	„**st**romal **i**nteraction **m**olecule-**1**“
TIE-2	„angiopoietin-1 recetor“; Synonym: CD202B
TKI	**T**yrosin **K**inase **I**nhibitor
TS	**T**hymidylat **S**ynthase
Tyr (Y)	**Tyr**osin
Val (V)	**Val**in
VCAM-1	„**v**ascular **c**ell **a**dhesion **m**olecule **1**“, Synonym: CD106
VEGF	„**v**ascular **e**ndothelial **g**rowth **f**actor“; vaskulo-endothelialem Wachstumsfaktor
VPCBAE	Abkürzung für Chemoterapeutika-Kombination: Vinblastin, Cisplatin, Cyclophosphamid, Bleomycin, Doxorubicin, Etoposid
WT1	**W**ilms' **T**umor **1** Protein
XL880	Foretinib

1 Einleitung

1.1 Das Ovarialkarzinom

Jährlich erkranken deutschlandweit etwa 7.500–7.900 Frauen (12,1 auf 100.000 Frauen (2010)) [1] mit einem mittleren Erkrankungsalter von 69 Jahren an einer malignem Form des Eierstockkrebs. Dies entspricht 3,5 % der jährlichen Krebserkrankungen bei Frauen und stellt somit die fünfthäufigste Tumorerkrankung (weltweit 3,6 %, Rang 7) [2] - hinter dem Mammakarzinom, Darmkrebs sowie Bronchial- und Pankreaskarzinom - dar. Mit 5,6 % (weltweit 4,3 %) der jährlichen Krebssterbefälle weist der Eierstockkrebs (Ovarialkarzinom) dabei die höchste Mortalitätsrate bezogen auf gynäkologische Tumore in Deutschland auf.

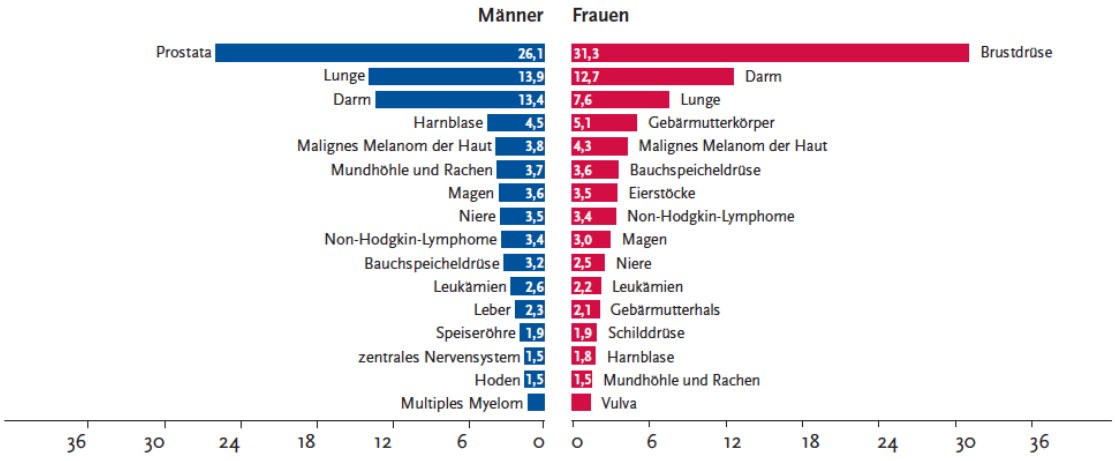

Abbildung 1-1: Prozentualer Anteil der häufigsten Tumorlokalisationen aller Krebssterbefällen in Deutschland (2010) [1].

Man unterscheidet je nach histologischer Tumorentität des Ovarialkarzinoms zwischen den epithelialen Ovarialtumoren (EOS, ca. 60 %), den Keimzelltumoren (ca. 20 %), den Keimstrang- und Stromatumoren (ca. 5 %) und Metastasen anderer Tumore (15-20 %) [3]. Des Weiteren werden Ovarialzysten von echten Neoplasien abgegrenzt. Echte Neoplasien werden wiederum in benigne und maligne Tumore sowie in Borderline Tumore eingeteilt. Eine international geltende Einteilung der gynäkologischen Tumore erfolgt z.B. in FIGO-Stadien (Federation Internationale de Gynécologie et d`Obstétrique) [4].

Tabelle 1.1 FIGO Stadieneinteilung für das Ovarialkarzinom [4] (Stand : 01. Januar 2014)

FIGO	Kriterien
I	Tumor auf die Ovarien beschränkt
I-A	auf ein Ovar beschränkt, Kapsel intakt, Ovarialoberfläche tumorfrei, negative Spülzytologie
I-B	Befall beider Ovarien, ansonsten wie Stadium IA
I-C	Tumor befällt ein Ovar oder beide Ovarien
I-C1	iatrogene Kapselruptur
I-C2	präoperative Kapselruptur oder Tumor auf der Ovarialoberfläche
I-C3	maligne Zellen im Aszites oder in der Spülzytologie nachweisbar
II	Tumor auf einem oder beiden Ovarien mit zytologisch oder histologisch nachgewiesener Ausbreitung in das kleine Becken oder primäres Peritonealkarzinom
II-A	Ausbreitung und/oder Tumorimplantate auf Uterus und/oder Tuben
II-B	Ausbreitung auf weitere intraperitoneale Strukturen im Bereich des kleinen Beckens
III	Tumor auf einem oder beiden Ovarien mit zytologisch oder histologisch nachgewiesener Ausbreitung außerhalb des kleinen Beckens und/oder retroperitoneale Lymphknotenmetastasen
III-A	retroperitoneale Lymphknotenmetastasen und/oder mikroskopische Metastasen außerhalb des kleinen Beckens
III-A1	ausschließlich retroperitoneale Lymphknotenmetastasen
III-A1(i)	Metastasen ≤ 10 mm
III-A1(ii)	Metastasen > 10 mm
III-A2	mikroskopische extrapelvine Ausbreitung auf das Peritoneum außerhalb des kleinen Beckens mit oder ohne retroperitoneale Lymphknotenmetastasen
III-B	makroskopische extrapelvine Ausbreitung auf das Peritoneum außerhalb des kleinen Beckens ≤ 2 cm mit oder ohne retroperitoneale Lymphknotenmetastasen; schließt eine Ausbreitung auf die Leberkapsel und die Milz ein
III-C	makroskopische extrapelvine Ausbreitung auf das Peritoneum außerhalb des kleinen Beckens > 2 cm mit oder ohne retroperitoneale Lymphknotenmetastasen; schließt eine Ausbreitung auf die Leberkapsel und die Milz ein
IV	Fernmetastasen mit Ausnahme peritonealer Metastasen
IV-A	Pleuraerguß mit positiver Zytologie
IV-B	Parenchymale Metastasen der Leber und/oder der Milz, Metastasen zu außerhalb des Abdomens gelegenen Organen (einschließlich inguinaler Lymphknotenmetastasen und/oder anderer außerhalb des Abdomens gelegener Lymphknotenmetastasen

Als Risikofaktoren für die Erkrankung an einem Ovarialkarzinom gelten zunehmendes Lebensalter, endokrine Faktoren (wiederholte Ovulation, frühe Menarche, späte Menopause, Nulliparität, primäre Sterilität, polyzystische Ovarien, Hormonsubstitution) und Keimbahn-

mutationen von *BRCA1* und *BRCA2* (das Lebenszeitrisiko an Eierstockkrebs zu erkranken liegt bei 40–60 %) [5,6]. Als protektive Faktoren gelten Ovulationshemmung, Tubenligatur, höhergradige Parität und eine lange Stillperiode [7-9].

Da mit dem Oberbegriff Ovarialkarzinom eine Vielzahl histologischer Subtypen des epithelialen Typs mit unterschiedlichen Entitäten beschrieben werden (serös, endometrioid, muzinös, klarzellig, transitionalzellig (Brenner Tumor), Karzinosarkom, gemischte epitheliale Tumoren, undifferenzierte Karzinome und andere) [10], formulierten Kurman und Shih [11-13] ein entsprechendes duales Modell zur verbesserten Einteilung der Tumore (Abbildung 1-2). Hierbei wird zwischen zwei möglichen Entstehungswegen unterschieden, dem („low-grade“) Typ-I und dem („high-grade“) Typ-II Tumor.

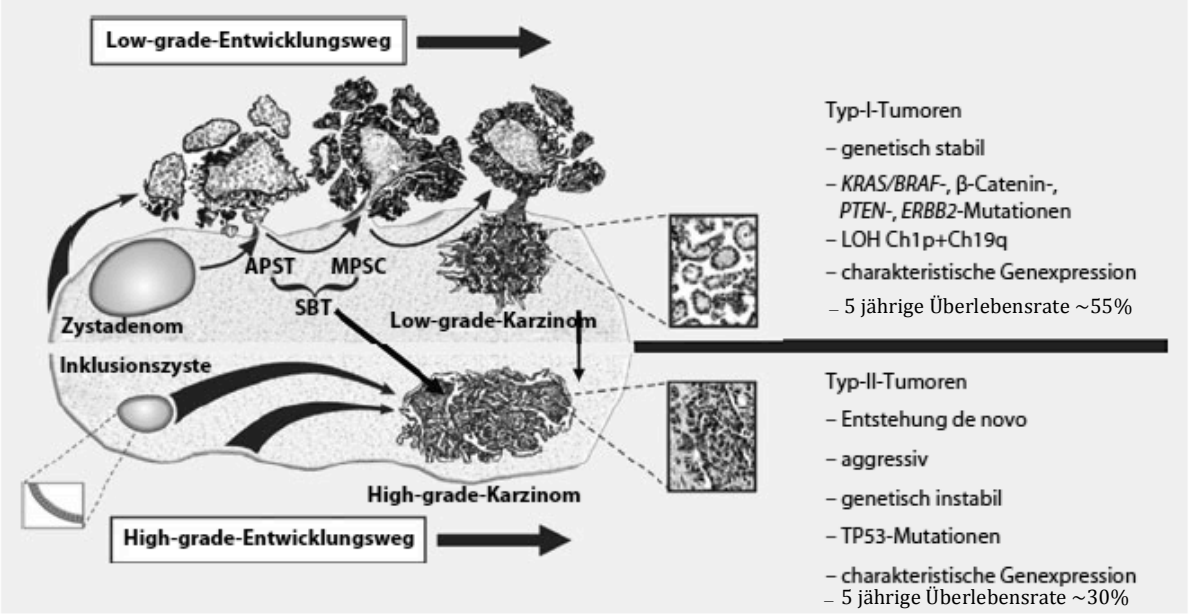

Abbildung 1-2: Dualistisches Progressionsmodell der serösen Ovarialkarzinome nach Shih und Kurman.
SBT (serous borderline tumor), APST (atypical proliferative serous tumor) MPSC (micropapillary serous carcinoma auch „nicht invasives mikropapilläres Karzinom“ genannt). **(**adaptiert nach Meinhold-Heerlein *et al.* [14])

Typ-I Tumore haben dabei zumeist Ihren Ursprung in benignen Tumoren (Adenome und Borderline-Tumore). Wie in Abbildung 1-2 dargestellt, entwickelt sich das hochgradig differenzierte Ovarialkarzinom an der Oberfläche des Ovars (Ovarialepithel) aus einem serösen Zystadenom - über ein Stadium, das als „invasives mikropapilläres seröses Zystadenom“ (MPSC) beschrieben wird. Zu den MPSC gehören die hochdifferenzierten serösen, muzinösen und endometroide „low-grade“-Karzinome sowie die malignen Brenner-Tumore. Charakteristisch für Tumore dieses Typs ist eine Häufung im Auftreten von *BRAF*- (V-RAF murine sarcoma viral oncogene homolog B1), *KRAS*- (kirsten rat sarcoma virus) und *ERBB*$_2$-

Mutationen [15,16], ein niedriger Proliferationsindex, eine geringe Rate an *P53*-Mutationen [15,17] und eine günstigere 5-jährige Überlebensrate von 55 %. Dagegen gehören die schlecht differenzierten, serösen und endometroiden Karzinome, die undifferenzierten und die malignen Müller-Mischtumoren zu den Typ-II Tumoren. Hierbei entsteht das Ovarialkarzinom „*de novo"* an der Ovaroberfläche oder an einem anderen Ort des Müller-Epithels und nicht, wie oben beschrieben, über eine tumoröse Vorläuferläsion. Charakteris-tisch für Typ-II Tumore ist ihr schnelles Wachstum und damit einhergehend eine schlechte Prognose. Des Weitern weisen sie im Vergleich zu den Typ-I Tumoren eine hohe genetische Instabilität und Mutationen im Gen *TP53* auf.

Erste *in vitro* Ergebnisse und klinische Untersuchungen [18-20] konnten zeigen, dass die langsam proliferierenden „low-grade" serösen Typ-I Tumore nicht dieselbe Sensitivität im Vergleich zu den „high-grade" serösen Karzinomen bezüglich der Standard Platin/Taxan-basierten Chemotherapie zeigen. Diese Daten zeigen, dass mindestens für diesen Subtyp neue Wege/Therapeutika zur effektiven Behandlung komplett fehlen und erforscht werden müssen. Im Hinblick auf diese inadäquate Behandlung mit platinhaltigen Präparaten konnten erste erfolgsversprechende *in vitro* und *in vivo* Ergebnisse mit dem MAPK (Mitogen-aktivierte Proteinkinase)-Inhibitor CI-1040 bei Tumorzellen mit *KRAS* oder *BRAF* Mutationen gezeigt werden [21]. Mit der Applikation von Selumetinib, einem weiteren MAPK-Inhibitor, konnte bspw. bei einer Patientin mit einem rezidivierten, serösen, „low-grade" Ovarialtumor eine 11-monatige progressionsfreie Zeit beobachtet werden [22]. Im Hinblick auf die Wirksamkeit von MAPK-Inhibitoren geht auch die Suche nach Inhibitoren weiter, die in der Signalkaskade oberhalb (upstream) von MAPK angesiedelt sind. Von immer größer werdendem Interesse sind spezifische Moleküle, die gerichtet auf die Angiogenese und/oder auf die proliferative Kapazität von Krebszellen wirken. Als Target würden hierfür zum Beispiel FGFs (fibroblast-growth factor), PDGFs (platelet-derived growth factor) [23], VEGF (vascular endothelial growth factor) [24], und HGF (hepatocyte growth factor)/c-Met (hepatocyte growth factor receptor) [25] von großem Interesse sein.

Nach den Leitlinien der Deutschen Krebsgesellschaft erfolgt als Standardtherapie bei Ovarialtumoren mit einem FIGO-Stadium von I bis II-A nach der operativen Entfernung aller makroskopisch erkennbaren Tumormaterialen eine Primärtherapie von 6 Zyklen einer platin-haltigen, adjuvanten Chemotherapie (ggf. kann bei einem Stadium von „I" auf eine Chemo-therapie verzichtet werden).

Tumore, bei denen das Stadium FIGO II-B bis IV diagnostiziert wurde, sollen nach einer möglichst kompletten Resektion des Tumormaterial mit einer primären, 6 Zyklen Carboplatin und Paclitaxel beinhaltenden, systemischen Chemotherapie behandelt werden [26].

In ca. 3/4 der Fälle tritt trotz einer optimierten Therapie bei fortgeschrittenen Ovarialtumoren ein Rezidiv auf [14]. Von einem Frührezidiv spricht man, wenn es weniger als 6 Monate nach Abschluss der Primärtherapie diagnostiziert wird. In den meisten Fällen weist das Frührezidiv eine Resistenz gegenüber Platinpräparaten auf, sofern diese Bestandteil der Primärtherapie waren. In diesen Fällen können die Patientinnen entweder mit pegyliertem, liposomalen Doxorubicin, Topotecan oder mit Gemcitabin und Paclitaxel behandelt werden.

Als Spätrezidiv werden Tumore bezeichnet, die frühestens 6 Monate nach Therapieende auftreten. Sie gelten im Allgemeinen als platinsensibel und werden in einer Reinduktions-therapie erneut mit einer platinhaltigen Kombinationstherapie behandelt. Folgende Wirkstoff-kombinationen haben sich als effektiv herausgestellt: Carboplatin + pegyliertes liposomales Doxorubicin oder Paclitaxel oder Gemcitabin oder Gemcitabin + Bevacizumab [26].

1.2 Kleinzelliges Ovarialkarzinom vom hyperkalzämischen Typ (SCCOHT)

Als eigenständige pathologische Einheit klassifizierte Robert E. Scully 1979 erstmals das kleinzellige Ovarialkarzinom im Atlas für Tumorpathologie [27]. Es wird dabei zwischen drei Varianten unterschieden: dem hyperkalzämischen-Typ (SCCOHT), dem pulmonalen-Typ (SCCOPT) und dem nicht-kleinzelligen-Typ (NSCSCC, non-small-cell carcinoma). Diese drei Typen des kleinzelligen Ovarialkarzinoms repräsentieren zusammen ungefähr 1 % der jährlichen Ovarialkarzinom Erkrankungen [28]. In einer ersten Publikation zum SCCOHT wurden 11 Patientenfälle mit 3 ähnlichen, schon publizierten Fällen [29,30] beschrieben und verglichen. Das Tumormaterial wurde lichtmikroskopisch und elektronenmikroskopisch untersucht. Hieraus schlussfolgerte Dickersin *et al.* eine epitheliale Natur dieser Neoplasien, konnte aber keinen spezifischen Subtyp oder Ursprung diagnostizieren. Im ersten Jahrzehnt nach der Festlegung, dass es sich bei SCCOHT um ein eigenständiges Krankheitsbild handelt, folgten erste Fallberichte und Studien von Behandlungsversuchen [31-37].

Folgende histologische Merkmale von SCCOHT-Tumoren wurden in der Literatur beschrieben:

- wenig differenzierte, kleine, runde Zellen mit hyperchromatischen Kernen, wenig Zytoplasma und eine hohe Mitoserate [38,39],
- diffuses, zuweilen spindelartiges Wachstum von dicht gepackten Zellen [39],
- die Tumore weisen häufig diffuse, folikelähnliche Bereiche auf, die zumeist mit eosinophiler Flüssigkeit gefüllt sind [39].

Bezüglich des Ursprungs der Histogenese von SCCOHT gibt es bis heute kein klares Ergebnis. In der Literatur werden verschiedene Ursprünge diskutiert: oberflächliche epitheliale Zellen, Keimzellen oder Keimstrang-Stromazellen [34,39-41]. Die WHO klassifizierte sie im Jahr 2003 in der Gruppe „misscellaneous tumor oft the ovary“ [42].
Im Klinikalltag bereitet die Unterscheidung zwischen einem SCCOHT und einem epithelialen Ovarialtumor oft große Probleme. Zumeist wächst das SCCOHT symptomlos und sehr schnell im kleinen Becken [43]. In über 50 % der Fälle ist bei der Erstdiagnose das SCCOHT nicht mehr auf das Ovar beschränkt, sodass es mit FIGO-Stadium ≥ II charakterisiert wird [44]. In einer retrospektiven Studie identifizierten Estel *et al*. 135 SCCOHT-Fälle mit umfangreichen Patientendaten, die in einem Zeitraum von 1975 bis 2010 lagen und werteten diese Daten statistisch aus. Die Ergebnisse dieser umfangreichen Studie lauten wie folgt [44]:

- Durchschnittsalter: 23,4 Jahre (SD 10,6; [14 Monate–71 Jahre])
- Durchschnittliche Zeit zwischen den ersten Symptomen und Diagnose:
  6,6 Wochen (SD 9,2; [1–52 Wochen])
- Größe des Primärtumors: 14,7cm im Durchmesser (n = 85, SD 4,8; [6–30 cm])
- Tumorvolumen: 2.213 cm^3 (n = 47, SD 2.479; [117–15.000 cm^3])
- Tumorgewicht: 1.378 g (n = 20, SD 2.045; [329–10.000 g])
- Tumormarker CA125 (Serumlevel): beschrieben in 26 Fällen und in 20 Fällen (76.9 %) lag ein erhöhter Messwert 176 U/ml (SD 176; [25–691 U/ml])
- Tumorstaging: FIGO „I“ 48,6 % (50/102), FIGO „II“ 11,6 % (12/102), FIGO „III“ 35,9 % (37/102) und FIGO „IV“ 3,9 % (4/102)
- Pathologische Beurteilung des Tumors:
  - Intratumorale Hämorrhagie: 28
  - Nekrose: 31
  - Zystische Bereiche: 28
- Ovarektomie: 97 % (128/132), unilateral 69,7 % (89/128), bilateral 30,5 % (39/128)

- Chemotherapie nach Operation: 86,3 % (101/117)
    - Carboplatin oder Cisplatin 87,1 % (88/101)
    - Etoposid 52,5 % (53/101)
    - Alkylierungsmittel 39,6 % (40/101)
    - Bleomycin 29,7 % (30/101)
    - Anthracycline 27,7 % (28/101)
    - Vinca-Alkaloide 27,7 % (28/101)
    - Taxane 20,8 % (21/101)
- Strahlentherapie: 27,2 % (28/103)
- Rezidiv: 65,1 % (82/126)
    - Dauer der Rezidiventwicklung: 11,5 Monate (n = 50, SD 13,3; [1–70 Monate])
    - Operation: 81,3 % (26/32)
    - Chemotherapie: 90,2 % (37/41)
    - Strahlentherapie: 44,4 % (12/27)
    - Zeit zwischen aufgetretenem Rezidiv und tumorbedingtem Tod: 15,7 Monate (SD 26,4; [1–159 Monate])

Die statistische Auswertung dieser Daten von Estel *et al*. zeigen mittels Überlebenskurve nach Kaplan-Meier und dem Log-Rank-Test, dass Bleomycin, Cyclophosphamid, Anthrazykline und Taxane keinen Effekt auf das Überleben der Patientinnen haben und damit hier therapeutisch unwirksam sind. Die Anwendung von Etoposid (Log Rank = 18,5; df = 1; p > 0,001), Cisplatin oder Carboplatin (Log Rank = 5,9; df = 1; p > 0,015) oder Vinca Alkaloide (Log Rank = 3,9; df = 1; p > 0,047) ist begleitet mit einem verlängertem Überleben der Patientinnen. Diese Ergebnisse unterstreichen Daten von Pautier *et al*. [45], wobei 27 Patientinnen eine PAVEP (Cisplatin, Adriamycin, Vepesid, Cyklophosphamid) basierte Chemotherapie verabreicht wurde mit dem Ergebnis, dass 49 % der Patientinnen einige Jahre überlebt haben (aber nur (1/13) der Stage-III Patientinnen überlebte die Krankheit mit dieser Therapie). Ein weiteres Chemo-Behandlungsschemata für das SCCOHT umfasst folgende Wirkstoffkombination VPCBAE (Vinblastin, Cisplatin, Cyclophosphamid, Bleomycin, Doxorubicin, Etoposid) [37,46-50]. Harrison *et al.* [51] berichtet in seiner Studie, dass die langzeitüberlebenden Patientinnen eine Kombinationstherapie von Cisplatin und Etoposid erhalten haben. Auf Basis dieser sehr spärlichen und heterogenen Ergebnislage gibt es bis zum jetzigen Zeitpunkt allerdings keine Standardtherapie für SCCOHT Patientinnen, so dass weiterhin Mithilfe von individuellen Heilversuchen (Case-Report) und der Grundlagen-

forschung (*in vitro* und *in vivo*) neue Wege für einen SCCOHT Therapieansatz gefunden werden müssen.

Ein physiologisch begleitendes Merkmal der SCCOHT Tumorerkrankung ist die Entwicklung einer Hyperkalzämie bei ca. 60 % der Patientinnen [39]. Als Hyperkalzämie bezeichnet man einen erhöhten Kalziumspiegel im Serum (Normalbereich: 2,0–2,5 mmol/L, milder Typ: 2,5–3,0 mmol/L, moderater Typ: 3,0–3,5 mmol/L, hyperkalzämische Krise: > 3,5 mmol/L) [52].

Neben der Hyperkalzämie gab es bis zum Jahr 2014 keinen spezifischen Marker, welcher es Pathologen ermöglichte, Tumorschnitte eindeutig dem SCCOHT zuzuordnen. Zwar kann ein erfahrener Pathologe mit Hilfe von charakteristischen Zellmerkmalen für SCCOHT mittels H/E-Färbung (Hämatoxylin-Eosin) und durch gezielten IHC-Färbungen (Immunhistochemie) von EMA (epithelial membran antigen, Synonyme: MUC1, CD227) und WT1 (Wilms-Tumor-Protein) [38,53] das Krankheitsbild bestätigen. Da diese IHC-Marker aber nicht zu 100 % spezifisch für SCCOHT sind, sind Fehlinterpretationen möglich.
Durch umfangreiche Forschungen zeigten fast gleichzeitig drei Arbeitsgruppen [54-56], dass SCCOHT durch eine Mutation des Gens *SMARCA4* (Proteinprodukt: BRG-1) charakterisiert werden kann (Verlust der Proteinexpression bei 64/69). Das BRG-1 Protein ist eine zentrale katalytische Komponente des „SWI/SNF chromatin-remodeling gene complex“ und ist an der Kontrolle der Gentranskription in der Zelle beteiligt [55]. Dieser Komplex wurde schon in einer Vielzahl unterschiedlicher Karzinome beschrieben [57,58]. Eine weitere Mutation in einem Mitglied des SWI/SNF Komplex, *SMARCB1*, zeigt zu 95 % bei Rhabdoiden Tumoren keine Expression des Proteinprodukts INI1 [55]. In einer ersten, darauffolgenden vergleichenden IHC-Studie konnte Karania-Philippe *et al.* [59] durch eine Analyse von 122 Tumoren, darunter 116 gynäkologische Tumore inklusive von 12 SCCOHT Fällen zeigen, dass das Fehlen von BRG-1 Expression und das gleichzeitige Vorhandensein von INI1 Expression eine geeignete Markerkombination zur Charakterisierung von SCCOHT darstellt. In vereinzelten Fällen kann es aber auch zu konträren Ergebnissen kommen, die nicht in das erwartete Muster passen [60].

Aufgrund von einigen Gemeinsamkeiten zwischen dem SCCOHT und den rhabdoiden Tumoren spekulieren einige Wissenschaftler über deren Verwandtschaftsgrad [44,61]. Andere Forscher gehen soweit und fordern eine Umbenennung des SCCOHT zu „malignant rhabdoid tumor of the ovary“ (MRTO) [55,62].

1.3 Zelllinien des kleinzelligen Ovarialkarzinom vom hyperkalzämischen Typ

In der Literatur wurden bis 2015 drei Zelllinien vom Typ des SCCOHT beschrieben:
1. BIN-67 [63,64]
[2. OS-1, allerdings ohne Tumorigenität] [65]
3. SCCOHT-1 [66]

Die Zelllinie BIN-67 wurde erstmals 1986 bei Upchurch *et al.* [64] erwähnt, aber erst 2013 durch Gamwell *et al.* [63] ausführlich charakterisiert. Die Zellen zeigen eine typische Morphologie von adhärenten, kleinen Zellen mit wenig Zytoplasma. Im Orginaltumor wurden eng gepackte, epitheliale Zellen mit follikelähnlicher Struktur beschrieben. Intensive IHC-Färbung von Vimentin und WT-1, eine moderate IHC-Färbung von KIT, Pgp9.5 und P53, sowie eine unregelmäßige IHC-Färbung von Zytokeratin und alpha-Synaptophysin wurden im Tumor festgestellt. In über 95 % der Zellen konnte ein diploider (46, XX) Chromosomensatz und in einer sub-Population eine Tetraploidie (92, XXXX) festgestellt werden. Es wurden keine *TP53*, *KRAS* und *BRAF* Genmutationen charakterisiert. Die Zelllinie zeigt nach sehr langer Inkubationszeit tumorigenes Potential und es konnte bei den tumortragenden Mäusen eine Entwicklung einer Hyperkalzämie beobachtet werden. Die Zelllinie BIN-67 zeigt *in vitro* eine Resistenz gegen Cis- und Carboplatin Präparate sowie Taxol.

Die Zelllinie OS-1 stammt von einem metastasiertem Herd des Uterus einer 25 jährigen Japanerin (ohne Hyperkalzämie) und wurde erstmals 2004 durch Ohi *et al*. [65] beschrieben. Die Zellen wachsen *in vitro* als kleine, runde, nicht-adhärente Cluster. Sie wachsen adhärent auf Kollagen1 beschichteten Schalen. Die Populationsverdopplungszeit der Zellen beträgt 30 h und sie besitzen zu 75 % (57/76) einen normalen Karyotyp (46, XX). Elektronen-mikroskopische Beobachtungen zeigen runde Zellen mit einem Kern. In den Zellen befindet sich eine gut entwickelte Golgi-Apparatur, ausgedehnte ERs und glykogene Partikel. Des Weiteren wurden Desmosomen beobachtet. Im Kulturmedium konnte eine erhöhte Konzentration von ACTH, PTH und PTHrP nach der Kultivierung der Zellen beobachtet werden. Die Zellen sind *in vitro* sensibel gegen Vinblastin, Docetaxel, Irinotecan und haben eine Resistenz gegenüber Cis- und Carboplatin, Etoposid und Vincristin. Die Zelllinie OS-1 zeigt allerdings keine tumorigene Kapazität *in vivo* und ist daher als Zellmodell für das SCCOHT unbrauchbar.

Die Zelllinie SCCOHT-1 wurde in unserem Labor durch Ralf Hass 2009 etabliert und erstmals 2012 in der Literatur von Otte *et al.* beschrieben. Die Zellen stammen von einer 31 jährigen Frau mit einem diagnostiziertem SCCOHT (FIGO Ia). 11 Monate nach der Primärtherapie entwickelte die Patientin ein Rezidiv mit begleitender Hyperkalzämie (2,87 mmol/L). Die Patientin verstarb 13 Monate nach Diagnosestellung.

Lichtmikroskopisch sind spindelförmige, adhärente Zellen sowie abgerundete Zellen zu beobachten. Elektronenmikroskopisch konnte eine Vielzahl an filopodienähnlichen Ausstülpungen beobachtet werden. Des Weiteren konnten viele längliche Mitochondrien, freie Ribosomen im Zytoplasma und gebundene am ER beobachtet werden (Abbildung 1-3). Die Zellen besitzen in Suspension einen Durchmesser von 13 µm und eine ungefähre Verdopplungszeit von 36 h.

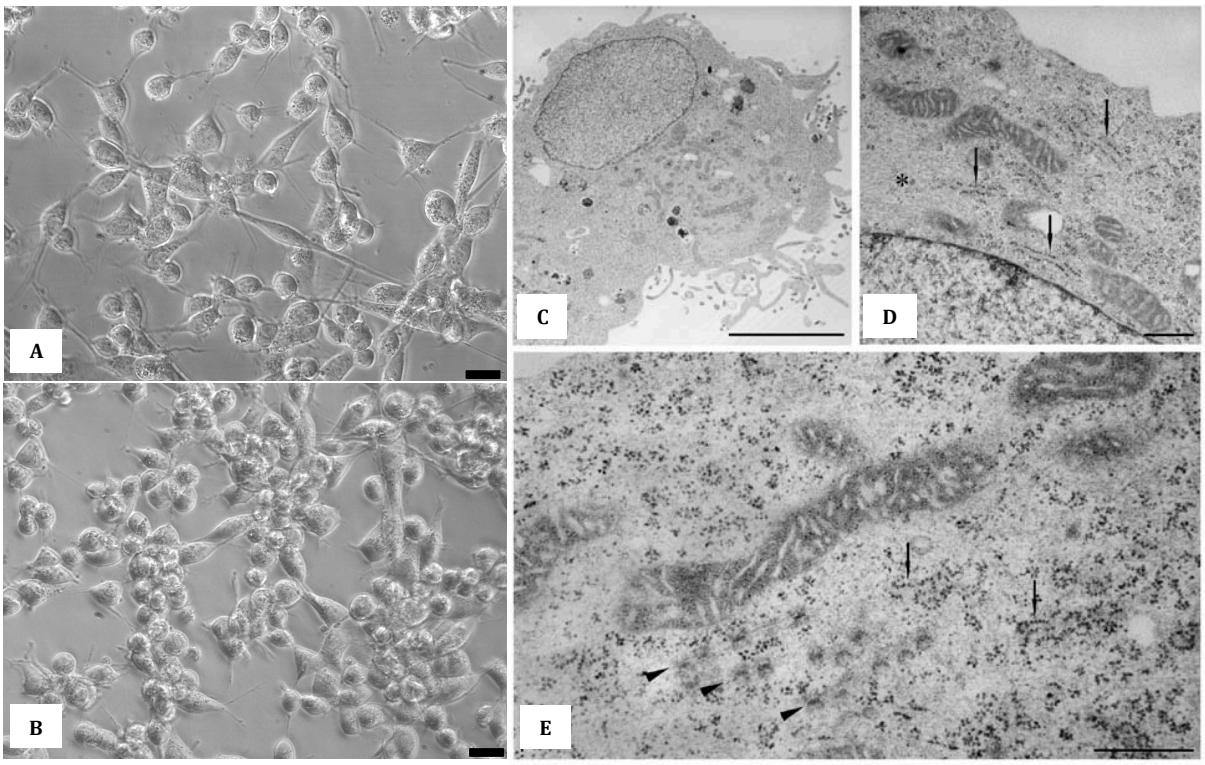

Abbildung 1-3: Morphologie von SCCOHT-1. A-B) Typische Phasenkontrastmikroskopische Aufnahmen von SCCOHT-1 mit adhärenten (A) und komplexen dreidimensionalen Strukturen (B). Die adhärenten Zellen bilden eine spindelförmige Morphologie aus (A) wohingegen bei den dreidimensionalen Strukturen abgerundete Zellen zu beobachten sind. Bei diesen abgerundeten Zellen handelt es sich aber nicht um abgelöste Zellen. **C-E)** In den Transmissionselektronenmikroskopischen Aufnahmen konnten unterschiedlich stark ausgeprägte apikale Oberflächen (C) beobachtet werden. Im Zytoplasma konnten viele Ribosomen frei oder gebunden am rauen endoplasmatischen Retikulum (D+E) beobachtet werden. Es konnten des Weiteren gut ausgeprägte Mitochondrien (C-E) und euchromatinreiche Zellkerne (C+D) beobachtet werden. (Balken A+B: 25 µm, C: 5 µm und E: 0,5 µm). (adaptiert nach Otte *et al.* [66])

In 18 von 21 Zellen konnte ein normaler Karyotyp (46, XX) (Abbildung 1-4) gefunden werden. Mit der Hilfe von einer FACS-basierten Analyse der Oberflächenmarker der

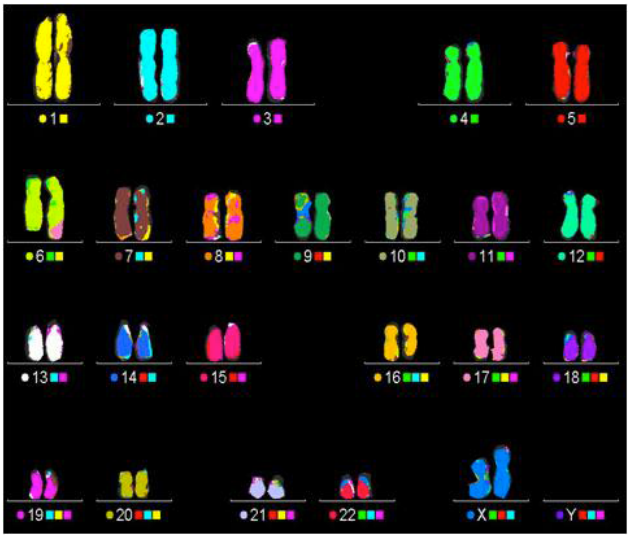

Abbildung 1-4: Karyotyp Analyse von SCCOHT-1.

Die Chromosomenanalyse wurde mittels klassischer Bänderungstechnik analysiert. Es konnten 3 von 21 unbalancierte Translokationen mittels mFISH-Analyse diagnostiziert werden. ISCN-Karyotyp: 46,XX,der(6)t(6;17)(q26;q22)[3]/46,XX[18]. (aus Otte *et al.* [66])

Zelllinie konnte eine Expression von CD15, CD29, CD44, CD90, panCK und Vimentin beobachtet werden. Die Zellen sind zu 100 % tumorigen in NODscid Mäusen und es entwickelt sich parallel eine Hyperkalzämie in den Mäusen. Histopathologisch zeigen die SCCOHT-1 induzierten Maustumore im Vergleich zum ursprünglichen Patiententumor-gewebe große Übereinstimmungen. Damit stellen insbesondere SCCOHT-1 Zellen ein geeignetes Zellsystem für *in vitro* und *in vivo* Studien zu dieser Tumorerkrankung dar.

1.4 Untersuchte Therapeutika

1.4.1 5'-Fluoruracil (5'-FU) – Antimetabolit

5'-FU gehört zu der Wirkstoffklasse der Zytostatika und zählt zu den Antimetaboliten, da es denselben Transportmechanismus wie Uracil verwendet [67]. Bei 5'-FU handelt es sich um ein Strukturanaloga von Uracil mit einem Fluor-Atom an der C-5 Position anstelle eines Wasserstoff-Atoms. In der Zelle wird 5'-FU in einige aktive Metaboliten umgewandelt (FdUMP, FdUTP und FUTP). Diese Stoffwechselprodukte stören die RNA-Synthese und die Wirkung des Enzyms Thymidylat-Synthase (TS). 1. Der 5'-FU Metabolit FdUMP verdrängt das Uracil bei der Bindung mit dem Enzym TS. Hierdurch kommt es zu einer verringerten Menge an synthetisiertem Thymidin, das für die Zellreplikation benötigt wird und somit zu einer verringerten Zellzahl führt. 2. FdUTP wird in Ermangelung von ausreichend Thymidin in die Zellen eingebaut, wobei eine fehlerhafte DNA entsteht, die mittels eines aufwendigen

Reparaturmechanismus korrigiert werden muss (Verlangsamung bis hin zum Erliegen kommende Zellreplikation). Durch die Überlastung der Reparationsmechanismus werden nicht alle Fehler entsprechend behoben und dies führt zu konsekutiven Strangbrüchen, die wiederum Apoptose induzieren.

1.4.2 Cytosin-Arabinosid (Ara-C) – Antimetabolit

Ara-C gehört ebenfalls zur Stoffklasse der Antimetaboliten und ist ein Analog des Nukleotids Cytosin. Es wurde erstmals um 1960 zur Behandlung von akuter myeloischer Leukämie (AML) zugelassen [68]. Intrazellulär wird Ara-C in seine aktive Form, dem Ara-C-Triphosphat phosphoryliert. Dies führt durch dessen Einbau in die DNA und einer damit einhergehenden Hemmung der DNA-Polymerase zum Zelltod durch die Blockierung der DNA-Replikation und dessen Reparatur [69,70]. Demnach spielt Ara-C nur während der DNA-Synthesephase eine entscheidende Rolle.

1.4.3 Methotrexat (MTX) – Antagonist

Methotrexat gehört zu der Klasse der Folsäure-Antagonisten [71]. Die Wirkung beruht auf einer Inhibition des für die Zellproliferation essentiellen Enzyms Dihydrofolatreduktase (DHFR). Die Aufgabe dieses Enzyms beruht auf der Metabolisierung von Folsäure zum Tetrahydrofolat als aktive Form, welche wiederum für die Synthese von Purinen und Thymidylaten benötigt wird. Als Folge dessen stehen für die DNA-Synthese nicht genügend Bausteine zur Verfügung, was zu einer verminderten Zellreplikation führt [72].

1.4.4 Doxorubicin – Anthracyclin und Interkalation

Doxorubicin gehört zu den Zytostatika aus der Stoffgruppe der Anthracycline und zur Wirkstoffgruppe der Interkalantien. Einer der Wirkstoffmechanismen beruht darauf, dass Doxorubicin sich zwischen benachbarte Nukleotide in der DNA schiebt und somit die Transkription blockiert wird [73]. Der zweite Wirkmechanismus beruht auf der enzymatischen Inhibition von Topoisomerase II durch Doxorubicin, die ein Schlüsselenzym der DNA-Synthese ist [74].

1.4.5 Topotecan – Topoisomerase I Inhibitor

Topotecan gehört zu der Stoffklasse der Zytostatika und ist ein Topoisomerase I Hemmer. Bei Topotecan handelt es sich um ein Camptothecin Derivat, welches auch in der traditionellen chinesischen Medizin zur Behandlung von Tumorerkrankungen eingesetzt wird [75].
Topotecan stabilisiert den kovalenten Komplex der Topoisomerase I mit der zur Replikation in zwei Stränge aufgespaltenen DNA. Aufgrund der Stabilisierung dieses Komplexes kommt es zu einem Doppelstrangbruch, die Transkription und die damit verbundene Replikation der Zellen kommt zum Erliegen und die Zellen gehen in die Apoptose [76-79]. Die Wirkung von Topotecan ist S-Phase spezifisch.

1.4.6 Cyclophosphamid – Alkylanz

Cyclophosphamid gehört zu der Gruppe der alkylierenden Wirkstoffe. Alkylanzien bauen Alkylgruppen in Amino-, Carboxyl-, Hydroxyl-, Phosphat- und Sulfhydrylgruppen der DNA ein und vernetzen damit die RNA bzw. DNA-Stränge miteinander. Dies führt wiederum zu einer insuffizienten Replikation der DNA, gefolgt von Substanz induzierten Strangbrüchen und wirkt somit direkt schädigend auf die DNA ein. Cyclophosphamid ist ein sogenanntes „Prodrug“, das erst durch eine enzymatische Reaktionen in der Leber aktiviert wird. Hierbei hydroxyliert das Cytochrom P450 System das Cyclophosphamid zu 4-Hydroxy-cyclophosphamid-Aldophosphamid. In einem weiteren Schritt wird Acrolin abgespalten, es entsteht das zytotoxische reaktive Produkt Phosphoramid-Mustard [80].

1.4.7 Platinverbindungen Cis- und Carboplatin

Das chemische Molekül „Cisplatin“ (cis-$PtCl_2(NH_3)_2$ wurde erstmals 1845 durch Michel Peyrone in der Literatur erwähnt. Seine zytostatische Wirkung wurde allerdings erst um 1960 durch ein Zufall entdeckt. Im Jahr 1971 wurde es erstmals in klinischen Studien für die Krebstherapie getestet. Die Wirkungsweise beruht auf der Bildung eines Platinkomplex im Zellinneren, der sich an die DNA bindet und sie quervernetzt.

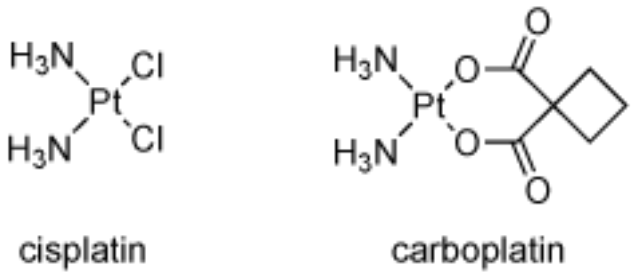

Abbildung 1-5: Strukturformel von Cis- und Carboplatin

Hierbei handelt es sich um eine nukleophile Substitutionsreaktion. In wässriger Umgebung des Körpers wird das Chlorid-Ion durch eine Hydroxyl-Gruppe ausgetauscht. Nach der intrazellulären Aktivierung bildet das positiv geladene Platinatom mit den nukleophilen Bindungsstellen der DNA (bevorzugt an den Guanin- oder Adeninbasen) eine kovalente Bindung aus. Die so entstehenden Quervernetzungen am selben Strang (Intrastrang-Vernetzung), sowie zwischen den Strängen der Doppelhelix (Interstrang-Vernetzung) haben eine Verkürzung der DNA, und somit eine Störung in der Stapelung der Basen, gefolgt von einer Verzerrung der Sekundärstruktur zur Folge. Dies kann zu einer Entwindung der Doppelhelix führen und hat den Verlust der thermischen Stabilität zur Folge. Als Folge ist bei Cisplatin behandelten Zellen keine Transkription und Replikation mehr möglich [81].
Carboplatin zeigt eine geringere Reaktivität und eine langsamere DNA-Bindungskinetik, obwohl das gleiche Endprodukt ausgebildet wird.

1.4.8 Paclitaxel (Taxol®) – Tubulin-interagierende Substanz

Taxol gehört zu der Stoffklasse der Taxane, die natürlich vorkommende Zytostatika sind. Die Substanz wurde erstmals 1971 durch Extraktion des Wirkstoffs aus der Rinde der pazifischen Eibe (Taxus brevifolia) von Wani *et al.* isoliert und charakterisiert [82].
Die krebshemmende Wirkung von Taxol und den unter 1.4.9 beschriebenen Epothilone beruht auf der Hemmung der Depolymerisierung von Mikrotubuli (Heterodimer aufgebaut aus je einer α- und β-Tubulinuntereinheit) und damit auf der Stabilisierung des polymeren Zustands [83]. Eine zentrale Rolle spielen die Mikrotubuli bei der Zellteilung (mitotischen Zellspindel), sowie beim Aufbau des Spindelapparates, dem intrazellulären Transport und dem Aufbau des Zytoskeletts in Zellen [84].
Durch die Bindung des Moleküls an β-Tubulin wird die Dissoziationsgeschwindigkeit in dem Tubulindimer beeinflusst. Dies führt zu einer Stabilisierung der Mikrotubuli, als Folge

können keine korrekten mitotischen Spindeln auf- und wieder abgebaut werden, der Zellzyklus wird in der G_2/M Phase arretiert und der Zelltod wird eingeleitet [83-85].

1.4.9 Epothilon A, Epothilon B und Ixabepilon – Tubulin-stabilisierende Substanz

Erstmals isolierten Wissenschaftler im Jahr 1987 beim Fermentationsprozess von Bodenbakterien, die sie am Flussufer des Sambesi in Afrika gefunden hatten, die Produktklasse der Epothilone [86,87]. Epothilone stellen eine Klasse von Zytostatika dar, dessen Wirkstoff aus dem Myxobakterium *Sorangium cellulosum* isoliert wurde [88].

Der Name Epothilon leitet sich von der chemischen Struktur des Naturstoffes (Abbildung 1-6) ab. Das Grundgerüst repräsentiert ein 16-gliedriges Makrolid mit **Epo**xid, **Thi**azol und Ket**on** als funktionellen Gruppen [85,87].

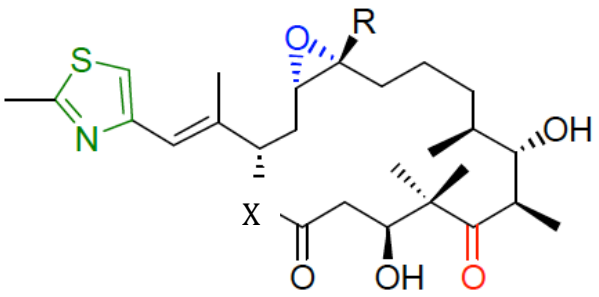

Epothilon A: R = H und X = O
Epothilon B: R = CH_3 und X = O
Ixabepilon: R = CH_3 und X = N

Epoxid, Thiazol, Keton = Epothilon

Abbildung 1-6: Strukturformel von Epothilon und deren Derivate Epothilon A, Epothilon B und Ixabepilon

Eine aktuelle PubChem Suche (http://pubchem.ncbi.nml.nih.gov) ergab bei einer Schlagwortsuche nach „epothilone“ 44 Treffer und für „ixabepilone“ 2 Treffer, darunter Epothilon A bis K, sowie semisynthetische Epothilone wie Ixabepilon und vollsynthetische Epothilone. Wie in Abbildung 1-6 zu erkennen ist, liegt der Unterschied zwischen Epothilon A und B in einer zusätzlichen Methylgruppe am Kohlenstoffatom der Epoxidgruppe, bei Ixabepilon ist anstelle des Sauerstoffatoms im Makolid-Ring (Epo A und Epo B) ein Stickstoffatom ausgetauscht.

Der Wirkstoffmechanismus beruht genau wie bei den Taxanen auf der Stabilisierung von Mikrotubuli in Tumorzellen (siehe unter 1.4.8).

1.4.10 Tyrosin Kinase Inhibitoren (TKI) des Tyrosin Kinase Rezeptor (RTK)

Tyrosin-Kinase Inhibitoren (TKI) sind kleine organische Verbindungen mit niedrigem Molekulargewicht (500–900 Dalton) [89,90]. Durch Bindung eines TKIs an eine ATP-Bindungsstelle der Tyrosinkinase-Domäne von Rezeptor-Tyrosinkinasen (RTK) wird dessen Kinaseaktivität inhibiert, die normalerweise nach Bindung eines spezifischen Wachstumsfaktors durch Dimerisierung mit anschließender Autophosphorylierung eines Tyrosinrestes aktiviert würde (Abbildung 1-8). Durch den Einsatz von TKI`s wird diese Autophosphorylierung an der Tyrosinkinase-Domäne inhibiert und die nachfolgende Signaltransduktion blockiert [91].

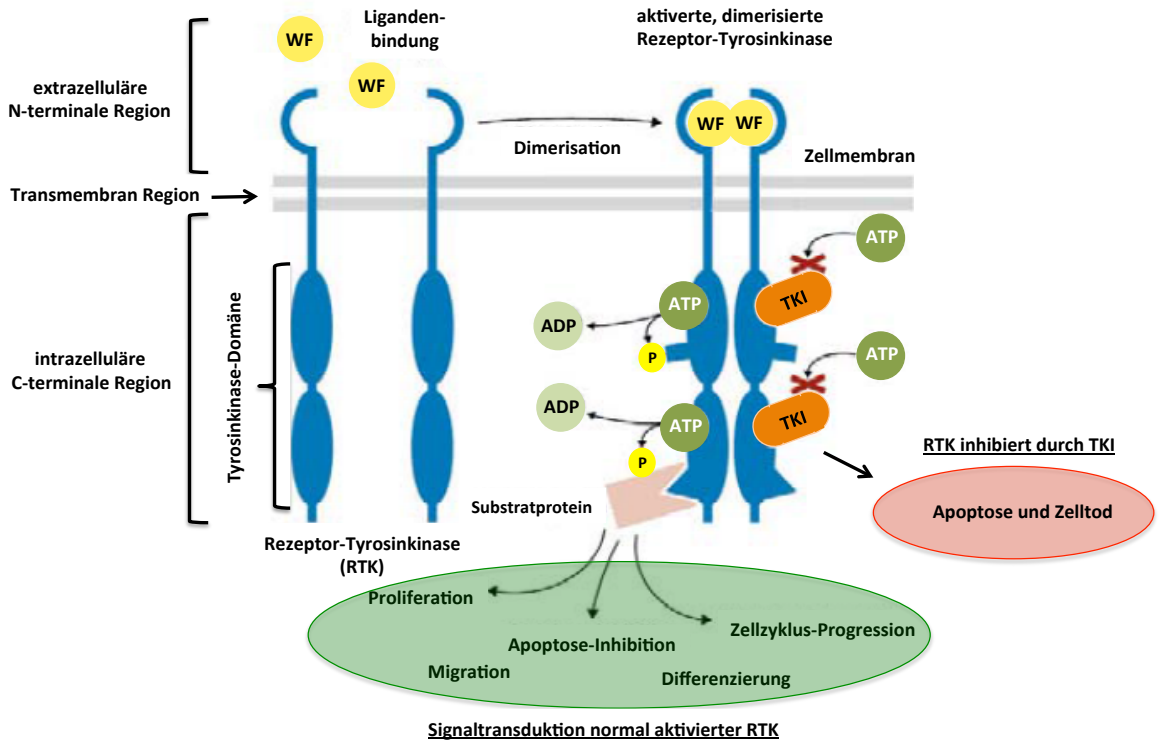

Abbildung 1-7: Schematische Darstellung von Rezeptor-Tyrosinkinasen. Allen Rezeptor-Tyrosinkinasen (RTK) gemein ist ihre Struktur, die aus drei Regionen besteht, der extrazellulären, der transmembranen und der zytoplasmatischen Region. Nach einer spezifischen Liganden Bindung erfolgt eine Dimerisierung gefolgt von einer Aktivierung des Tyrosinkinase-Rezeptors durch die Autophosphorvlierung von Tyrosinresten und die Aktivierung von Substratproteinen durch Tyrosinphosphorylierung. Daraufhin wird eine Signaltransduktionskaskade aktiviert (grüne Umrandung). Durch den Einsatz von kleinmolekularen Rezeptortyrosinkinase-Inhibitoren (TKI) wird über eine Bindung in der ATB-Bindungsstelle die Kinaseaktivität blockiert. (adaptiert nach Müller-Tidow *et al.* [92])

Beim Menschen sind derzeit 58 RTK`s bekannt, die in 20 Familien unterteilt werden. Darunter befinden sich 30 RTK`s, die bei der Onkogenese, einer Vielzahl von Tumoren, eine wichtige Rolle spielen [93]. Hierzu zählen z. B. die RTK`s der Familie vom EGF-Rezeptor

(Epidermaler Wachstumsfaktor Rezeptor), Insulin-Rezeptor, PDGF-Rezeptor (Blutplättchen-Wachstumsfaktor Rezeptor), FGF-Rezeptor (Fibroblasten-Wachstumsfaktor Rezeptor), VEGF-Rezeptor (vaskulo-endothelialem-Wachstumsfaktor Rezeptor), HGF-Rezeptor (Hepatozyten-Wachstumsfaktor Rezeptor) und weitere Rezeptoren.

1.4.10.1 Hepatozyten-Wachstumsfaktor (HGF) und dessen korrespondierende Rezeptor Tyrosinkinase c-Met

Der Tyrosinkinase Rezeptor c-Met, der durch das proto-Onkogen *MET* auf dem Chromosom 7q21-31 codiert wird, kontrolliert eine Vielzahl von Prozessen während der Entwicklung und Embryogenese von Wirbel- und Säugetieren [94]. Es handelt sich hierbei um einen membranständigen Rezeptor, der auf epithelialen Zellen von einer Vielzahl an Organen (Leber, Pankreas, Prostata, Niere, Muskeln und Knochenmark, während der Embryogenese und im Erwachsenenalter) zu finden ist [95].

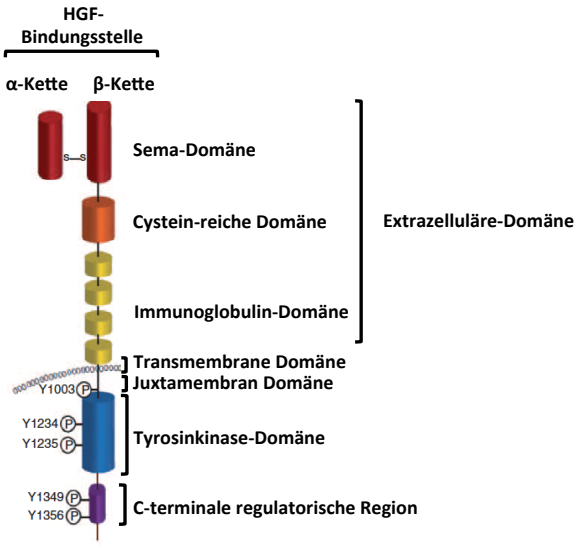

Abbildung 1-8: Schematischer Aufbau des c-Met-Rezeptors. Die Abbildung zeigt schematisch den Aufbau des transmembranen c-Met Proteins. Die extrazellulären Domänen: Sema- Domänen, eine Cystein-reiche-Domäne und vier Immunglobulin-Domänen. Der intrazelluläre Teil besteht aus der Juxtamembran- und der Tyrosinkinase-Domäne sowie aus der regulatorischen Region an der sich die Multisubstrat-Bindungsstelle befindet. Diese Extrazellulären Bereiche werden durch eine Transmembran-Domäne mit den intrazellulären Domänen verbunden. (adaptiert nach Organ *et al.* [94])

Der c-Met Rezeptor wird im post-Golgi-Kompartment durch [96] eine proteolytische Spaltung des inaktiven Proteins mit Furin zwischen den Aminosäuren 307 und 308 gebildet. Die aktive Form von c-Met besteht aus einer kurzen α- und einer langen β-Kette, die mittels einer Disulfid-Brücke miteinander verbunden sind [96]. Der extrazelluläre Bereich von c-Met besteht aus der spezifischen Bindungsstelle für HGF, auch bezeichnet als Sema-Domäne,

gefolgt von einer Cystein-reichen Domäne und vier Immunglobulin-Domänen. Der zytoplasmatische Bereich des Proteins besteht aus der membranständigen Juxtamembran-Domäne, der Tyrosinkinase-Domäne und der C-terminalen Region, die für die Signalübertragung verantwortlich ist.
Ende 1980 entdeckten zwei Wissenschaftler unabhängig voneinander den später als Ligand vom c-Met Rezeptor identifizierten Wachstumsfaktor HGF bzw. scatter-factor (SF) [97-100]. HGF wird als einkettige, biologisch inerte Vorläufer-Form (pro-HGF/SF) von mesenchymalen Zellen sekretiert. Durch eine proteolytische Spaltung der Bindung zwischen den Aminosäuren Arg494 und Val495 durch HGFA (Hepatozyten-Wachstums-Aktivator) wird das pro-HGF in ein aktives Dimer gespalten, welche durch eine Disulfidgruppe miteinander verbunden sind [101,102].

Durch die Bindung des Liganden HGF/SF an c-Met erfolgt eine Homodimerisierung des Rezeptors, gefolgt von einer Autophosphorylierung zweier Tyrosinreste (Y1234 und Y1235) in der katalytischen Schleife der Tyrosinkinase-Domäne [103]. Dies induziert die intrinsische Kinase-Aktivität des Moleküls und es folgen weitere Phosphorylierungen von Tyrosin-Resten in der C-terminalen Region (Y1349 und Y1356) sowie in der membrannahen Juxtamembran-Domäne (Y1003).

Die zentrale Voraussetzung für das Ablaufen der durch c-Met aktivierten Signalkaskaden ist die Bildung der Multisubstrat-Bindungsstelle für verschiedene Effektorproteine mit SH2- (Src homology 2) bzw. PTB- (phosphotyrosine binding) Domänen oder Met Bindungs-Domänen durch die Phosphorylierung der Tyrosin-Reste Y1349 und Y1356 in der Tyrosinkinase-Domäne [104,105]. Dabei können an dieser Multisubstrat-Bindungsstelle Proteine ohne enzymatische Aktivität (wie die Adapterproteine GRB2 (growth-factor receptor-bound protein), SHC (Src-homology-2 (SH2)-domain-containing), CRK (v-crk avin sarcoma virus CT10 oncogene homolog), CRKL (Crk-like) und GAB1 (growth factor receptor-bound protein 2 (GRB2) associated-binding protein 1)) und Proteine mit enzymatischer Aktivität (wie Src-Kinasen (Proto-oncogene tyrosine-protein kinase Src), PI3K (phosphatidylinositol 3-kinase), PLC-γ1 (phospholipase C- γ1), SHIP-2 (src homology 2 domain-containing 5' inositol phosphatase), STAT-3 (signal transducer and activator of transcription), SOS (Ras guanine nucleotide exchange factor son-of-seven), PTPs (protein tyrosine phosphatases) und SHP2 (Src homology 2 domain-containing phosphatase-2) binden [105-113]. Den

Adapterproteinen kommt dabei die zentrale Aufgabe zu, als Plattform für die Rekrutierung von Signalproteinen an der Zellmembran zu dienen.

Eine Schlüsselrolle bei diesen Signalkaskaden nimmt das Adapterprotein GAB1 ein, das sich direkt oder indirekt über GRB2 an c-Met bindet und dadurch phosphoryliert wird. Durch diese Phosphorylierung entstehen am Gab1 neue Bindungsstellen für nachgeschaltete Signalmoleküle. Dies führt zur Aktivierung des MAPK (mitogen activated protein kinase) – Signalweg und/oder zur PI3K vermittelten Aktivierung des Akt/PKB-Signalweges (Abbildung 1-9).

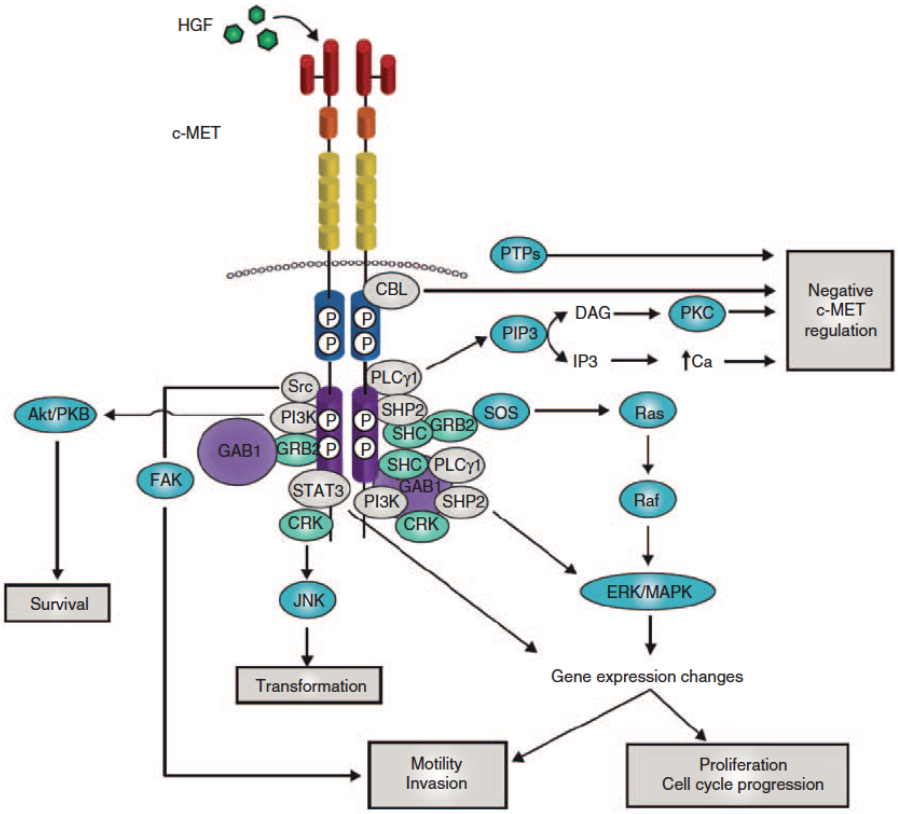

Abbildung 1-9: Schematischer Darstellung der HGF indizierten c-Met Signalwege.
Hier dargestellt sind der MAPK-Signalwegs (Proliferation, Migration, Apoptose und Differenzierung), PI3K/Akt-Signalweg (Zellwachstum, Überleben uns Proliferation), STAT3-Signalwegs (induziert Transkription von Genen zur Proliferation und Differenzierung) und die Negativ Regulierung**.** (aus Organ *et al.* [94])

Zusammenfassend führt eine HGF-Bindung an den Rezeptor c-Met zu dessen Aktivierung und damit zu einer Rezeptorphosphorylierung. Dies wiederum führt zur Rekrutierung von Adaptermolekülen, mit nachgeschalteter Stimulation weiterer Signaltransduktionskaskaden, u.a. der Aktivierung von MAPK.

MAPK-Signalweg

Die Aktivierung der MAPK über die c-Met Signalkaskade kann durch die Bindung des Adapterproteins GRB2 erfolgen, das wiederum konstitutiv mit dem Guaninnukleotid - Austauscher SOS (son of sevenless) an der Multisubstrat-Bindungsstelle assoziiert. Es folgt die Aktivierung von RAS (rat sarcoma viral oncogene homolog) durch SOS, indem es die Freisetzung von GDP und so den Austausch mit GTP an RAS ermöglicht [111]. RAS-GTP bindet daraufhin das Effektorprotein RAF (v-raf murine sarcoma viral oncogene homolog B1), dies führt zur Aktivierung von RAF, was in der Folge die Kinase MEK (MAPK effektor kinase) durch Phosphorylierung aktiviert. Schlussendlich phosphoryliert aktiviertes MEK die Kinase ERK/MAPK. Dies translociert in den Zellkern und aktiviert dort eine Reihe von Transkriptionsfaktoren, die für die Regulation einer Vielzahl an Genen (Proliferation, Motilität und Zellzyklus Progression) verantwortlich sind [113,114]. Im Gegenzug reguliert die Phosphatase SHP2 die Dauer der MAPK Phosphorylierung durch entsprechende Dephosphorylierung der RAS-GAP- (RAS GTPase activating protein) Bindungsstellen am GAB1, hierdurch kommt es zu keiner negativen Regulierung von RAS durch RAS-GAP [115,116].

Aktiviertes RAS kann darüberhinaus auch die Aktivierung von PI3K veranlassen, die über weitere Zwischenreaktionen die Kinasen P38 und JNK aktiviert. Diese beiden Kinasen kontrollieren auch eine Vielzahl an zellulären Prozesse (Transformation, Proliferation, Differenzierung und Apoptose) [109,117,118].

AKT/PKB-Signalweg

Durch die Bindung von p85, der regulatorischen Untereinheit von PI3K, kommt es zur Aktivierung von PI3K. Dies führt zur Generierung des sekundären Botenstoffs PIP3 (phosphatidylinositol (3,4,5)-triphosphat) aus PIP2 (phosphatidylinositol (4,5)-bisphosphat). Durch die Interaktion von PIP3 mit der PH- (pleckstrin homology) Domäne wird AKT an die Plasmamembran rekrutiert. Dort erfährt AKT eine Konformationsänderung und wird anschließend von den Kinasen PDK1 (phosphoinositide depending kinase 1) und mTORC2 (mammalian target of rapamycin complex 2) phosphoryliert und aktiviert. Der AKT-Signalweg ist an der Übermittelung von Wachstumssignalen (Proliferation, Motilität und Angiogenese) an Zellen beteiligt und verhindert, dass diese in die Apoptose gehen (Phosphorylierung von Bad (BCL-2 antagonist of the cell death) und MDM2 (E3 ubiquitin-protein ligase) durch AKT) [97,119].

STAT3-Signalweg

Durch die Bindung von STAT3 an die phosphorylierte Multisubstrat-Bindungsstelle von c-Met erfolgt eine Phosphorylierung von STAT3 über dessen SH2-Domäne. Dies ist assoziiert mit der Dimerisierung von STAT3 und der Translokation zum Zellkern. Hier veranlasst das STAT3 Dimer als Transkriptionsfaktor die Expression von Genen, die an der Differenzierung und Proliferation beteiligt sind.

An der negativen Regulation des c-Met Rezeptors sind verschiedene Mechanismen beteiligt. Eine wichtige Polle als negativer Regulator spielt dabei der Tyrosin-Rest Y1003. Dieser wird durch die Bindung der E3-Ubiquitin-Ligase c-CBL (casitas B-linage lymphoma) an den phosphorylierten Tyrosin-Rest Y1003 ubiquitiniert. Es folgt Endozytose, Transport und abschließend die proteasomale Degradierung des c-Met Rezeptors [120-123]. Ein weiterer Mechanismus der negativen Regulation erfolgt durch die Bindung von PLCγ1 an den c-Met-Rezeptor. Dadurch wird PLCγ1 aktiviert und setzt dabei den „second messenger“ IP3 (Inositoltriphosphat) und DAG (Diacylglycerol) frei. Dies führt unter anderem zu der Aktivierung von PKC (Protein Kinase C), die über einen negativen Feedback-Mechanismus die Tyrosinkinase Aktivität des c-Met Rezeptors herunterreguliert [124,125]. Unabhängig von der PKC-Aktivierung kann ein Anstieg an intrazellulärem Kalzium zu einer negativen Regulation von c-Met führen [126]. Ebenfalls können PTP`s die Tyrosin-Reste in der Kinase-Domäne bzw. an der Multisubstrat-Bindungsstelle für die Adaptorproteine dephosphorylieren [94].

Somit wird deutlich, dass ein weit verzweigtes Netzwerk unterschiedlicher Signalkaskaden für die komplexe zelluläre Antwort auf HGF/Met-Signale verantwortlich ist.

1.4.10.2 Crizotinib

Crizotinib (PF-02341066) ist ein Tyrosinkinase Inhibitor und wurde im Jahr 2010 durch die Firma Pfizer als Arzneimittel der Fachwelt vorgestellt. Die Substanz wurde mit Hilfe eines Arzneimittelscreening entwickelt, basierend auf dem c-Met-Inhibitor PHA 665752. Im Rahmen dieser Optimierung wurden verschiedene funktionelle Gruppen des ursprünglichen Moleküls (PHA 665752) verändert, so dass bei dem neu entwickelten Molekül Crizotinib eine effizientere Bindung des Moleküls an der ATP-Bindungstasche der Kinase-Domäne von c-Met festzustellen war. Somit wird die Bindung von ATP an die Kinase-Domäne blockiert

und die Autophosphorylierung der Tyrosinreste verhindert)[127,128]. Zudem zeigt Crizotinib auch für den Tyrosinkinase Rezeptor ALK (Anaplastic lymphoma kinase) und ROS1 (ROS proto-oncogene 1, receptor tyrosine kinase) inhibierendes Potenzial [129]. Seit dem Jahr 2012 ist Crizotinib unter dem Handelsnahmen Xalkori in Europa bekannt und seit August 2011 in den USA zur Behandlung von ALK-positiven nicht-kleinzelligen Bronchialkarzinomen (NSCLC) zugelassen. Bei der Durchführung von klinischen Studien konnten die pharmako-kinetischen Eigenschaften von Crizotinib sowie resultierende Nebenwirkungen untersucht werden. Dies waren zumeist gastrointestinale Nebenwirkungen (Übelkeit und Diarrhö), die höchste Plasmakonzentration nach einmaliger Einnahme vom 250 mg Crizotinib wurde nach 4 h erreicht. Hierbei liegt die Konzentration des freien Arzneistoffs im Plasmaspiegel bei 57 nM (274 ng/ml) und somit im effektiven Konzentrationsbereich für c-Met (~13 nM) und ALK (~26 nM) [130,131].

1.4.10.3 Foretinib

Der als Medikament oral verabreichte Tyrosinkinase Inhibitor Foretinib (GSK1363089, XL880) wurde von der Firma Exelixis entwickelt und anschließend an die Firma GlaxoSmithKline auslizensiert. Foretinib zeigt eine gewisse Spezifität mit hoher Bindungsaffinität bei c-Met (IC50: 0,4 nM) und VEGF/KDR (IC50: 0,9 nM) und eine geringere Bindungsaffinität bei anderen Wachstumsfaktorrezeptoren wie PDGFRα (IC50: 3,6 nM), PDGFRβ (IC50: 9,6 nM), RON (IC50: 3 nM), c-KIT (IC50: 6,7 nM), FLT-3 (IC50: 3,6 nM) und TIE-2 (IC50: 1,1 nM) [132-135] und eine geringe Bindungsaffinität bei FGFR1 (IC50: 660 nM), und EGFR (IC50: 2,9 μM). Durch die Assoziation des Inhibitors an die Rezeptor-Tyrosinkinasen kommt es zu einer Änderung der Konformation in der Kinase-struktur. Hierdurch kommt es zu einer stabileren Bindung von Foretinib mit den Tyrosin-Resten in den ATP-Bindungstaschen. Eder *et al*. fand heraus, dass die Foretinib/ Tyrosinkinase Rezeptorbindung länger als 24 Stunden stabil bleibt [133]. Aktuell gibt es folgende klinische Studien mit Foretinib (clinicaltrials.gov, updated on 2015-06-27): Phase I: solide Tumore, orale Applikation (abgeschlossen); Phase I: solide Tumore, tägliche Applikation (abgeschlossen); Phase I: Leberkrebs, multizentrisch (aktiv); Phase I: randomisiert, solide Tumore (abgeschlossen); Phase I/II: nicht kleinzelliges Lungenkarzinom (NSCLC) nach Erlotinib Therapie (abgeschlossen); Phase I/II: Metastasierender Brustkrebs mit HER2- (human epidermal growth factor receptor2) Überexpression, (abgeschlossen); Phase II: „triple negative“ Brustkrebs (abgeschlossen); Phase II: Nierenkrebs (abgeschlossen);

Phase II: genomische Subpopulationen des nicht kleinzelligen Lungenkarzinoms (NSCLC), (aktiv); Phase II: metastasierter Magenkrebs (abgeschlossen); Phase II: Rezidiv oder metastasiertes Plattenepithelkarzinom (abgeschlossen).

1.5 Zielsetzung der Arbeit

Wird bei einer Patientin die Diagnose gestellt, dass sie an einem kleinzelligen Ovarialkarzinom vom hyperkalzämischen Typ (SCCOHT) erkrankt ist, so kann man davon ausgehen, dass diese Frau innerhalb der nachfolgenden 5 Jahre an dieser Erkrankung versterben wird. Seit der erstmaligen Erwähnung des SCCOHT von Dr. Robert E. Scully im Atlas für Tumorpathologie vor 36 Jahren wurden in der Fachliteratur zwar einige Fallberichte publiziert, aber es fehlt an Arbeiten, die sich mit den mechanistischen Grundlagen dieser Krankheit eingehend beschäftigen. Aus dieser Unkenntnis ist der momentane Therapieansatz beim SCCOHT fast identisch mit der Therapie, die beim Ovarialkarzinom Anwendung findet. Ein schwerwiegendes Problem stellt die Seltenheit dieser Erkrankung dar, weil dies im entscheidenden Maße das für die Forschung dringend benötigte Ausgangsmaterial limitiert. Es fehlten hierfür zuverlässige Modellsysteme, mit deren Hilfe dieses Krankheitsbild zunächst auf Zellbasis (*in vitro*) studiert werden konnte. Diese Voraussetzungen geeigneter Zellkulturmodelle sind bei einer Vielzahl gut erforschter Tumorerkankungen wie beispielsweise dem Ovarialkarzinom, dem Lungenkarzinom oder Leukämie gegeben, um therapeutische Hypothesen testen zu können.

Diese entscheidende Lücke beim SCCOHT konnte durch eine erfolgreiche Etablierung zweier Zellsysteme in den letzten Jahren geschlossen werden. Eines dieser Zellsysteme ist die Zelllinie SCCOHT-1, die im Jahr 2009 von Prof. Ralf Hass aus dem Tumormaterial einer Patientin mit einem SCCOHT Rezidiv isoliert und etabliert werden konnte. Im Rahmen von Vorarbeiten aus der Arbeitsgruppe um Ralf Hass, der medizinischen Doktorarbeit von Finn Rauprich und meiner eigenen Diplomarbeit konnten die Zellen grundlegend charakterisiert werden. Dabei zeigten die Zellen im Mausmodell ein solides tumorigenes Potenzial, das für die in dieser Arbeit durchgeführten *in vivo* Untersuchungen das Fundament darstellte. In der hier vorgestellten Arbeit sollte der Effekt verschiedenster Chemotherapeutika und deren Einfluss auf unterschiedliche Signalwege der SCCOHT-1 Zellen untersucht werden. Die aus diesen *in vitro* Testreihen resultierenden Ergebnisse sollten anschließend im *in vivo* Modell auf ihre Wirksamkeit hin überprüft werden.

Anknüpfend an die Arbeit von Finn Rauprich, der zeigen konnte, dass die SCCOHT-1 gegenüber einer erhöhten Kalziumkonzentration im Zellkulturmedium mit einer verminderten Proliferation reagierten, sollte dieses Phänomen weitergehend und im Vergleich zu zwei humanen ovarialen Adenokarzinom-Zelllinien (SK-OV-3 und NIH:OVCAR-3) untersucht werden. Des Weiteren sollte geprüft werden, was das exogen hinzugefügte Kalzium auf molekularer Ebene in den Zellen auslöst. Die aus den *in vitro* Untersuchungen generierten Ergebnisse sollten ebenfalls *in vivo* auf ihre Relevanz hin getestet werden. Darüber hinaus sollte durch den parallelen Einsatz von Chemotherapeutika in Verbindung mit exogenem Kalzium geprüft werden, wie sich diese Kombination auf das proliferative Verhalten der SCCOHT-1 Tumorzellen *in vitro* und *in vivo* auswirkt.

2 Publikationen

2.1 Interference of Ca^{2+} with the proliferation of SCCOHT-1 and ovarian adenocarcinoma cells

Anna Otte, Finn Rauprich, Juliane von der Ohe, Peter Hillemanns und Ralf Hass

publiziert in
Inernational Journal of Oncology
45(3), 2014, 1151 - 1158
doi: 10.3892/ijo.2014.2517

INTERNATIONAL JOURNAL OF ONCOLOGY 45: 1151-1158, 2014

Interference of Ca^{2+} with the proliferation of SCCOHT-1 and ovarian adenocarcinoma cells

ANNA OTTE, FINN RAUPRICH, JULIANE VON DER OHE, PETER HILLEMANNS and RALF HASS

Biochemistry and Tumor Biology Laboratory, Department of Obstetrics and Gynecology, Hannover Medical School, Hannover, Germany

Received April 14, 2014; Accepted May 27, 2014

DOI: 10.3892/ijo.2014.2518

Abstract. A recently established cellular model for the rare small cell carcinoma of the ovary hypercalcemic type (SCCOHT-1) was characterized in comparison to ovarian adenocarcinoma cells (NIH:OVCAR-3 and SK-OV-3). The different cancer populations exhibited a common sensitivity in acidic pH milieu and a continuous proliferation in alkaline medium of pH 8.0-9.0. In the presence of elevated Ca^{2+} concentrations, the ovarian cancer cells demonstrated a progressively reduced proliferation within 72 h in contrast to other tumor types such as breast cancer cells. This significant growth inhibition was calcium-specific since the proliferation was unaffected after culture of the ovarian cancer cells in the presence of similar concentrations of other cations. The Ca^{2+} effects on the ovarian cancer cells were associated with marked differences in the activation of intracellular signaling pathways including enhanced phosphorylation of the p42/44 MAP kinase (Thr202/Tyr204). Further analysis of the signaling pathway revealed a significantly enhanced Ca^{2+}-dependent and p42/44 MAP kinase activation-mediated prostaglandin E2 (PGE2) production in SK-OV-3 and SCCOHT-1 and to a lesser extent in NIH:OVCAR-3 cells. Vice versa, exogenous PGE2 did not affect the proliferative capacity of the ovarian cancer cells and inhibition of the Ca^{2+}-mediated MAP kinase activation did not abolish the Ca^{2+}-mediated cytotoxicity. Collectively, these data suggest that multiple pathways are activated by exogenous Ca^{2+} in the different ovarian cancer cells, including a specific MAP kinase signaling cascade with subsequent PGE2 production and a parallel pathway for the induction of cell death.

Correspondence to: Professor Ralf Hass, Biochemistry and Tumor Biology Laboratory, Gynecology Research Unit, Department of Gynecology and Obstetrics, Hannover Medical University, Carl-Neuberg-Str. 1, D-30625 Hannover, Germany
E-mail: hass.ralf@mh-hannover.de

Key words: small cell carcinoma of the ovary hypercalcemic type, ovarian cancer, tumor growth, Ca^{2+}-signaling, cell cycle, prostaglandin E2 production

Introduction

Ovarian cancer still represents one of the most lethal gynecologic malignancies. Within this type of gynecological cancer the small cell ovarian carcinoma of the hypercalcemic type (SCCOHT) is defined as a rare form of an aggressive ovarian tumor predominantly affecting young women between ages of 13 to 35 which is mostly associated with paraendocrine hypercalcemia (1-3). Following the initial histopathological evaluation of several clinical cases, the SCCOHT has been classified as a separate pathological entity (2). Recent studies revealed a mutation in the *SMARCA4* gene as a potential marker for the SCCOHT (4-6).

The SCCOHT tumor disease is associated with poor prognosis and appears different and clearly distinguishable from other ovarian cancer types such as ovarian epithelial tumors and ovarian germ cell tumors (7). Initial immunohistochemical analysis of the SCCOHT postulated a germ cell-derived tumor (8). Another study reported SCCOHT as an epithelial-like originating tumor (3). In fact, some cells stained positive for epithelial cell markers, however, the intermediate filament protein vimentin predominantly associated with cells of a mesenchymal phenotype has been identified in the majority of cells in the SCCOHT (9). Further investigations using additional genetic analysis of SCCOHT tumor specimen suggested a heterogeneous tumor entity but did not confirm a germ cell-derived or an epithelial cell-derived tumor origin (9-11). The heterogeneity of these data may be explained in part by the rare and limited tumor material from patients. Considering these controversial reports, the histogenesis of SCCOHT and the mechanism of the development and physiological role of an accompanying hypercalcemia still remain unclear. Likewise, reasonable approaches for a sufficient (chemo)therapeutic management to treat SCCOHT patients are completely unknown. Although a multi-modality platform is suggested including surgery followed by chemotherapy and radiotherapy (12,13), only very few patients survived longer than the following two years (14-17).

Recently, we developed a cellular model for the SCCOHT and the resulting SCCOHT-1 tumor cells were derived from a primary culture of biopsy material from a 31-year-old patient with recurrent SCCOHT. *In vivo* studies with these primary cells substantiated a SCCOHT phenotype with histopathological similarities between the mouse xenograft-developed

tumors and the original patient tumor. Moreover, development of SCCOHT-1-induced tumor xenografts displayed an accompanying hypercalcemia in NOD/scid mice with serum calcium levels above 3.5 mmol/l (1).

Using this unique cellular model, we examined in the present study the effects of exogenous calcium representing a hypercalcemia on SCCOHT-1 in comparison to established human ovarian adenocarcinoma cell lines including NIH:OVCAR-3 and SK-OV-3 cells. Moreover, different calcium-mediated signaling pathways were analysed in these ovarian cancer cells, which may be supportive in search of an appropriate therapeutic approach, particularly in SCCOHT.

Materials and methods

Cell culture

Primary human SCCOHT-1 cells. SCCOHT-1 cells were derived as a spontaneous, permanently growing primary culture from a tumor biopsy after surgery of a 31-year-old patient with recurrent SCCOHT (1). Informed written consent was obtained from the patient for the use of this material and the study was approved by the Ethics Committee of Hannover Medical School, Project #3916, June 15, 2005. The SCCOHT-1 cells were cultured in RPMI-1640 supplemented with 1 or 10% (v/v) fetal calf serum, 100 U/ml L-glutamine, 100 U/ml penicillin and 100 μg/ml streptomycin. The tissue culture was performed at 37˚C in a humidified atmosphere of 5% (v/v) CO_2 and the medium was changed at intervals of 3 to 4 days. For subculture, the cells were centrifuged (320 g/6 min) and resuspended in growth medium and the proliferative capacity at various conditions and the population doublings in parallel to the cell viability during culture was determined in a hemocytometer using the trypan blue exclusion test. In an alternative fluorescence-based proliferation assay the SCCOHT-1 cells have been transduced with a 3rd generation lentiviral SIN vector containing the eGFP gene (SCCOHT-1^{GFP}) as previously described for these cells (1).

Human ovarian adenocarcinoma cell lines. Human NIH:OVCAR-3 ovarian cancer cells (ATCC® #HTB-161™) were commercially obtained in passage 76 (P76) from the Institute for Applied Cell Culture (IAZ), Munich, Germany. The SK-OV-3 ovarian cancer cells (ATCC® #HTB-77™) were commercially obtained in P25 from the ATCC, Manassas, VA, USA. These ovarian adenocarcinoma cell lines were originally established from the malignant ascites of a patient with progressive adenocarcinoma of the ovary, respectively. The cells were cultivated at about 1,750 cells/cm^2 in RPMI-1640 supplemented with 1 or 10% (v/v) fetal calf serum, 100 U/ml L-glutamine, 100 U/ml penicillin and 100 μg/ml streptomycin. Subculture was performed by trypsin/EDTA (Biochrom GmbH, Berlin, Germany) treatment for 5 min at 37˚C. For the experiments NIH:OVCAR-3 cells were used in P86 to P118 and SK-OV-3 cells were used in P37 to P39. For fluorescence measurement in an appropriate proliferation assay the NIH:OVCAR-3 as well as the SK-OV-3 cells were also transduced with a eGFP gene vector (NIH:OVCAR-3^{GFP} and SK-OV-3^{GFP}) similar to SCCOHT-1^{GFP} cells.

Human breast cancer cell line. Human MDA-MB-231 breast cancer cells (MDA) were obtained from the ATCC (#HTB-26). This cell line was analyzed in a short tandem repeat (STR)-based authentication by the Institute for Legal Medicine at the University Hospital Schleswig-Holstein as recently documented (18). MDA cells were cultivated at about 1,500 cells/cm^2 in Leibovitz's L-15-medium (Invitrogen) with 10% (v/v) FCS, 2 mM L-glutamin and 1 mM penicillin/streptomycin. For fluorescence measurement MDA-MB-231^{GFP} cells were also generated after transduction with the eGFP gene vector.

Cell line authentication. Authentication of SCCOHT-1, NIH:OVCAR-3, SK-OV-3, and MDA-MB-231 cells was performed by short tandem repeat (STR) fragment analysis using the GenomeLab human STR primer set (Beckman Coulter Inc., Fullerton, CA, USA). Following DNA isolation of the cell lines and amplification by polymerase chain reaction (PCR) with the STR primer set, the appropriate PCR products were sequenced in the CEQ8000 Genetic Analysis System (Beckman Coulter) using the GenomeLab DNA size standard kit-600 (Beckman Coulter). Comparison of the sequencing results from SCCOHT-1 were similar to the original SCCOHT patient cells cultured in our lab. Moreover, the NIH:OVCAR-3, SK-OV-3 and MDA-MB-231 cell lines demonstrated a similar STR pattern according to the STR database provided by the Deutsche Sammlung von Mikroorganismen und Zellkulturen (DSMZ, Braunschweig, Germany) for these cell lines.

Proliferation and cell cycle analysis

For fluorescence measurement the different eGFP-transduced ovarian cancer populations were cultured in flat bottom 96-well plates (Nunc/ThermoFischer, Roskilde, Denmark) and incubated with 1.6, 3.2 and 6.4 mM Ca^{2+}, respectively, for 24 to 72 h. At different time points, the medium was removed and the cells were lysed with 5% (w/v) sodium dodecylsulfate (SDS). Thereafter, the fluorescence intensities of GFP in the cell homogenate which corresponded to the appropriate cell number of ovarian cancer cells, were measured at excitation 485 nm/emission 520 nm using the Fluoroscan Ascent Fl (Thermo Fisher Scientific) fluorescence plate reader.

To substantiate these results in an alternative assay, wild-type ovarian cancer populations were incubated similarly with 1.6, 3.2 and 6.4 mM Ca^{2+}, respectively, for 24 to 72 h and the cells were counted at the appropriate time points in a hemocytometer following trypan blue staining.

The cell cycle analysis was performed as described previously (19) using untreated compared to 1.6 mM Ca^{2+}- and 6.4 mM Ca^{2+}-stimulated SCCOHT-1^{GFP}, NIH:OVCAR-3^{GFP} and SK-OV-3^{GFP} ovarian cancer cells after 48 h. Briefly, $5x10^5$ cells were fixed in 70% (v/v) ice-cold ethanol at 4˚C for 24 h. Thereafter, the fixed cells were stained with CyStain DNA 2 step kit (Partec GmbH, Münster, Germany) and filtered through a 50 μm filter. The samples were then analyzed in a Galaxy flow cytometer (Partec) using the MultiCycle cell cycle software (Phoenix Flow Systems Inc., San Diego, CA, USA).

Immunoblot analysis

Following culture of SCCOHT-1^{GFP} cells in culture medium with 1% FCS, untreated control cells and Ca^{2+}-stimulated cells were washed three times in ice-cold PBS and lysed in a reswelling buffer containing 8 M urea (Carl Roth GmbH Co KG, Karlsruhe, Germany), 1% CHAPS (3-[(3-cholamidopropyl) dimethylammonio]-1-propanesulfonate) (Carl Roth GmbH

Co KG), 0.5% (v/v) pharmalyte 3-10 (GE Healthcare Europe GmbH, Freiburg, Germany), 0.002% (w/v) bromophenol blue (Serva Electrophoresis GmbH, Heidelberg, Germany) and freshly prepared 0.4% (w/v) dithiothreitol (DTT) (Carl Roth GmbH Co KG). Protein concentration was adjusted using the colorimetric BCA-assay (Perbio Science Deutschland, Bonn, Germany), subjected to SDS-polyacrylamide gel electrophoresis and transferred to a Hybond C Extra Nitrocellulose membrane (GE Healthcare Life Science). The membranes were blocked with PBS containing 5% FCS and 0.05% Tween-20 (PBS/Tween). After washing four times with PBS/Tween, the membranes were incubated with the primary antibodies (polyclonal anti-phospho-p44/42 MAPK$^{Thr202/Tyr204}$ (Cell Signaling Technology Inc.); polyclonal anti-Stim-1 (clone D88E10; Cell Signaling Technology Inc.); polyclonal anti-IP3 receptor (clone D53A5; Cell Signaling Technology Inc.); monoclonal anti-GAPDH (clone 6C5, Santa Cruz Biotechnology, Santa Cruz, CA, USA) at 4˚C overnight. Thereafter, the membranes were washed four times with PBS/Tween and incubated with the appropriate horseradish peroxidase-conjugated secondary antibody (all from Santa Cruz Biotechnology) for 1 h/25˚C. The membranes were washed with PBS/Tween and visualized by autoradiography using the ECL-detection kit (GE Healthcare Europe GmbH).

Prostaglandin E2 (PGE2) ELISA

SCCOHT-1^{WT}, SK-OV-3^{WT} and NIH:OVCAR-3^{WT} cells were seeded in 24-well plates at 10^6 cells/well (Nunc/ThermoFischer, Roskilde, Denmark) with 500 μl culture medium per well. In comparison to untreated control cells, the populations were stimulated with 1.6, 3.2 and 6.4 mM Ca^{2+}, respectively, in the absence or presence of a 1-h pre-incubation with 50 μM of the MAP kinase inhibitor PD98059 (Cell Signaling Technology Inc.). The conditioned medium was collected after 12 and 24 h, respectively, and centrifuged at 1,000 rpm/10 min. Thereafter, 50 μl aliquots of the supernatant were applied to the appropriate PGE2 measurements which were performed in an ELISA system according to the manufacturer's recommendation (R&D Systems Ltd., Abingdon, UK).

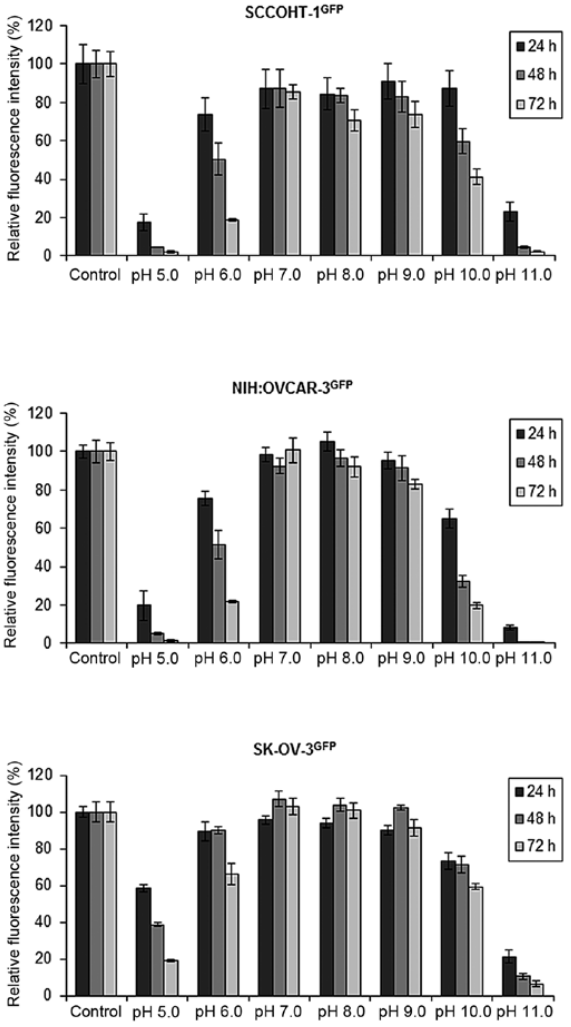

Figure 1. The proliferation of different ovarian cancer cell types (SCCOHT-1^{GFP}, NIH:OVCAR-3^{GFP} and SK-OV-3^{GFP} cells) was evaluated in a fluorescence-based assay under various pH conditions in the range of pH 5.0 to pH 11.0 as compared to control cells cultured at pH 7.4 for 24 to 72 h. Every 24 h, the medium was exchanged with newly established pH following appropriate adjustments by HCl or NaOH, respectively. Data represent the mean ± SD (n=5).

Results

Proliferation. All three ovarian cancer cell types exhibited sensitivity for an acidic culture milieu and continued maximal proliferation in alkaline medium of approximately pH 9.0 (Fig. 2). The proliferative capacity of SCCOHT-1 and NIH:OVCAR-3 cells was progressively inhibited by about 80% at pH 6.0 within 72 h (n=5) whereas SK-OV-3 cells demonstrated more stability with a growth reduction of about 30% (n=6). At pH 10.0 the proliferation progressively declined by 59±4% (n=5) in SCCOHT-1 cells after 72 h. A higher sensitivity with 80±2% (n=5) was observed in NIH:OVCAR-3 cells at pH 10.0 after 72 h and SK-OV-3 cells revealed 41±6% (n=5) growth inhibition at similar conditions (Fig. 1).

According to the hypercalcemia associated with SCCOHT, exogenous stimulation with calcium was tested and revealed a significant growth inhibition in all three ovarian carcinoma cell types in a concentration- and time-dependent manner. Whereas the culture medium constitutively contained about 0.8 mM Ca^{2+} and Mg^{2+} during steady-state culture conditions, the proliferative capacity of SK-OV-3 cells after exogenous addition of 1.6 mM Ca^{2+} up to 6.4 mM Ca^{2+} was progressively reduced to 17.8±6.2% (n=10) within 72 h. These growth-inhibitory effects of 6.4 mM Ca^{2+} were even more pronounced in SCCOHT-1 with growth reduction down to 11.4±5.0% (n=9) and were maximal in NIH:OVCAR-3 cells reaching only 3.8±0.5% (n=10) of proliferative capacity after 72 h as compared to control cells in normal culture medium (Fig. 2A). In contrast to these significant growth-inhibitory effects of Ca^{2+}, incubation of the three ovarian carcinoma cell populations with 6.4 mM Mg^{2+} demonstrated little if any effect on the cell growth and remained at a normal growth rate of approximately 100% within 72 h (Fig. 2A). Moreover, culture of the breast cancer cell line MDA-MB-231 in the

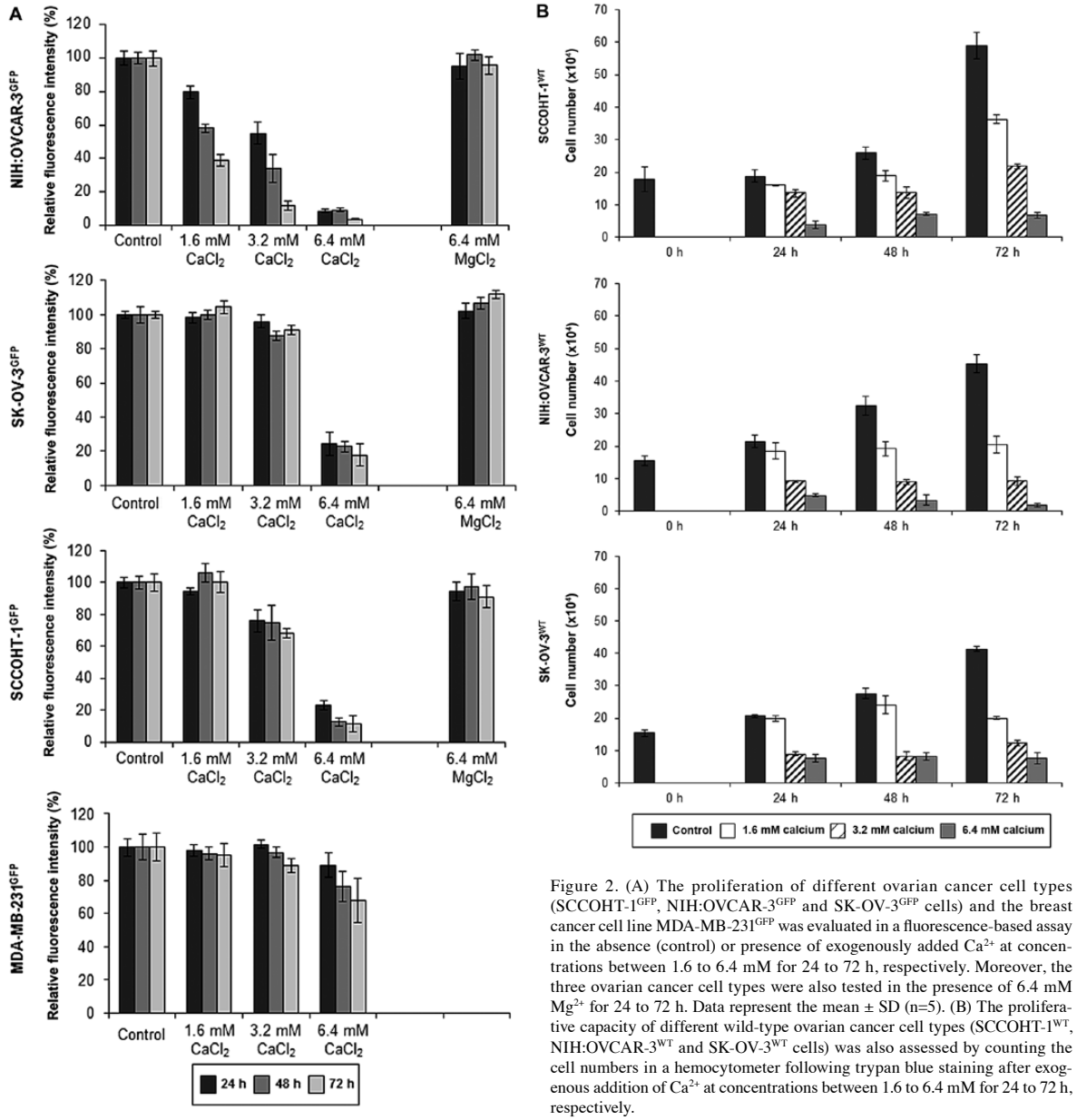

Figure 2. (A) The proliferation of different ovarian cancer cell types (SCCOHT-1^{GFP}, NIH:OVCAR-3^{GFP} and SK-OV-3^{GFP} cells) and the breast cancer cell line MDA-MB-231^{GFP} was evaluated in a fluorescence-based assay in the absence (control) or presence of exogenously added Ca^{2+} at concentrations between 1.6 to 6.4 mM for 24 to 72 h, respectively. Moreover, the three ovarian cancer cell types were also tested in the presence of 6.4 mM Mg^{2+} for 24 to 72 h. Data represent the mean ± SD (n=5). (B) The proliferative capacity of different wild-type ovarian cancer cell types (SCCOHT-1^{WT}, NIH:OVCAR-3^{WT} and SK-OV-3^{WT} cells) was also assessed by counting the cell numbers in a hemocytometer following trypan blue staining after exogenous addition of Ca^{2+} at concentrations between 1.6 to 6.4 mM for 24 to 72 h, respectively.

presence of 6.4 mM Ca^{2+} was associated with a growth rate of 68.1±13.2% (n=6) compared to a control culture after 72 h (Fig. 2A). Similar results of a marked Ca^{2+}-mediated concentration- and time-dependent growth inhibition were also obtained with the appropriate wild-type ovarian cancer cell populations by cell counting in a trypan blue exclusion assay (Fig. 2B). The results from the proliferation assays were also accompanied by appropriate morphological changes. Whereas the different ovarian cancer cell types demonstrated their typical morphology in phase contrast microscopy of the control cultures together with a GFP expression of the lentiviral eGPF-transduced cultures, a significant cell death with rounded and granulated cell bodies was observed in NIH:OVCAR-3^{GFP} cells following exposure to 6.4 mM Ca^{2+} for 72 h (Fig. 3, upper panel). Moreover, little if any fluorescence was detectable anymore in NIH:OVCAR-3^{GFP} cells. Only few GFP-expressing viable cells remained in the SCCOHT-1^{GFP} culture after incubation with 6.4 mM Ca^{2+} for 72 h (Fig. 3, middle panel). SK-OV-3^{GFP} cells also exhibited a significant granulation after incubation with exogenous Ca^{2+} with some more GFP-positive viable cells which substantiated the results of the proliferation assay (Fig. 3, lower panel).

Cell cycle analysis revealed a significant arrest of SCCOHT-1^{GFP} cells in the G_2 phase after 48 h in the presence of 1.6 mM Ca^{2+}. An elevation to 6.4 mM Ca^{2+} was associated with increased cell death by an accumulation of SCCOHT-1^{GFP}

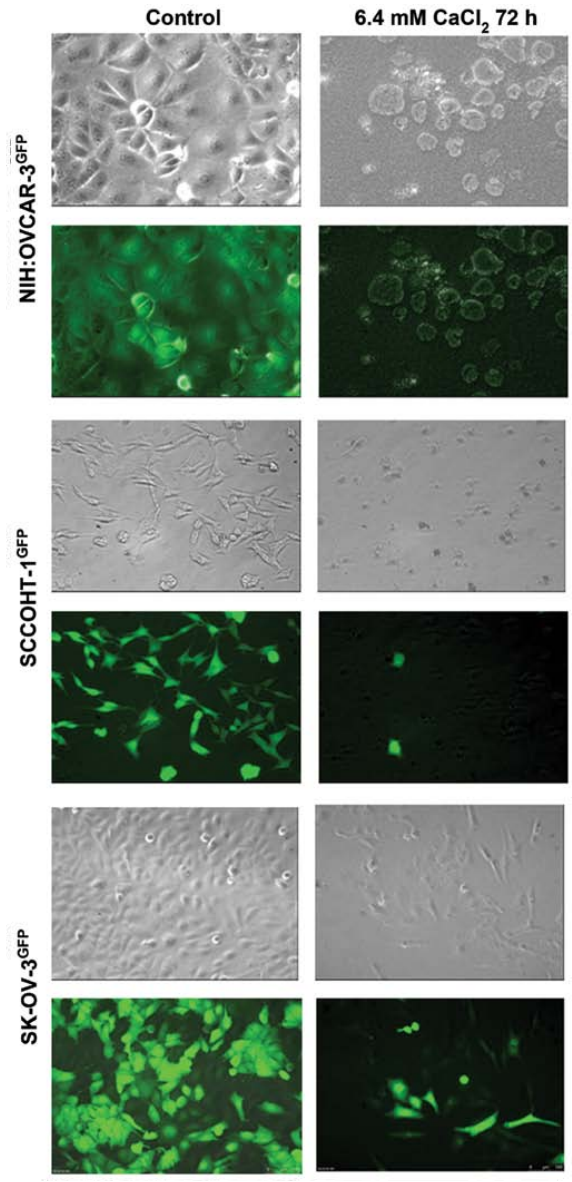

Figure 3. The morphology of NIH:OVCAR-3^{GFP} (upper panel), SCCOHT-1^{GFP} (middle panel) and SK-OV-3^{GFP} (lower panel) cells was documented by phase contrast (grey) and fluorescence microscopy (green) in untreated control cells and after incubation in the presence of 6.4 mM Ca^{2+} for 72 h.

cells in the subG$_1$ phase. Similar findings were observed in 6.4 mM Ca^{2+}-exposed NIH:OVCAR-3^{GFP} cells with significantly elevated levels of cells in the subG$_1$ phase after 48 h whereas the cell cycle of the lesser Ca^{2+}-sensitive SK-OV-3^{GFP} cells still remained unaltered (Fig. 4).

Together, these findings suggested an optimal growth of the different ovarian cancer cells in a neutral to alkaline pH range whereby enhanced exogenous Ca^{2+} significantly reduced the proliferative capacity and tumor cell viability. Western blot analysis was performed to further investigate specific signaling effects of Ca^{2+} in the different ovarian cancer cells. Exposure to 1.6 mM Ca^{2+} revealed a marked appearance of phosphorylated p42/44 MAP kinase (Thr202/Tyr204) within 2 h in SCCOHT-1 cells and this phosphorylation signal sustained for at least 24 h (Fig. 5A). A constitutive p42/44 MAP kinase phosphorylation in NIH:OVCAR-3 and SK-OV-3 cells was initially reduced by exogenous Ca^{2+} and significantly increased after 4 to 8 h before this signal was markedly reduced again within 24 h (Fig. 5B and C). Ca^{2+}-sensitizing proteins were also investigated, including stromal interaction molecule-1 (Stim-1) which determines differences in [Ca^{2+}] in the endoplasmic reticulum and can oscillate for stimulatory interactions with the ORAI1 calcium ion channels to the plasma membrane (20). The Stim-1 expression was enhanced between 1 and 2 h of 1.6 mM Ca^{2+} treatment of SCCOHT-1 cells (Fig. 5A), whereas little, if any, different Stim-1 protein levels were observed in NIH:OVCAR-3 and SK-OV-3 cells until a decrease was observed after 24 h (Fig. 5B and C). With respect to the IP3 receptor which releases Ca^{2+} from endoplasmic storage compartments upon phospholipase C-mediated PI-breakdown and inositol trisphosphate generation, there was only marginal if any change in the IP3 receptor protein levels following Ca^{2+} stimulation of the ovarian cancer cells. The unaltered GAPDH expression served as loading control (Fig. 5A).

Ca^{2+}-mediated phosphorylation of p42/44 MAP kinase (Thr202/Tyr204) was associated with enhanced PGE2 production in the ovarian cancer cells. Thus, stimulation of SK-OV-3 cells with increasing [Ca^{2+}] between 1.6 and 6.4 mM exhibited progressively increasing PGE2 release after 12 h, which was significantly further elevated after 24 h following Ca^{2+} stimulation (Fig. 6A). Moreover, pre-treatment with the p42/44 MAP kinase inhibitor PD98059 completely abolished even the highest levels of Ca^{2+}-mediated PGE2 production (Fig. 6A). Similar results were obtained in SCCOHT-1 cells with 40.4±24.1 pg/ml PGE2 after 1.6 mM Ca^{2+} and 232.5±37.9 pg/ml PGE2 after 6.4 mM Ca^{2+} stimulation for 12 h. Likewise, NIH:OVCAR-3 cells produced 41.2±0.1 pg/ml PGE2 after 1.6 mM Ca^{2+} and 48.4±0.1 pg/ml PGE2 after 6.4 mM Ca^{2+} incubation within 24 h whereas non-stimulated control cells displayed 12.1±0.1 pg/ml PGE2 and the PGE2 concentrations in the presence of the MAP kinase inhibitor PD98059 were below detection limit. To test any potential growth-inhibitory effects of PGE2 on the different ovarian cancer populations, SCCOHT-1, NIH:OVCAR-3 and SK-OV-3 cells were incubated with various PGE2 concentrations between 1 pg/ml to 10 ng/ml and revealed little if any effect on the proliferative capacity of the tumor cells (Fig. 6B). Together, these findings suggested that the Ca^{2+}-mediated p42/44 MAP kinase phosphorylation and subsequent stimulation of PGE2 production was independent of the Ca^{2+}-mediated growth inhibition. Indeed, this suggestion was substantiated by the MAP kinase inhibitor PD98059 which completely abolished the Ca^{2+}-mediated p42/44 MAP kinase phosphorylation in SCCOHT-1 cells (Fig. 7A). Moreover, MAP kinase inhibition did not demonstrate any effect on the increased G$_2$ arrest by 1.6 mM Ca^{2+} nor on the pronounced cell death of SCCOHT-1 cells in subG1 phase by 6.4 mM Ca^{2+} after 48 h similar to the results in Fig. 4 (Fig. 7B).

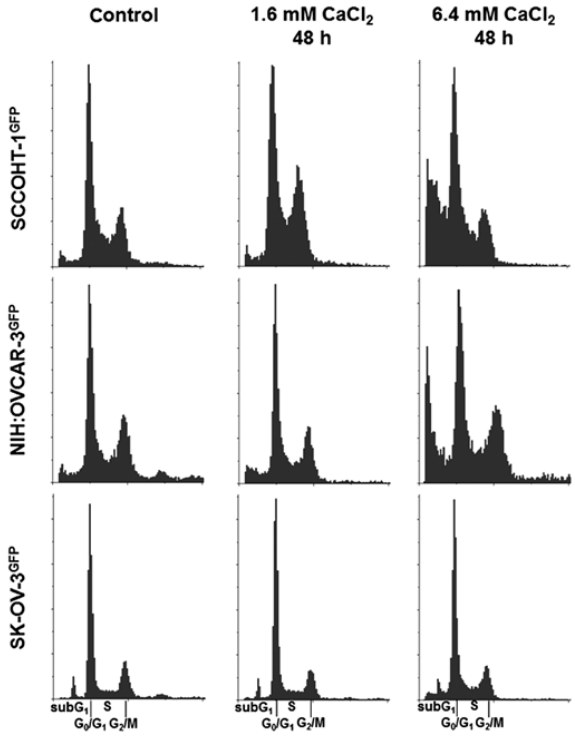

Figure 4. Cell cycle analysis was performed in SCCOHT-1^{GFP} (upper panel), NIH:OVCAR-3^{GFP} (middle panel) and SK-OV-3^{GFP} (lower panel) cells in the absence (control) or presence of exogenously added Ca^{2+} at concentrations of 1.6 and 6.4 mM for 48 h, respectively.

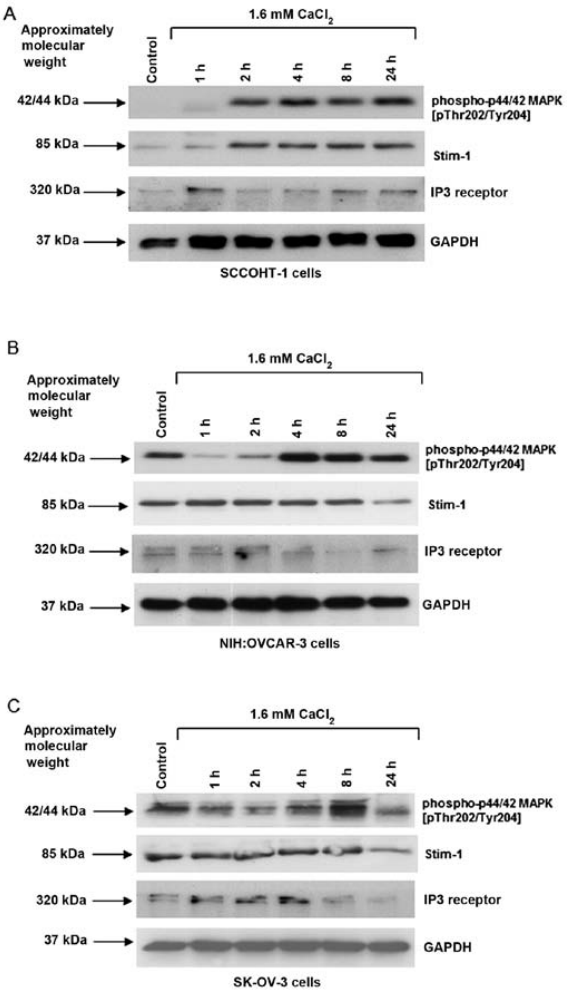

Figure 5. Western blot analysis was performed with proteins from (A) SCCOHT-1^{GFP}, (B) NIH:OVCAR-3^{GFP} and (C) SK-OV-3^{GFP} cells following incubation in the absence (control) or presence of 1.6 mM exogenously added Ca^{2+} for 1 h up to 24 h, respectively. The blots were incubated with the anti-phospho-p44/42 $MAPK^{Thr202/Tyr204}$, anti-Stim-1 and anti-IP3 receptor antibody, respectively. Protein levels of GAPDH served as a loading control.

Discussion

Ovarian cancer represents the predominant cause of gynecological cancer-related deaths affecting approximately 65,000 females in economically-developed countries in 2011 (21). As a rare form and special kind of ovarian cancer, the SCCOHT represents an aggressive tumor with poor prognosis and characteristics as compared to other ovarian carcinoma types remain unclear. The *in vitro* results in this study revealed common pH sensitivity in acidic milieu and continuous proliferation in neutral/low alkaline environment. Whereas young patients diagnosed with SCCOHT often present with a concomitant serum hypercalcemia, it was of interest to focus on calcium effects in ovarian cancer cells.

According to normal serum calcium levels of 2 to 2.5 mmol/l, hypercalcemia is considered as a mild type at concentrations between 2.5 to 3.0 mmol/l serum calcium and as a moderate type at concentrations between 3.0 to 3.5 mmol/l serum calcium. Patients with serum calcium levels above 3.5 mmol/l are diagnosed with a hypercalcemic crisis. Of interest, a recent study in a variety of ovarian cancer patients reports elevated blood calcium levels whereby $[Ca^{2+}]$ was proposed a potential predictive marker for ovarian cancer (22).

To test different levels of hypercalcemia *in vitro*, calcium concentrations of 1.6, 3.2 and 6.4 mmol/l were applied to the various ovarian cancer cells and revealed already significant growth-inhibitory effects between mild and moderate hypercalcemia. These growth-inhibitory effects were calcium-specific, since none of these results were obtained with similar concentrations of Mg^{2+} or further cations. Moreover, other tumor types such as breast cancer cells demonstrated much less responsiveness to high Ca^{2+} concentrations as compared to the different ovarian cancer cells. This calcium sensitivity of ovarian cancer cells suggested that elevated $[Ca^{2+}]$ is supportive for a therapeutic approach particularly in SCCOHT. Additional examination of these growth-inhibitory effects of high $[Ca^{2+}]$ *in vitro* demonstrated a morphological disintegration of the ovarian cancer cells. This was associated with increased cell death as revealed by cell cycle analysis. Interference with the calcium homeostasis can induce cell damage and eventually initiate cell death (23), whereby

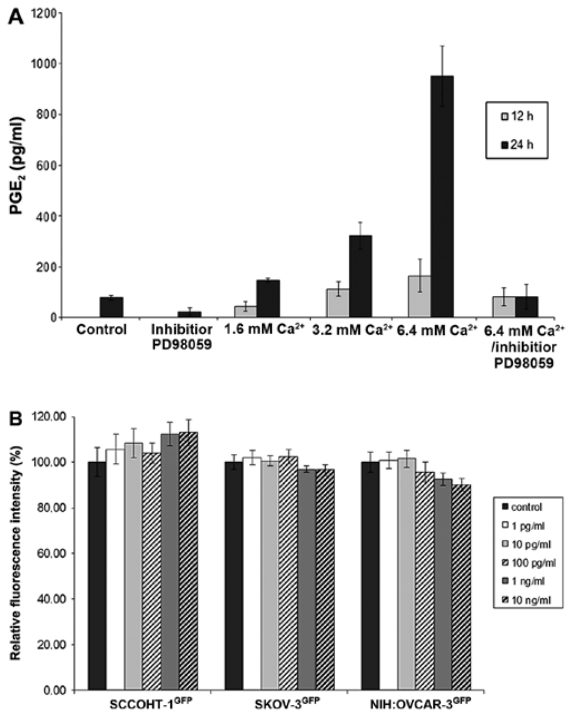

Figure 6. (A) The amount of released prostaglandin E2 (PGE2) was evaluated by ELISA in the supernatant of SK-OV-3^{WT} cells following stimulation in the absence (control) or exogenous addition of Ca^{2+} at concentrations between 1.6 to 6.4 mM for 12 and 24 h, respectively. Moreover, PGE2 levels were measured in the supernatant of control cells after incubation with 50 μM of the p44/42 MAPK inhibitor PD98059 for 24 h (inhibitor PD98059), and following stimulation of the cells with 6.4 mM Ca^{2+} in the presence of the MAPK inhibitor PD98059 for 12 and 24 h, respectively. Data represent the mean + SD (n=3). (B) The proliferation of different ovarian cancer cell types (SCCOHT-1^{GFP}, NIH:OVCAR-3^{GFP} and SK-OV-3^{GFP} cells) was evaluated in a fluorescence-based assay following stimulation of the different populations with various concentration of PGE2 between 1 pg/ml to 10 ng/ml for 72 h. Data represent the mean ± SD (n=5).

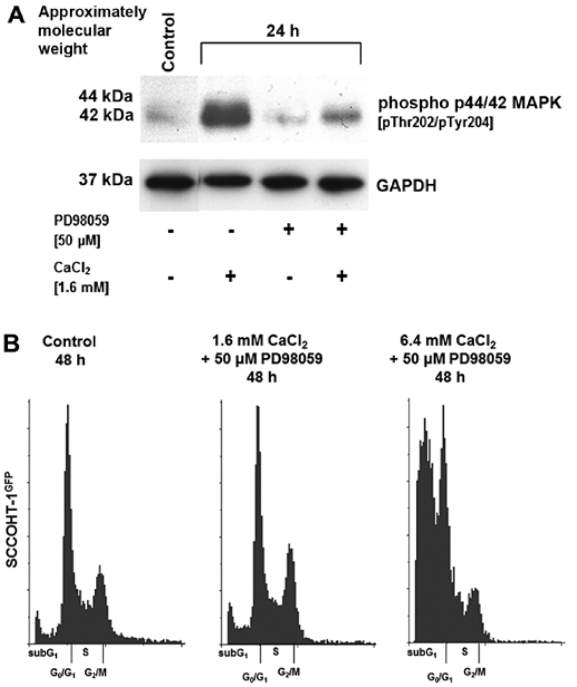

Figure 7. (A) Western blot analysis was performed for the anti-phospho-p44/42 MAPK$^{Thr202/Tyr204}$ protein levels in SCCOHT-1^{GFP} cells following incubation in the absence (control) or presence of 1.6 mM exogenously added Ca^{2+}, 50 μM of the p44/42 MAPK inhibitor PD98059 or both, 1.6 mM Ca^{2+} and 50 μM PD98059 for 24 h, respectively. Incubation of the blot with anti-GAPDH antibody served as a loading control. (B) Cell cycle analysis was performed in SCCOHT-1^{GFP} cells pre-incubated for 1 h with 50 μM of the p44/42 MAPK inhibitor PD98059 and further cultured in the absence (control) or presence of exogenously added Ca^{2+} at concentrations of 1.6 and 6.4 mM for 48 h, respectively.

recent studies proposed a process of programmed necrosis (necroptosis) upon cytosolic calcium accumulation in mouse xenografts of human neuroblastoma (24). These findings further substantiate our hypothesis that suitable chemotherapeutic compounds in combination with increased calcium levels contribute to an enhanced promotion of tumor cell death particularly in SCCOHT-1 cells. In this context, the hypercalcemia associated with SCCOHT may reflect a physiological anti-tumor response. However, due to a certain protection of the tumor cells within the tumor microenvironment and potential interactions with other cell types including immune cells and mesenchymal stem/stroma cells as documented for other tumor types such as breast cancer (18,25,26), the hypercalcemic effects achieve only a limited threshold and therefore, remain unresponsive and inefficient without further support to directly target the SCCOHT cancer cells.

At the molecular level, high [Ca^{2+}] was associated with increased activation/phosphorylation of the p42/p44 MAPK in the ovarian cancer cells. Activated p42/p44 MAPK can further relay phosphorylation signals to eventually stimulate phospholipase A2 (27). Upon cleavage of polyunsaturated fatty acids including arachidonic acid from the C2-position of membrane phospholipids by activated phospholipase A2, the elevated levels of arachidonic acid can be further metabolized via cyclooxygenase isoforms (COX-1, COX-2) into prostanoids and predominantly PGE2 (28,29). Indeed, the data obtained in the present study substantiated such a signaling pathway, whereby stimulation of the ovarian cancer cells with increasing calcium concentration resulted in appropriately increasing PGE2 production both, in a concentration- and time-dependent manner. Enhanced PGE2-synthesis accompanied by an increased expression of COX-1 and COX-2 has been documented in certain epithelial ovarian cancer (30) indicating potential metabolic alterations with the malignant transformation and progression. PGE2 can mediate suppressive effects via ligation to the E prostanoid receptors EP2 and EP4 followed by enhanced production of cyclic AMP. However, PGE2 binding to EP3 can also exert immune-stimulatory properties by decreasing cAMP levels. Therefore, PGE2-mediated immune-modulation by tumors can alter immune surveillance by re-educating the infiltrating inflammatory and immune cells to support tumorigenesis (31). Whereby no direct proliferative effects of PGE2 on the ovarian cancer cells were detectable, our work also demonstrated

that the calcium-mediated PGE2 production was p42/p44 MAPK-dependent since MAPK inhibition abolished the PGE2 production in the different ovarian cancer cells.

Together, increased calcium concentrations can specifically stimulate PGE2 production via p42/p44 MAPK activation and in parallel, contribute to the induction of cell death in ovarian cancer cells, whereby these calcium-mediated effects are relayed via different signaling pathways. Although the appearance of a serum hypercalcemia in SCCOHT patients and a variety of other ovarian cancer patient exhibit only a limited and insufficient threshold, the present findings indicate that elevated Ca^{2+} levels can enhance a physiological antitumor strategy for SCCOHT in support of a combined therapeutic approach against this rare but severe type of ovarian cancer.

Acknowledgements

This study was supported by a grant from the Niedersächsische Krebsgesellschaft e.V. to R.H.

References

1. Otte A, Gohring G, Steinemann D, *et al*: A tumor-derived population (SCCOHT-1) as cellular model for a small cell ovarian carcinoma of the hypercalcemic type. Int J Oncol 41: 765-775, 2012.
2. Dickersin GR, Kline IW and Scully RE: Small cell carcinoma of the ovary with hypercalcemia: a report of eleven cases. Cancer 49: 188-197, 1982.
3. Young RH, Oliva E and Scully RE: Small cell carcinoma of the hypercalcemic type in the ovary. Gynecol Oncol 57: 7-8, 1995.
4. Jelinic P, Mueller JJ, Olvera N, *et al*: Recurrent SMARCA4 mutations in small cell carcinoma of the ovary. Nat Genet 46: 424-426, 2014.
5. Witkowski L, Carrot-Zhang J, Albrecht S, *et al*: Germline and somatic SMARCA4 mutations characterize small cell carcinoma of the ovary, hypercalcemic type. Nat Genet 46: 438-443, 2014.
6. Ramos P, Karnezis AN, Craig DW, *et al*: Small cell carcinoma of the ovary, hypercalcemic type, displays frequent inactivating germline and somatic mutations in SMARCA4. Nat Genet 46: 427-429, 2014.
7. Scully RE: Atlas of Tumor Pathology: Tumors of the Ovary and Maldeveloped Gonads. Armed Forces Institute of Pathology, Washington, DC, 1979.
8. Ulbright TM, Roth LM, Stehman FB, Talerman A and Senekjian EK: Poorly differentiated (small cell) carcinoma of the ovary in young women: evidence supporting a germ cell origin. Hum Pathol 18: 175-184, 1987.
9. Aguirre P, Thor AD and Scully RE: Ovarian small cell carcinoma. Histogenetic considerations based on immunohistochemical and other findings. Am J Clin Pathol 92: 140-149, 1989.
10. Walt H, Hornung R, Fink D, *et al*: Hypercalcemic-type of small cell carcinoma of the ovary: characterization of a new tumor line. Anticancer Res 21: 3253-3259, 2001.
11. McCluggage WG, Oliva E, Connolly LE, McBride HA and Young RH: An immunohistochemical analysis of ovarian small cell carcinoma of hypercalcemic type. Int J Gynecol Pathol 23: 330-336, 2004.
12. Harrison ML, Hoskins P, du Bois A, *et al*: Small cell of the ovary, hypercalcemic type - analysis of combined experience and recommendation for management. A GCIG study. Gynecol Oncol 100: 233-238, 2006.
13. Shrimali RK, Correa PD and Reed NS: Dose-dense and dose-intense chemotherapy for small cell ovarian cancer: 2 cases and review of literature. Med Oncol 28: 766-770, 2011.
14. Benrubi GI, Pitel P and Lammert N: Small cell carcinoma of the ovary with hypercalcemia responsive to sequencing chemotherapy. South Med J 86: 247-248, 1993.
15. Reed WC: Small cell carcinoma of the ovary with hypercalcemia: report of a case of survival without recurrence 5 years after surgery and chemotherapy. Gynecol Oncol 56: 452-455, 1995.
16. Dykgraaf RH, de Jong D, van Veen M, Ewing-Graham PC, Helmerhorst TJ and van der Burg ME: Clinical management of ovarian small-cell carcinoma of the hypercalcemic type: a proposal for conservative surgery in an advanced stage of disease. Int J Gynecol Cancer 19: 348-353, 2009.
17. Barondeau J, Rodgers M, Braun L, Azarow K, Forouhar M and Faucette K: Small cell ovarian carcinoma: a rare, aggressive tumor masquerading as constipation in a teenager with a fatal outcome. J Pediatr Hematol Oncol 32: e139-e141, 2010.
18. Mandel K, Yang Y, Schambach A, Glage S, Otte A and Hass R: Mesenchymal stem cells directly interact with breast cancer cells and promote tumor cell growth in vitro and in vivo. Stem Cells Dev 22: 3114-3127, 2013.
19. Bertram C and Hass R: Cellular senescence of human mammary epithelial cells (HMEC) is associated with an altered MMP-7/HB-EGF signaling and increased formation of elastin-like structures. Mech Ageing Dev 130: 657-669, 2009.
20. Putney JW: Capacitative calcium entry: from concept to molecules. Immunol Rev 231: 10-22, 2009.
21. Jemal A, Bray F, Center MM, Ferlay J, Ward E and Forman D: Global cancer statistics. CA Cancer J Clin 61: 69-90, 2011.
22. Schwartz GG and Skinner HG: Prospective studies of total and ionized serum calcium in relation to incident and fatal ovarian cancer. Gynecol Oncol 129: 169-172, 2013.
23. Trump BF and Berezesky IK: Calcium-mediated cell injury and cell death. FASEB J 9: 219-228, 1995.
24. Nomura M, Ueno A, Saga K, Fukuzawa M and Kaneda Y: Accumulation of cytosolic calcium induces necroptotic cell death in human neuroblastoma. Cancer Res 74: 1056-1066, 2014.
25. Ungefroren H, Sebens S, Seidl D, Lehnert H and Hass R: Interaction of tumor cells with the microenvironment. Cell Commun Signal 9: 18, 2011.
26. Hass R and Otte A: Mesenchymal stem cells as all-round supporters in a normal and neoplastic microenvironment. Cell Commun Signal 10: 26, 2012.
27. Van Rossum GS, Klooster R, van den Bosch H, Verkleij AJ and Boonstra J: Phosphorylation of p42/44(MAPK) by various signal transduction pathways activates cytosolic phospholipase A(2) to variable degrees. J Biol Chem 276: 28976-28983, 2001.
28. Koehler L, Hass R, DeWitt DL, Resch K and Goppelt-Struebe M: Glucocorticoid-induced reduction of prostanoid synthesis in TPA-differentiated U937 cells is mainly due to a reduced cyclooxygenase activity. Biochem Pharmacol 40: 1307-1316, 1990.
29. Rehfeldt W, Hass R and Goppelt-Struebe M: Characterization of phospholipase A2 in monocytic cell lines. Functional and biochemical aspects of membrane association. Biochem J 276: 631-636, 1991.
30. Rask K, Zhu Y, Wang W, Hedin L and Sundfeldt K: Ovarian epithelial cancer: a role for PGE2-synthesis and signalling in malignant transformation and progression. Mol Cancer 5: 62, 2006.
31. Medeiros A, Peres-Buzalaf C, Fortino Verdan F and Serezani CH: Prostaglandin E2 and the suppression of phagocyte innate immune responses in different organs. Mediators Inflamm 2012: 327568, 2012.

2.2 *In vitro* and *in vivo* therapeutic approach for a small cell carcinoma of the ovary hypercalcaemic type using a SCCOHT-1 cellular model

Anna Otte, Finn Rauprich, Peter Hillemanns, Tjoung-Won Park-Simon, Juliane von der Ohe und Ralf Hass

publiziert in
Orphanet Journal of Rare Disease
9 : 126, 2014
doi: 10.1186/s13023-014-0126-4

Otte et al. Orphanet Journal of Rare Diseases 2014, 9:126
http://www.ojrd.com/content/9/1/126

ORPHANET JOURNAL OF RARE DISEASES

RESEARCH Open Access

In vitro and *in vivo* therapeutic approach for a small cell carcinoma of the ovary hypercalcaemic type using a SCCOHT-1 cellular model

Anna Otte, Finn Rauprich, Peter Hillemanns, Tjoung-Won Park-Simon, Juliane von der Ohe and Ralf Hass*

Abstract

Background: The small cell ovarian carcinoma of the hypercalcemic type (SCCOHT) which preferably affects young women during regenerative age represents a rare and aggressive form of ovarian tumors with poor prognosis and lacks an efficient therapy.

Methods and results: *In vitro* chemotherapy testing in a fluorescence assay using a recently developed cellular model from a recurrent SCCOHT revealed sensitivity for certain epothilones, methotrexate and topotecan whereas little if any cytotoxicity was observed with other chemotherapeutics including platin-based compounds. In particular, epothilone B demonstrated a high sensitivity in contrast to ixabepilone with only little detectable effects. Western blot and cell cycle analysis revealed that the epothilone B sensitivity was associated with increased Ser^{15} phosphorylation of p53, a significant G_1 and G_2 cell cycle accumulation and subsequent cell death in subG_1 phase. Moreover, tubulinβ3 expression in SMARCA4/BRG1-defective SCCOHT-1 in contrast to other ovarian cancer cells was also affected during chemotherapy treatment. Increased extracellular Ca^{2+} levels further enhanced the epothilone B cytotoxicity in SCCOHT-1 cells. These *in vitro* effects were also confirmed *in vivo* in NOD/scid mouse xenografts demonstrating an attenuated tumor growth in epothilone B / Ca^{2+}-treated mice. After 4d of subsequent treatment, the tumor sizes were reduced by about 90% as compared to continuously growing control tumors. In parallel, a hypercalcemia in control tumor-carrying mice was reverted to normal serum Ca^{2+} levels after epothilone B / Ca^{2+} therapy.

Conclusions: Taken together, these data demonstrated anti-tumorigenic effects of epothilone B / Ca^{2+} in SCCOHT providing a focused therapeutic approach against this rare disease and arising recurrent tumors.

Keywords: SCCOHT, Ovarian cancer, Tumor growth, Chemotherapy

Background

Ovarian cancer represents one of the most lethal gynecologic malignancy. A rare form of an aggressive ovarian tumor is displayed by the small cell ovarian carcinoma of the hypercalcemic type (SCCOHT). So far, no histogenetic origin of SCCOHT has been identified and accordingly, only little is known about tumor tissue characteristics of SCCOHT. Initial immunohistochemical analysis of the SCCOHT has postulated a germ cell-derived tumor [1] although electron microscopy evaluations of tumor specimen reported SCCOHT as an epithelial-like originating tumor [2]. Further analysis of SCCOHT tumor specimen suggested an inhomogeneous tumor entity which neither confirmed a germ cell-derived nor an epithelial cell-derived tumor origin [3-5]. The heterogeneity of these data may be explained in part by the limitations of biopsy material from patients. An appropriate cellular model for this tumor entity is represented by the BIN-67 cells [6]. Due to the unknown etiology, the SCCOHT which represents an aggressive form of ovarian tumors still remains with poor prognosis and no efficient therapy. Thus, the SCCOHT which is mostly accompanied by a paraendocrine hypercalcemia [2,7] preferably affects young women between ages of 13 to 35 with lethal outcome in a short period of time after diagnosis.

Potential therapeutic approaches to date are based predominantly on certain histological SCCOHT tissue examinations. The findings revealed that some areas of

* Correspondence: hass.ralf@mh-hannover.de
Biochemistry and Tumor Biology Laboratory, Department of Gynecology and Obstetrics Medical, University Hannover, Carl-Neuberg-Str. 1, D – 30625 Hannover, Germany

SCCOHT tumor stained positive for epithelial cell markers whereas the intermediate filament protein vimentin has been described in the majority of cells [3]. In addition, cell cycle analysis of several SCCOHT tumors by flow cytometry reported a broad distribution with 4.7% to 18% of S phase cells and 1.5% to 19.5% of G_2/M phase cells [8], however, the histogenesis and further cell biological properties of the SCCOHT still remained poorly understood. Recent studies of a variety of SCCOHT tissue samples revealed a mutation in the *SMARCA4* gene as a potential marker for the SCCOHT [9-11].

Moreover, interaction of the tumor cells with adjacent populations within the tumor microenvironment including endothelial cells and mesenchymal stem cells support tumor vascularization and growth, however, such interaction alters the functionality and induces differentiation processes of the stem cells which can contribute to protect the tumorigenic target cells [12,13]. Consequently, reasonable approaches for the treatment of SCCOHT patients or a sufficient (chemo)therapeutic management are difficult and remain unclear. A recently developed cellular model of SCCOHT-1 cells derived from a primary culture of biopsy material after surgery of a 31-year-old patient with recurrent SCCOHT confirmed a cell type with epithelial/mesenchymal properties by partially expressing epithelial cytokeratins as well as the mesenchymal-type intermediate filament vimentin. Expression of surface markers in SCCOHT-1 includes CD15, CD29, CD44 and CD90 [14]. Based upon this cellular model of SCCOHT-1 cells, we examined in the present study cytotoxic effects of a variety of anti-tumor compounds in comparison to established human ovarian adenocarcinoma cell lines including NIH:OVCAR-3 and SK-OV-3 with known resistance to cisplatin [15]. The obtained *in vitro* effects in SCCOHT-1 cells with a focus on microtubule-stabilizing chemotherapeutics including epothilone B were investigated at the protein level to identify certain molecular effects and mechanisms. Moreover, epothilone B in combination with calcium was applied in NOD/scid mouse tumor xenografts to verify the *in vitro* therapeutic effects also *in vivo*. Our findings provide a more detailed understanding of potential compounds to target ovarian cancer cells exhibiting resistance to a variety of chemotherapeutics.

Material and methods

Cell culture

Primary human SCCOHT-1 cells

SCCOHT-1 cells were derived as a spontaneously permanent growing primary culture from a tumor biopsy after surgery of a 31-year-old patient with recurrent SCCOHT [14]. Informed written consent was obtained from the patient for the use of this material and the study has been approved by the Ethics Committee of Hannover Medical School, Project #3916 on June 15th, 2005. The SCCOHT-1 cells were cultured in RPMI 1640 supplemented with 10% (v/v) fetal calf serum, 2mM L-glutamine, 100U/ml penicillin and 100 μg/ml streptomycin. The tissue culture was performed at 37°C in a humidified atmosphere of 5% (v/v) CO_2 and the medium was changed at intervals of 3 to 4 days. For subculture, the loosely attached cells were mechanically collected, centrifuged (320 g/6 min), and resuspended in growth medium at a cell viability of >95% as determined in a hemocytometer using the trypan blue exclusion test. The proliferation of SCCOHT-1 cells was measured in a fluorescence-based microtiter plate assay following transduction of SCCOHT-1 cells with a 3rd generation lentiviral SIN vector containing the eGFP gene as previously described for these cells [14].

The human SCCOHT cell line BIN-67 (kindly provided by Dr. Barbara Vanderhyden, University of Ottawa, Canada) was cultured with DMEM/F12 : DMEM medium (1:1) (Sigma Aldrich, St. Louis, MO) supplemented with 20% (v/v) fetal calf serum, 2mM L-glutamine, 100U/ml penicillin and 100 μg/ml streptomycin.

Human alveolar adenocarcinoma A549 cell line (kindly provided by Dr. Detlef Neumann, Hannover Medical School, Germany) were cultured with DMEM (Sigma) supplemented with 10% (v/v) fetal calf serum, 2mM L-glutamine, 100U/ml penicillin and 100 μg/ml streptomycin.

Human ovarian adenocarcinoma cell lines

Human NIH:OVCAR-3 ovarian cancer cells (ATCC® #HTB-161™) were commercially obtained in passage 76 (P76) from the Institute for Applied Cell Culture (IAZ), Munich, Germany. The SK-OV-3 ovarian cancer cells (ATCC® #HTB-77™) were commercially obtained in P25 from the ATCC, Manassas, VA, USA. These ovarian adenocarcinoma cell lines were originally established from the malignant ascites of a patient with progressive adenocarcinoma of the ovary, respectively. The cells were cultivated at about 1,750 cells/cm^2 in RPMI 1640 supplemented with 10% (v/v) fetal calf serum, 2mM L-glutamine, 100U/ml penicillin and 100 μg/ml streptomycin. Subculture was performed by trypsin/EDTA (Biochrom GmbH, Berlin, Germany) treatment for 5 min at 37°C. For the experiments NIH:OVCAR-3 cells were used in P86 to P118 and SK-OV-3 cells were used in P37 to P39. For fluorescence measurement in an appropriate proliferation assay the NIH:OVCAR-3 as well as the SK-OV-3 cells have also been transduced with a 3rd generation lentiviral SIN vector containing the eGFP gene similar to SCCOHT-1 cells.

Authentication of SCCOHT-1, NIH:OVCAR-3, and SK-OV-3 cells was performed by short tandem repeat (STR) fragment analysis using the GenomeLab human STR primer set (Beckman Coulter Inc., Fullerton, CA, USA). PCR products were sequenced in a CEQ8000

Genetic Analysis System (Beckman Coulter) using the GenomeLab DNA size standard kit-600 (Beckman Coulter). The results of SCCOHT-1 were similar to the original SCCOHT patient cells cultured in our lab and the NIH:OVCAR-3 and SK-OV-3 cell lines results were similar to the STR database provided by the Deutsche Sammlung von Mikroorganismen und Zellkulturen (DSMZ, Braunschweig, Germany).

Proliferation measurement by fluoroscan assay

The ovarian cancer cells were incubated with different concentrations for each of the chemotherapeutic compounds. The compounds and their concentrations used in the cell culture are:

carboplatin (320 μM; Carbomedac, Medac GmbH, Hamburg, Germany), cisplatin (320 μM; Bristol-Myers-Squibb), cyclophosphamide (1.28 mM; Cyclophostin, Pharmacia GmbH, Erlangen, Germany), cytarabine (320 μM; Ara C, Sigma Aldrich GmbH, München, Germany), 5'-fluorouracil (320 μM; Gry-Pharma GmbH, Kirchzarten, Germany), doxorubicin (1.28 μM; Sigma), methotrexate (320nM; Hexal AG, Holzkirchen, Germany), topotecan (320nM; Glaxo Smithkline GmbH&Co KG, Munich), taxol (160nM; Paclitaxel, Bristol-Myers-Squibb GmbH&Co KGaA, Munich), epothilone A (160nM; GBF Braunschweig, Germany), epothilone B (40nM; GBF Braunschweig, Germany), and ixabepilone (80 μM; Bristol-Myers-Squibb), respectively.

For fluorescence measurement the different eGFP-transduced ovarian cancer populations were seeded at 3,000 cells/well with standard culture medium (100 μL/well) in flat bottom 96-well plates (Nunc/ThermoFischer, Roskilde, Denmark) and incubated overnight to allow attachment. Thereafter, 100 μl of culture medium was added to the cells as control and in further wells 100 μl of culture medium with the maximal solvent concentration was added to the cells as solvent control, respectively. Moreover, 100 μl of the chemotherapeutic compounds were added to the cells and dosed in a 2-fold serial dilution. Each plate was applied with a cells-only control in culture medium and a maximal solvent concentration control, respectively (Table 1). The cell viability obtained with the appropriate chemotherapeutic compounds was then normalized to these controls on a plate by plate basis and a drug-dose–response analysis was performed for the different compounds in the 3 different ovarian cancer cell populations. Following incubation of the cells for 72 h, the medium was removed and the cells were lysed with 5% (w/v) SDS. Afterwards, the fluorescence intensities of GFP in the cell homogenate which corresponded to the appropriate cell number of ovarian cancer cells was measured at excitation 485 nm/emission 520 nm using the Fluoroscan Ascent Fl (Thermo Fisher Scientific). The resulting fluorescent signal was first normalized to the mean signal of the cells only wells to control for seeding variability and then to the mean signal of the solvent-only control.

Cell cycle analysis

The cell cycle analysis was performed as described previously [16]. Briefly, 9.3×10^3 cells/cm^2 were seeded in culture plates (diameter 10 cm; Greiner Bio-one GmbH, Frickenhausen, Germany) overnight to allow attachment of the cells and adjustment to the culture conditions. Following incubation with 1 μM cisplatin, or 1 μM carboplatin, or 2nM epothilone B for 48 h, the cells were fixed in 70% (v/v) ice-cold ethanol at 4°C for 24 h. Thereafter, about 5×10^5 fixed cells were stained with CyStain DNA 2 step kit (Partec GmbH, Münster, Germany) and filtered through a 50 μm filter. The samples were then analyzed in a Galaxy flow cytometer (Partec) using the MultiCycle cell cycle software (Phoenix Flow Systems Inc., San Diego, CA).

Immunoblot analysis

For immunoblot analysis, untreated and chemotherapeutic agents-stimulated SCCOHT-1^{GFP}, NIH:OVCAR-3^{GFP} and SK-OV-3^{GFP} cells were washed three times in ice-cold PBS and lysed in a reswelling buffer containing 8 M urea (Carl Roth GmbH Co KG, Karlsruhe, Germany), 1% CHAPS (3-[(3-Cholamidopropyl)dimethylammonio]-1-propanesulfonate) (Carl Roth GmbH Co KG), 0.5% (v/v) Pharmalyte 3 –10 (GE Healthcare Europe GmbH, Freiburg, Germany), 0.002% (w/v) bromophenol blue (SERVA Electrophoresis GmbH, Heidelberg, Germany) and freshly prepared 0.4% (w/v) DTT (Dithiothreitol) (Carl Roth GmbH Co KG). Protein concentration was adjusted using the colorimetric BCA-assay (ThermoScientic, Rockford, IL, USA), subjected to SDS-polyacrylamide gel electrophoresis and transferred to a hybond-C extra nitrocellulose membrane (GE Healthcare). The membranes were blocked with PBS containing 5% FCS and 0.05% Tween-20 (PBS/Tween). After washing four times with PBS/Tween, the membranes were incubated with the primary antibodies (monoclonal anti-BRG-1 (dilution 1:1,000; ab110641; Abcam plc, Cambridge, UK); polyclonal anti-p53$^{[pSer15]}$ (dilution 1:1,000; Cell Signaling Technology, Beverly, MA, USA); polyclonal anti-p53 (dilution 1:1,000; Cell Signaling Technology); monoclonal anti-HSP27$^{[pSer82]}$ (dilution 1:200; clone 5B9, Enzo GmbH, Lörrach, Germany); monoclonal anti-tubulinβ3 (dilution 1:500; clone TU-20, Novus Biologicals Ltd., Cambridge, UK); monoclonal anti-β-actin (dilution 1:5,000; clone AC-15; Sigma-Aldrich) and monoclonal anti-GAPDH (dilution 1:200; clone AC-15 (Santa Cruz Biotechnology, Santa Cruz, CA, USA)) overnight at 4°C. Thereafter, the membranes were washed four times with PBS/Tween and incubated with the appropriate horseradish peroxidase-conjugated anti-mouse IgG (dilution 1:5,000) or anti-rabbit

Table 1 Concentrations of chemotherapeutic compounds used in human ovarian cancer cells

Chemotherapeutic compound	Maximal solvent concentration [%]	Maximal chemotherapeutic compound concentration	IC50 [M]		
			SCCOHT-1	SK-OV-3	NIH:OVCAR-3
Cytarabine	1.6×10^{0} H_2O	160 μM	8.1×10^{-6}	1.0×10^{-6}	1.1×10^{-7}
Cisplatin	2.0×10^{-2} NaCl	160 μM	2.3×10^{-5}	3.3×10^{-6}	1.7×10^{-6}
Carboplatin	5.0×10^{-3} NaCl	160 μM	7.9×10^{-5}	8.8×10^{-6}	7.0×10^{-6}
Cyclophosphamide	7.5×10^{-3} NaCl	640 μM	1.0×10^{-5}	2.3×10^{-4}	1.0×10^{-4}
Methotrexate	3.0×10^{-5} NaCl/ 2.0×10^{-1} PBS	160 nM	4.7×10^{-9}	5.7×10^{-9}	5.9×10^{-9}
Topotecan	7.0×10^{-3} H_2O/ 2.0×10^{-1} PBS	160 nM	3.6×10^{-9}	1.8×10^{-8}	5.0×10^{-9}
Doxorubicin	3.0×10^{-2} H_2O/ 2.0×10^{-1} PBS	640 nM	2.0×10^{-8}	1.3×10^{-7}	2.9×10^{-8}
5'-fluorouracil	4.0×10^{-4} NaCl/ 2.0×10^{-1} PBS	160 μM	1.9×10^{-5}	3.5×10^{-6}	1.1×10^{-6}
Epothilone A	8.0×10^{-3} DMSO/ 2.0×10^{-1} PBS	80 nM	3.3×10^{-9}	2.9×10^{-9}	2.2×10^{-9}
Epothilone B	2.0×10^{-3} DMSO/ 2.0×10^{-1} PBS	20 nM	1.5×10^{-9}	2.9×10^{-10}	9.8×10^{-11}
Taxol	6.0×10^{-4} ethanlol/ 2.0×10^{-1} PBS	80 nM	2.2×10^{-9}	2.4×10^{-9}	1.4×10^{-9}
Ixabepilone	2.0×10^{-1} ethanol	40 μM	1.1×10^{-6}	1.6×10^{-6}	9.8×10^{-7}

The maximal chemotherapeutic compound concentration indicates the highest initial concentration on the cells in the well followed by 2-fold serial dilutions. The IC50 values of the appropriate chemotherapeutic compounds were calculated from the drug-dose–response curves after normalization to the mean signal of the cells-only control and then to the mean signal of the solvent-only control.

IgG (dilution 1:10,000) secondary antibody, respectively, (all from GE Healthcare, Freiburg, Germany) for 1 h/room temperature. The membranes were washed with PBS/Tween and visualized by autoradiography using the ECL-detection kit (GE Healthcare). Quantification of the blots was performed by densitometry scanning using the Image J program.

In vivo experiments

Animal research using NOD/scid mice was carried out by following internationally recognized guidelines on animal welfare and has been approved by the institutional licensing committee ref. #33.14-42502-04-12/0814 on June 22nd, 2012.

About 1 x 10^6 GFP-labeled SCCOHT-1 cells previously cultured in serum-free HybridoMed DIF 1000 medium to avoid non-specific serum effects were injected subcutaneously into 5 to 6 weeks old female NOD/scid mice, respectively. After about 18 days post injection, all mice with SCCOHT-1^{GFP} cells had developed subcutaneous tumors. A therapeutic approach of the tumors was first tested with a daily subcutaneous injection of only 200 μl epithilone B (10 μM Epo B) at the tumor site for 2 days. To test possible synergistic effects of calcium and epothilone B in a further set of experiments, tumor-carrying mice were divided into 3 treatment groups. The first group represented the control tumor group with 5 animals and was injected subcutaneously with 200 μl of 0.9% NaCl at the tumor site every day. The second group with 5 animals was injected subcutaneously with 200 μl Ca^{2+} (5 mM) in 0.9% NaCl at the tumor site every day. The third group of 5 animals with tumor-carrying mice was injected subcutaneously with 200 μl Ca^{2+} (5 mM) together with 10 μM Epo B in 0.9% NaCl at the tumor site every day. The tumor length (L) and width (W) in each animal was measured on a daily basis and the resulting tumor size was calculated as ½ L × W^2 where L is the longer of the 2 measurements according to the calculation of ellipsoid tumor forms [17]. The treatment was started at an initial tumor size of approximately 2 to 3 mm^3.

At the end of the experiments, the animals were sacrificed by CO_2 anesthesia and cervical dislocation. Following UV light examination for the detection of GFP positive tissue, the tumors were dissected whereby tumor weight and the corresponding animal weight were determined.

For calcium measurements cardial blood was taken from the tumor-carrying NOD/scid mice after therapy and serum was prepared and analyzed for Ca^{2+} concentration using the Calcium Gen.2 reagent kit (Roche Diagnostics, Mannheim, Germany). The Ca^{2+} test is based on a color reaction with the chromophor 5-nitro-5'-methyl-1,2-bis(o-aminophenoxy) ethane- N,N,N',N'-tetraacetic acid (NM-BAPTA) according to the manufacturer's instruction (Roche Diagnostics).

Results

To date, little if any successful chemotherapy is available for the poor prognosis SCCOHT and therefore, *in vitro* testing was performed using a recently developed cellular model of human SCCOHT-1 cells derived from a recurrent small cell ovarian carcinoma of the hypercalcemic type [14]. The proliferative capacity of SCCOHT-1 cells was tested in comparison to NIH:OVCAR-3 and SK-OV-3

ovarian carcinoma cells in a fluorescence-based assay of GFP-labeled cells following treatment with different chemotherapeutic compounds for 72 h (Figure 1A-C). DMSO as an initial solvent for certain compounds was diluted to less than 0.1% (v/v) in the final concentration whereby incubation of the cells with even 0.2% (v/v) DMSO displayed no detectable effects as compared to control cells without DMSO reaching a proliferation rate of 104.3% ± 9.2% (n = 6) after 72 h.

Incubation of the cells with cisplatin revealed an IC50 of 2.3×10^{-5} M in SCCOHT-1^{GFP} cells and 3.3×10^{-6} M and $1.7x10^{-6}$ M in SK-OV-3^{GFP} and NIH:OVCAR-3^{GFP} cells, respectively (Figure 1A). Likewise, little effects on the proliferation of these 3 ovarian cancer populations were observed after exposure to carboplatin for up to 72 h (Figure 1A, Table 1). Only a marginal growth inhibition of SCCOHT-1^{GFP}, SK-OV-3^{GFP} and NIH:OVCAR-3^{GFP} cells was also detectable following incubation of the cells with cytarabine and even less with cyclophosphamide (Figure 1A, Table 1). Similarly, 5'-fluoruracil displayed only little effects on the proliferation of the 3 ovarian cancer cell types (Figure 1B, Table 1). In contrast, exposure to doxorubicin, topotecan and methotrexate was associated with a significantly elevated inhibiton of the proliferative capacity in SCCOHT-1^{GFP}, SK-OV-3^{GFP} and NIH:OVCAR-3^{GFP} cells, respectively (Figure 1B, Table 1).

Mitotic inhibitors which stabilize the microtubules including taxol and epothilones exhibited different antiproliferative effects. Thus, taxol revealed a growth reduction of in SCCOHT-1^{GFP} with a IC50 of 2.2nM which was enhanced in NIH:OVCAR-3 cells displaying an IC50 of 1.4nM but less pronounced in SK-OV-3^{GFP} cells with an IC50 of 2.4nM (Figure 1C, Table 1). Whereas epothilone A demonstrated a slightly reduced sensitivity as compared to taxol, treatment of the 3 different ovarian cancer cell populations to epothilone B revealed the highest growth inhibition tested in this study displaying an IC50 of 1.5nM for SCCOHT-1^{GFP}, 0.3nM for SK-OV-3^{GFP}, and 0.098nM for NIH:OVCAR-3^{GFP} cells (Figure 1C, Table 1). In contrast, only a low responsiveness of the cells was observed to ixabepilone with IC50 value in the micromolar range (Figure 1C, Table 1).

Together, these findings demonstrated differences in the chemotherapeutic sensitivity of these 3 ovarian cancer populations. Moreover, topotecan, methotrexate, taxol and epothilone B appeared as the most potent chemotherapeutic

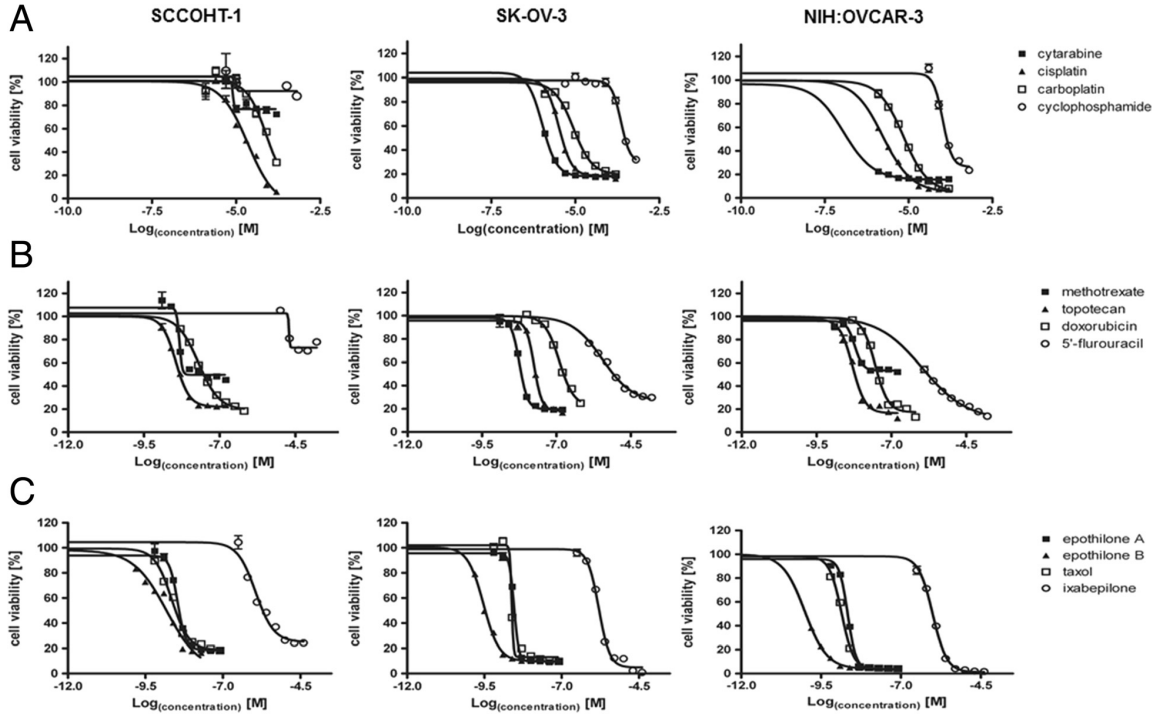

Figure 1 Sensitivity of human ovarian cancer cells for chemotherapeutic compounds (A-C). SCCOHT-1^{GFP} cells, NIH:OVCAR-3^{GFP} and SK-OV-3^{GFP} cells were incubated with different concentrations of chemotherapeutic compounds for 72 h, respectively, and the proliferative capacity was measured by the fluoroscan assay. Analysis of a drug-dose–response to define IC50 concentrations for all compounds was performed using GraphPad Prism-6. For calculation of the drug-dose–response curves, the data were normalized to the cells-only control in culture medium and to the maximal solvent concentration control of the corresponding compound, respectively.

compounds for SCCOHT-1^{GFP} cells *in vitro* with the highest potency for epothilone B.

Further analysis was performed to test the effects of epothilone B on the cell cycle progression of the ovarian cancer cells in comparison to cisplatin or carboplatin which are frequently used in a combination with etoposide or taxol, respectively, for treatment of the SCCOHT [18,19]. Flow cytometric cell cycle analysis of logarithmically-growing SCCOHT-1^{GFP} cells revealed a distribution of continuously proliferating cells with about 68% in G_0/G_1 phase, 9% in S phase and 23% in the mitotic G_2/M phase as evaluated by the MultiCycle cell cycle software (Figure 2A). A similar cell cycle distribution of continuously proliferating cells was observed following incubation of SCCOHT-1^{GFP} cells with either 1 μM cisplatin or 1 μM carboplatin for 48 h. In contrast, treatment of SCCOHT-1^{GFP} cells with a 500-fold reduced concentration of 2 nM epothilone B for 48 h was associated with G_0/G_1 cell cycle arrest and a significant accumulation of dead cells in the subG$_1$ phase (Figure 2A). Likewise, the platin-resistent ovarian cancer cell lines NIH:OVCAR-3 and SK-OV-3 demonstrated a paralleled cell cycle pattern following exposure to 1 μM cisplatin or 1 μM carboplatin or 2 nM epothilone B for 48 h whereby SK-OV-3 also displayed an accumulation in G_2/M upon epothilone B exposure (Figure 2A). The SCCOHT-derived cell line BIN-67 demonstrated platin-compound resistance although some subG1 accumulation was detectable following treatment with 1 μM carboplatine for 48 h. Moreover, incubation of BIN-67 cells to 2 nM epothilone B revealed an accumulation in G_2/M phase (Figure 2A). These findings substantiated the unresponsiveness of BIN-67 and SCCOHT-1 cells as well as NIH:OVCAR-3 and SK-OV-3 cells to platin-based compounds. Moreover, growth inhibitory effects of epothilone B associated with significant cellular damage and cell death were confirmed in the ovarian cancer lines except for BIN-67 cells with a markedly reduced sensitivity.

Differences between ovarian cancer cells and cells derived from SCCOHT have been previously reported by a mutation in the *SMARCA4* gene as a potential marker for the SCCOHT [9-11]. Western blot analysis of BRG-1 as the protein product of the *SMARCA4* gene revealed a pronounced expression in the NIH:OVCAR-3 and SK-OV-3 ovarian cancer cells, however, little if any BRG-1 protein was detectable in SCCOHT-1 cells (Figure 2B). Likewise, BRG-1 was absent in human alveolar adenocarcinoma A549 cells and in the BIN-67 cell line as previously reported [11] (Figure 2B), suggesting also a *SMARCA4* defect in SCCOHT-1 cells. Detection of β-actin expression was used as a loading control (Figure 2B).

Whereas cellular and DNA damage activate a cascade of repair mechanisms involving p53 and distinct phosphorylation processes of this tumor suppressor protein, the different responses of SCCOHT-1 cells observed with taxol and certain epothilones, particularly epothilone B and ixabepilone, were evaluated by Western blot analysis. Thus, only marginal differences were observed for the protein level of p53 expression in SCCOHT-1 cells following treatment with either taxol, epithilone A, epithilone B, or ixabepilone. However, there was a significantly enhanced detection of phosphorylated p53 at serine15 (p53$^{[pSer15]}$) particularly between 24 h to 48 h after epothilone B treatment (Figure 3). Likewise, an elevated phosphorylation of the heat shock protein HSP27 at serine 82 (HSP27$^{[pSer82]}$) could be detected within 24 h to 48 h of epothilone B exposure together with unchanged control expression of GAPDH (Figure 3). Quantification by densitometry scanning also revealed an elevated expression of p53$^{[pSer15]}$ in taxol-stimulated SCCOHT-1 cells, however, these levels remained significantly lower as compared to those observed after epithilone B treatment.

A comparison of distinct chemotherapeutic effects between SCCOHT-1 and NIH:OVCAR-3 cells revealed little if any change in p53 protein expression of the investigated compounds, whereby densitometric analysis revealed slightly induced p53 levels in the compound-treated NIH:OVCAR-3 as compared to SCCOHT-1 cells (Figure 4). A significant difference, however, was observed for the tubulinβ3 protein level which was constitutively expressed already in untreated SCCOHT-1 cells and decreased after methotrexate treatment in contrast to undetectable tubulinβ3 protein in NIH:OVCAR-3 cells (Figure 4). Conversely, HSP27$^{[pSer82]}$ was significantly higher and unaltered expressed in NIH:OVCAR-3 cells as in SCCOHT-1 cells whereby incubation with epothilone B for 24 h was associated with an increase of HSP27$^{[pSer82]}$ protein levels in SCCOHT-1 cells (Figure 4). SK-OV-3 cells are reported as p53 defective and a similar expression pattern as compared to NIH:OVCAR-3 cells was also observed for HSP27$^{[pSer82]}$ and undetectable tubulinβ3 (data not shown).

To further address the question whether these *in vitro* effects of epothilone B on SCCOHT-1 cells may also be effective *in vivo*, subcutaneous tumors were induced in NOD/scid mouse xenografts. Injection of 10^6 GFP-labeled SCCOHT-1 cells resulted in a detectable tumor development within 2–3 weeks. First, NOD/scid mouse tumors were dissected and re-cultured to investigate whether the cells obtained from the re-cultured tumors maintain a similar chemotherapeutic sensitivity observed during previous *in vitro* culture of SCCOHT-1^{GFP} cells. Indeed, incubation of the NOD/scid mouse tumors re-cultured cells demonstrated a significantly increased sensitivity for epothilone B after 48 h and 72 h, respectively, whereas the responsiveness to topotecan-treated cells remained unaltered (Figure 5A). Conversely, a higher

Otte *et al. Orphanet Journal of Rare Diseases* 2014, **9**:126
http://www.ojrd.com/content/9/1/126

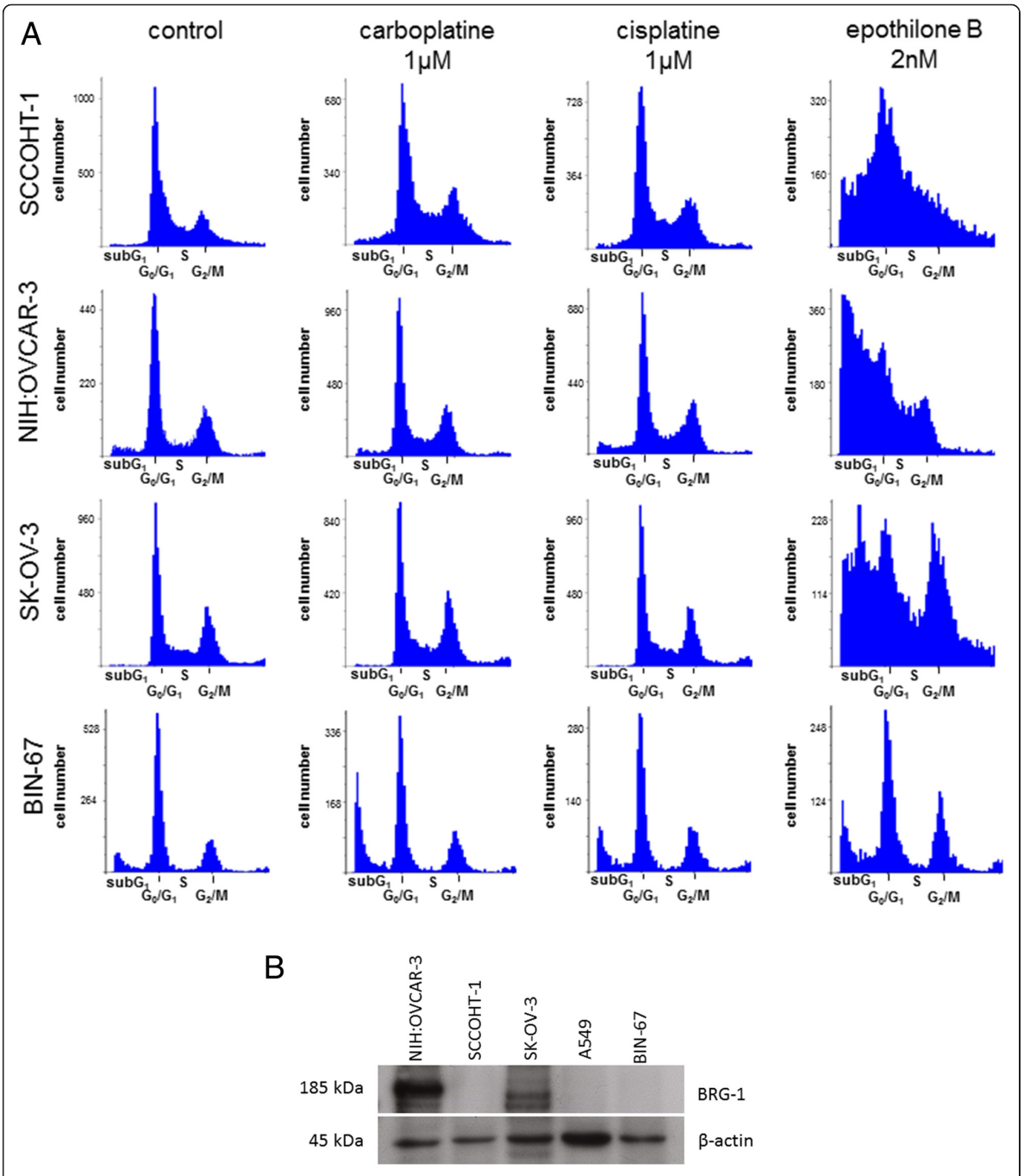

Figure 2 Cell cycle analysis of ovarian cancer cells after chemotherapeutic compound application (A) and SMARCA4/BRG-1 protein expression in human ovarian cancer cells (B). Cell cycle analysis **(A)** was performed by flow cytometry in SCCOHT-1^{GFP}, NIH:OVCAR-3^{GFP}, SK-OV-3^{GFP} and BIN-67 cells after treatment with 1 µM cisplatin, or 1 µM carboplatin, or 2 nM epothilone B for 48 h, respectively. Western blot analysis **(B)** of BRG-1 protein was performed in steady state of two ovarian carcinoma cell lines (NIH:OVCAR-3 and SK-OV-3) as compared to SCCOHT-derived cells (SCCOHT-1 and BIN-67). The absence of BRG-1 in human alveolar adenocarcinoma A549 cells was used as a control and expression of β-actin served as a loading control.

Otte et al. Orphanet Journal of Rare Diseases 2014, 9:126
http://www.ojrd.com/content/9/1/126

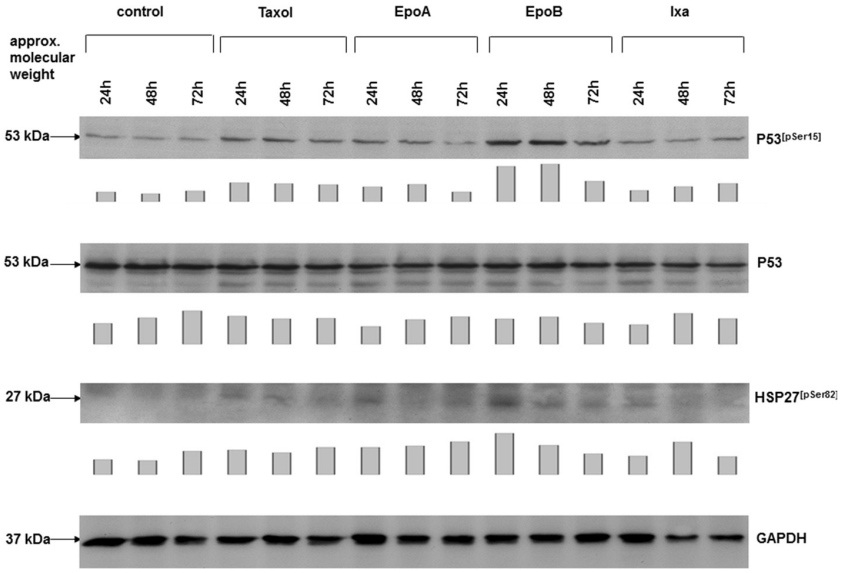

Figure 3 Western blot analysis was performed in SCCOHT-1 cells, treated with 4 nM of either taxol, epothilone A (EpoA), epothilone B (EpoB), or ixabepilone (Ixa) for 24 h, 48 h, and 72 h, respectively. Protein aliquots of the corresponding cell homogenates were analysed for the expression of p53, phosphorylated p53 at serine-15, and phosphorylated heat shock protein (HSP27) at serine-82. The unaltered expression of GAPDH served as a control for equal loading. Quantification of the blots by densitometry scanning was normalized against the appropriate GAPDH expression and the relative expression levels were documented as bar diagram below the corresponding Western blots.

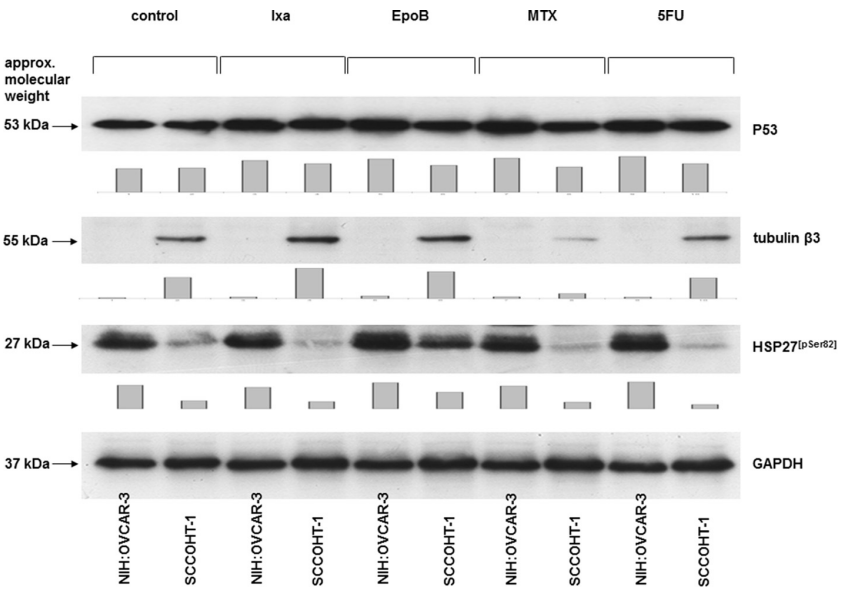

Figure 4 Comparison of protein expression in SCCOHT-1 and NIH:OVACAR-3 cells. Western blot analysis was performed in SCCOHT-1^{GFP} and NIH:OVCAR-3^{GFP}, to compare the protein expression levels of p53, tubulinβ3, and phosphorylated heat shock protein (HSP27) at serine-82 after a 24 h incubation of the 2 cell types with 2 nM of ixabepilone (Ixa), epothilone B (EpoB), methotrexate (MTX), and 5′-fluorouracil (5FU), respectively. The unaltered expression of GAPDH served as a control for equal loading, respectively. Quantification of the blots by densitometry scanning was normalized against the appropriate GAPDH expression and the relative expression levels were documented as bar diagram below the corresponding Western blots.

Otte et al. Orphanet Journal of Rare Diseases 2014, 9:126
http://www.ojrd.com/content/9/1/126

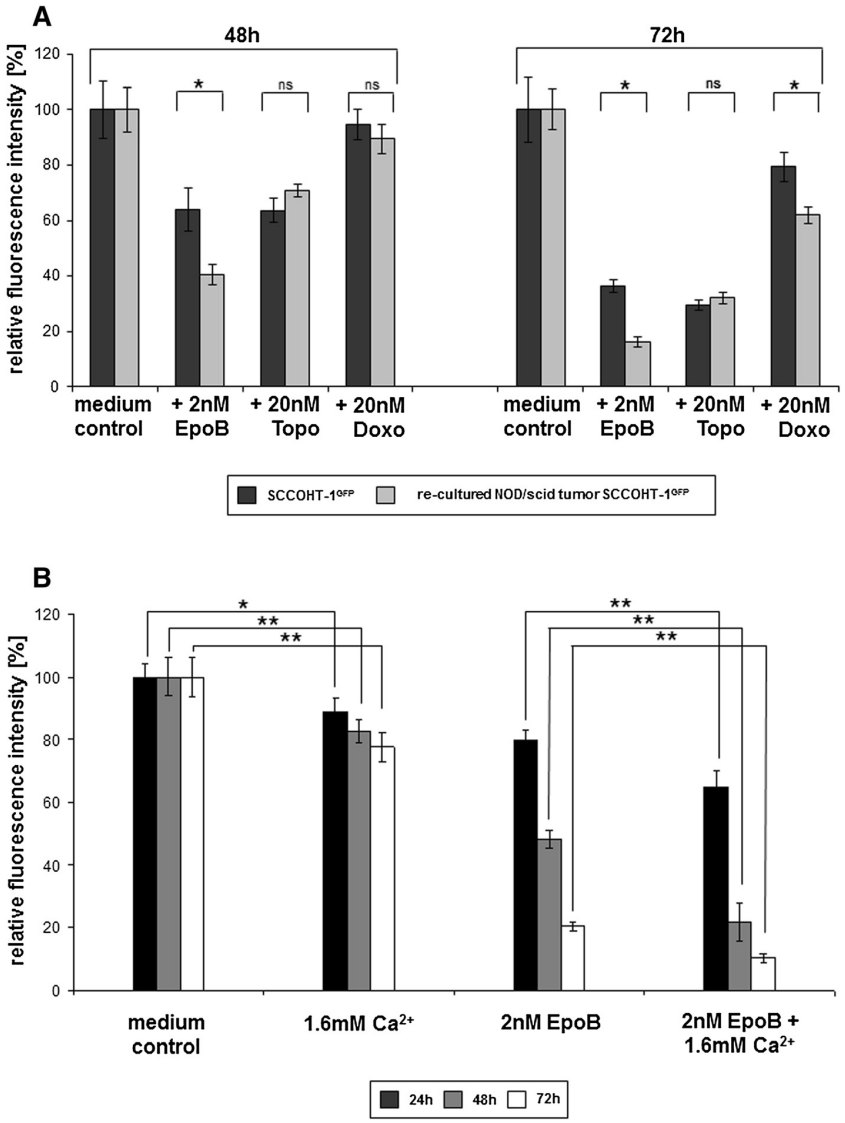

Figure 5 Chemotherapeutic sensitivity of re-cultured SCCOHT-1^{GFP} cells from xenograft tumors (A) and sensitivity of SCCOHT-1 cells to Ca^{2+} and Epo B (B). SCCOHT-1^{GFP} cells and re-cultured cells obtained from a SCCOHT-1^{GFP}-induced tumor in NOD/scid mice **(A)** were incubated with 2 nM epothilone B (EpoB), 20 nM topotecan (Topo), and 20 nM doxorubicin (Doxo) for 48 h and 72 h, respectively, and the proliferative capacity was measured by the fluoroscan assay. Fluorescence data of the non-treated control cells were calculated as 100% of relative fluorescence intensity. Data represent the mean ± s.d. (n = 10 for each control; n = 9 for each chemotherapeutic compounds). Statistical analysis between the SCCOHT-1^{GFP} cells and re-cultured NOD/scid tumor SCCOHT-1^{GFP} cells after treatment with the chemotherapeutics was calculated by 2-way ANOVA following Tukey's multiple comparison test (ns = not significant; *= significant ($p < 0.0001$)). SCCOHT-1^{GFP} cells were incubated with either 1.6 mM $CaCl_2$ (1.6 mM Ca^{2+}), 2 nM epothilone B (EpoB), or a combination of 2 nM EpoB + 1.6 mM Ca^{2+} in a fluoroscan assay for 24 h up to 72 h **(B)**, respectively. Fluorescence data of the non-treated control cells were calculated as 100% of relative fluorescence intensity. Data represent the mean ± s.d. (n = 10). Statistical analysis was conducted between SCCOHT-1^{GFP} cells in control medium and after exposure to 1.6 mM Ca^{2+} as well as between SCCOHT-1^{GFP} cells in the presence of 2 nM Epo B and SCCOHT-1^{GFP} cells after exposure to 2 nM EpoB + 1.6 mM Ca^{2+} by unpaired Student's t-test (*$P < 0.0001$; **$P < 0.00001$).

sensitivity was observed for doxorubicin which became significant after 72 h as statistically analyzed by 2-way ANOVA (Figure 5A). According to the hypercalcemia which accompanies this tumor disease, additional questions were addressed whether exogenous calcium affects SCCOHT-1 tumor cell growth *in vitro* together with

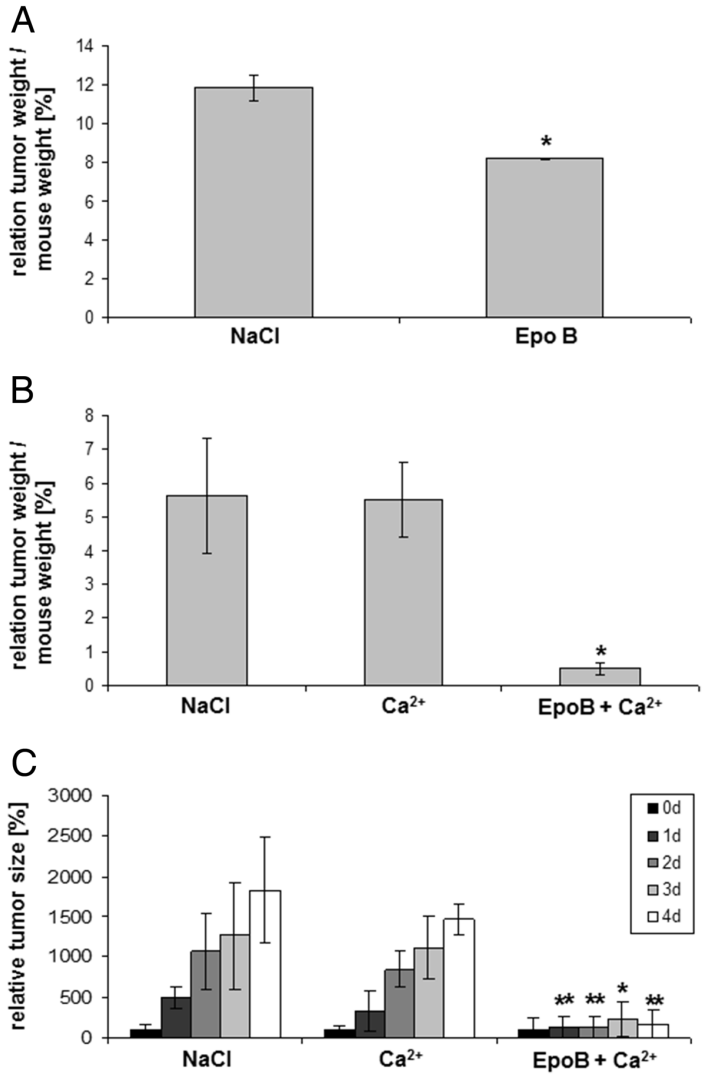

Figure 6 ***In vivo*** **effects of different therapeutic approaches were examined in NOD/scid mice by evaluation of the tumor size each day in the course of the therapy and by calculation of the relation of tumor weight/mouse weight after tumor dissection at the end of the experiment**. Subcutaneous tumors were induced in NOD/scid mice within 18d following injection of about 10^6 SCCOHT-1^{GFP} cells. Thereafter, different therapeutic approaches were applied by injection of 200 μl of either 0.9% NaCl, or 5 mM $CaCl_2$, or 10 μM epothilone B (EpoB), or 5 mM $CaCl_2$ + 10 μM EpoB each day. **A**. The relation of tumor weight / mouse weight was calculated after 2d of subsequent injections for control tumors (NaCl) (n = 2) and EpoB-treated tumors (n = 2). **B**. The relation of tumor weight / mouse weight was calculated after 4d of subsequent injections as the mean ± s.d. for control tumors (NaCl) (n = 5), Ca^{2+}-treated tumors (n = 5), and Ca^{2+} + EpoB-treated tumors (n = 4). Statistical analysis was conducted by 1-way ANOVA test (*p = 0.027). **C**. The tumor size was evaluated each day at 4 consecutive days of subsequent injections as the mean ± s.d. for control tumors (NaCl) (n = 5), Ca^{2+}-treated tumors (n = 5), and Ca^{2+} + EpoB-treated tumors (n = 4). Statistical analysis was calculated by unpaired Student's t-test between Ca^{2+}-treated tumors and the NaCl-treated tumor sizes as well as between Ca^{2+} + EpoB-treated tumors and the NaCl-treated tumor sizes at the corresponding time points, respectively (*P < 0.05; **P < 0.01).

epothilone B. Indeed, addition of 1.6 mM $CaCl_2$ was associated with a continuously reduced proliferation of SCCOHT-1 cells in the fluoroscan assay by about 22.4% ± 4.6% (n = 10) after 72 h (Figure 5B). However, Ca^{2+} exhibited at least additive effects together with epothilone B and further diminished the epothilone B-mediated progressive growth reduction of SCCOHT-1 cells. Thus, the effects of epothilone B which reduced the SCCOHT-1 cell growth by 20.3% ± 3.6% (n = 10) after 24 h was further enhanced to 35.0% ± 5.3% (n = 10) together with Ca^{2+}. Similar synergistic effects of Ca^{2+} together with an epothilone B-conferred growth inhibition of SCCOHT-1 cells

were observed after 48 h and 72 h, respectively (Figure 5B).

Based upon these results, further NOD/scid mouse tumors were examined for a successful therapeutic approach by a daily injection of epothilone B at the tumor site. Testing various concentrations revealed detectable effects with 10 μM epothilone B already after 48 h (=2 treatments) with a tumor size of 2.1 ± 0.2 cm^3 as compared to 2.5 ± 0.1 cm^3 in NaCl-treated control tumors and a relation of tumor weight to mouse weight of 8.2 ± 0.1 in the epothilone B-treated tumor mice as compared to 11.8 ± 0.6 in the NaCl-treated control tumors (Figure 6A). Although in this first therapeutic approach, the mice had to be sacrificed after 2 days for ethical reasons due to the tumor size, these data demonstrated already a reduction in tumor size by about 16% and a reduction in the relation of tumor weight to mouse weight by about 30% after solely epothilone B treatment.

Since addition of exogenous Ca^{2+} supported the growth-inhibitory effects of epothilone B *in vitro*, a further therapeutic approach was tested *in vivo* whereby 200 μl of 5 mM $CaCl_2$ were injected at the tumor site and compared to the effects of a co-injection of 5 mM $CaCl_2$ + 10 μM epothilone B. Although Ca^{2+} alone demonstrated little if any effects on the *in vivo* tumor growth, the combined treatment of Ca^{2+} + epothilone B was associated with a significant reduction by about 90% in the relation of tumor weight to mouse weight after tumor dissection of the sacrificed mice (Figure 6B). Thus, a therapeutic approach with $CaCl_2$ + epothilone B reached a relation of tumor weight to mouse weight of 0.5 ± 0.2 (n = 3) after 4d, however, Ca^{2+} alone and the NaCl control injection reached a relation of tumor weight to mouse weight of 5.5 ± 1.0 (n = 4) and 5.6 ± 1.7 (n = 4), respectively. Statistical analysis by 1-way ANOVA revealed a significant tumor reduction (p = 0.027) (Figure 6B). Daily consecutive measurements and corresponding calculations of the tumor size normalized to the size at the beginning of the therapy (day 0) confirmed a more than 90% reduced tumor size in $CaCl_2$ + epothilone B-treated mice. A consecutive NaCl control treatment and solely Ca^{2+} treatment revealed a rapidly growing and continuously increasing tumor size to 1827% ± 656% (n = 5) and 1472% ± 196% (n = 5) after 4d (Figure 6C). In contrast, consecutive treatment with $CaCl_2$ + epothilone B for 4d was associated with an attenuation of tumor growth reaching an average tumor size of 165% ± 186% (n = 4). These findings suggested that a significantly reduced tumor growth of the SCCOHT *in vivo* by epothilone B treatment could be further enhanced by the addition of exogenous Ca^{2+} to the epothilone B therapy. This therapeutic effect of Ca^{2+}/epothilone B was also accompanied by an abolished hypercalcemia in the mice. Whereas NaCl-treated control tumor-carrying mice and Ca^{2+}-treated mice exhibited a hypercalcemia with average calcium levels in the blood serum of 3.11 ± 0.75 mmol/L (n = 3) and 3.20 ± 0.40 mmol/L (n = 4), respectively, the combined treatment of Ca^{2+}/epothilone B demonstrated normal calcium serum levels of 2.16 ± 0.53 mmol/L (n = 3).

Discussion

SCCOHT represents an aggressive female tumor with poor prognosis and previous work has suggested a multimodality treatment for the SCCOHT including surgery and a subsequent chemotherapy consisting of cisplatin- and etoposide-based or carboplatin- and taxane-based components followed by a radiotherapy [18,19]. Despite this multi-modality approach, however, the level of tumor relapses remains high and only very few patients survived for more than two years [20-23]. Thus, the data obtained in this study demonstrated a certain resistance of SCCOHT-1 cells to a cisplatin- or carboplatin-based chemotherapy since both compounds were ineffective to decrease the proliferative capacity *in vitro*. Resistance to the platin chemotherapeutics has also been confirmed for the NIH:OVCAR-3 and SK-OV-3 ovarian cancer cells. Moreover, the continuous and unaltered cell cycle progression of SCCOHT-1 cells in the presence of both platin compounds is further questioning the effectiveness of these drugs in patients with SCCOHT. Our findings are also supported by studies in BIN-67 cells, displaying a resistance to platinum and other standard chemotherapeutic agents [24]. In contrast, microtubule-stabilizing compounds such as taxol and more importantly, epothilone B demonstrated significant anti-proliferative effects in SCCOHT-1 as well as in NIH:OVCAR-3 and SK-OV-3 cells *in vitro*. The growth-inhibitory effects of epothilone B were associated with an activation of the cellular and DNA damage response machinery including enhanced detection of $HSP27^{[pSer82]}$ and $p53^{[pSer15]}$, respectively, followed by increased cell death as determined via $subG_1$ phase cell cycle accumulation in SCCOHT-1 cells. HSP27 phosphorylation can be mediated by PKD upon cellular stress and plays an important role in cellular protection [25]. Moreover, DNA damage response and cell cycle arrest is relayed via p53 phosphorylation including accumulation of $p53^{[pSer15]}$ [26]. Treatment of human A2780 ovarian cancer cells with taxol has been reported with p53 phosphorylation at serin 20 [27] whereby taxol and epothilone B may confer signals for different phosphorylation sites at p53. In addition, epothilone-mediated cytotoxicity is relayed via different forms of p53 [28].

These significant cytotoxic effects of epothilone B in SCCOHT-1 cells *in vitro* could also be substantiated in a therapeutic approach of NOD/scid mouse tumor xenografts *in vivo* leading to an attenuated tumor growth. The differences in epothilone B concentrations used *in vitro* and *in vivo* can be related to protective effects

by the tumor stroma *in vivo*. Thus, the tumor cells *in vitro* can be exposed directly to the drug whereas *in vivo*, the tumor microenvironment of extracellular matrix with embedded adjacent cell populations including immune cells, endothelial cells, cancer-associated fibroblasts and mesenchymal stem cells contribute to a border which requires higher chemotherapeutic concentrations to target the tumor cells [12,13].

In this context, it is remarkable to note that the closely related compound ixabepilone, which differs in only one atom by the exchange of oxygen against nitrogen within the ester bridge of the molecule, displayed no detectable effects on SCCOHT-1 cell growth and viability even at a 250-fold higher concentration as compared to epothilone B. These significantly different cellular effects of structurally very similar compounds are related to molecular differences in the interactions with tubulins and the associated stability of the microtubules. Whereas tubulinα and tubulinβ proteins associate to a heterodimer and form a taxane binding pocket at intradimer interfaces, epothilone B binding to this taxane site exhibits a tight interaction with the heterodimeric tubulin molecule and a rather static conformation. In contrast, ixabepilone retains a significant degree of flexibility within the atomic and molecular environment of this taxane binding pocket and therefore displays different effects on the interaction and stability with the tubulin heterodimeric molecule [29]. Such molecular interactions may also apply to the isotype form tubulinβ3 which is present predominantly in aggressive and drug-resistant tumors [30,31]. Indeed, a markedly detectable expression of tubulinβ3 has been identified in SCCOHT-1 cells in contrast to the NIH:OVCAR-3 and SK-OV-3 ovarian cancer cells which substantiates the aggressiveness of SCCOHT.

The significant epothilone B-mediated growth reduction of SCCOHT-1 cells *in vitro* was maintained in re-cultured cells from induced mouse xenograft tumors and these findings could also be confirmed *in vivo* demonstrating a tumor reduction by epothilone B in SCCOHT-1-induced mouse xenografts. Moreover, the tumor-reducing effects of epothilone B could be synergistically enhanced by exogenous calcium *in vitro* and *in vivo* and resulted in an attenuated tumor growth. The concomitant reduction of the hypercalcemic serum levels back to normal calcium serum levels observed in calcium + epothilone B-treated mice in contrast to the sustained hypercalcemia in untreated and solely calcium-treated tumors appear somewhat paradoxical and suggests an important but so far unexplained physiological role of calcium in this tumor entity. Since increased calcium levels can exhibit cytotoxic effects in ovarian cancer cells *in vitro* [32], hypercalcemia may partially represent a defense mechanism of the organism to antagonize the rapid and aggressive tumor growth and exogenously added calcium may further raise these levels for a sufficient synergy with epothilone B. However, the underlying mechanisms of this synergism remain unanswered and require further investigation.

Conclusion

Whereas only little therapeutic strategies for unresponsive ovarian carcinoma are available, the present findings provide a more detailed understanding of potential compounds to target ovarian cancer cells exhibiting resistance to a variety of chemotherapeutics. Moreover, this work demonstrates a promising disease-focused approach including some molecular explanation for targeting the small cell carcinoma of the ovary hypercalcaemic type which may be embedded into a multi-modality therapeutic approach for a better targeted treatment of this rare cancerous disease.

Abbreviations

SCCOHT: Small cell carcinoma of the ovary hypercalcemic type; GFP: Green fluorescent protein; PKD: Protein kinase D.

Competing interests

The authors declare no financial, personal, or professional conflicts of interest.

Authors' contributions

AO, FR and JO performed the proliferation tests with the various chemotherapeutics, the cell cycle analysis and the Western blots. RH and AO exhibited the *in vivo* studies. PH and TPS critically read and revised the manuscript and contributed clinical background. RH designed and supervised the study and drafted the manuscript. All authors read and approved the final manuscript.

Acknowledgements

The authors are grateful to Dr. N. von Neuhoff, Hannover Medical School, for the support with the cell line authentication by STR profiling analysis, and to Prof. Dr. R. Lichtinghagen, Hannover Medical School, for support with the calcium measurement. This work was supported by a grant from the Niedersächsische Krebsgesellschaft e.V. to Ralf Hass.

Received: 1 April 2014 Accepted: 23 July 2014
Published: 8 August 2014

References

1. Ulbright TM, Roth LM, Stehman FB, Talerman A, Senekjian EK: **Poorly differentiated (small cell) carcinoma of the ovary in young women: evidence supporting a germ cell origin.** *Hum Pathol* 1987, **18:**175–184.
2. Young RH, Oliva E, Scully RE: **Small cell carcinoma of the hypercalcemic type in the ovary.** *Gynecol Oncol* 1995, **57:**7–8.
3. Aguirre P, Thor AD, Scully RE: **Ovarian small cell carcinoma. Histogenetic considerations based on immunohistochemical and other findings.** *Am J Clin Pathol* 1989, **92:**140–149.
4. Walt H, Hornung R, Fink D, Dobler-Girdziunaite D, Stallmach T, Spycher MA, Maly F, Haller U, Burki N: **Hypercalcemic-type of small cell carcinoma of the ovary: characterization of a new tumor line.** *Anticancer Res* 2001, **21:**3253–3259.
5. McCluggage WG, Oliva E, Connolly LE, McBride HA, Young RH: **An immunohistochemical analysis of ovarian small cell carcinoma of hypercalcemic type.** *Int J Gynecol Pathol* 2004, **23:**330–336.
6. Upchurch KS, Parker LM, Scully RE, Krane SM: **Differential cyclic AMP responses to calcitonin among human ovarian carcinoma cell lines: a calcitonin-responsive line derived from a rare tumor type.** *J Bone Miner Res* 1986, **1:**299–304.
7. Dickersin GR, Kline IW, Scully RE: **Small cell carcinoma of the ovary with hypercalcemia: a report of eleven cases.** *Cancer* 1982, **49:**188–197.

8. Eichhorn JH, Bell DA, Young RH, Swymer CM, Flotte TJ, Preffer RI, Scully RE: **DNA content and proliferative activity in ovarian small cell carcinomas of the hypercalcemic type. Implications for diagnosis, prognosis, and histogenesis.** *Am J Clin Pathol* 1992, **98:**579–586.
9. Jelinic P, Mueller JJ, Olvera N, Dao F, Scott SN, Shah R, Gao J, Schultz N, Gonen M, Soslow RA, Berger MF, Levine DA: **Recurrent SMARCA4 mutations in small cell carcinoma of the ovary.** *Nat Genet* 2014, **46:**424–426.
10. Witkowski L, Carrot-Zhang J, Albrecht S, Fahiminiya S, Hamel N, Tomiak E, Grynspan D, Saloustros E, Nadaf J, Rivera B, Gilpin C, Castellsague E, Silva-Smith R, Plourde F, Wu M, Saskin A, Arseneault M, Karabakhtsian RG, Reilly EA, Ueland FR, Margiolaki A, Pavlakis K, Castellino SM, Lamovec J, Mackay HJ, Roth LM, Ulbright TM, Bender TA, Georgoulias V, Longy M, *et al*: **Germline and somatic SMARCA4 mutations characterize small cell carcinoma of the ovary, hypercalcemic type.** *Nat Genet* 2014, **46:**438–443.
11. Ramos P, Karnezis AN, Craig DW, Sekulic A, Russell ML, Hendricks WP, Corneveaux JJ, Barrett MT, Shumansky K, Yang Y, Shah SP, Prentice LM, Marra MA, Kiefer J, Zismann VL, McEachron TA, Salhia B, Prat J, D'Angelo E, Clarke BA, Pressey JG, Farley JH, Anthony SP, Roden RB, Cunliffe HE, Huntsman DG, Trent JM: **Small cell carcinoma of the ovary, hypercalcemic type, displays frequent inactivating germline and somatic mutations in SMARCA4.** *Nat Genet* 2014, **46:**427–429.
12. Ungefroren H, Sebens S, Seidl D, Lehnert H, Hass R: **Interaction of tumor cells with the microenvironment.** *Cell Commun Signal* 2011, **9:**18.
13. Hass R, Otte A: **Mesenchymal stem cells as all-round supporters in a normal and neoplastic microenvironment.** *Cell Commun Signal* 2012, **10:**26.
14. Otte A, Gohring G, Steinemann D, Schlegelberger B, Groos S, Langer F, Kreipe HH, Schambach A, Neumann T, Hillemanns P, Park-Simon TW, Hass R: **A tumor-derived population (SCCOHT-1) as cellular model for a small cell ovarian carcinoma of the hypercalcemic type.** *Int J Oncol* 2012, **41:**765–775.
15. Bernhardt G, Muller R, Gust R, Reile H, Keller C, Spruss T, Schonenberger H: **Dichloro-[1-(hydroxyphenyl)-2-phenylethylenediamine]platinum(II) complexes: testing on the human ovarian cancer cell lines NIH: OVCAR3 and SK OV 3.** *Arch Pharm* 1992, **325:**93–99.
16. Bertram C, Hass R: **Cellular senescence of human mammary epithelial cells (HMEC) is associated with an altered MMP-7/HB-EGF signaling and increased formation of elastin-like structures.** *Mech Ageing Dev* 2009, **130:**657–669.
17. Tomayko MM, Reynolds CP: **Determination of subcutaneous tumor size in athymic (nude) mice.** *Cancer Chemother Pharmacol* 1989, **24:**148–154.
18. Shrimali RK, Correa PD, Reed NS: **Dose-dense and dose-intense chemotherapy for small cell ovarian cancer: 2 cases and review of literature.** *Med Oncol (Northwood London England)* 2012, **28:**766–770.
19. Harrison ML, Hoskins P, du Bois A, Quinn M, Rustin GJ, Ledermann JA, Baron-Hay S, Friedlander ML: **Small cell of the ovary, hypercalcemic type – analysis of combined experience and recommendation for management.** *A GCIG Study Gynecol Oncol* 2006, **100:**233–238.
20. Benrubi GI, Pitel P, Lammert N: **Small cell carcinoma of the ovary with hypercalcemia responsive to sequencing chemotherapy.** *South Med J* 1993, **86:**247–248.
21. Reed WC: **Small cell carcinoma of the ovary with hypercalcemia: report of a case of survival without recurrence 5 years after surgery and chemotherapy.** *Gynecol Oncol* 1995, **56:**452–455.
22. Dykgraaf RH, de Jong D, van Veen M, Ewing-Graham PC, Helmerhorst TJ, van der Burg ME: **Clinical management of ovarian small-cell carcinoma of the hypercalcemic type: a proposal for conservative surgery in an advanced stage of disease.** *Int J Gynecol Cancer* 2009, **19:**348–353.
23. Barondeau J, Rodgers M, Braun L, Azarow K, Forouhar M, Faucette K: **Small cell ovarian carcinoma: a rare, aggressive tumor masquerading as constipation in a teenager with a fatal outcome.** *J Pediatr Hematol Oncol* 2010, **32:**e139–e141.
24. Gamwell LF, Gambaro K, Merziotis M, Crane C, Arcand SL, Bourada V, Davis C, Squire JA, Huntsman DG, Tonin PN, Vanderhyden BC: **Small cell ovarian carcinoma: genomic stability and responsiveness to therapeutics.** *Orphanet J Rare Dis* 2010, **8:**33.
25. Stetler RA, Gao Y, Zhang L, Weng Z, Zhang F, Hu X, Wang S, Vosler P, Cao G, Sun D, Graham SH, Chen J: **Phosphorylation of HSP27 by protein kinase D is essential for mediating neuroprotection against ischemic neuronal injury.** *J Neurosci* 2012, **32:**2667–2682.
26. Bertram C, Hass R: **Cellular responses to reactive oxygen species-induced DNA damage and aging.** *Biol Chem* 2008, **389:**211–220.
27. Damia G, Filiberti L, Vikhanskaya F, Carrassa L, Taya Y, D'Incalci M, Broggini M: **Cisplatinum and taxol induce different patterns of p53 phosphorylation.** *Neoplasia (New York, NY* 2001, **3:**10–16.
28. Ioffe ML, White E, Nelson DA, Dvorzhinski D, DiPaola RS: **Epothilone induced cytotoxicity is dependent on p53 status in prostate cells.** *Prostate* 2004, **61:**243–247.
29. Khrapunovich-Baine M, Menon V, Yang CP, Northcote PT, Miller JH, Angeletti RH, Fiser A, Horwitz SB, Xiao H: **Hallmarks of molecular action of microtubule stabilizing agents: effects of epothilone B, ixabepilone, peloruside A, and laulimalide on microtubule conformation.** *J Biol Chem* 2011, **286:**11765–11778.
30. Kavallaris M: **Microtubules and resistance to tubulin-binding agents.** *Nat Rev* 2010, **10:**194–204.
31. Seve P, Dumontet C: **Is class III beta-tubulin a predictive factor in patients receiving tubulin-binding agents?** *Lancet Oncol* 2008, **9:**168–175.
32. Otte A, Rauprich F, von der Ohe J, Hillemanns P, Hass R: **Interference of Ca^{2+} with the proliferation of SCCOHT-1 and ovarian adenocarcinoma cells.** *Int J Oncol* 2014, **45:**1151–1158.

doi:10.1186/s13023-014-0126-4
Cite this article as: Otte *et al.*: *In vitro* and *in vivo* therapeutic approach for a small cell carcinoma of the ovary hypercalcaemic type using a SCCOHT-1 cellular model. *Orphanet Journal of Rare Diseases* 2014 **9**:126.

2.3 c-Met inhibitors attenuate tumor growth of small cell hypercalcemic ovarian carcinoma (SCCOHT) populations

Anna Otte, Finn Rauprich, Juliane von der Ohe, Yuanyuan Yang, Friedrich Kommoss, Friedrich Feuerhake, Peter Hillemanns und Ralf Hass

publiziert in
Oncotarget
6(31), 2015, 31640-31658
doi: 10.18632/oncotarget.5151

www.impactjournals.com/oncotarget/ Oncotarget, Advance Publications 2015

c-Met inhibitors attenuate tumor growth of small cell hypercalcemic ovarian carcinoma (SCCOHT) populations

Anna Otte[1], Finn Rauprich[1], Juliane von der Ohe[1], Yuanyuan Yang[1], Friedrich Kommoss[2], Friedrich Feuerhake[3], Peter Hillemanns[1], Ralf Hass[1]

[1]Biochemistry and Tumor Biology Lab, Department of Obstetrics and Gynecology, Hannover Medical School, Hannover, Germany

[2]Synlab MVZ Pathologie Mannheim GmbH, Referral Center for Gynecopathology, Mannheim, Germany

[3]Institute for Pathology, Hannover Medical School, Hannover, Germany

Correspondence to:
Ralf Hass, **e-mail:** hass.ralf@mh-hannover.de

Keywords: *SCCOHT, small cell ovarian cancer, c-Met inhibitor, foretinib, tumor growth*

Received: *February 16, 2015* ***Accepted:*** *September 18, 2015* ***Published:*** *September 30, 2015*

ABSTRACT

A cellular model (SCCOHT-1) of the aggressive small cell hypercalcemic ovarian carcinoma demonstrated constitutive chemokine and growth factor production including HGF. A simultaneous presence of c-Met in 41% SCCOHT-1 cells suggested an autocrine growth mechanism. Expression of c-Met was also observed at low levels in the corresponding BIN-67 cell line (6.5%) and at high levels in ovarian adenocarcinoma cells (NIH:OVCAR-3 (84.4%) and SK-OV-3 (99.3%)). Immunohistochemistry of c-Met expression in SCCOHT tumors revealed a heterogeneous distribution between undetectable levels and 80%. Further characterization of SCCOHT-1 and BIN-67 cells by cell surface markers including CD90 and EpCAM demonstrated similar patterns with differences to the ovarian adenocarcinoma cells. HGF stimulation of SCCOHT-1 cells was associated with c-Met phosphorylation at Tyr^{1349} and downstream Thr^{202}/Tyr^{204} phosphorylation of p44/42 MAP kinase. This HGF-induced signaling cascade was abolished by the c-Met inhibitor foretinib. Cell cycle analysis after foretinib treatment demonstrated enhanced G2 accumulation and increasing apoptosis within 72 h. Moreover, the IC_{50} of foretinib revealed 12.4 nM in SCCOHT-1 cells compared to 411 nM and 481 nM in NIH:OVCAR-3 and SK-OV-3 cells, respectively, suggesting potential therapeutic effects. Indeed, SCCOHT-1 and BIN-67 tumor xenografts in NOD^{scid} mice exhibited an approximately 10-fold and 5-fold reduced tumor size following systemic application of foretinib, respectively. Furthermore, foretinib-treated tumors revealed a significantly reduced vascularization and little if any c-Met-mediated signal transduction. Similar findings of reduced proliferative capacity and declined tumor size were observed after siRNA-mediated c-Met knock-down in SCCOHT-1 cells demonstrating that *in vivo* inhibition of these pathways contributed to an attenuation of SCCOHT tumor growth.

INTRODUCTION

One of the most lethal gynecologic malignancies is caused by ovarian cancer. A variety of different epithelial ovarian cancers have been categorized into two types, whereby type I tumors include low-grade serous, endometrioid, clear cell and mucinous carcinomas which appear clinically indolent. In contrast, type II tumors are characterized by high-grade serous, high-grade endometrioid and undifferentiated carcinomas, as well as malignant mixed mesodermal tumors (carcinosarcomas) with papillary, glandular, and solid patterns displaying highly aggressive cancer cells predominantly observed in advanced tumor stages [1–3]. This differentiated histopathological categorization of ovarian tumor types is also supported by molecular differences. Thus, gene mutations including KRAS, BRAF, ERBB2, PTEN, CTNNB1, and PIK3CA are predominantly detected in

type I ovarian tumors. Vice versa, type II tumors often display genetic instabilities with a high frequency of TP53 mutations and cyclin E1 amplifications which directly regulate the proliferative capacity and cell cycle progression [4, 5].

Upon variations of this type of malignant neoplasia, the small cell ovarian carcinoma of the hypercalcemic type (SCCOHT) represents a rare form of an aggressive ovarian tumor which is predominantly observed in young women between ages of 13 to 35. The SCCOHT has a poor prognosis and is associated in most cases with paraendocrine hypercalcemia [6, 7].

Histopathological evaluation of several clinical cases have classified the SCCOHT as a separate pathological entity [6] since this tumor appears different from other ovarian cancer types including ovarian epithelial tumors and ovarian germ cell tumors [8]. However, the etiology of the SCCOHT still remains obscure. Whereas immunohistochemical analysis of the SCCOHT postulated a germ cell-derived tumor [9], other work has also discussed SCCOHT as an epithelial-like originating tumor [7] and genetic analysis of SCCOHT tumor specimen have documented an inhomogeneous tumor entity [10–12]. Genome sequencing of SCCOHT tumor biopsies revealed both, germline and somatic mutations of the *SMARCA4* gene including a stop codon mutation p.Arg1077* and a frameshift p.Pro1180fs [13]. The SMARCA4 gene encodes the transcription activator BRG1 which represents an ATP-dependent helicase of the SWI/SNF family and its mutation was suggested as a potential molecular marker for the SCCOHT [14–16].

Cellular models for the SCCOHT are represented by the BIN-67 [17] and the SCCOHT-1 [18] cell lines. In line with the SCCOHT histology, characterization of BIN-67 and SCCOHT-1 tumor cells indicated heterogeneous populations with certain epithelial and mesenchymal properties. Moreover, SCCOHT-1 tumor cells are carrying a defective *SMARCA4* gene with a loss of BRG1 protein expression [19] and likewise, BIN-67 cells demonstrated biallelic deleterious *SMARCA4* gene mutations [15] which confirms the results in SCCOHT patient biopsies. Whereas mutations in the *SMARCA4* gene and the related *SMARCB1* gene also occur in malignant rhabdoid tumors, further similarities by whole exome sequencing suggested SCCOHT as malignant rhabdoid tumor of the ovary [20]. Furthermore, BIN-67 and SCCOHT-1 cells developed appropriate tumors in xenotransplants and exhibited multiple chemotherapeutic resistances by continued tumor growth [21, 22]. Consistently, various resistant effects are also observed in SCCOHT patients and therefore, reasonable approaches for the treatment of this tumor disease remain unknown. It was thus the aim of the present study, to identify a potential molecular target for a growth arrest of these tumor cells by investigating effects of growth factors such as HGF and the related receptor c-Met in SCCOHT-1 cell cultures in comparison to BIN-67 cells and the established human ovarian adenocarcinoma NIH:OVCAR-3 and SK-OV-3 cell line.

RESULTS

The constitutive production and release of certain cytokines and growth factors by SCCOHT-1 cells was measured in a customized human multiplex ELISA system. Little if any release of ICAM-1, PDGF-BB and TNF-α was detectable in SCCOHT-1 cell culture medium after 24 h and 48 h, respectively. However, there was a significant production of HGF by 4,868 ± 464ng/2 × 10^5 cells after 24 h which raised to 24,590 ± 1,580ng/2 × 10^5 cells (n = 4) after 48 h (Fig.1). Moreover, an increase in IL8 production was also paralleled by elevated PDGF-AA levels from 11 ± 2 ng/ml in control medium to 666 ± 100ng/2 × 10^5 cells after 24 h and 2,167 ± 279ng/2 × 10^5 cells after 48 h (n = 4), respectively. Likewise, release of VCAM-1 and VEGF was significantly elevated by SCCOHT-1 cells (Fig. 1).

According to the constitutive production and release of HGF by SCCOHT-1 cells, simultaneous expression of the corresponding receptor c-Met was investigated. Analysis by flow cytometry revealed c-Met receptor expression in 6.5 ± 0.1% (n = 3) of BIN-67 cells, 40.9 ± 3.8% (n = 3) of SCCOHT-1 cells and a majority in ovarian adenocarcinoma cells with 84.4 ± 9.2% (n = 3) in NIH:OVCAR-3 cells and 99.3 ± 0.4% (n = 3) in SK-OV-3 cells (Fig. 2A). Similar results were obtained by Western blots with the lowest levels of c-Met proteins in BIN-67 cells and high expression levels in NIH:OVCAR-3 cells and SK-OV-3 cells (Fig. 2B).

Although different levels of c-Met expression were observed in SCCOHT-1 and BIN-67 cells, these two populations shared a variety of similar markers and could be distinguished from other ovarian adenocarcinoma cells. Flow cytometry analysis revealed a common expression of surface markers for cell-cell communication including the beta-1 integrin subunit CD29 among all of these ovarian cancer populations which i.e. can function as the α3β1 integrin and may play a role during metastatic diffusion of certain tumor cells. However, marked differences were observed for a variety of other cell surface markers in SCCOHT-1 and BIN-67 cells compared to NIH:OVCAR-3 and SK-OV-3 cells indicating altered tumor cell functionalities. One of these differences included the glycosyl phosphatidyl inositol (GPI)-anchored CD90 antigen expression, also present on some immune cells, hematopoietic stem cells, and a property of mesenchymal stem cells in a normoxic and hypoxic microenvironment [23, 24]. Increased CD90 and vimentin levels were detected during epithelial to mesenchymal transition of non small cell lung cancer (NSCLC) cells [25] and CD90 protein expression by

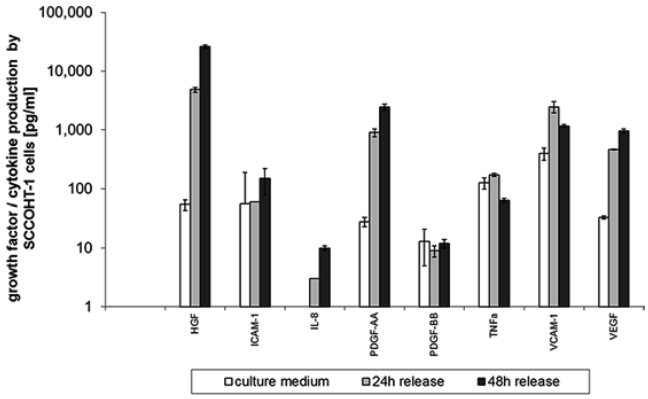

Figure 1: Quantitative production of distinct growth factors and cytokines was measured in supernatants of SCCOHT-1 (2×10^5 cells/ml) after 24 h and 48 h, respectively, using a multiplexed human chemokine assay system. Data represent the amount of cytokine/growth factor production [pg/2×10^5 cells] ± s.d. (n = 4). (HGF = hepatocyte growth/scatter factor; ICAM-1 = intercellular cell adhesion molecule-1; IL-8 = interleukin-8; PDGF = platelet-derived growth factor; TNFa = tumor necrosis factor-alpha; VCAM-1 = vascular cell adhesion molecule-1; VEGF = vascular endothelial growth factor)

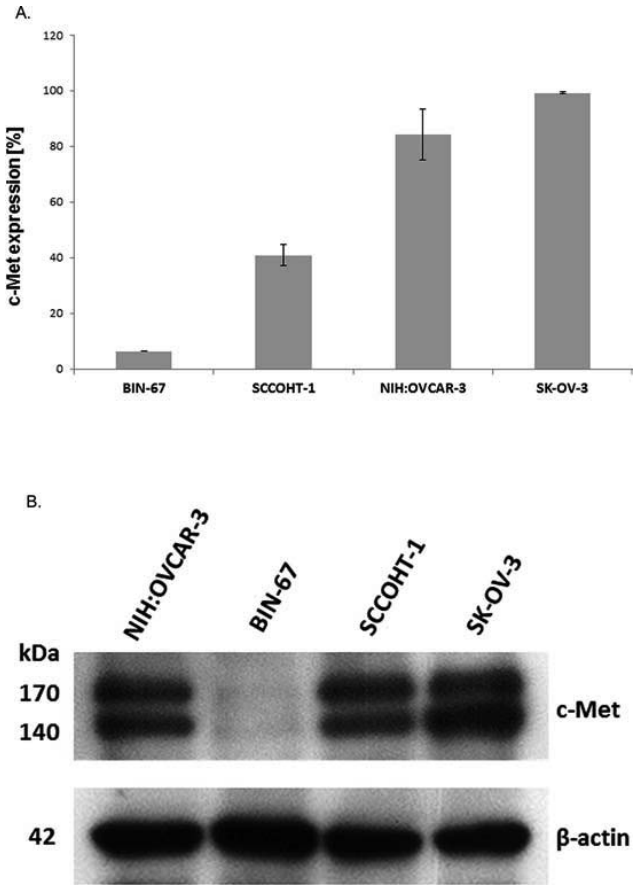

Figure 2: A. Expression of c-Met protein was measured by flow cytometry in BIN-67, SCCOHT-1, NIH:OVCAR-3 and SK-OV-3 cells, respectively. Data represent the percentage of c-Met expression ± s.d. (n = 4). **B.** Western blot of c-Met expression in the 4 different ovarian cancer cell populations with GAPDH expression as control.

SCCOHT-1 and BIN-67 cells was in contrast to little if any detectable CD90 in NIH:OVCAR-3 and SK-OV-3 cells (suppl. Fig. S1). Moreover, mesothelin as part of the outer plasma membrane by GPI linkage is overexpressed in several human tumors, including mesothelioma as well as pancreatic and ovarian adenocarcinoma [26] and was detectable in NIH:OVCAR-3 and SK-OV-3 cells in contrast to SCCOHT-1 and BIN-67 cells. In addition, the epithelial cell adhesion molecule (CD326/EpCAM) functions as a transmembrane glycoprotein mediating Ca^{2+}-independent homotypic cell-cell adhesion in epithelia and in contrast to an extensive expression in NIH:OVCAR-3 and SK-OV-3 cells this adhesion molecule was undetectable in SCCOHT-1 and BIN-67 cells. Furthermore, the mesenchymal intermediate filament vimentin could be observed in SCCOHT-1, BIN-67 and SK-OV-3 cells and to about 7% NIH:OVCAR-3 cells. In addition, cytokeratins as part of the epithelial intermediate filament proteins were strongly expressed in NIH:OVCAR-3 and SK-OV-3 cells and only to about 27% in SCCOHT-1 and about 2% in BIN-67 cells (suppl. Fig. S1). Together, these findings suggested differences in cell-cell and cell-matrix interactions between the small cell hypercalcemic ovarian tumor cell types and the ovarian adenocarcinoma cell lines.

C-Met expression was also examined by immunohistochemistry (IHC) in 16 different SCCOHT patient tumor tissues (Fig. 3). The SCCOHT-1 cell-originating patient tumor demonstrated c-Met expression in about 40% of the cells (Fig. 3A) which is in line with our flow cytometry data. In addition, a series of 15 centrally reviewed primary SCCOHT was retrieved from the archives of the Mannheim referral center for gynecopathology by one of the authors (FK) and stained for c-Met expression by standard immunohistochemistry. While 6/15 tumors were c-Met negative, 4/15 tumors showed very low levels of c-Met expression (<1% positive cells), and 5/15 tumors were weakly to moderately c-Met positive (<10–80% positive cells, Fig. 3B). These results suggest heterogeneity of c-Met expression in individual SCCOHT tumors.

Accordingly, c-Met signaling was investigated in the different ovarian cancer cells. Exogenous stimulation of SCCOHT-1, SK-OV-3 and NIH:OVCAR-3 cells with 20 ng/ml HGF was associated with enhanced phosphorylation of c-Met at Tyr1349 after 30 min which was abolished in the presence of 2.5 μM crizotinib and 1.25 μM foretinib, respectively (Fig. 4). BIN-67 cells demonstrated barely detectable phosphorylation signals due to the low constitutive expression levels of c-Met (Fig. 4). Whereby constitutive c-Met expression remained unaltered, HGF stimulation was also accompanied by downstream signaling of enhanced p44/p42 MAP kinase phosphorylation at Thr202/Tyr204 particularly in SK-OV-3 and NIH:OVCAR-3 cells. Likewise, these HGF-mediated phosphorylation signals were partially diminished by a parallel incubation with 2.5 μM crizotinib and even more reduced in the presence of 1.25 μM foretinib (Fig. 4) suggesting the c-Met inhibitor foretinib a potent signaling inhibitor in these tumor cells.

Effects of crizotinib and foretinib were also tested on the cell cycle progression and proliferative capacity of the ovarian cancer cells. Cell cycle analysis after incubation of SCCOHT-1 (Fig. 5A) and BIN-67 cells (Fig. 5B) with 0.25 μM up to 1.25 μM foretinib or 0.625 μM up to 2.5 μM crizotinib revealed a significant initial G2/M accumulation after 12 h which continuously declined until 72 h (Fig. 5A, 5B). This was paralleled by a progressively increasing apoptosis in sub G1 phase within 12 h to 72 h. Moreover, some aberrant mitosis was detectable by DNA doubling without cell division and therefore, appearance of populations with 2 × G2/M or more DNA content (>2 × G2/M) (Fig. 5A, 5B). A detailed time course of incubation with these c-Met inhibitors demonstrated similar effects also in NIH:OVCAR-3 and SK-OV-3 cells which substantiated a continuously increasing and significant G2/M phase accumulation already within 8 h to 12 h in the 4 different cell types (suppl. Figs. S2A to S2D).

Examination of the IC_{50} for the two c-Met inhibitors demonstrated an about 10-fold increased sensitivity of SCCOHT-1 cells for foretinib (12.4 nM) compared to crizotinib (128 nM). Moreover, the ovarian adenocarcinoma cells NIH:OVCAR-3 and SK-OV-3 exhibited an about 2- and 3-fold enhanced sensitivity for foretinib whereas only little and insensitive differences were observed for BIN-67 cells (Fig. 5C). Together, these findings suggested a more specific growth inhibition associated with foretinib.

To test potential growth-inhibitory effects of foretinib *in vivo*, xenograft tumors were induced in NOD^{scid} mice by the two SCCOHT cell lines. Following a subcutaneous injection of 3×10^6 cells SCCOHT-1-induced mouse tumors ($n = 3$) could be detected already after 8d. A daily oral application of 200 μl foretinib (50 mg/kg) for 10 subsequent days revealed a white/yellow-colored tumor tissue with an about 10- to 20-fold reduced tumor mass compared to red-colored SCCOHT-1 control tumors ($n = 3$) after similar daily treatment with the solvent only (Fig. 6A). Following continuous tumor size measurements with corresponding calculation of the tumor volume, progressively increasing control tumors volumes were observed in contrast to an unaltered size of foretinib-treated tumors (Fig. 6B, upper panel). The relation of tumor weight / mouse weight after 10d of treatment revealed 1.46 ± 0.62% ($n = 3$) in control tumors and an about 15-fold reduced relation of 0.10 ± 0.02% ($n = 3$) in foretinib-treated SCCOHT-1 tumors (Fig. 6B, lower panel). Effects of foretinib treatment on the body weight of mice carrying SCCOHT-1 tumor xenografts revealed

A.

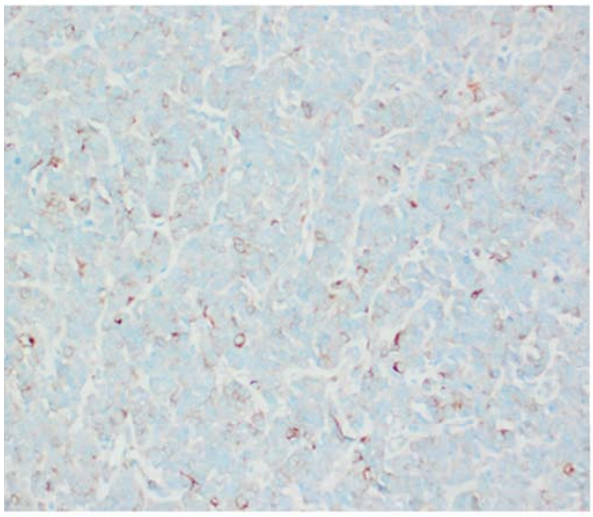

B.

Case ID#	Intensity	Average positive %	Remarks
MA1a	2+	60%	focal staining pattern
MA2a	0	0	
MA3a	0	0	
MA4	2+	80%	partially focal pattern
MA5a	0	0	
MA6a	2+	<1%	small positive foci
MA7a	0	0	
MA8a	1+	70%	
MA9a	2+	<10%	
MA10	0	0	
MA11	2+	<1%	focal staining pattern
MA12a	2+	<10%	focal staining pattern
MA13	1+	<1%	focal staining pattern
MA14a	1+	<1%	single diffusely distributed cells
MA15	0	0	

c-Met immunohistochemistry in SCCOHT patient tumors

Figure 3: Immunhistochemical (IHC) detection of c-Met was performed in specimen of 16 different patients with confirmed SCCOHT. A. IHC analysis in the primary patient tumor (origin of SCCOHT-1 cells) confirmed c-Met expression at variable levels with predominantly membrane-bound staining. **B.** An additional pilot series (n = 15) of primary SCCOHT showed microscopically detectable c-Met expression together with the SCCOHT-1 originating tumor predominantly in 6/16 cases. The staining confirmed significant c-Met expression in a subset of SCCOHT and showed striking variability across cases and within individual tumors, suggesting intra- and intertumoral heterogeneity of c-Met expression.

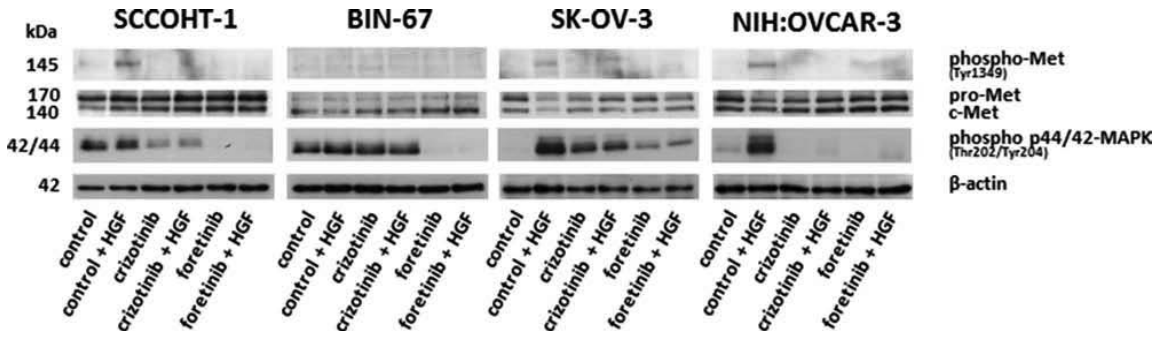

Figure 4: Western blot analysis was performed for c-Met phosphorylation at Tyr1349 and p44/p42 MAP kinase phosphorylation at Thre202/Tyr204 in SCCOHT-1, BIN-67, NIH:OVCAR-3 and SK-OV-3 ovarian cancer cells following 30 min of HGF stimulation in the presence or absence of the c-Met inhibitors crizotinib or foretinib, respectively.

less than 20% differences (up to 17%; n = 3; $p < 0.01$) compared to control treatment after 10d (suppl. Fig. S4, left panel).

BIN-67-induced mouse tumors (n = 3) appeared after 71d of subcutaneous tumor cell injection which took much longer to develop than SCCOHT-1 xenografts. This is also supported by the significantly reduced proliferative capacity of BIN-67 cells with an average cell doubling of approximately 75 h to 90 h compared to SCCOHT-1 cells representing a cell doubling time between 24 h to 36 h (suppl. Fig. S3).

A similar foretinib treatment of BIN-67-induced mouse tumors (daily oral application of 200 µl foretinib (50 mg/kg) for 10d) was associated with an approximately 5-fold reduced tumor mass (Fig. 6C, left panel) and accordingly, the relation of tumor weight / mouse weight after 10d of treatment declined by 4.6-fold from 0.83 ± 0.07% (n = 3) in control tumors to 0.18 ± 0.03% (n = 3) in

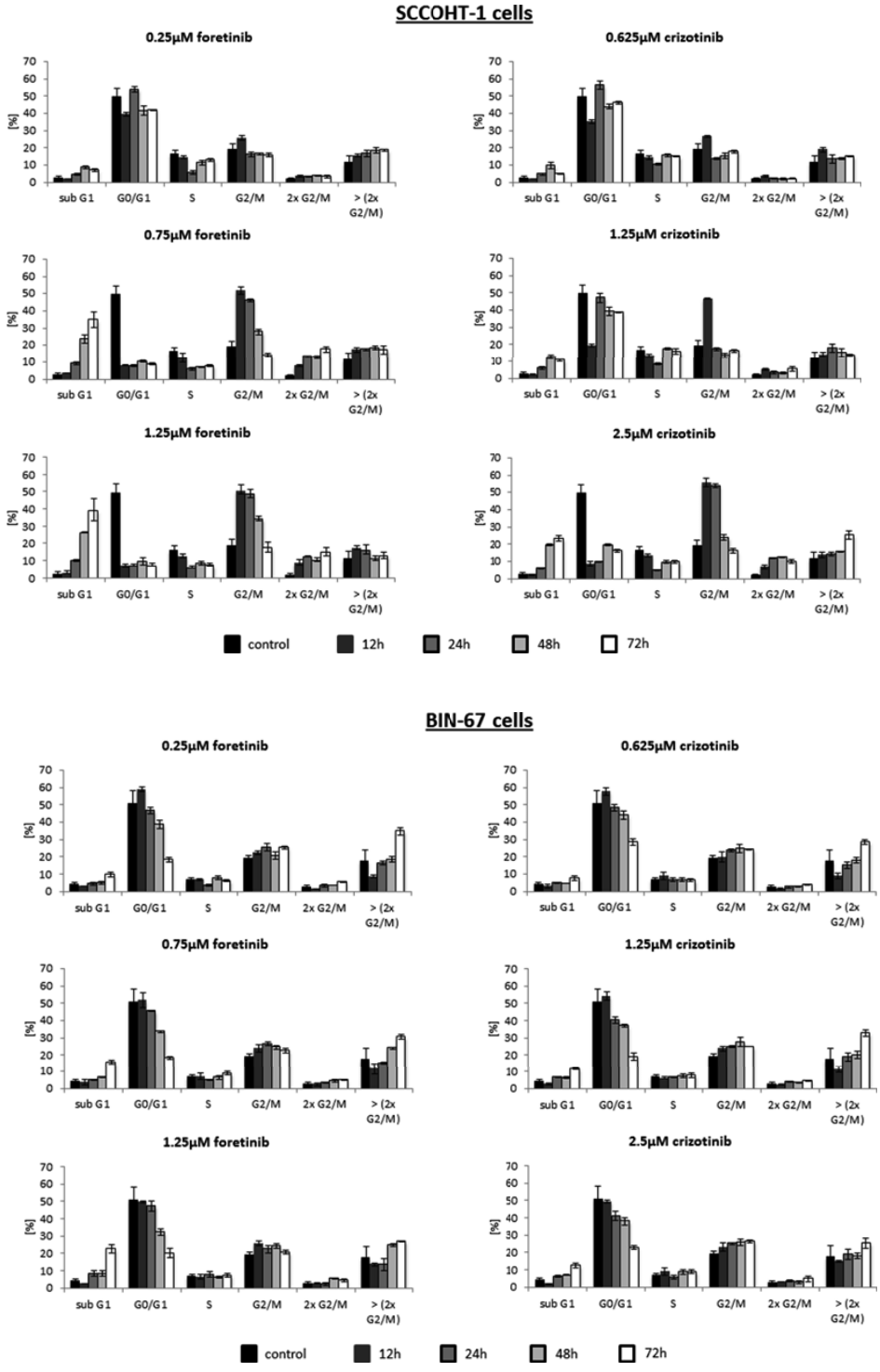

Figure 5: A. Cell cycle analysis was performed in SCCOHT-1, BIN-67 cells in the absence or presence of different concentrations of the c-Met inhibitors crizotinib and foretinib for 12 h up to 72 h, respectively. Quantification of the different cell cycle phases represent the mean ± s.d. (n = 3).

(*Continued*)

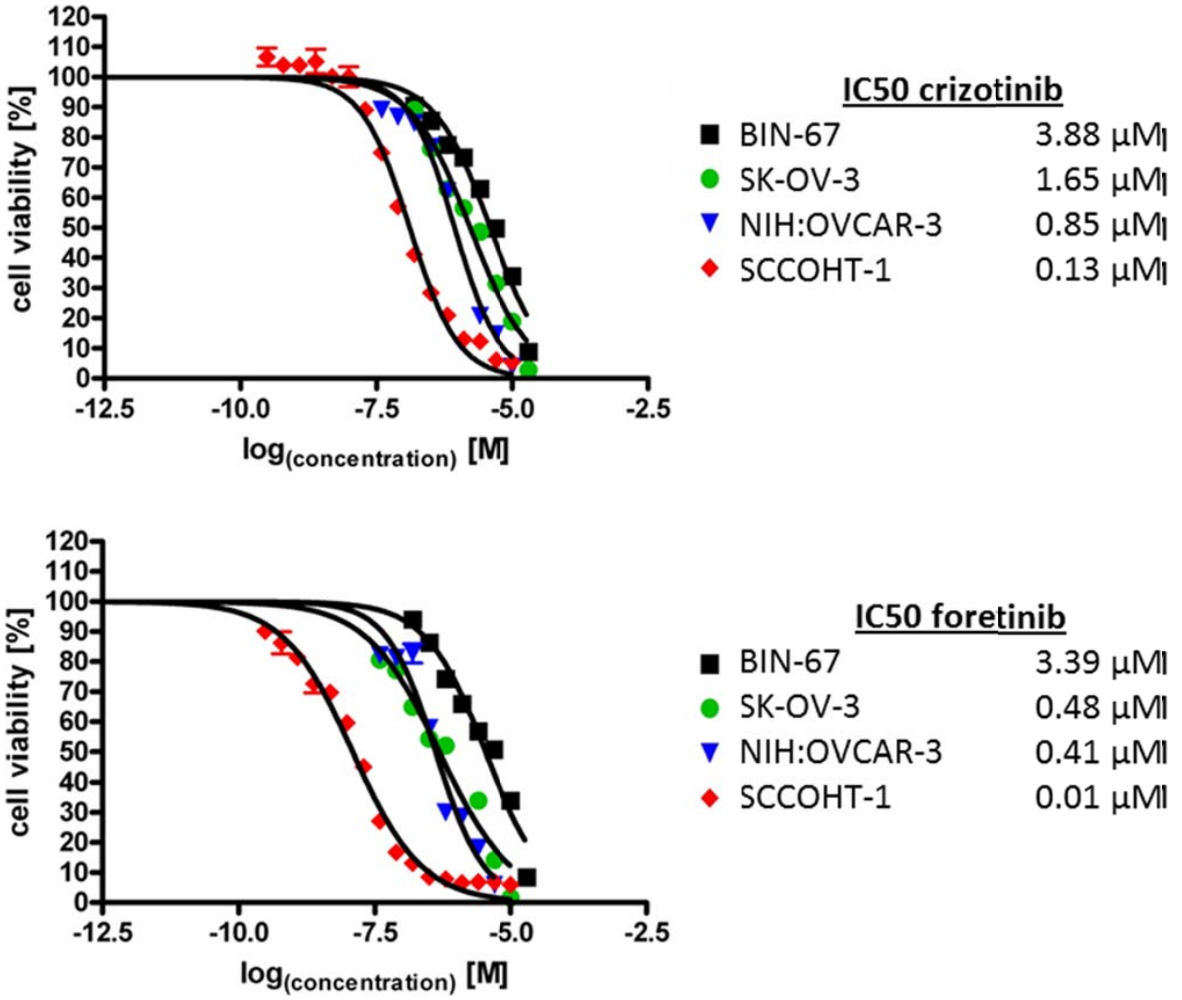

Figure 5: (*Continued*) B. SCCOHT-1^{GFP}, BIN-67^{GFP}, NIH:OVCAR-3^{GFP} and SK-OV-3^{GFP} ovarian cancer cells were incubated with different concentrations of crizotinib and foretinib for 72 h, respectively, and the proliferative capacity was measured by the fluoroscan assay**.** Analysis of a drug-dose-response to define IC50 concentrations for crizotinib and foretinib was performed using GraphPad Prism-6. For calculation of the drug-dose-response curves, the data were normalized to the cells-only control in culture medium and to the maximal solvent (DMSO) concentration control of the two compounds, respectively.

foretinib-treated BIN-67 tumors (Fig. 6C, right panel). In parallel, the body weight of mice carrying BIN-67 tumor xenografts remained relatively constant and revealed no significant differences during foretinib treatment (suppl. Fig. S4, right panel).

Further analysis by RT-PCR revealed a strong c-Met expression in SK-OV-3 and NIH:OVCAR-3 cells and low levels in BIN-67 cells. Expression of c-Met in SCCOHT-1 cells was also detectable in the original SCCOHT patient tumor and in SCCOHT-1-induced and BIN-67-induced tumor xenografts whereas a reduced expression appeared in both foretinib-treated tumors (Fig. 6D). Low levels of HGF transcripts in NIH:OVCAR-3, SK-OV-3, and BIN-67 cells were paralleled by nearly unaltered levels in SCCOHT-1 cells and the SCCOHT-1 *in vivo* tumors whereas the low HGF expression in BIN-67 *in vivo* tumors decreased to undetectable signals after foretinib treatment. Differences in the CD90 and EpCAM mRNA transcripts between the ovarian adenocarcinoma NIH:OVCAR-3 and SK-OV-3 compared to BIN-67 and SCCOHT-1 cells and associated *in vivo* tumors substantiated the special entity of SCCOHT tumors (Fig. 6D).

Analysis of c-Met protein expression in control tumor xenografts by Western blot revealed a reduction in both, the 170kDa preform and the 140kDa active HGF receptor following a 10 day foretinib treatment of the mice. Moreover, the phosphorylation signal of c-Met at Tyr1003 present in the control tumors was abolished after foretinib

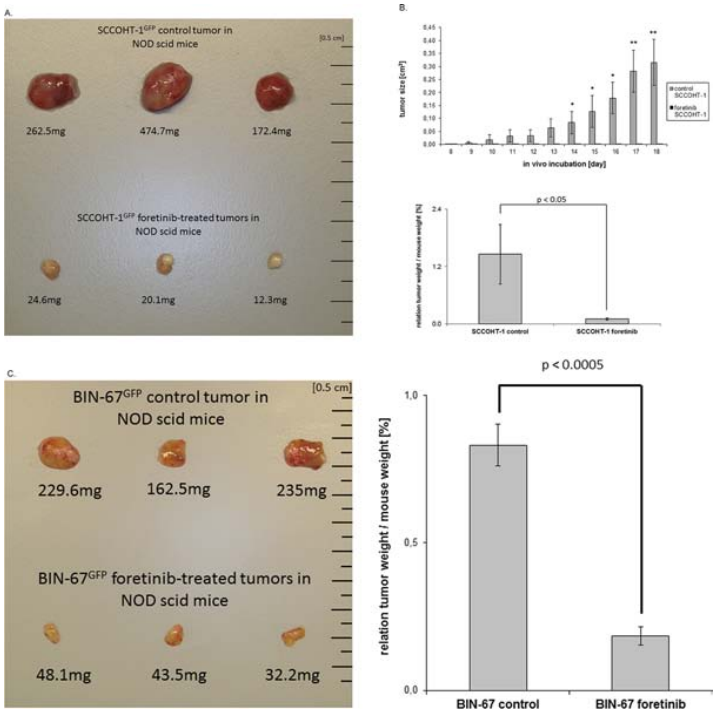

Figure 6: A. Size and weight of SCCOHT-1^{GFP}-induced tumors in NOD^{scid} mice was compared in the absence or presence of a 10 days therapeutic approach with foretinib. Following initial tumor detection, daily oral application was performed in 3 mice with 200 µl foretinib at a concentration of 50 mg/kg dissolved in 30% (v/v) propylene glycol, 5% (v/v) Tween 80, and 65% (v/v) of a 5% (w/v) dextrose solution in H_2O. The other 3 mice were used as controls by a daily oral application of 200 µl of the solvent (30% (v/v) propylene glycol, 5% (v/v) Tween 80, and 65% (v/v) of a 5% (w/v) dextrose solution in H2O). After 10d of therapy, all 6 mice were sacrificed by cervical dislocation and the GFP-positive tumors were dissected under UV light, washed in PBS, and weighted. **B.** The tumor size (upper panel) of SCCOHT-1^{GFP}-induced tumors in NOD^{scid} mice in the absence or presence of foretinib treatment was evaluated each day at 10 consecutive days of daily oral application as the mean ± s.d. for control tumors ($n = 3$) and foretinib-treated tumors ($n = 3$). Statistical analysis was calculated by unpaired Student's t-test (*$P < 0.05$; **$P < 0.01$). In the bottom panel, the relation of SCCOHT-1 tumor weight / mouse weight was calculated after 10d of subsequent treatment as the mean ± s.d. for control tumors ($n = 3$) and foretinib-treated tumors ($n = 3$). Statistical analysis was conducted by unpaired Student's t-test (*$P < 0.05$). **C.** Size and weight of BIN-67^{GFP}-induced tumors in NOD^{scid} mice was compared in the absence or presence of a 10 days therapeutic approach with foretinib (left panel). The relation of BIN-67 tumor weight / mouse weight (right panel) was calculated after 10d of subsequent treatment as the mean ± s.d. for control tumors ($n = 3$) and foretinib-treated tumors ($n = 3$). Statistical analysis was conducted by unpaired Student's t-test (*$P < 0.0005$).

application (Fig. 6E). In addition, downstream signaling by phosphorylation of p44/42 MAPK remained undetectable in foretinib-treated tumors whereby GAPDH expression was used as a control (Fig. 6E). These data suggested that the significantly reduced tumor size was associated at least in part with interruption of c-Met signaling followed by growth arrest after foretinib exposure. Supportive data were obtained by immunohistochemistry of the *in vivo* SCCOHT-1 (Fig. 6F) and BIN-67 (Fig. 6G) tumors. Staining with hematoxylin/eosin (HE) revealed various mitotic tumor cells in control tumor tissue in the vicinity of capillaries and microvessels. In contrast, less mitotic tumor cells and a significantly reduced vascularization were observed in the foretinib-treated tumors (Fig. 6F and 6G, upper panel). Moreover, the proliferation marker Ki-67 stained the majority of cells in the control tumor (about 91% in SCCOHT-1 and 31% in BIN-67) whereas only about 54% of Ki-67-positive SCCOHT-1 cells and about 17% of Ki-67-positive BIN-67 cells were detectable after foretinib application (Fig. 6F and 6G, lower panel). Together, these findings substantiated an attenuation of SCCOHT-1- and BIN-67-mediated tumor growth paralleled by a reduced vascularization in the yellow foretinib-treated tumors, respectively.

The involvement of c-Met on cell growth was also tested by c-Met siRNA knock-down in SCCOHT-1. Transfection efficiency using an appropriate green fluorescing probe revealed about 92% (suppl. Fig. S5).

Effects of the c-Met siRNA were confirmed by Western blot analysis. A pronounced c-Met expression was detectable in control SCCOHT-1 cells, in cells using the transfection reagent alone (transfection control), and in cells transfected with 25 nM of a non-targeting control siRNA after 24 h (Fig. 7A). In contrast, down-modulation of c-Met protein was observed in c-Met siRNA-transfected SCCOHT-1 cells for up to 120 h (Fig. 7A). This down-modulation of c-Met in SCCOHT-1 caused a progressive growth reduction with a proliferative capacity of 35.1% ± 1.4% in c-Met siRNA-transfected cells as compared to about 100% in control cells and control transfectants after 72 h (Fig. 7B, upper panel). Moreover, c-Met siRNA-mediated growth inhibition in SCCOHT-1 cells was also accompanied by an accumulation of apoptotic cells in subG1 and an increase in G0/G1 cell cycle phase with reduced S phase (Fig.7B, lower panel).

C-Met siRNA knock-down also abolished HGF-mediated phosphorylation signaling of the receptor. Whereas SCCOHT-1 transfection control and cells transfected with a non-targeting siRNA demonstrated increased c-Met phosphorylation at Tyr1349 as well as more downstream an increased p44/p42 MAP kinase phosphorylation at Thr202/Tyr204 after 5 min to 20 min of stimulation with 20 ng/ml HGF, little if any phosphorylation signal was observed in c-Met siRNA-transfected SCCOHT-1 cells (Fig. 7C). Likewise, expression of the c-Met receptor itself remained undetectable in c-Met siRNA-transfected SCCOHT-1 cells in contrast to constitutive c-Met expression in SCCOHT-1 transfection control and cells transfected with a non-targeting siRNA (Fig. 7C).

At a more functional level, down-modulation of c-Met in SCCOHT-1 cells also reduced tumor growth *in vivo*. Whereas 1 mouse with a control tumor died during the experiment, 5 mice developed pronounced and partially red-colored tumors within 22d (Fig. 7D, upper panel) indicating an appropriate tumor vascularization. Similar data were obtained from tumors of 6 mice injected with non-coding siRNA-transfected SCCOHT-1^{GFP} cells (Fig. 7D, lower panel). In contrast, mouse tumor xenografts of c-Met siRNA-transfected SCCOHT-1^{GFP} cells were observed only in 4/6 mice and appeared much smaller and less vascularized (Fig. 7D, middle panel). Calculation of the relation of tumor weight/mouse weight revealed 0.92 ± 0.51 (n = 5) for the transfection control and 0.94 ± 0.8 (n = 6) for the non-targeting siRNA-induced tumors. In contrast, c-Met siRNA-mediated

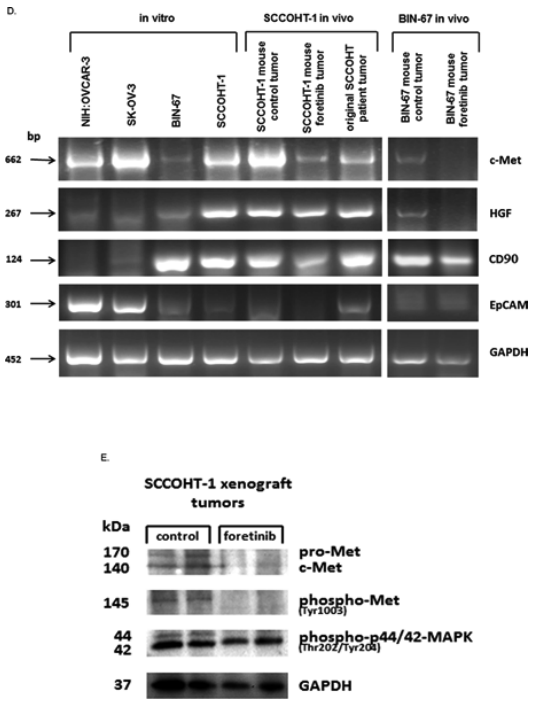

Figure 6: (*Continued*) D. The mRNA expression levels of various genes were analyzed by RT-PCR in the 4 ovarian cancer cell lines in vitro and compared to the in vivo NOD^{scid} SCCOHT-1 xenograft tumors together with the original patient tumor and to the in vivo BIN-67^{GFP} xenograft tumors following daily oral foretinib application for 10 consecutive days. **E.** Analysis of c-Met protein expression and associated phosphorylation signals in 2 control tumor xenografts (#1.2 and #1.3) was compared to 2 foretinib-treated tumor xenografts (#2.3 and #2.4) by Western blot analysis.

(*Continued*)

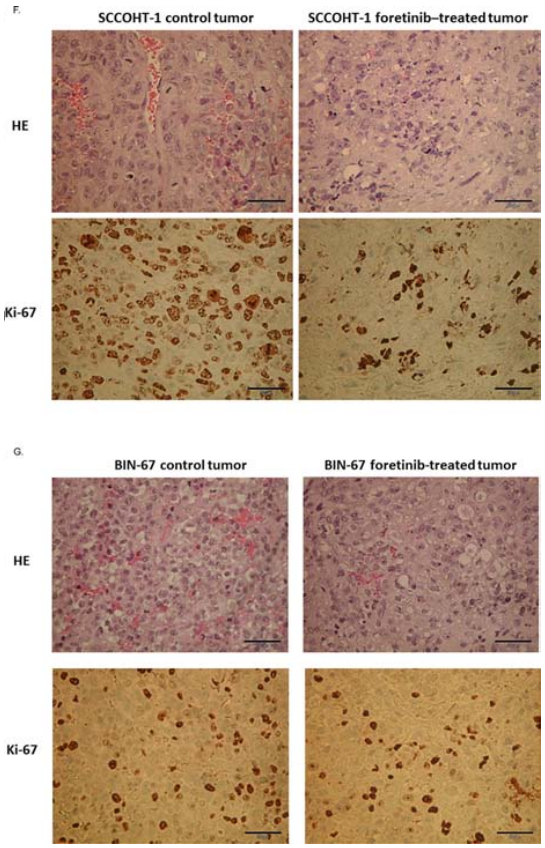

Figure 6: (*Continued*) F. Tissue sections (4 μm) were prepared by hematoxylin/eosin staining (HE) of SCCOHT-1^{GFP}-induced control and foretinib-treated tumors in NOD^{scid} mice (upper panel; bars represent 50 μm). In addition, tissue sections (4 μm) of control and foretinib-treated tumor xenografts were compared by immune histochemistry using the proliferation marker Ki-67 (lower panel; bars represent 50 μm). **G.** Tissue sections (4 μm) were prepared by hematoxylin/eosin staining (HE) of BIN-67^{GFP}-induced control and foretinib-treated tumors in NOD^{scid} mice (upper panel; bars represent 50 μm). In addition, tissue sections (4 μm) of control and foretinib-treated tumor xenografts were compared by immune histochemistry using the proliferation marker Ki-67 (lower panel; bars represent 50 μm).

tumors displayed an approximately 20-fold reduced ratio of 0.04 ± 0.04 (n = 6) (Fig. 7E).

Together, these data demonstrated an attenuation of tumor growth in SCCOHT-1 cells by targeting c-Met via antisense or via c-Met signaling interference compounds including foretinib. However, BIN-67 cells express only background levels of c-Met although foretinib treatment exhibited a significant tumor reduction which suggested additional effects of this compound. Indeed, foretinib treatment was also associated with interference of vascular endothelial growth factor (VEGF) signaling. Whereas VEGF was expressed by the ovarian tumor cell lines and by the SCCOHT tumors, transcripts of the related receptor VEGFR2 appeared species-specific and were observed exclusively in the corresponding human and mouse tumors, respectively (Fig. 7F). In particular, VEGFR2 expression exclusively in the original SCCOHT patient tumor but not in the corresponding SCCOHT-1 cells which were derived from this human tumor suggested paracrine VEGF effects by expression of this receptor in tumor-associated tissue rather than in the tumor cells. Moreover, foretinib treatment significantly reduced the VEGFR2 expression in the mouse tumors furthermore supporting additional effects of this drug also on the tumor microenvironment e.g. by reduced vascularization (Fig.7F).

DISCUSSION

SCCOHT represents a rare and aggressive tumor type with unclear etiology and insufficient therapeutic strategies. Whereas mutations in the *SMARCA4* gene and certain similarities to malignant rhabdoid tumors are known for this cancerous disease [14–16, 20] further characterization of the corresponding cellular models SCCOHT-1 and BIN-67 demonstrated significant

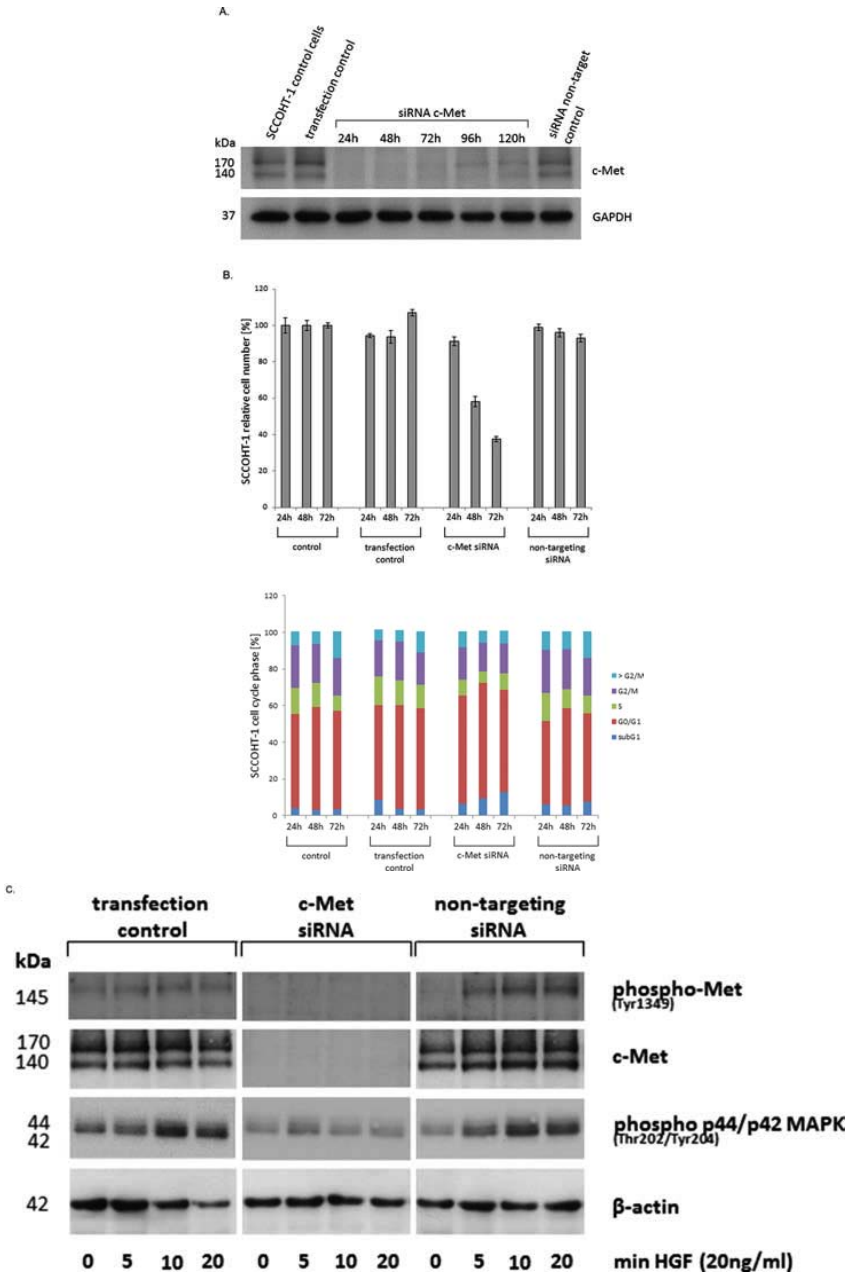

Figure 7: A. Western blot of c-Met in SCCOHT-1 steady state control cells, in cells using the transfection reagent alone (transfection control), and in cells with 25 nM of a non-targeting control siRNA was performed 24 h after transfection. For c-Met siRNA-transfected SCCOHT-1 cells Western blots were performed between 24 h and 120 h post transfection. Analysis for GAPDH served as a loading control. **B.** Proliferative capacity (upper panel) and percentage of cell cycle phases (lower panel) of steady state SCCOHT-1 cells (control) was compared to cells after 24 h in the presence of the transfection reagent (transfection control), to cells transfected with c-Met siRNA (c-Met siRNA) and to cells transfected with a non-targeting siRNA (non-targeting siRNA). Cell numbers were counted for 24 h to 72 h and normalized ot the cell number of control cells (=100%). Data represent the mean ± s.d. of 3 independent experiments. **C.** Western blot of c-Met signaling was examined in SCCOHT-1 cells incubated with the transfection reagent for 24 h (transfection control), in cells transfected with 25 nM c-Met siRNA (c-Met siRNA), and in cells transfected with 25 nM of a non-targeting siRNA (non-targeting siRNA). In comparison to non-stimulated cells (0), the different populations were incubated with 20 ng/ml HGF for 5 min, 10 min, and 20 min, respectively. Expression of β-actin was used as a loading control.

(*Continued*)

differences in surface marker and filament expression compared to ovarian adenocarcinoma cells and therefore confirmed SCCOHT as a separate tumor entity with distinct growth properties. However, the growth factor receptor c-Met revealed common presences in the ovarian adenocarcinoma cells and to a lesser extend in SCCOHT-1 and BIN-67 cells.

The membrane receptor c-Met (Mesenchymal epithelial transition factor), also known as hepatocyte growth factor/scatter factor receptor is essential for embryonic development and wound healing [27]. In tumors, however, including ovarian cancer, c-MET overexpression and paralleled hyperactivation correlates with poor prognosis by triggering tumor growth, metastasis and angiogenesis [28–30]. Constitutive c-Met expression and enhanced angiogenic properties in SCCOHT-1 cells are also supported by their capacity of to produce and release VEGF and VCAM-1 into the tumor microenvironment which are essential for tumor neo-vascularization. Likewise, IL-8 (CXCL8) is associated with angiogenesis besides an involvement in inflammatory processes [31]. Moreover, the distinct chemokine/growth factor production by SCCOHT-1 cells including a constitutive HGF production suggested an autocrine loop for c-Met-relayed proliferation signals which could serve as a more specific therapeutic target in these cells. Additional exogenous HGF stimulation resulted in c-Met phosphorylation and enhanced downstream signaling by elevated p44/42-MAP kinase activation in SCCOHT-1 and the ovarian adenocarcinoma cells. Indeed, several phosphorylation sites are identified in the cytoplasmic c-Met domain to confer Erk/MAP kinase activation for induced proliferation and cell cycle progression in a variety of different tumor types including ovarian cancer [32–34]. Targeted approaches to antagonize aberrant c-Met signaling include therapeutic intervention in 1) ligand/receptor interaction, 2) inhibition of the tyrosine kinase catalytic activity, and 3) blockade of activated receptor/effector interaction. Thus, crizotinib and foretinib represent multi-targeted tyrosine kinase inhibitors to block c-Met signaling whereby foretinib was even more efficient to completely abolish both, constitutive and HGF-induced

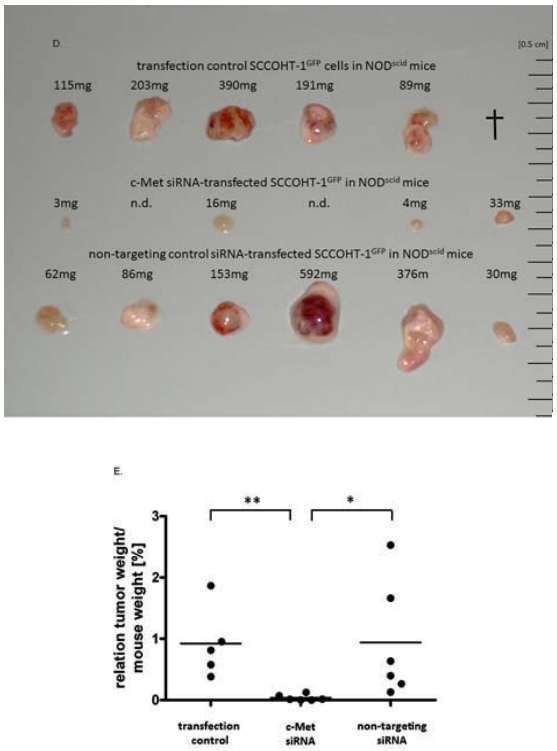

Figure 7: (*Continued*) D. *In vivo* tumor development was evaluated after 22d of subcutaneous injection of 3×10^6 SCCOHT-1^{GFP} cells 24 h after transfection into 6 NOD^{scid} mice, respectively. Steady state control cells with transfection reagent (upper row) were compared to c-Met siRNA-mediated tumors (middle row) and tumors of a non-targeting control siRNA (lower row). In the control tumor section 1 mouse died in the course of the experiment (†, upper row). In the c-Met siRNA-transfected SCCOHT-1 cells 2 tumor developments were not detectable (n.d., middle row). Each tumor was verified by fluorescence microcopy demonstrating GFP expression. **E.** The relation of tumor weight / mouse weight of tumors from Fig. 7D was calculated Statistical analysis was conducted by unpaired Student's *t*-test (*****$P < 0.05$; ******$P < 0.005$).

(*Continued*)

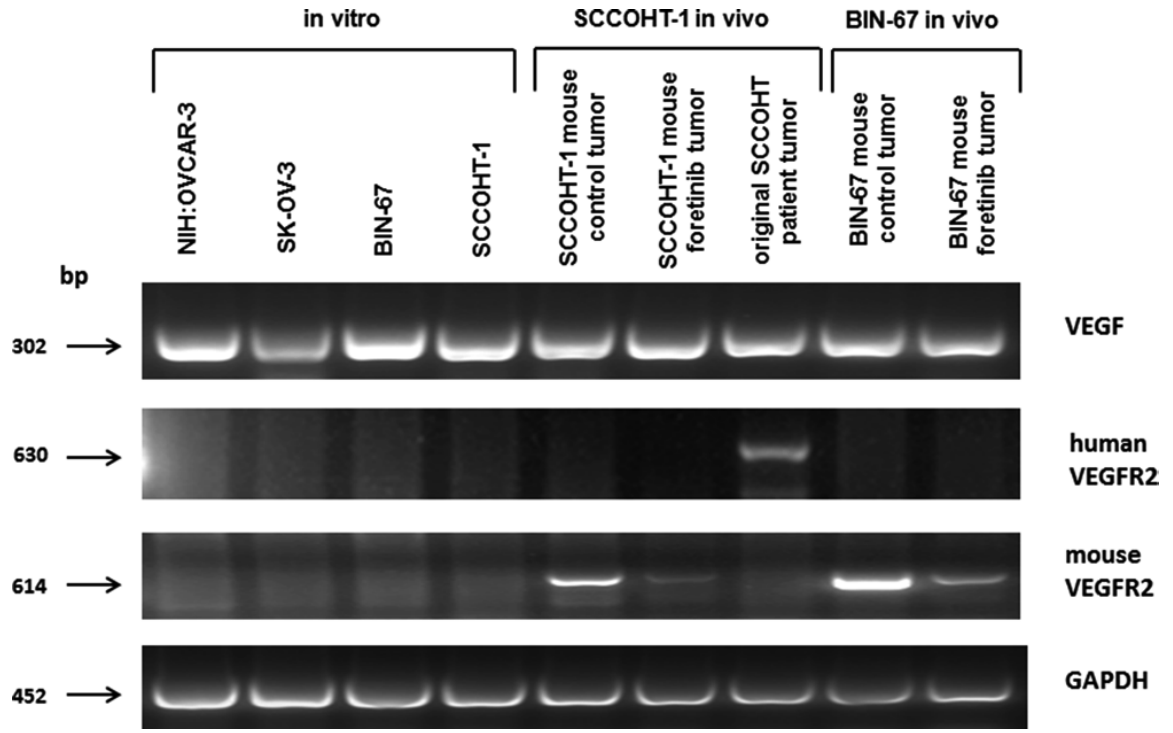

Figure 7: (*Continued*) F. The mRNA expression levels of VEGF and human and mouse VEGFR2 was analyzed by RT-PCR in the 4 ovarian cancer cell lines *in vitro* and compared to the *in vivo* NOD^{scid} SCCOHT-1 and BIN-67^{GFP} xenograft tumors together with the original patient tumor of SCCOHT-1 cells. GAPDH expression levels served as a control.

c-Met and subsequent MAP kinase phosphorylation in the ovarian adenocarcinoma as well as in the small cell hypercalcemic ovarian cancer cells. Simultaneously, these c-Met inhibitors effectively inhibited proliferation of the tumor cells by a pronounced G2/M cell cycle arrest and confirmed previous findings in foretinib-treated SK-OV-3 cells [35]. Since foretinib appears as a more potent inhibitor than crizotinib also in patients with ROS1-rearranged non-small-cell lung carcinoma [36], further *in vivo* studies revealed anti-tumorigenic effects of foretinib in lung metastasis [37] and in patients with sonic hedgehog-driven medulloblastoma [38]. In the present study, we could demonstrate a substantial therapeutic effect of foretinib by attenuating growth of SCCOHT-1- and BIN-67-induced tumors although SCCOHT-1 xenograft tumors developed much more rapidly. Both populations provide a cellular model for the rare SCCOHT whereby detectable c-Met expression was observed preferably in SCCOHT-1 cells and in the majority of SCCOHT tumor samples. Consequently, c-Met and associated targets by foretinib treatment represent a potential therapeutic approach for this tumor entity. Moreover, foretinib displayed additional effects by down-modulation of the VEGFR2 within the SCCOHT tumor microenvironment and thereby reduced cancer growth also in BIN-67-induced tumors with little or barely detectable c-Met expression.

Together, interference with c-Met signaling *in vivo* significantly diminished the SCCOHT-1 and BIN-67 tumor sizes, respectively. This effect was paralleled by a marked reduction of growth-associated structures in the tumor microenvironment such as tumor vascularization. Supportive evidence for anti-tumor activity of foretinib by inhibition of c-Met and vascular endothelial growth factor receptor 2 was obtained in models of hepatocellular carcinoma [39], renal cell carcinoma [40], and gastric cancer [41] which also underscores the importance to simultaneously target the tumor microenvironment by blocking neo-vascularization. In this context, interaction of SCCOHT-1 tumor cells by a close vicinity to mesenchymal stroma/stem cells in the tumor microenvironment can transfer proteins, RNAs and further biological material thereby altering cellular functionality and contributing to increased tumor heterogeneity [42–46].

In conclusion, the data suggested that in all presently available models of the rare SCCOHT tumor entity the attenuation of *in vivo* SCCOHT-1 or BIN-67 tumor growth and vascularization blockage by foretinib provides a specific target to further support a combination with cytotoxic agents in a promising therapeutic approach.

MATERIAL AND METHODS

Cell Culture

Culture of human SCCOHT cells

Cellular models of SCCOHT are represented by the two cell lines BIN-67 and SCCOHT-1. BIN-67 were kindly provided by Dr. Barbara Vanderhyden (University of Ottawa, Canada) and cultured with DMEM/F12 : DMEM medium (1:1) (Sigma Aldrich, St. Louis, MO) supplemented with 20% (v/v) fetal calf serum, 2 mM L-glutamine, 100 U/ml penicillin and 100 µg/ml streptomycin [21].

SCCOHT-1 cells were generated in our lab as a spontaneously growing primary culture derived from a tumor biopsy of a 31-year-old patient with recurrent SCCOHT [18]. The study has been approved by the Ethics Committee of Hannover Medical School, Project #3916 on June 15th, 2005 and informed written consent was obtained from the patient for the use of this material. The SCCOHT-1 cells were cultured in RPMI 1640 supplemented with 10% (v/v) fetal calf serum, 100 U/ml L-glutamine, 100 U/ml penicillin and 100 µg/ml streptomycin. Serum-free cultures of SCCOHT-1 were maintained in HybridoMed DIF 1000 medium (Biochrom, Berlin, Germany). The cell culture was performed at 37°C in a humidified atmosphere of 5% (v/v) CO_2 and the culture medium was changed at intervals of 3 to 4 days. For subculture, the cells were centrifuged (320 g/6 min) and resuspended in the appropriate growth medium.

Human ovarian adenocarcinoma cell lines

Human NIH:OVCAR-3 ovarian cancer cells (ATCC® #HTB-161™) were commercially obtained in passage 76 (P76) from the Institute for Applied Cell Culture (IAZ), Munich, Germany. The SK-OV-3 ovarian cancer cells (ATCC® #HTB-77™) were commercially obtained in P25 from the ATCC, Manassas, VA, USA. These two cell lines were originally established from the malignant ascites of a patient with progressive adenocarcinoma of the ovary, respectively. Both cell types were cultivated at about 1,750 cells/cm^2 in RPMI 1640 supplemented with 10% (v/v) fetal calf serum, 100 U/ml L-glutamine, 100 U/ml penicillin and 100 µg/ml streptomycin. Subculture was performed by trypsin/EDTA (Biochrom GmbH, Berlin, Germany) treatment for 5 min at 37°C.

Cell line authentication

All cells were tested for mycoplasma by the luminometric MycoAlert Plus mycoplasma detection kit (Lonza Inc., Rockland, ME, USA) according to the manufacturer's recommendations. Moreover, authentication of SCCOHT-1, BIN-67, NIH:OVCAR-3, and SK-OV-3 cell lines was performed by short tandem repeat (STR) fragment analysis using the GenomeLab human STR primer set (Beckman Coulter Inc., Fullerton, CA, USA). The fragment analysis for the NIH:OVCAR-3 and SK-OV-3 cell lines demonstrated a similar STR pattern according to the STR database provided by the Deutsche Sammlung von Mikroorganismen und Zellkulturen (DSMZ, Braunschweig, Germany).

Whereas no STR patterns are available for SCCOHT-1 and BIN-67 cells to date, repeated STR fragment analyses were performed for these two cell populations. Data from different SCCOHT-1 culture periods (n = 3) confirmed similar patterns and these STR pattern were presented in suppl. Fig. S6.

Cytokine production and release

Following culture of 2 × 10^5/ml SCCOHT-1 cells in serum-free HybridoMed DIF 1000 medium, supernatants were collected after 48 h and 72 h, respectively. The conditioned medium was filtered in a 0,2 µm filter (Sartorius Stedim Biotech GmbH, Göttingen, Germany) to remove cells and debris, and aliquots were shockfrozen in liquid nitrogen and stored at -80°C until measurement. Aliquots of the supernatants were applied to a Quantibody® array (RayBiotech Inc., Norcross, GA, USA / tebu-bio GmbH, Offenbach, Germany), which represents a quantitative array platform by using a multiplexed sandwich ELISA-based technology. This method allows to simultaneously and quantitatively determine the concentration of multiple cytokines. Membranes of the Quantibody Human Chemokine Array (RayBiotech Inc./ tebu-bio GmbH) were incubated with the cell supernatants in comparison to control medium in quadruplicates and developed by chemiluminescence according to the manufacturer's instructions. Chemokine concentrations were measured (based on internal controls) in pg/ml + s.d. (n = 4) using appropriate manufacturer's software.

Analysis of surface markers by flow cytometry

Continuously proliferating SCCOHT-1, BIN-67, NIH:OVCAR-3 and SK-OV-3 cells in logarithmic growth phase were harvested and analyzed for cell surface marker expression by flow cytometry. After blocking non-specific binding to Fc-receptors by incubation of 10^6 cells with 2% FCS for 30 min at 4°C and washing with PBS-BSA, the cells were incubated with the following appropriately-labeled monoclonal anti-human antibodies, respectively: c-Met-FITC (clone eBioclone97, IgG1, eBioscience, Inc., San Diego, CA, USA); CD29-PE (clone MAR4, IgG1, BD Biosciences, Heidelberg, Germany); CD44-FITC (clone G44–26, IgG2b, BD Biosciences); CD90-PE (clone 5E10, IgG1, BioLegend Inc., San Diego, CA, USA); CD105-PE (clone 43A3, IgG1, BioLegend Inc.); CD326-PE (clone G9C4, IgG2b, BioLegend Inc.); vimentin-PE (clone VI-RE-1, IgG1, antibodies-online Inc., Atlanta, GA, USA); pan-cytokeratin-PE (clone C-11, IgG1, Acris Antibodies GmbH, Herford, Germany); Following antibody staining,

all samples were washed twice with PBS-BSA. Moreover, SCCOHT-1, BIN-67, NIH:OVACAR-3 and SK-OV-3 cells were incubated with a primary monoclonal anti-human mesothelin antibody (clone K1, IgG1, abcam plc, Cambridge, UK), respectively, followed by two washes with PBS-BSA and subsequent addition of a secondary PE-labeled polyclonal rabbit anti-mouse antibody (DakoCytomation Inc., Glostrup, Denmark).

A parallel incubation of the cells with appropriately-labeled antibodies of the corresponding Ig subclass were used as controls. Flow cytometry analysis was performed in a Galaxy FACSan (Partec) using FloMax analysis software (Partec).

Immunohistochemical c-Met analysis in SCCOHT patient tumors

Immunohistochemistry was performed on an automated staining instrument (Benchmark Ultra; Ventana, Tuscon, U.S.A) using the CC1 mild antigen retrieval procedure and a monoclonal anti-c-Met antibody (clone D1C2, rabbit, Cell Signaling Technology, Danvers, MA, USA), diluted at 1:100 in primary antibody diluent following the manufacturer's recommendations. Semiquantitative slide evaluation by two observers (RH/FF) included scoring of staining intensity (0, 1+, 2+, 3+) and estimation of percentage of positive cells in 10% increments.

Immunoblot analysis

Cell lysates of SCCOHT-1, BIN-67, NIH:OVCAR-3 or SK-OV-3 cells were prepared in reswelling buffer containing 8 M urea (Carl Roth GmbH Co KG, Karlsruhe, Germany), 1% CHAPS (3-[(3-Cholamidopropyl)-dimethylammonio]-1-propanesulfonate) (Carl Roth GmbH Co KG), 0.5% (v/v) Pharmalyte 3 –10 (GE Healthcare Europe GmbH, Freiburg, Germany), 0.002% (w/v) bromophenol blue (SERVA Electrophoresis GmbH, Heidelberg, Germany) and freshly prepared 0.4% (w/v) DTT (Dithiothreitol) (Carl Roth GmbH Co KG). Protein concentration of the cell lysates was adjusted using the colorimetric BCA-assay (Thermo Scientific, Schwerte, Germany). Aliquots of 40 µg protein were subjected to SDS-polyacrylamide gel electrophoresis and transferred to a Amersham™ Protran™-Supported 0.45 µm nitrocellulose membrane (GE Healthcare). The membranes were blocked with PBS containing 5% low fat milk and 0.05% Tween-20 (PBS/Tween). After washing four times with PBS/Tween, the membranes were incubated with the primary antibodies: monoclonal anti-c-Met (clone D1C2, rabbit, (dilution 1:1,000); Cell Signaling Technology, Danvers, MA, USA); monoclonal anti-phospho-Met (Tyr1349) (clone 130H2, rabbit, (dilution 1:1,000); Cell Signaling Technology); monoclonal anti-phospho-Met (Tyr1003) (clone 13D11, rabbit, (dilution 1:1000), Cell Signaling Technology); polyclonal anti-phospho p44/42 MAP kinase (Thr202/Tyr204) (rabbit, (dilution 1:1,000), Cell Signaling Technology); monoclonal anti-GAPDH (clone 6C5, mouse, (dilution 1:200), Santa Cruz Biotechnology Inc., Dallas, Texas, USA); monoclonal anti-β-actin (clone AC-15, mouse, (dilution 1:1,000), Sigma, St. Louis, Missouri, USA). Thereafter, the membranes were washed four times with PBS/Tween and incubated with the appropriate horseradish peroxidase-conjugated anti-mouse IgG (dilution 1:5,000) or anti-rabbit IgG (dilution 1:2,000) secondary antibody, respectively, (all from GE Healthcare, Freiburg, Germany) for 1 h/room temperature. The membranes were washed with PBS/Tween and visualized by autoradiography using SuperSignal West Pico Chemiluminescent Substrate (Thermo Scientific, Schwerte, Germany).

Cell cycle analysis

Cell cycle analysis compared to untreated controls was performed in 5×10^5 SCCOHT-1, BIN-67, NIH:OVCAR-3 or SK-OV-3 cells after culture either in the presence of 0.025% (v/v) DMSO (Sigma) as solvent, 2.5 µM crizotinib, or 1.25 µM foretinib (= GSK1363089; = PF-02341066) (both from Selleck Chemicals LLC, Houston,TX,USA) for up to 72 h, respectively. The cells were fixed in 70% (v/v) ice-cold ethanol at 4°C for 24 h. Thereafter, the fixed cells were stained with CyStain DNA 2 step kit (Partec GmbH, Münster, Germany) and filtered through a 50 µm filter. Flow cytometry analysis was performed in a Galaxy FACSan (Partec) using FloMax analysis software (Partec).

Proliferation rate

The proliferative capacity and the sensitivity of SCCOHT-1, BIN-67, NIH:OVCAR-3 and SK-OV-3 cells was determined for different concentrations of crizotinib and foretinib. In a fluorescence-based proliferation assay the ovarian cancer cell types were transduced with a 3rd generation lentiviral SIN vector containing the eGFP gene as previously described for these cells [18, 19]. The different eGFP-transduced ovarian cancer cell populations (SCCOHT-1^{GFP}, BIN-67^{GFP}, NIH:OVCAR-3^{GFP} and SK-OV-3^{GFP}) were incubated with culture medium in flat bottom 96-well plates (Nunc/ThermoFischer) at a density of 3×10^3 cells/well and following incubation for 24 h, 48 h, and 72 h, the medium was removed and the cells were lysed with 5% (w/v) SDS. Afterwards, the fluorescence intensities of GFP in the cell homogenate which corresponded to the appropriate cell number of ovarian cancer cells was measured at excitation 485 nm / emission 520 nm using the Fluoroscan Ascent Fl (Thermo Fisher Scientific).

In vivo experiments

Animal research using NOD^{scid} mice was carried out by following internationally recognized guidelines on animal welfare and has been approved by the institutional licensing committee ref. #33.14–42502-04–12/0814 on June 26th, 2012.

About 3 × 10^6 SCCOHT-1^{GFP} or BIN-67^{GFP} cells were injected subcutaneously into 5 weeks old female NOD^{scid} mice (n = 6 for each cell line). Within 8 days, the 6 SCCOHT-1-treated mice and after 71d the other 6 BIN-67-treated mice had developed small subcutaneous tumors. Systemic therapy was performed in 3 mice of both cell line-induced tumors by a daily oral application of 200 µl foretinib (GSK1363089) (50 mg/kg) (Selleck Chemicals LLC) dissolved in 30% (v/v) propylene glycol, 5% (v/v) Tween 80, and 65% (v/v) of a 5% (w/v) dextrose solution in H_2O. The other 3 mice of both cell line-induced tumors were used as controls by a daily oral application of 200 µl of the solvent (30% (v/v) propylene glycol, 5% (v/v) Tween 80, and 65% (v/v) of a 5% (w/v) dextrose solution in H_2O). Although foretinib in clinical studies is administered to patients between 3.6 mg/kg to 4.5 mg/kg [47], *in vivo* mouse experiments including recent studies are performed at foretinib concentrations of 60 mg/kg to 100 mg/kg [38].

Oral application was performed using plastic feeding tubes (18 ga × 30 mm) (Instech Laboratories, Plymouth, PA, USA). Following 10d of therapy, the 6 mice of each cell line-induced tumors were sacrificed by cervical dislocation. Tumor volumes (V) of SCCOHT-1 tumors were calculated with the longitudinal diameter (length) and the transverse diameter (width) in the modified ellipsoidal formula $V = \pi/6 * \text{width} * (\text{length})^2$ [48].

The GFP-positive tumors were dissected under UV light, washed in PBS, weighted and either cryo-preserved in liquid nitrogen for subsequent PCR and Western blot analysis or fixed in 4% glutardialdehyde solution for histopathological evaluations.

Transcript analysis by RT-PCR

Total RNA was isolated from cells and tumor tissues using RNeasy Mini Kit (Qiagen, Hilden, Germany) according to the manufacturer's instructions. One µg RNA was reverse transcribed into cDNA using 500 µM of dNTP (R0193), 5 µM Oligo(dT)18 primer (S0132), 5 µM Random Hexan primer (S0142), 1 U RiboLockTM RNase Inhibitor (E00381) and 5 U RevertAidTM M-MuLV Reverse Transcriptase (EP0441) in the supplied reaction buffer (all reagents from Thermo Scientific, Schwerte, Germany). The cDNA reactions were performed for 10 min/25°C, 1 h/37°C and stopped at 72°C for 10 min. As a template 2.5 µl of cDNA was used with primers specific for:

- Hepatocyte growth factor (scatter factor) (HGF) (sense: 5′-AGG AGA AGG CTA CAG GGG CAC-3′; antisense: 5′-TTT TTG CCA TTC CCA CGA TAA-3′; amplification product 267 bp) [49];
- c-Met (sense: 5′-CAG GCA GTG CAG CAT GTA GTG-3′; antisense: 5′-TAA GGT GGG GCT CCT CTT GTC A-3′; amplification product 662 bp) [50];
- CD90 (sense: 5′-GGA CTG AGA TCC CAG AAC CA-3′; antisense: 5′-ACG AAG GCT CTG GTC CAC TA-3′; amplification product 124 bp) [51]);
- EpCAM (sense: 5′-GAA GGC TGA GAT AAA GGA GAT GGG-3′; antisense: 5′-TTA ACG ATG GAG TCC AAG TTC TGG-3′ amplification product 301 bp) [52];
- VEGF-A (sense: 5′-CCT CAG TGG GCA CAC ACT CC-3′; antisense: 5′-CGA AAC CAT GAA CTT TCT GC-3′ amplification product 302bp) [53]
- human VEGF-R2 (sense: 5′-TTA CAG ATC TCC ATT TAT TGC-3′; antisense: 5′-TTC ATC TCA CTC CCA GAC T-3′ amplification product 630bp) [54]
- mouse VEGF-R2 (sense: 5′-ATA ACC TGG CTG ACC CGA TTC -3′; antisense: 5′-TCG GTG ATG TAC ACG ATG CC-3′ amplification product 614 bp)
- GAPDH as a control PCR (sense: 5′-ACC ACA GTC CAT GCC ATC AC-3′; antisense: 5′-TCC ACC ACC CTG TTG CTG TA-3′; amplification product 452 bp [55])

was performed (all primers customized by Eurofins, MWG GmbH, Ebersberg, Germany). PCR reactions included 0.2 µM of each primer, 200 µM of dNTP (R0193, Thermo Scientific) and 0.05 U Taq DNA Polymerase (EPO402, Thermo Scientific) in the supplied reaction buffer. PCR cycling conditions were performed 30 sec at 94°C, 1 min at 60°C and 72°C for 1 min respectively, including an initial 30 sec denaturation step at 94°C and a final 10 min extension step at 72°C (35 cycles). Aliquots of 25 µl of each RT-PCR product were separated on a 2% agarose gel including the standard GeneRuler 100 bp DNA Ladder (Thermo Scientific) and visualized by GelRedTM (Biotium Inc., Hayward, CA, US) staining.

siRNA knock-down of c-Met

For c-Met knock-down a transfection protocol was applied according to the manufacturer's instructions (Dharmacon, GE Healthcare, Uppsala, Sweden) using c-Met small interfering RNA (siRNA). Briefly, SCCOHT-1 cells were transfected with 25 nM c-Met siRNA (siGENOME human MET SMARTpool, cat. #D-003156-02) or with 25 nM of a non-targeting control siRNA (non-targeting #3 control, cat. #D-001210-03, Dharmacon, GE Healthcare, Uppsala, Sweden) using a 1:1,000 dilution of the DharmaFECT 4 transfection reagent (Dharmacon) in transfection medium (RPMI-1640 medium supplemented with 2% (v/v) fetal calf serum, 100U/ml L-glutamine) for 24 h. For evaluation of the transfection efficiency, SCCOHT-1 cells were transfected

with 25 nM of the green fluorescing siGLO^{green} (cat. #D-001630-01, Dharmacon). Thereafter, the cells were washed and cultured in normal growth medium.

ACKNOWLEDGMENT AND FUNDING

The authors are grateful to Dr. Marc-Jens Kleppa for helpful advices and providing some transfection reagent.

CONFLICTS OF INTEREST

The authors declare no conflict of interest. All authors have critically read and approved the present manuscript.

GRANT SUPPORT

This work was supported by a grant from the Niedersächsiche Krebsgesellschaft to Ralf Hass.

REFERENCES

1. Kurman RJ, Visvanathan K, Roden R, Wu TC, Shih Ie M. Early detection and treatment of ovarian cancer: shifting from early stage to minimal volume of disease based on a new model of carcinogenesis. American journal of obstetrics and gynecology. 2008; 198:351–356.
2. Kurman RJ, Shih Ie M. The origin and pathogenesis of epithelial ovarian cancer: a proposed unifying theory. The American journal of surgical pathology. 2010; 34:433–443.
3. Kim A, Ueda Y, Naka T, Enomoto T. Therapeutic strategies in epithelial ovarian cancer. J Exp Clin Cancer Res. 2012; 31:14.
4. Dubeau L. The cell of origin of ovarian epithelial tumours. The Lancet. 2008; 9:1191–1197.
5. Hafner N, Nicolaus K, Weiss S, Frey M, Diebolder H, Rengsberger M, Durst M, Runnebaum IB. p53-autoantibody may be more sensitive than CA-125 in monitoring microscopic and macroscopic residual disease after primary therapy for epithelial ovarian cancer. Journal of cancer research and clinical oncology. 2013; 139:1207–1210.
6. Dickersin GR, Kline IW, Scully RE. Small cell carcinoma of the ovary with hypercalcemia: a report of eleven cases. Cancer. 1982; 49:188–197.
7. Young RH, Oliva E, Scully RE. Small cell carcinoma of the hypercalcemic type in the ovary. Gynecologic oncology. 1995; 57:7–8.
8. Scully RE. Tumors of the Ovary and Maldeveloped Gonads. Atlas of Tumor Pathology: Washington, DC, Armed Forces Institute of Pathologym, 1979; 233–242.
9. Ulbright TM, Roth LM, Stehman FB, Talerman A, Senekjian EK. Poorly differentiated (small cell) carcinoma of the ovary in young women: evidence supporting a germ cell origin. Human pathology. 1987; 18:175–184.
10. Aguirre P, Thor AD, Scully RE. Ovarian small cell carcinoma. Histogenetic considerations based on immunohistochemical and other findings. American journal of clinical pathology. 1989; 92:140–149.
11. Walt H, Hornung R, Fink D, Dobler-Girdziunaite D, Stallmach T, Spycher MA, Maly F, Haller U, Burki N. Hypercalcemic-type of small cell carcinoma of the ovary: characterization of a new tumor line. Anticancer research. 2001; 21:3253–3259.
12. McCluggage WG, Oliva E, Connolly LE, McBride HA, Young RH. An immunohistochemical analysis of ovarian small cell carcinoma of hypercalcemic type. Int J Gynecol Pathol. 2004; 23:330–336.
13. Ramos P, Karnezis AN, Hendricks WP, Wang Y, Tembe W, Zismann VL, Legendre C, Liang WS, Russell ML, Craig DW, Farley JH, Monk BJ, Anthony SP, Sekulic A, Cunliffe HE, Huntsman DG, et al. Loss of the tumor suppressor SMARCA4 in small cell carcinoma of the ovary, hypercalcemic type (SCCOHT). Rare Diseases. 2014; 2:e967148.
14. Jelinic P, Mueller JJ, Olvera N, Dao F, Scott SN, Shah R, Gao J, Schultz N, Gonen M, Soslow RA, Berger MF, Levine DA. Recurrent SMARCA4 mutations in small cell carcinoma of the ovary. Nature genetics. 2014; 46:424–426.
15. Witkowski L, Carrot-Zhang J, Albrecht S, Fahiminiya S, Hamel N, Tomiak E, Grynspan D, Saloustros E, Nadaf J, Rivera B, Gilpin C, Castellsague E, Silva-Smith R, Plourde F, Wu M, Saskin A, et al. Germline and somatic SMARCA4 mutations characterize small cell carcinoma of the ovary, hypercalcemic type. Nature genetics. 2014; 46:438–443.
16. Ramos P, Karnezis AN, Craig DW, Sekulic A, Russell ML, Hendricks WP, Corneveaux JJ, Barrett MT, Shumansky K, Yang Y, Shah SP, Prentice LM, Marra MA, Kiefer J, Zismann VL, McEachron TA, et al. Small cell carcinoma of the ovary, hypercalcemic type, displays frequent inactivating germline and somatic mutations in SMARCA4. Nature genetics. 2014; 46:427–429.
17. Upchurch KS, Parker LM, Scully RE, Krane SM. Differential cyclic AMP responses to calcitonin among human ovarian carcinoma cell lines: a calcitonin-responsive line derived from a rare tumor type. J Bone Miner Res. 1986; 1:299–304.
18. Otte A, Gohring G, Steinemann D, Schlegelberger B, Groos S, Langer F, Kreipe HH, Schambach A, Neumann T, Hillemanns P, Park-Simon TW, Hass R. A tumor-derived population (SCCOHT-1) as cellular model for a small cell ovarian carcinoma of the hypercalcemic type. International journal of oncology. 2012; 41:765–775.
19. Otte A, Rauprich F, Hillemanns P, Park-Simon TW, von der Ohe J, Hass R. *In vitro* and *in vivo* therapeutic approach for a small cell carcinoma of the ovary hypercalcaemic type using a SCCOHT-1 cellular model. Orphanet journal of rare diseases. 2014; 9:126.
20. Foulkes WD, Clarke BA, Hasselblatt M, Majewski J, Albrecht S, McCluggage WG. No small surprise - small cell

carcinoma of the ovary, hypercalcaemic type, is a malignant rhabdoid tumour. The Journal of pathology. 2014; 233:209–214.

21. Gamwell L, Gambaro K, Merziotis M, Crane C, Arcand SL, Bourada V, Davis C, Squire JA, Huntsman DG, Tonin PN, Vanderhyden BC. Small cell ovarian carcinoma: genomic stability and responsiveness to therapeutics. Orphanet journal of rare diseases. 2013; 8.
22. Otte A, Rauprich F, von der Ohe J, Hillemanns P, Hass R. Interference of Ca(2)(+) with the proliferation of SCCOHT-1 and ovarian adenocarcinoma cells. International journal of oncology. 2014; 45:1151–1158.
23. Majore I, Moretti P, Hass R, Kasper C. Identification of subpopulations in mesenchymal stem cell-like cultures from human umbilical cord. Cell Commun Signal. 2009; 7:6.
24. Lavrentieva A, Majore I, Kasper C, Hass R. Effects of hypoxic culture conditions on umbilical cord-derived human mesenchymal stem cells. Cell Commun Signal. 2010; 8:18.
25. Pirozzi G, Tirino V, Camerlingo R, Franco R, La Rocca A, Liguori E, Martucci N, Paino F, Normanno N, Rocco G. Epithelial to mesenchymal transition by TGFbeta-1 induction increases stemness characteristics in primary non small cell lung cancer cell line. PloS one. 2011; 6:e21548.
26. Chang K, Pastan I. Molecular cloning of mesothelin, a differentiation antigen present on mesothelium, mesotheliomas, and ovarian cancers. Proceedings of the National Academy of Sciences of the United States of America. 1996; 93:136–140.
27. Birchmeier C, Birchmeier W, Gherardi E, Vande Woude GF. Met, metastasis, motility and more. Nature reviews. 2003; 4:915–925.
28. Parr C, Jiang WG. Expression of hepatocyte growth factor/scatter factor, its activator, inhibitors and the c-Met receptor in human cancer cells. International journal of oncology. 2001; 19:857–863.
29. Yamashita Y, Akatsuka S, Shinjo K, Yatabe Y, Kobayashi H, Seko H, Kajiyama H, Kikkawa F, Takahashi T, Toyokuni S. Met is the most frequently amplified gene in endometriosis-associated ovarian clear cell adenocarcinoma and correlates with worsened prognosis. PloS one. 2013; 8:e57724.
30. Tang C, Jardim DL, Hong D. MET in ovarian cancer: metastasis and resistance? Cell cycle. Georgetown, Tex: 2014; 13:1220–1221.
31. Brat DJ, Bellail AC, Van Meir EG. The role of interleukin-8 and its receptors in gliomagenesis and tumoral angiogenesis. Neuro-oncology. 2005; 7:122–133.
32. Organ SL, Tsao MS. An overview of the c-MET signaling pathway. Therapeutic advances in medical oncology. 2011; 3:S7–S19.
33. Mhawech-Fauceglia P, Afkhami M, Pejovic T. MET/HGF Signaling Pathway in Ovarian Carcinoma: Clinical Implications and Future Direction. Pathology research international. 2012; 2012:960327.
34. Blumenschein GR, Jr., Mills GB, Gonzalez-Angulo AM. Targeting the hepatocyte growth factor-cMET axis in cancer therapy. J Clin Oncol. 2012; 30:3287–3296.
35. Zillhardt M, Park SM, Romero IL, Sawada K, Montag A, Krausz T, Yamada SD, Peter ME, Lengyel E. Foretinib (GSK1363089), an orally available multikinase inhibitor of c-Met and VEGFR-2, blocks proliferation, induces anoikis, and impairs ovarian cancer metastasis. Clin Cancer Res. 2011; 17:4042–4051.
36. Davare MA, Saborowski A, Eide CA, Tognon C, Smith RL, Elferich J, Agarwal A, Tyner JW, Shinde UP, Lowe SW, Druker BJ. Foretinib is a potent inhibitor of oncogenic ROS1 fusion proteins. Proceedings of the National Academy of Sciences of the United States of America. 2013; 110:19519–19524.
37. Qian F, Engst S, Yamaguchi K, Yu P, Won KA, Mock L, Lou T, Tan J, Li C, Tam D, Lougheed J, Yakes FM, Bentzien F, Xu W, Zaks T, Wooster R, et al. Inhibition of tumor cell growth, invasion, and metastasis by EXEL-2880 (XL880, GSK1363089), a novel inhibitor of HGF and VEGF receptor tyrosine kinases. Cancer research. 2009; 69:8009–8016.
38. Faria CC, Golbourn BJ, Dubuc AM, Remke M, Diaz RJ, Agnihotri S, Luck A, Sabha N, Olsen S, Wu X, Garzia L, Ramaswamy V, Mack SC, Wang X, Leadley M, Reynaud D, et al. Foretinib is effective therapy for metastatic sonic hedgehog medulloblastoma. Cancer research. 2015; 75:134–146.
39. Huynh H, Ong R, Soo KC. Foretinib demonstrates antitumor activity and improves overall survival in preclinical models of hepatocellular carcinoma. Angiogenesis. 2012; 15:59–70.
40. Choueiri TK, Vaishampayan U, Rosenberg JE, Logan TF, Harzstark AL, Bukowski RM, Rini BI, Srinivas S, Stein MN, Adams LM, Ottesen LH, Laubscher KH, Sherman L, McDermott DF, Haas NB, Flaherty KT, et al. Phase II and biomarker study of the dual MET/VEGFR2 inhibitor foretinib in patients with papillary renal cell carcinoma. J Clin Oncol. 2013; 31:181–186.
41. Shah MA, Wainberg ZA, Catenacci DV, Hochster HS, Ford J, Kunz P, Lee FC, Kallender H, Cecchi F, Rabe DC, Keer H, Martin AM, Liu Y, Gagnon R, Bonate P, Liu L, et al. Phase II study evaluating 2 dosing schedules of oral foretinib (GSK1363089), cMET/VEGFR2 inhibitor, in patients with metastatic gastric cancer. PloS one. 2013; 8:e54014.
42. Ungefroren H, Sebens S, Seidl D, Lehnert H, Hass R. Interaction of tumor cells with the microenvironment. Cell Commun Signal. 2011; 9:18.
43. Hass R, Otte A. Mesenchymal stem cells as all-round supporters in a normal and neoplastic microenvironment. Cell Commun Signal. 2012; 10:26.
44. Mandel K, Yang Y, Schambach A, Glage S, Otte A, HassR. Mesenchymal stem cells directly interact with breast cancer

cells and promote tumor cell growth *in vitro* and *in vivo*. Stem cells and development. 2013; 22:3114–3127.

45. Yang Y, Otte A, Hass R. Human mesenchymal stroma/stem cells exchange membrane proteins and alter functionality during interaction with different tumor cell lines. Stem cells and development. 2015; 24:1205–1222.
46. Yang Y, Bucan V, Baehre H, von der Ohe J, Otte A, Hass R. Acquisition of new tumor cell properties by MSC-derived exosomes. International journal of oncology. 2015; 47:244–252.
47. Eder JP, Shapiro GI, Appleman LJ, Zhu AX, Miles D, Keer H, Cancilla B, Chu F, Hitchcock-Bryan S, Sherman L, McCallum S, Heath EI, Boerner SA, LoRusso PM. A phase I study of foretinib, a multi-targeted inhibitor of c-Met and vascular endothelial growth factor receptor 2. Clin Cancer Res. 2010; 16:3507–3516.
48. Tomayko MM, Reynolds CP. Determination of subcutaneous tumor size in athymic (nude) mice. Cancer chemotherapy and pharmacology. 1989; 24:148–154.
49. Hollborn M, Krausse C, Iandiev I, Yafai Y, Tenckhoff S, Bigl M, Schnurrbusch UE, Limb GA, Reichenbach A, Kohen L, Wolf S, Wiedemann P, Bringmann A. Glial cell expression of hepatocyte growth factor in vitreoretinal proliferative disease. Laboratory investigation; a journal of technical methods and pathology. 2004; 84:963–972.
50. Pons E, Uphoff CC, Drexler HG. Expression of hepatocyte growth factor and its receptor c-met in human leukemia-lymphoma cell lines. Leukemia research. 1998; 22:797–804.
51. Montanucci P, Basta G, Pescara T, Pennoni I, Di Giovanni F, Calafiore R. New simple and rapid method for purification of mesenchymal stem cells from the human umbilical cord Wharton jelly. Tissue engineering. 2011; 17:2651–2661.
52. Andratschke M, Hagedorn H, Luebbers CW, Schmitt B, Lang S, Zeidler R, Wollenberg B. Limited suitability of EpCAM for molecular staging of tumor borders in head and neck cancer. Anticancer research. 2006; 26:153–158.
53. Simpson DA, Feeney S, Boyle C, Stitt AW. Retinal VEGF mRNA measured by SYBR green I fluorescence: A versatile approach to quantitative PCR. Molecular vision. 2000; 6:178–183.
54. Schuch G, Machluf M, Bartsch G, Jr., Nomi M, Richard H, Atala A, Soker S. *In vivo* administration of vascular endothelial growth factor (VEGF) and its antagonist, soluble neuropilin-1, predicts a role of VEGF in the progression of acute myeloid leukemia *in vivo*. Blood. 2002; 100:4622–4628.
55. Marconi C, Peppicelli S, Bianchini F, Calorini L. TNFalpha receptor1 drives hypoxia-promoted invasiveness of human melanoma cells. Experimental oncology. 2013; 35:187–191.i

www.impactjournals.com/oncotarget/ Oncotarget, Supplementary Materials 2015

SUPPLEMENTARY FIGURES

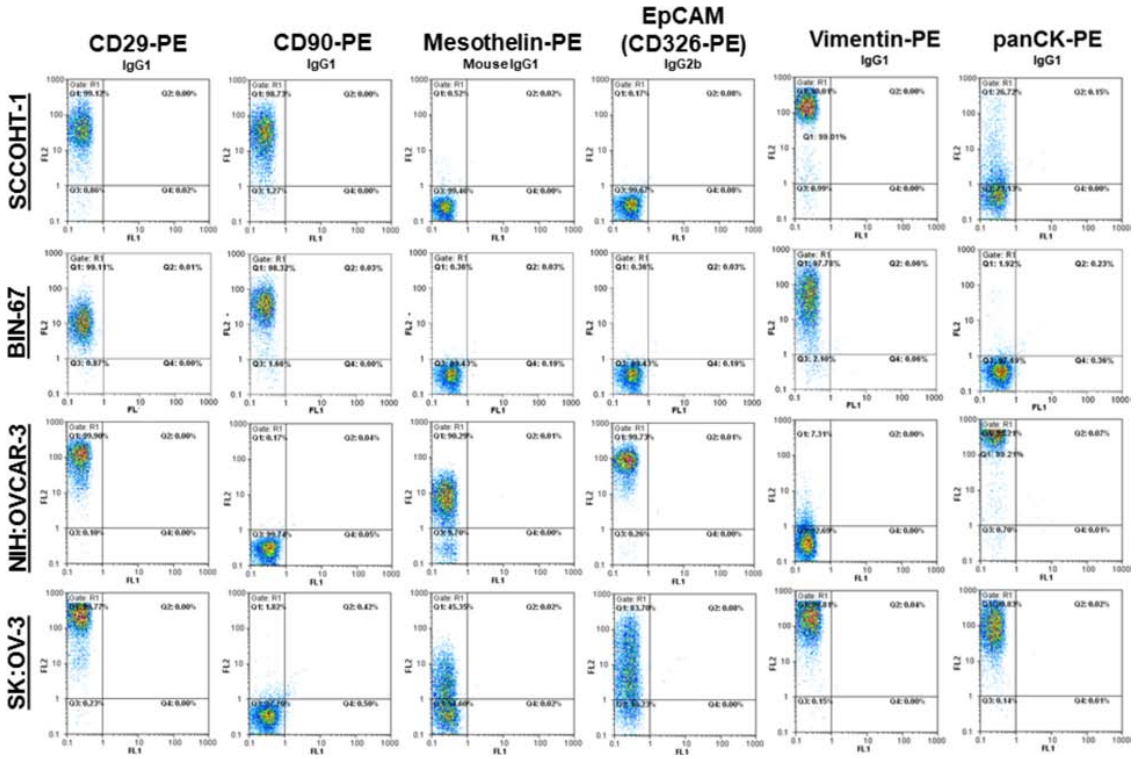

Supplementary Figure S1: Cell marker analysis was performed for a variety of different surface molecules and intermediate filament proteins (vimentin, cytokeratin (panCK)) in steady state-growing SCCOHT-1, BIN-67, NIH:OVCAR-3 and SK-OV-3 ovarian cancer cells by flow cytometry analysis according to the appropriate Ig isotype control.

www.impactjournals.com/oncotarget/ Oncotarget, Supplementary Materials 2015

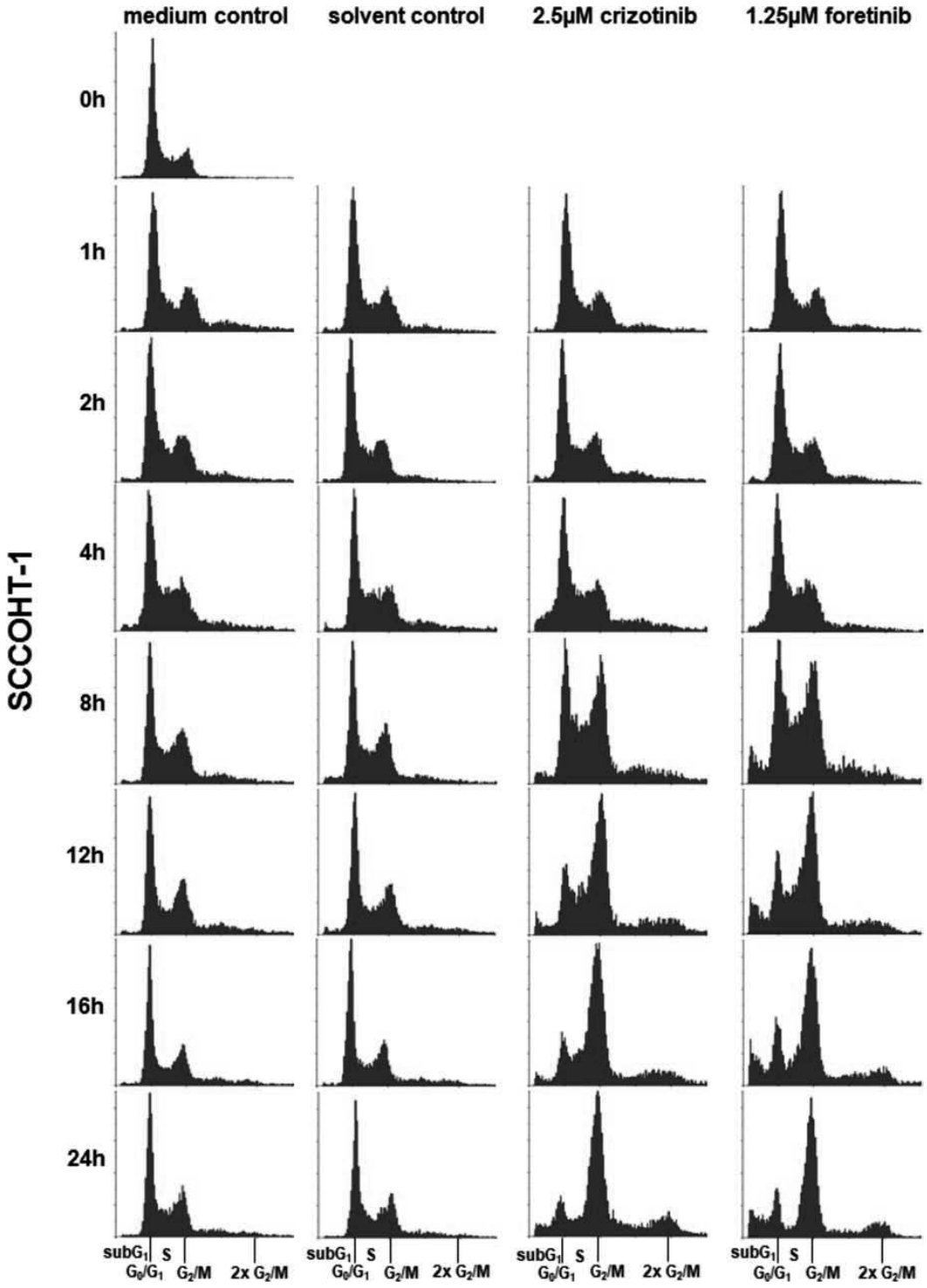

(*Contiuned*)

www.impactjournals.com/oncotarget/ Oncotarget, Supplementary Materials 2015

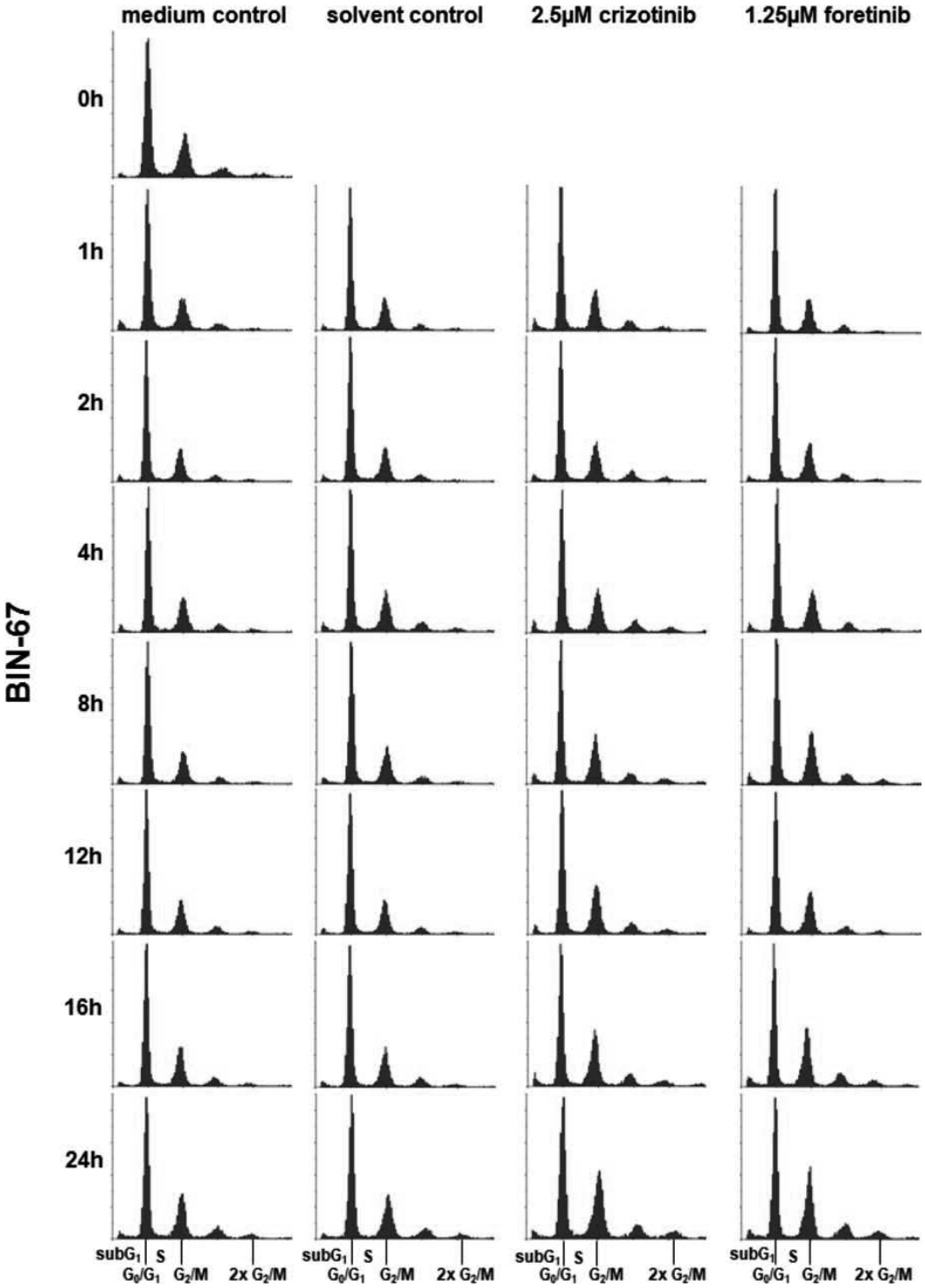

(*Contiuned*)

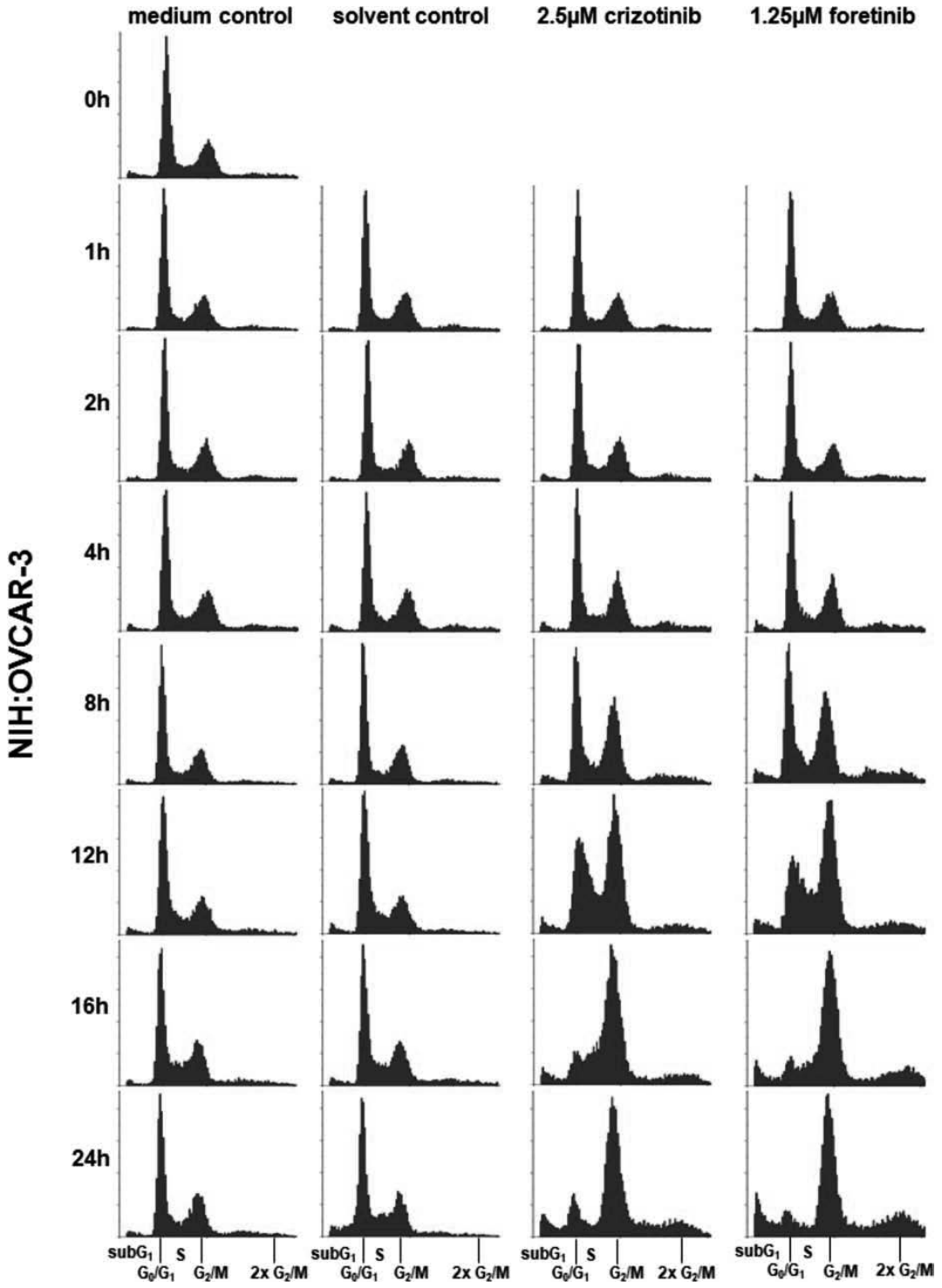
medium control
solvent control
2.5µM crizotinib
1.25µM foretinib
NIH:OVCAR-3
0h
1h
2h
4h
8h
12h
16h
24h
subG1
G0/G1
S
G2/M
2x G2/M

(*Contiuned*)

www.impactjournals.com/oncotarget/ Oncotarget, Supplementary Materials 2015

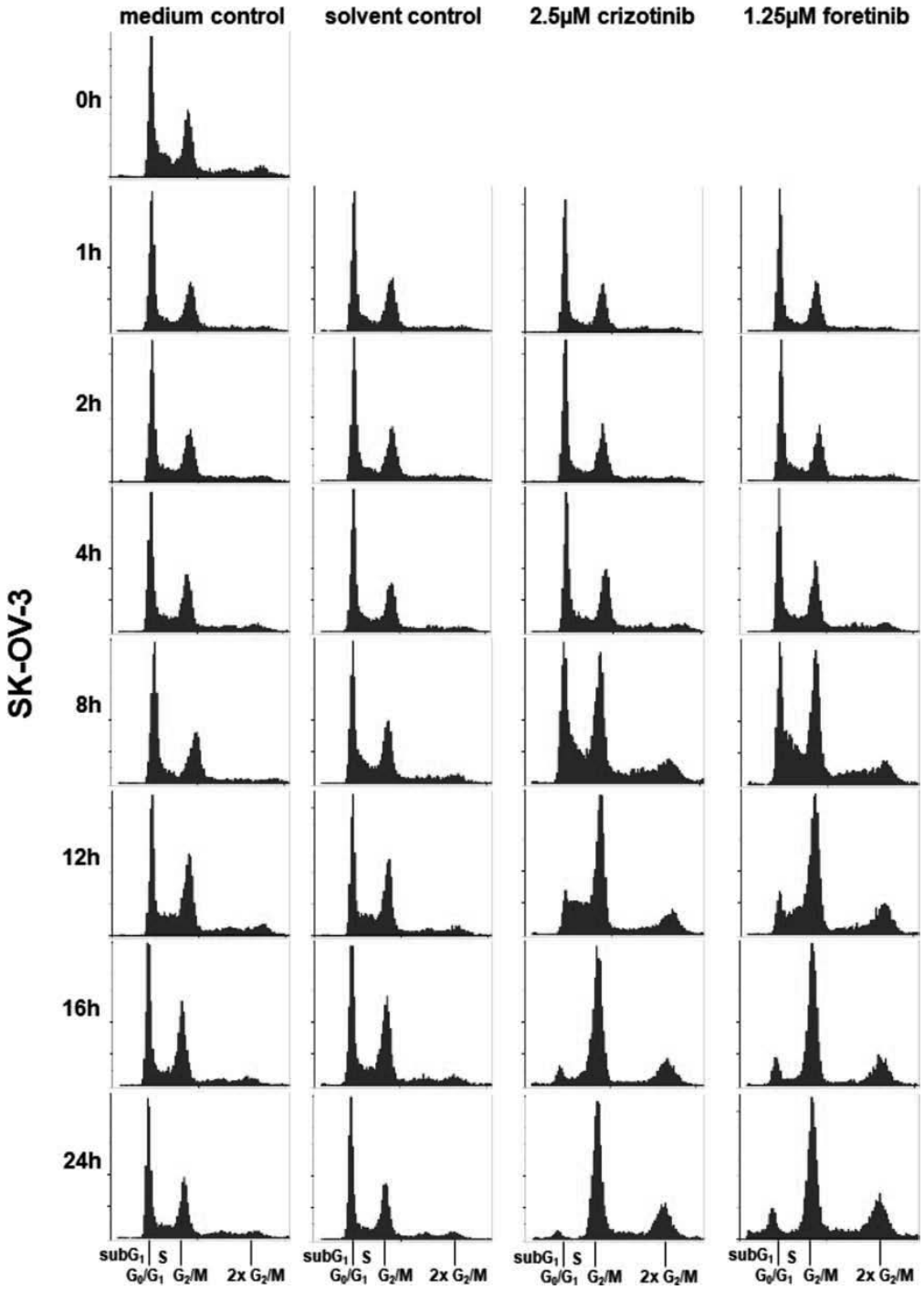

Supplementary Figure S2: Short term cell cycle analysis of A. SCCOHT-1, B. BIN-67, C. NIH:OVCAR-3 and D. SK-OV-3 ovarian cancer cells was performed in steady state controls, in solvent controls (0.025% (v/v) DMSO), or in the presence of the c-Met inhibitors 2.5 µM crizotinib and 1.25 µM foretinib for up to 24 h, respectively.

www.impactjournals.com/oncotarget/ Oncotarget, Supplementary Materials 2015

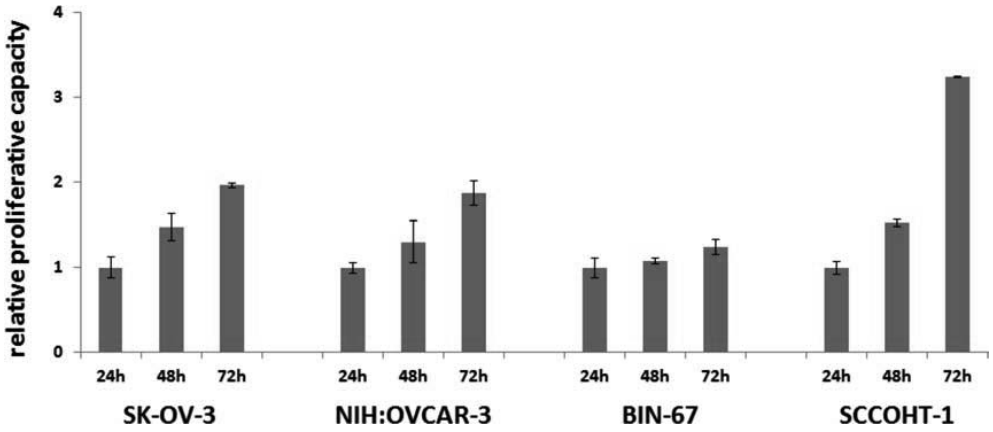

Supplementary Figure S3: Relative proliferative capacity of SCCOHT-1, BIN-67, NIH:OVCAR-3 and SK-OV-3 cells was determined in 24-well plates using the trypan blue exclusion test between 24 h to 72 h. Data represent the mean ± s.d. of 3 independent experiments.

www.impactjournals.com/oncotarget/ Oncotarget, Supplementary Materials 2015

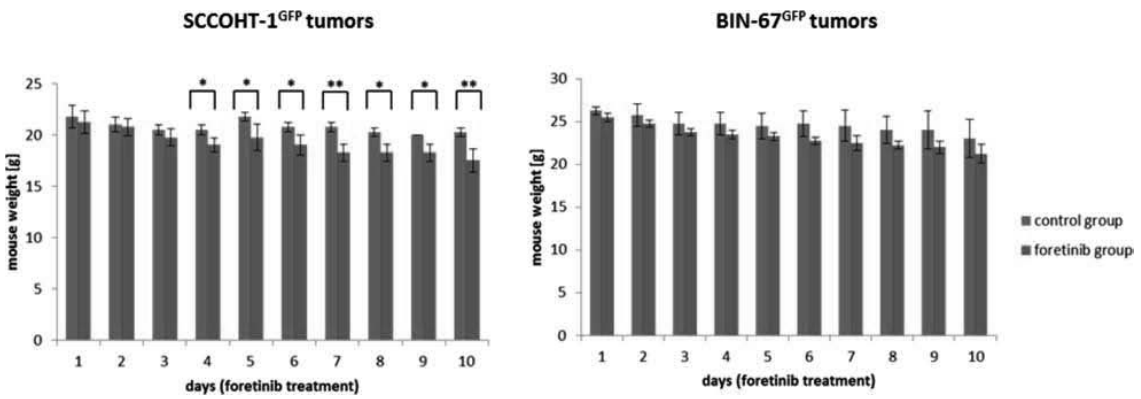

Supplementary Figure S4: Body weight was determined in mice carrying SCCOHT-1^{GFP} (left panel) and BIN-67^{GFP} (right panel) tumor xenografts receiving control treatment compared to foretinib treatment over 10 days. Data represent the mean ± s.d. of 3 animals in each experiments. Statistical analysis was performed by unpaired Student's t-test (*$P < 0.05$; **$P < 0.01$).

www.impactjournals.com/oncotarget/ Oncotarget, Supplementary Materials 2015

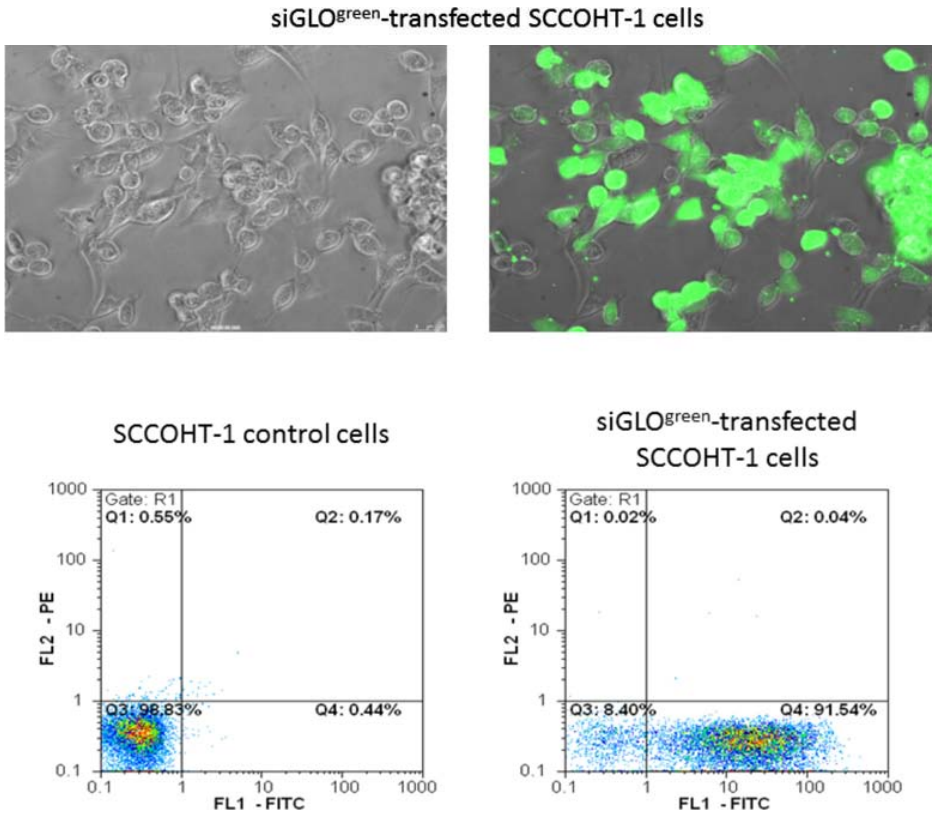

Supplementary Figure S5: Transfection efficiency of SCCOHT-1 cells with 25 nM siGLO^{green} was evaluated by microscopy (upper panels) and by flow cytometry (lower panels) 24h after transfection.

www.impactjournals.com/oncotarget/ Oncotarget, Supplementary Materials 2015

STR fragment	SCCOHT-1	BIN-67
Penta D A1	12	9
Penta D A2	15	9
Penta E A1	10	14
Penta E A2	13	16
AMEL A1	X-chr	X-chr
AMEL A2	X-chr	X-chr
CSF1PO A1	10	10
CSF1PO A2	11	12
D13S317 A1	8	10
D13S317 A2	12	12
D16S539 A1	9	12
D16S539 A2	13	12
D18S51 A1	13	13
D18S51 A2	13	19
D3S1358 A1	15	15
D3S1358 A2	17	19
D7S820 A1	10	9
D7S820 A2	11	9
D8S1179 A1	13	14
D8S1179 A2	14	14
TH01 A1	7	6
TH01 A2	8	9.3
TPOX A1	8	11
TPOX A2	9	11

Supplementary Figure S6: Short tandem repeat (STR) fragment analysis using the GenomeLab human STR primer set was performed for SCCOHT-1 and BIN-67 cell populations. Data from different culture periods of SCCOHT-1 (n = 3), respectively, confirmed reproducible STR patterns for each cell type.

2.4 Human mesenchymal stroma/stem cell exchange membran proteins and alter functionality during interaction with different tumor cell lines

Yuanyuan Yang, **Anna Otte** und Ralf Hass

publiziert in
STEM CELLS AND DEVELOPMENT
24 (10), 2015, 1205-1222
doi: 10.1089/scd.2014.0413

STEM CELLS AND DEVELOPMENT
Volume 24, Number 10, 2015

DOI: 10.1089/scd.2014.0413

Human Mesenchymal Stroma/Stem Cells Exchange Membrane Proteins and Alter Functionality During Interaction with Different Tumor Cell Lines

Yuanyuan Yang,[1,2] Anna Otte,[1] and Ralf Hass[1]

To analyze effects of cellular interaction between human mesenchymal stroma/stem cells (MSC) and different cancer cells, direct co-cultures were performed and revealed significant growth stimulation of the tumor populations and a variety of protein exchanges. More than 90% of MCF-7 and primary human HBCEC699 breast cancer cells as well as NIH:OVCAR-3 ovarian adenocarcinoma cells acquired CD90 proteins during MSC co-culture, respectively. Furthermore, SK-OV-3 ovarian cancer cells progressively elevated CD105 and CD90 proteins in co-culture with MSC. Primary small cell hypercalcemic ovarian carcinoma cells (SCCOHT-1) demonstrated undetectable levels of CD73 and CD105; however, both proteins were significantly increased in the presence of MSC. This co-culture-mediated protein induction was also observed at transcriptional levels and changed functionality of SCCOHT-1 cells by an acquired capability to metabolize 5′cAMP. Moreover, exchange between tumor cells and MSC worked bidirectional, as undetectable expression of epithelial cell adhesion molecule (EpCAM) in MSC significantly increased after co-culture with SK-OV-3 or NIH:OVCAR-3 cells. In addition, a small population of chimeric/hybrid cells appeared in each MSC/tumor cell co-culture by spontaneous cell fusion. Immune fluorescence demonstrated nanotube structures and exosomes between MSC and tumor cells, whereas cytochalasin-D partially abolished the intercellular protein transfer. More detailed functional analysis of FACS-separated MSC and NIH:OVCAR-3 cells after co-culture revealed the acquisition of epithelial cell-specific properties by MSC, including increased gene expression for cytokeratins and epithelial-like differentiation factors. Vice versa, a variety of transcriptional regulatory genes were down-modulated in NIH:OVCAR-3 cells after co-culture with MSC. Together, these mutual cellular interactions contributed to functional alterations in MSC and tumor cells.

Introduction

Human mesenchymal stroma/stem cells (MSC) can be derived as a multipotent stromal population from a large variety of different sources. MSC represent a heterogeneous cell population due to their diverse origin from nearly all vascularized organs and tissues and exhibit migratory capability and regenerative potential [1]. According to their heterogeneity, no specific marker but a broad range of properties are characterized for these stem cells, including the capacity for plastic adherence, simultaneous expression of the CD73, CD90, and CD105 surface molecules with concomitant absence of other cell type-specific markers, including CD14, CD31, CD34 CD45, and HLA-DR, and at least a tri-lineage differentiation potential along the osteogenic, chondrogenic, and adipogenic phenotype [2,3]. Some additional surface markers can be detected in certain subpopulations such as Stro-1 [4], or the chemokine receptors VCAM-1 (CD106) and ICAM-1 (CD54) [5] predominantly found in bone marrow-derived MSC, or the more embryonic-like stem cell markers Oct-4 and Sox2 [6], all of which depend on the local microenvironment and contribute to the multi-facetted functionalities as a part of the heterogeneous MSC population.

MSC can be attracted by inflammatory cytokines/chemokines to migrate toward local tissue injuries in support of tissue regeneration and repair. During this process, MSC get into contact with a variety of different cell types and display mutual cellular interactions, including the release of bioactive molecules [7] and exosomes [8] as well as direct cell-to-cell interactions via integrins and gap junctional intercellular communication (GJIC). At the sites of tissue damage, MSC exhibit immune-modulatory functions predominantly for T cells, NK cells, and macrophages to facilitate repair

[1]Biochemistry and Tumor Biology Lab, Department of Obstetrics and Gynecology, Hannover Medical School, Hannover, Germany.
[2]Tongji Hospital Affiliated by Tongji University, Shanghai, China.

[9–11]. Moreover, MSC are involved in endothelial cell interactions for the promotion of angiogenesis and neovascularization in the damaged area [12,13].

Invasive tumor growth such as breast or ovarian cancer also causes local tissue damage and inflammation and, consequently, attracts immune cells and MSC to contribute to the required repair machinery. Thus, MSC can be detected within the adipose breast tissue and the fibroglandular tissue of the breast, thereby forming close vicinity to normal human mammary epithelial cells (HMEC) and to breast cancer cells within the tumor microenvironment [14–16]. Likewise, MSC are also present in tissues of the ovary and their tumorigenic counterparts. Ovarian cancer similar to breast cancer represents one of the most lethal gynecologic malignancies and can be categorized into different low-grade serous type I tumors in contrast to high-grade type II tumors with aggressive cancer cells predominantly observed in advanced tumor stages [17–19]. Moreover, the small cell carcinoma of the ovary hypercalcemic type (SCCOHT) represents a rare form of an aggressive tumor, which often affects young women during reproductive age. SCCOHT characterizes a separate tumor entity apart from ovarian cancer [20]. However, it remains unclear how MSC interact with these different kinds of breast, ovarian, or other cancer types.

In this study, we established several co-culture models for a variety of MSC populations together with different kinds of tumor cells, including tumor cell lines and primary cells from tumor biopsies of breast and ovarian cancer patients. It was the aim of this study to address potential cell biological effects during direct interaction between the stroma/stem cells and the various tumor cell types. Our co-culture experiments demonstrated elevated growth of the tumor cells in the presence of MSC and mutual exchange of cellular material between MSC and the different tumor cell types.

Materials and Methods

Cell culture

The use of primary cells from human tumor biopsies and the use of primary human mesenchymal stem cells after explant culture have been approved by the Ethics Committee of Hannover Medical School, Project #3916 on June 15th, 2005, and Project #443 on February 26th, 2009, respectively, and informed written consent was obtained from all patients.

Breast cancer cells. Human MCF-7 breast carcinoma cell line was obtained from the American Type Culture Collection and grown in Dulbecco's modified Eagle's medium with medium supplements [10% (v/v) fetal calf serum (FCS), 2 mM L-glutamine, 100 U/mL penicillin, and 100 µg/mL streptomycin; all from Sigma Chemie GmbH]. Cultures were maintained at 37°C in a humidified atmosphere with 5% CO_2.

Primary human breast cancer-derived epithelial cells (HBCEC) were obtained from explant cultures of human breast cancer biopsies after negative testing for HIV-1, hepatitis B & C, bacteria, yeast, and fungi, respectively, as described [21]. The primary HBCEC 699 were cultured further in serum-free and phenol red-free mammary epithelial cell growth medium (MEGM; Lonza Ltd.).

Ovarian cancer cells. The human NIH:OVCAR-3 ovarian adenocarcinoma cell line (ATCC® #HTB-161™) was commercially obtained in passage 76 (P76) from the Institute for Applied Cell Culture (IAZ). The SK-OV-3 epithelial-like ovarian cancer cells (ATCC #HTB-77™) were commercially obtained in P25 from the ATCC. SCCOHT-1 represent a spontaneously proliferating population derived from a patient with recurrent SCCOHT [22]. These three different cancer cell types were cultivated at about 1,750 cells/cm^2 in RPMI 1640 with medium supplements, respectively. NIH:OVCAR-3 and SK-OV-3 cells were subcultured by trypsin/EDTA (Biochrom GmbH) treatment for 5 min at 37°C.

Mesenchymal stroma/stem cells. MSC-like cells were isolated from human umbilical cords as previously reported [23,24]. The cells were obtained from six different patients after delivery of full-term (38–40 weeks) infants either spontaneously or by Cesarean section. MSC were cultured in αMEM supplemented with 10% of allogeneic human AB-serum (HS, commercially obtained from blood bank, University Campus Lübeck, Germany), 100 U/mL penicillin, 100 µg/mL streptomycin, and 2 mM L-glutamine (Sigma) at 37°C in a humidified atmosphere with 5% CO_2. For the experiments, MSC primary cultures from the six different donors in different passages (P2 to P6) were used (MSC240113 in P2; MSC280313 in P3, P4 and P5; MSC131113 in P3 and P4; MSC101213 in P5; MSC100314 in P3; and MSC180314 in P3 and P6), respectively.

Human mammary epithelial cells. Primary cultures of normal human mammary epithelial cells (HMEC) were commercially provided by BioWhittaker, Inc. (Lot #1F1012). Juvenile and proliferating HMEC in P13 were cultured at 2,500 cells/cm^2 in mammary epithelial cell growth medium (PromoCell) as previously described [25].

Cell line authentication. Cells were tested for mycoplasma by the luminometric MycoAlert Plus mycoplasma detection kit (Lonza, Inc.) according to the manufacturer's recommendations. Moreover, authentication of the cell lines was performed by short tandem repeat (STR) fragment analysis using the GenomeLab human STR primer set (Beckman Coulter, Inc.) demonstrating a similar STR pattern according to the STR database provided by the Deutsche Sammlung von Mikroorganismen und Zellkulturen (DSMZ).

Co-culture and proliferation measurement of tumor cell lines and primary cultures with MSC after lentiviral transduction

For discrimination of the different tumor cells in co-culture with MSC and for proliferation measurements, all tumor cell populations were transduced with a third generation lentiviral SIN vector containing the mcherry gene. Likewise, the different MSC populations were similarly transduced with an eGFP gene-containing vector as previously described [26].

A co-culture of 60% GFP-labeled human mesenchymal stem cells (MSC^{GFP}) and 40% mcherry-labeled tumor cells (for MCF-7^{cherry} and MSC^{GFP} the initial ratio was 20% to 80%) were incubated in MSC culture medium till 9 days in cell culture plates (diameter 10 cm; Greiner BioOne GmbH) at an initial density between 500 and 2,000 cells/cm^2 as indicated in the experiments.

For proliferation measurement of the co-culture at different time points, the medium was removed and the cells

were lysed with 10% SDS. The fluorescence intensity of mcherry (excitation 584 nm/emission 612 nm) and GFP (excitation 485 nm/emission 520 nm) that corresponded to the appropriate cell number of tumor cells and MSC, respectively, was measured in aliquots of the lysate using the Fluoroscan Ascent Fl (Thermo Fisher Scientific). Appropriate mono-cultures of tumor^{cherry} cells and MSC^{GFP} demonstrated no artificial cross-fluorescence.

In an additional independent evaluation of the cell numbers, the different cell cultures were trypsinized at the appropriate time points and the cells were counted after trypan blue staining in a fluorescence microscope (Olympus IX50) using the green and red fluorescence filters, respectively, as well as an FITC/TRIC fluorescence dual band filter.

Analysis of surface markers and cell cycle by flow cytometry

Continuously proliferating mono- and co-culture cells were harvested and analyzed for cell surface marker expression by flow cytometry. After blocking nonspecific binding to Fc-receptors by incubation of 10^6 cells with 2% bovine serum albumin in phosphate-buffered saline (PBS-BSA) for 30 min at 4°C and washing with PBS-BSA, the cells were incubated with the following appropriately labeled monoclonal anti-human antibodies, respectively: CD73-PE (clone AD2; BD Bioscience); CD90-PE (clone 5E10, IgG1; BioLegend, Inc.); CD105-PE (clone 43A3, IgG1; BioLegend, Inc.); and CD326-PE (=EpCAM-PE, clone G9C4, IgG2b; BioLegend, Inc.). After antibody staining, all samples were washed twice with PBS-BSA and measured by flow cytometry. Appropriately labeled antibodies of the corresponding Ig subclass were used as a control.

For cell cycle analysis, 5×10^5 cells were fixed in 70% (v/v) ice-cold ethanol at 4°C for 24 h. Thereafter, the fixed cells were stained with CyStain DNA 2 step kit (Partec GmbH) and filtered through a 50 μm filter. Flow cytometry analysis was performed in a Galaxy FACSan (Partec) using FloMax analysis software (Partec).

Analysis of 5′-AMP and adenosine

Steady-state SCCOHT-1 cells and SCCOHT-1 after FACS separation from a 7 days co-culture with MSC were cultivated in PBS with 20 μM 5′-AMP (Sigma) as a substrate for 30 min at 37°C. MSC mono-culture and MSC after FACS separation from a 7 day co-culture with SCCOHT-1 cells were used as a control after incubation with 20 μM 5′-AMP. Supernatants were collected and centrifuged (500 g/5 min) to remove additional cells and debris and cell-free supernatants were analyzed by HPLC-MS/MS using a Shimadzu HPLC-system (Shimadzu) coupled with a QTRAP5500TM triple quadrupole mass spectrometer (AB-SCIEX) operating in positive ionization mode to quantify the amount of 5′AMP as the substrate and the level of adenosine as the product.

Immunoblot analysis

Conditioned media (7 days) from mono-cultured MCF-7^{cherry}, SK-OV-3^{cherry}, SCCOHT-1^{cherry}, and NIH:OVCAR-3^{cherry} (initially seeded at 5×10^4 cells/mL) or MSC^{GFP} (initially seeded at 7.5×10^4 cells/mL) in comparison to co-cultured cells from MCF-7^{cherry}, SK-OV-3^{cherry}, SCCOHT-1^{cherry} and NIH:OVCAR-3^{cherry} with MSC^{GFP} (cell ratio 40:60; initially seeded at 1.25×10^5 cells/mL) was used, respectively. In addition, cell lysates of MSC^{GFP} were prepared in reswelling buffer containing 8 M urea (Carl Roth GmbH Co KG), 1% CHAPS (3-[(3-Cholamidopropyl)-dimethylammonio]-1-propanesulfonate; Carl Roth GmbH Co KG), 0.5% (v/v) Pharmalyte 3–10 (GE Healthcare Europe GmbH), 0.002% (w/v) bromophenol blue (SERVA Electrophoresis GmbH) and freshly prepared 0.4% (w/v) DTT (Dithiothreitol; Carl Roth GmbH Co KG). Protein concentration of the MSC lysate was adjusted using the colorimetric BCA-assay (Thermo Scientific). The protein samples (50 μg MSC cell lysate as control) and 40 μL aliquots of all appropriate conditioned media from mono- and co-cultures were subjected to SDS-polyacrylamide gel electrophoresis. In parallel, all conditioned media were concentrated 100-fold by applying Amicon Ultra-4 centrifugal filters (Merck Millipore Ltd.) with a molecular weight cut-off of ~10 kDa according to the manufacturer's instructions. Gels were transferred to a Amersham™ Protran™ Supported 0.45 μm nitrocellulose membrane (GE Healthcare). The membranes were blocked with PBS containing 5% FCS and 0.05% Tween-20 (PBS/Tween). After washing four times with PBS/Tween, the membranes were incubated with the primary antibodies [monoclonal anti-CD90 (EPR3132, rabbit, dilution 1:250, ab92574; Abcam plc); polyclonal anti-CD105 (N3C3, rabbit, dilution 1:500; Gene Tex, Inc.), and monoclonal anti-β-actin (mouse, dilution 1:1,000, clone AC-15; Sigma-Aldrich)] overnight at 4°C. Thereafter, the membranes were washed four times with PBS/Tween and incubated with the appropriate horseradish peroxidase-conjugated anti-mouse IgG (dilution 1:5,000) or anti-rabbit IgG (dilution 1:5,000) secondary antibody, respectively, (all from GE Healthcare) for 1 h/room temperature. The membranes were washed with PBS/Tween and visualized by autoradiography using SuperSignal West Pico Chemiluminescent Substrate (Thermo Scientific).

Transcript analysis by reverse transcription PCR

Total RNA was isolated using RNeasy Mini Kit (Qiagen) according to the manufacturer's instructions. One microgram RNA was reverse transcribed into cDNA using 500 μM of dNTP (R0193), 5 μM Oligo$(dT)_{18}$ primer (S0132), 5 μM Random Hexan primer (S0142), 1 U RiboLock™ RNase Inhibitor (E00381), and 5 U RevertAid™ M-MuLV Reverse Transcriptase (EP0441) in the supplied reaction buffer (all reagents from Thermo Scientific). The cDNA reactions were performed for 10 min/25°C, 1 h/37°C and stopped at 72°C for 10 min. As a template, 2.5 μL of cDNA was used with primers specific for CD73 (sense: 5′-CGC AAC AAT GGC ACA ATT AC-3′; antisense: 5′-CTC GAC ACT TGG TGC AAA GA-3′; amplification product 241 bp [27]), CD90 (sense: 5′-GGA CTG AGA TCC CAG AAC CA-3′; antisense: 5′-ACG AAG GCT CTG GTC CAC TA-3′; amplification product 124 bp [28]), and CD105 (sense: 5′-TGT CTC ACT TCA TGC CTC CAG CT-3′; antisense: 5′-AGG CTG TCC ATG TTG AGG CAG T-3′; amplification product 378 bp [29]). As a control, β-actin polymerase chain reaction (PCR) (sense: 5′-CGG ATG TCC ACG TCA CAC T-3′; antisense: 5′-CCA CTG GCA TCG TGA TGG A-3′;

amplification product 427 bp [30]) was performed (all primers customized by Eurofins, MWG GmbH). PCR reactions included 0.2 μM of each primer, 200 μM of dNTP (R0193; Thermo Scientific), and 0.03 U One Taq Hot Start DNA polymerase (New England Biolabs GmbH) in the supplied reaction buffer. PCR cycling conditions were performed for 30 s at 94°C, 1 min at 60°C, and 68°C for 1 min, respectively, including an initial 30 s denaturation step at 94°C and a final 5 min extension step at 68°C (35 cycles). Aliquots of 25 μL of each reverse transcription-PCR product were separated on a 2% agarose gel, including the standard GeneRuler 100 bp DNA Ladder (Thermo Scientific), and visualized by GelRed™ (Biotium, Inc.) staining.

FACS separation, RNA isolation, and microarray analysis of co-cultured MSC and NIH:OVCAR-3 cells

After RNA isolation using the RNeasy mini kit (Qiagen GmbH), 100 ng of total RNA from either steady-state control MSC^{GFP}, control NIH:OVCAR-3^{cherry}, and 7 days co-cultured MSC^{GFP}, or NIH:OVCAR-3^{cherry} cells after FACS separation were used to prepare aminoallyl-UTP-modified (aaUTP) cRNA (Amino Allyl MessageAmp™ II Kit, #AM1753; Life Technologies) as directed by the manufacturer. Labeling of aaUTP-cRNA was performed by CY3 POST-Labelling Reactive Dyes (25-8010-79; GE Healthcare Biosciences). Before the reverse transcription reaction, 1 μL of a 1:10,000 dilution of Agilent's ''One-Color spike-in kit stock solution'' (#5188-5282; Agilent Technologies) were added to each total RNA sample. cRNA fragmentation, hybridization, and washing steps were carried out as recommended and microarray analysis was performed by use of a refined version of the Whole Human Genome Oligo Microarray 4x44K v2 (AMADID 026652; Agilent Technologies), termed ''026652AsQuintuplicatesOn180k'' (AMADID 054261) and developed in the Research Core Unit Transcriptomics of Hannover Medical School. Microarray design was defined at Agilent's eArray portal using a 4x180k design format for mRNA expression as a template. All noncontrol probes of AMADID 026652 were printed five times onto one 180k Microarray (on-chip quintuplicates). Control probes required for proper Feature Extraction software algorithms were determined and placed automatically by eArray using recommended default settings. Slides were scanned on the Agilent Microarray Scanner G2565CA (pixel resolution 3 μm, bit depth 20). Data extraction was performed with the ''Feature Extraction Software V10.7.3.1'' using the extraction protocol file ''GE1_107_Sep09.xml.'' Processed intensity values of the green channel, ''gProcessedSignal'' (gPS) were normalized by global linear scaling: All gPS values of one sample were multiplied by an array-specific scaling factor. This factor was calculated by dividing a ''reference 75th Percentile value'' (set as 1,500 for the whole series) by the 75th Percentile value of the particular microarray (''Array I'' in the formula shown next). Accordingly, normalized gPS values for all samples (microarray data sets) were calculated by the following formula:

$$normalized\ gPS_{Array\ i} = gPS_{Array\ i} \times (1,500/75th\ Percentile_{Array\ i}$$

Measurements of on-chip replicates (quintuplicates) were averaged using the geometric mean of normalized gPS values. Measurements outside the interval of ''1.42× interquartile range'' regarding the normalized gPS distribution of the respective on-chip replicate population were excluded from averaging. A lower intensity threshold (surrogate value) was defined as 1% of the reference 75th Percentile value (= 15). All normalized gPS values below this intensity border were substituted by the respective surrogate value of 15. Gene expression levels of more than two-fold difference were compared between control MSC and co-cultured MSC as well as between control NIH:OVCAR-3 and co-cultured NIH:OVCAR-3 cells and stored at the NCBI-GEO database with the accession GSE60035 (www.ncbi.nlm.nih.gov/geo/query/acc.cgi?acc=GSE60035).

Results

Enhanced cell growth and membrane protein acquisition by cancer cells in the presence of MSC

Co-culture of human MCF-7^{cherry} breast cancer cells with three different individual MSC^{GFP} populations in separate assays was associated with reproducible data demonstrating continuous growth stimulation by MSC^{GFP} within 9 days (Fig. 1A). These growth-stimulatory effects by MSC predominantly required direct intercellular communication, as co-culture experiments performed in transwells carrying a sterile track-etched membrane with 0.4 mm sized-pores revealed no detectable effects in proliferative capacity similar to previous studies (data not shown) [25]. Direct cell counting of MCF-7^{cherry} cells in co-culture with MSC^{GFP} was also performed and compared with an appropriate amount of mono-cultured cells and confirmed a growth induction of the breast cancer cell line in contrast to a reduced MSC^{GFP} cell number during co-culture (Supplementary Fig. S1; Supplementary Data are available online at www.liebertpub.com/scd).

Moreover, the MCF-7^{cherry} cells revealed an acquisition of CD90 protein from about 1.4% ± 0.3% in mono-culture to 92.5% ± 2.0% ($n = 3$) in MCF-7^{cherry} co-cultured with MSC as evaluated in correspondence to the appropriate G1 cell cycle peaks of MCF-7^{cherry} and MSC^{GFP} (Fig. 1B). The co-cultures were prepared at an initial population ratio of 20% MCF-7^{cherry} and 80% MSC^{GFP} due to the high proliferation rate of the breast cancer cells. Similar data were obtained at an initial co-culture ratio of 40% MCF-7^{cherry} and 60% MSC^{GFP}; however, here MCF-7^{cherry} more rapidly overgrew the MSC^{GFP} representing already 95.7% of the population in co-culture with 57.6% of CD90-positive breast cancer cells after 7 days. These levels increased to 97.3% of MCF-7^{cherry} with 72.6% of CD90-carrying breast cancer cells after 8 days of co-culture (data not shown). The acquisition of CD90 by the breast cancer cells in co-culture was also dependent on the cell density. While MCF-7^{cherry} and MSC^{GFP} initially seeded at 500 cells/cm^2 demonstrated more than 90% of CD90 acquisition by the breast cancer cells after 9 days of co-culture (Fig. 1B), a four-fold increased density of 2,000 cells/cm^2 was accompanied by 92% of CD90-positive MCF-7 cells already after 3 days of co-culture (data not shown). A direct proof of CD90-carrying breast cancer cells was performed after cell sorting of MCF-7^{cherry} cells and

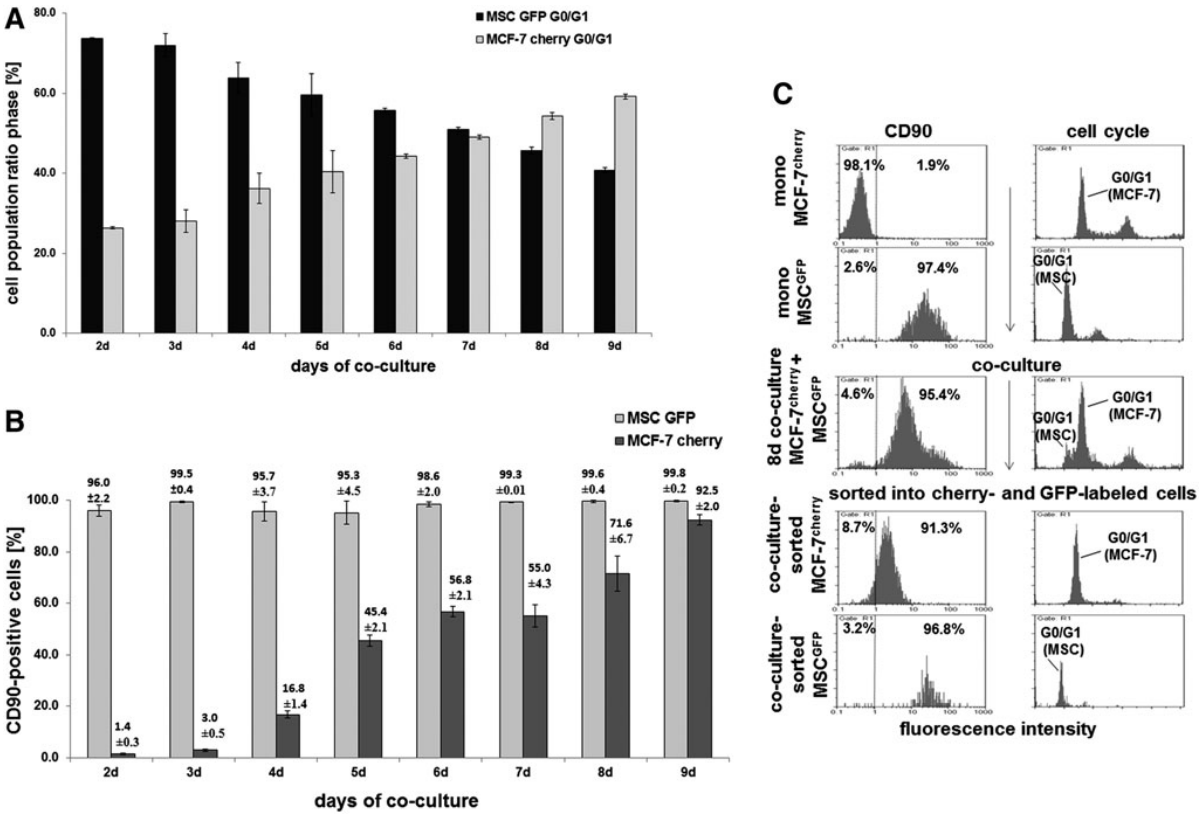

FIG. 1. MCF-7^{cherry} cells were incubated with three different human primary MSC populations (MSC240113^{GFP} P2, MSC280313^{GFP} P3, and MSC131113^{GFP} P3) in three separate co-cultures at a ratio of 20% MCF-7/80% MSC with 500 cells/cm^2 till 9 days. **(A)** Cell cycle analysis was performed in the co-cultures, and the ratio of the two populations (MCF-7^{cherry} and MSC^{GFP}) was quantified with the corresponding G1 peaks. Data represent the mean ± SD from the three separate co-cultures. **(B)** The percentage of CD90 expression in each population of the co-culture was quantified by flow cytometry. Data represent the mean ± SD from the three separate co-cultures. **(C)** Cell cycle analysis by flow cytometry and CD90 expression demonstrated little, if any, detection in MCF-7^{cherry} and 97.4% in MSC^{GFP} mono-cultures (*upper panels*), which were compared with an 8 day co-culture (*middle panel*). After separation of the co-cultured cells into cherry (red fluorescence) and GFP (green fluorescence) populations by sorting via FACS, subsequent flow cytometric analysis for CD90 and cell cycle revealed 91.3% CD90-positive MCF-7 cells. MSC, mesenchymal stroma/stem cells.

MSC^{GFP} after 8 days of co-culture into cherry- and GFP-positive cells, which revealed more than 90% of CD90 expression in the cherry-labeled MCF-7 cells in contrast to about 1.9% of CD90 in MCF-7 mono-cultured cells (Fig. 1C).

Similar to the MCF-7 breast cancer cell line, CD90 expression was also acquired by primary human breast cancer epithelial cells (HBCEC). HBCEC 699 corresponded to a benign phyllodes breast tumor as previously characterized [31,32] and exhibited little, if any, detectable CD90 expression (Fig. 2A). After mcherry transduction, the resulting HBCEC 699^{cherry} were seeded together with MSC^{GFP} at a ratio of 40% to 60%, respectively. After 10 days of co-culture, a ratio of 39.5% HBCEC 699^{cherry} and 58.7% MSC^{GFP} together with 1.8% of spontaneously fused yellow chimeric/hybrid cells was measured (Fig. 2B), whereby 91.6% of the whole co-culture population expressed CD90 (Fig. 2C), suggesting that the majority of HBCEC 699^{cherry} also acquired this antigen. Cell counting was performed with primary HBCEC 699^{GFP} and MSC^{cherry} and revealed a growth stimulation of the breast cancer cells in co-culture with MSC, whereas the cell number of MSC was decreased in co-culture compared with the appropriate amount of mono-cultured cells (Supplementary Fig. S2).

Co-culture of MSC with different ovarian cancer cell lines was also associated with growth stimulation of the tumor cells, alterations in the membrane protein composition, and the formation of a small population of spontaneously fused chimeric/hybrid cells. Thus, NIH:OVCAR-3^{cherry} cells increased from an initial population of about 40% to 73.3% in a co-culture with MSC^{GFP} after 7 days and conversely, the initially 60% MSC^{GFP} dropped to 26.7% together with transiently detectable chimeric/hybrid cells as evaluated by fluorescence cell counting using a hemocytometer (Fig. 3A). Similar results were obtained by flow cytometry with 67.0% NIH:OVCAR-3^{cherry} cells, 32.4% MSC^{GFP}, and 0.6% chimeric/hybrid cells after 7 days of co culture (Fig. 3B). CD90 expression was always detectable in about 99% of

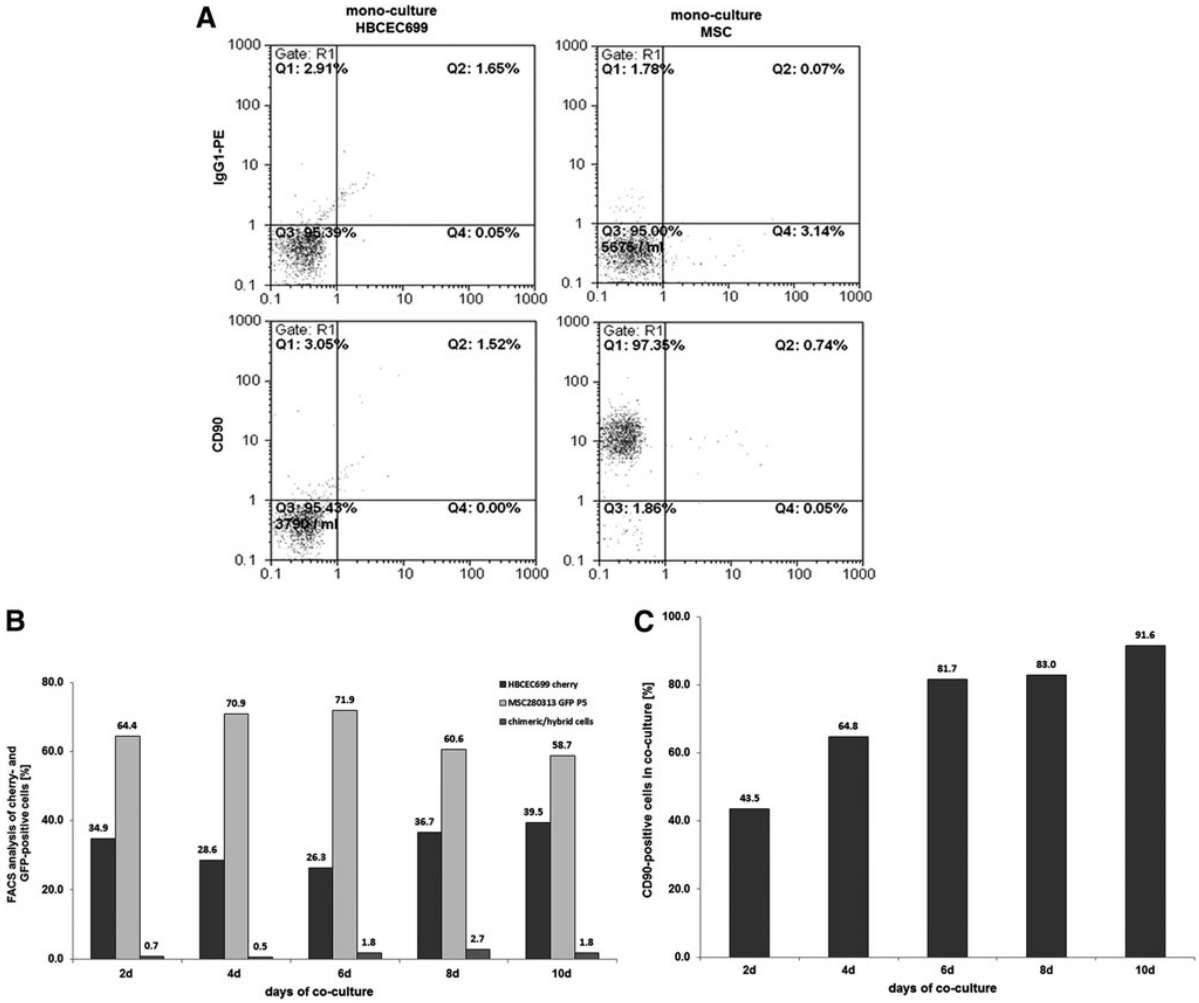

FIG. 2. Co-culture of primary MSC with human primary breast cancer epithelial cells at a ratio of 40% HBCEC 699/60% MSC with 500 cells/cm^2 till 10 days. **(A)** Detection and analysis of CD90 expression in mono-cultures of MSC280313 P5 and HBCEC 699. **(B)** Quantification of the percentage of MSC280313^{GFP} P5 and HBCEC 699^{cherry} and the formation of yellow chimeric/hybrid cells by flow cytometric analysis during a 10 day co-culture. **(C)** Quantification of the percentage of CD90-positive HBCEC 699 acquired during a 10 day co-culture with MSC. HBCEC, human breast cancer-derived epithelial cells.

MSC^{GFP} during co-culture similar to the corresponding MSC mono-cultures (Fig. 3C, D). Conversely, CD90 protein in NIH:OVCAR-3^{cherry} mono-culture was barely detectable (Fig. 3D); however, co-culture with MSC^{GFP} till 7 days continuously increased these levels from about 1.9% to 91.9% (Fig. 3C).

Steady-state human SK-OV-3 ovarian adenocarcinoma cells displayed little, if any, CD90 and CD105 expression in contrast to a pronounced presence of more than 95% of these markers in MSC (Fig. 4A). Co-culture of SK-OV-3^{cherry} with MSC^{GFP} till 7 days was associated with an elevated CD105 expression by about 12% (Fig. 4B), and CD90 expression constantly increased over time to about 69.3% in SK-OV-3^{cherry} cells (Fig. 4C). Simultaneously, the ovarian cancer cell population increased from about 40% to 58.7% by cell counting (Fig. 4D) or to 57.0% by flow cytometry analysis (Fig. 4E), whereas MSC declined from initially 60% to 41.3% by cell counting (Fig. 4D) or to 42.7% by flow cytometry analysis (Fig. 4E) within 7 days of co-culture.

The acquisition of these proteins by the tumor cells primarily required direct cell-to-cell interactions with the MSC, as western blot analysis revealed no detectable CD90 or CD105 proteins in the supernatant of the different mono- and co-cultures in contrast to a clear control staining in protein lysates of MSC (Supplementary Fig. S3).

Primary SCCOHT-1 cells expressed CD105 and functional ecto-5′-nucleotidase (CD73) after co-culture with MSC

The SCCOHT-1 cells, which represent a completely different tumor entity of a small cell hypercalcemic type as compared with other ovarian cancers constitutively,

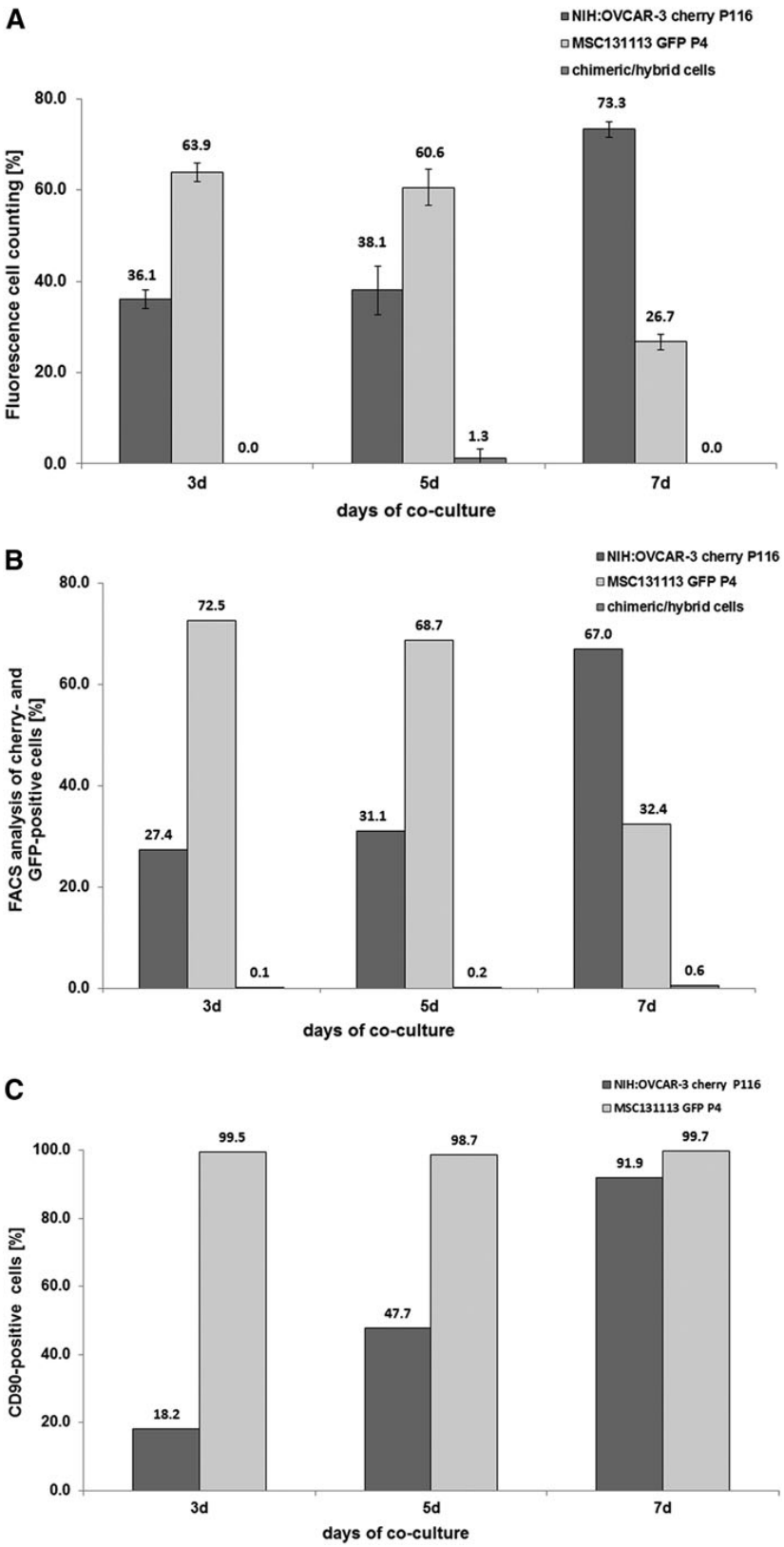

FIG. 3. Co-culture of primary MSC with human ovarian cancer cells at an initial ratio of 40% NIH:OVCAR-3/60% MSC with 2,000 cells/cm^2 till 7 days. **(A)** Cell counting of MSC131113^{GFP} P4 and NIH:OVCAR-3^{cherry} and yellow chimeric/hybrid cells using a fluorescence microscope (Olympus IX50) with a FITC/TRIC fluorescence dual band filter and calculation of the population percentage during a 7 day co-culture. **(B)** Quantification of the percentage of MSC131113^{GFP} P4 and NIH:OVCAR-3^{cherry} and the formation of yellow chimeric/hybrid cells by flow cytometric analysis during a 7 day co-culture. **(C)** Quantification of the percentage of CD90-positive NIH:OVCAR-3 cells acquired during a 7 day co-culture with MSC. **(D)** Detection and analysis of CD90 expression in mono-cultures of MSC and NIH:OVCAR-3 cells.

(*Figure continued*→)

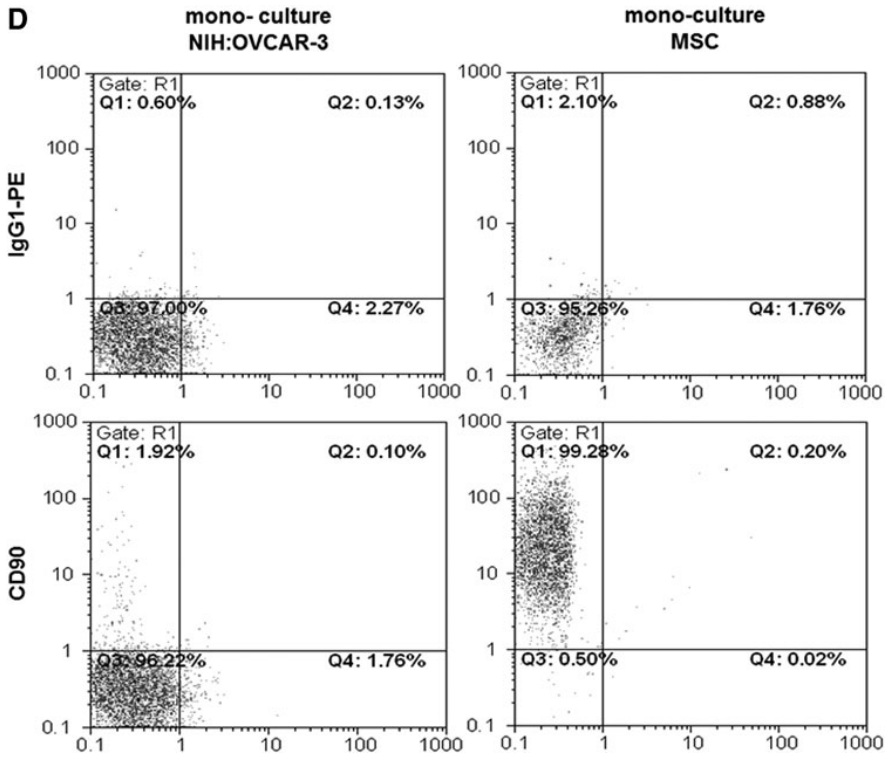

FIG. 3. (Continued).

expressed CD90 in more than 99% of the population-like MSC [22]. In contrast, little, if any, CD73 or CD105 was detectable in SCCOHT-1 cells as compared with MSC (Fig. 5A). However, co-culture of SCCOHT-1^{cherry} with MSC^{GFP} was associated with CD73 expression in 10.2% (Fig. 5B) and expression of CD105 in 12.1% of the cancer cell population at day 7, which already appeared after 3 days and remained at about this level (Fig. 5C). The appearance of CD73 (= ecto-5′-nucleotidase) in SCCOHT-1 after co-culture with MSC also demonstrated intact enzymatic activity by the acquired capability of SCCOHT-1 cells to metabolize purine 5′-mononucleotides. Thus, steady-state cultures of SCCOHT-1 demonstrated 5′-AMP substrate concentrations of 2,205 ± 18.7 pmol/100 μL ($n = 3$) during incubation with little detectable production of adenosine similar to a no cell PBS control displaying 2,071.7 ± 185.1 pmol/100 μL ($n = 3$) of the 5′-AMP substrate (Fig. 5D). In contrast, analysis by liquid chromatography coupled with tandem mass spectrometry revealed significantly decreased levels of 1,461.7 ± 86.1 pmol/100 μL ($n = 3$) 5′-AMP paralleled by a more than 13-fold increased adenosine production in co-cultured SCCOHT-1 cells. Indeed, the acquisition of 5′-AMP metabolization was detectable after FACS separation of SCCOHT-1 from a 5 days MSC co-culture with a purity of about 97.5% (Fig. 5E). As a control, constitutively CD73-expressing MSC mono-cultures produced 911.6 ± 100.9 pmol/100 μL ($n = 3$) adenosine with a paralleled decline of the 5′-AMP substrate to 218.0 ± 52.6 pmol/100 μL ($n = 3$). Similar data were obtained from MSC after FACS separation of a 5 days co-culture with SCCOHT-1 cells (Fig. 5D).

Transcript analysis of acquired MSC markers during co-culture

RNA isolation and PCR analysis was performed in mono-cultures and after separation of co-cultures by FACS to distinguish between the possibilities of transferring premade proteins as opposed to transferring mRNA and/or transcriptional regulators that induce expression of these proteins in co-cultured cells. Although little, if any, CD73 gene expression was measured in SCCOHT-1 cells and no detectable CD105 mRNAs in SCCOHT-1 and SK-OV-3 cells, both of these transcripts were significantly expressed after co-culture of the tumor cells in the presence of MSC (Fig. 5F, upper panel). Likewise, the absence of CD90 mRNAs in SK-OV-3 cells became detectable after co-culture with MSC (Fig. 5F, lower panel). Altered levels of distinct mRNAs were also observed during co-culture of MSC with HMEC as a nontumorigenic cell population. Although CD73 was constitutively expressed in HMEC (P13), little, if any, CD105 mRNAs were detectable in the HMEC mono-cultures. However, these transcripts were enhanced in HMEC after MSC co-culture (Fig. 5G).

Epithelial cell adhesion molecule (EpCAM/CD326) became detectable in MSC after co-culture with ovarian carcinoma cells

Acquisition of new proteins also worked in the opposite direction that MSC revealed new markers during interactions with cancer cells. There was little, if any, detectable expression of the CD326 epithelial cell adhesion molecule

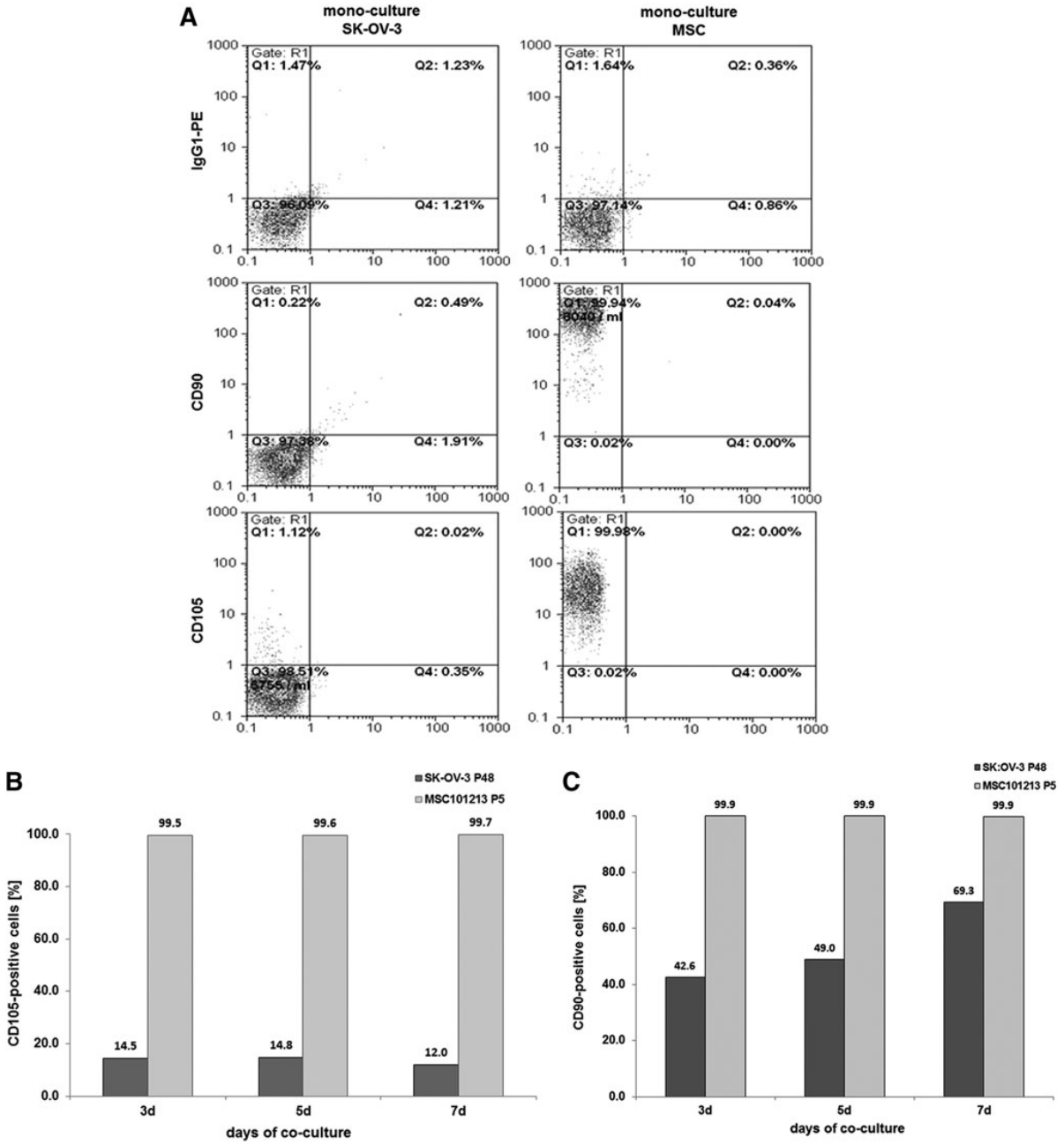

FIG. 4. Co-culture of primary MSC (MSC101213 P5 and MSC 131113 P4) with human ovarian adenocarcinoma cells at an initial ratio of 40% SK-OV-3/60% MSC with 2,000 cells/cm^2 till 7 days. **(A)** Detection and analysis of CD90 and CD105 expression in mono-cultures of SK-OV-3 cells and MSC. **(B)** Quantification of the percentage of CD105-positive SK-OV-3 cells acquired during a 7 day co-culture with MSC101213. **(C)** Quantification of the percentage of CD90-positive SK-OV-3 cells acquired during a 7 day co-culture with MSC101213. **(D)** Cell counting of MSC131113^{GFP} P4 and SK-OV-3^{cherry} and yellow chimeric/hybrid cells using a fluorescence microscope (Olympus IX50) with an FITC/TRIC fluorescence dual band filter and calculation of the population percentage during a 7 day co-culture. **(E)** Quantification of the percentage of MSC131113^{GFP} P4 and SK-OV-3^{cherry} and the formation of yellow chimeric/hybrid cells by flow cytometric analysis during a 7 day co-culture.

(*Figure continued*→)

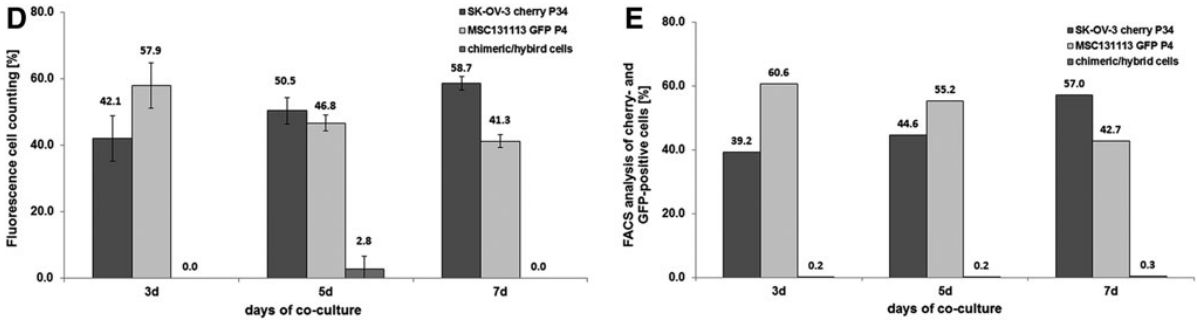

FIG. 4. (Continued).

(EpCAM) in MSC populations in contrast to a significant EpCAM expression of more than 99% in the epithelial-like ovarian tumor cells SK-OV-3 and NIH:OVCAR-3 (Fig. 6A). Co-culture of MSC with the ovarian tumor cells, however, was accompanied by continuously increasing EpCAM levels in MSC. About 23% of MSC displayed EpCAM after co-culture with SK-OV-3 cells (Fig. 6B), and about 45% of MSC demonstrated EpCAM expression after intercellular communication with NIH:OVCAR-3 cells till 7 days (Fig. 6C).

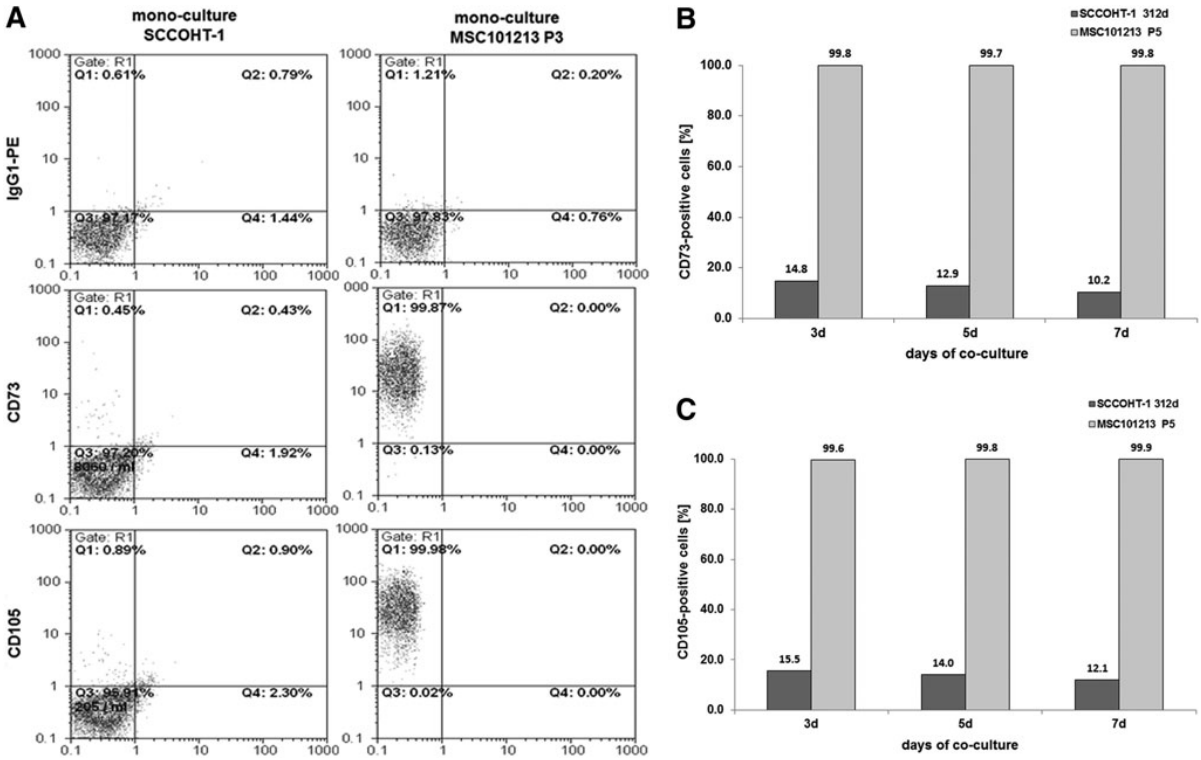

FIG. 5. Co-culture of primary MSC with human small cell ovarian carcinoma cells hypercalcemic type at an initial ratio of 40% SCCOHT-1/60% MSC with 2,000 cells/cm^2 till 7 days. **(A)** Detection and analysis of CD73 and CD105 expression in mono-cultures of SCCOHT-1 cells and MSC. **(B)** Quantification of the percentage of CD73-positive SCCOHT-1 cells acquired during a 7 day co-culture with MSC101213. **(C)** Quantification of the percentage of CD105-positive SCCOHT-1 cells acquired during a 7 day co-culture with MSC101213. **(D)** Quantification of acquired 5′ nucleotidase enzymatic activity by liquid chromatography/tandem mass spectrometry analysis of 5′AMP and adenosine. Data represent the mean ± SD of three independent experiments. A statistical analysis between the mono-culture and the corresponding population in co-culture was conducted by unpaired Student's *t*-test (**$P < 0.01$). **(E)** SCCOHT-1 cells previously co-cultured with MSC were separated by fluorescence-activated cell sorting (FACS), and sorted SCCOHT-1 cells were analyzed for purity by a GFP flow cytometry analysis. **(F)** RT-PCR of CD73 and CD105 transcripts (*upper panel*) and CD90 transcripts (*lower panel*) was performed in SCCOHT-1^{cherry} and SK-OV-3^{cherry} mono-cultures as compared with a 7 day co-culture with MSC^{GFP} and subsequent separation by fluorescence-activated cell sorting. **(G)** RT-PCR of transcripts in MSC^{GFP} and HMEC (P13) mono-cultures were compared with a 7 day co-culture and subsequent separation by fluorescence-activated cell sorting. Unaltered β-actin expression was used as a control. HMEC, human mammary epithelial cells; RT-PCR, reverse transcription PCR.

(*continued*)

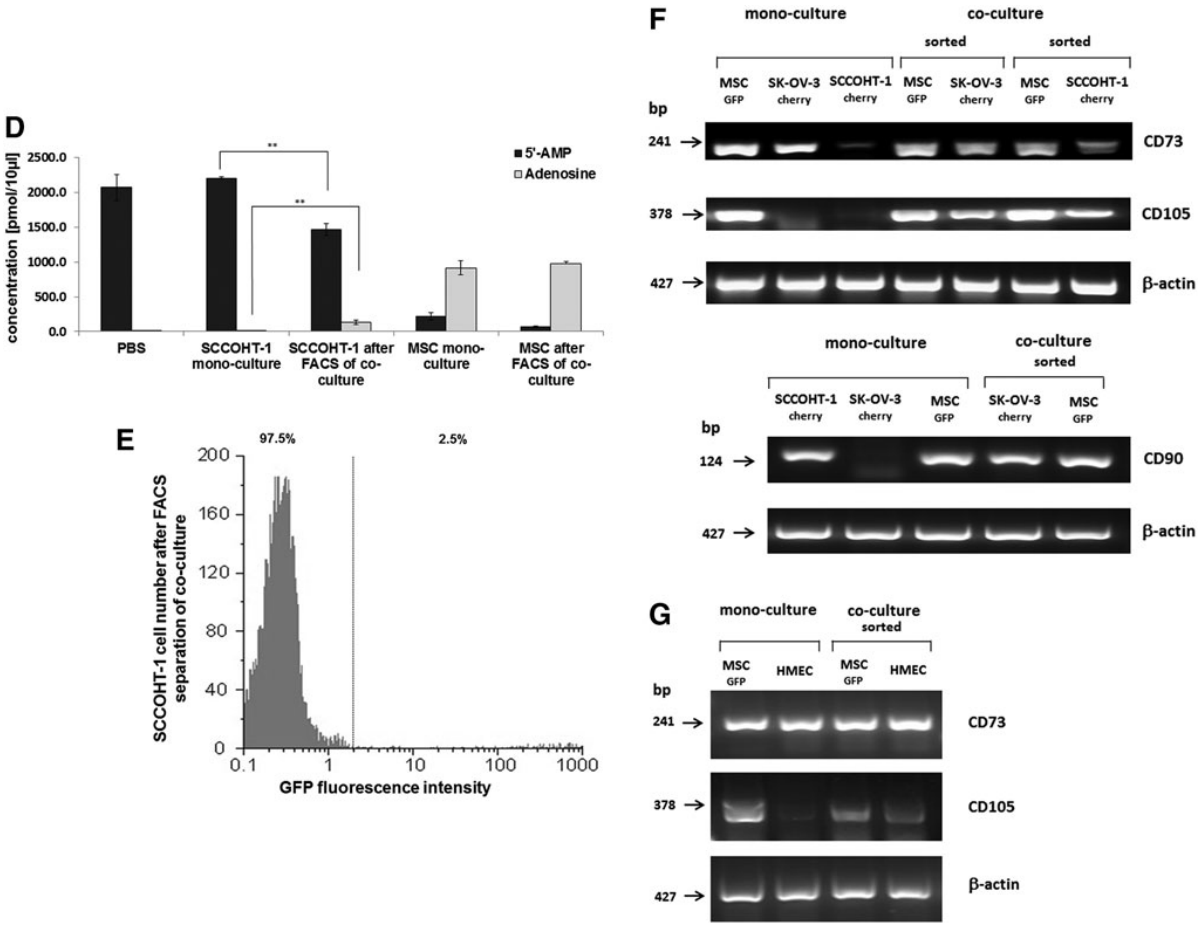

FIG. 5. (Continued).

Altered protein expression (CD90, CD105) could be abolished by cytochalasin D

Morphological evaluation of the cellular interactions between various MSC^{GFP} populations and different kinds of tumor cells, including MCF-7^{cherry} breast cancer cells (Fig. 7A), revealed cell contacts by the extension of small cytoplasmic protrusions (nanotubes) and exchange of small vesicles (exosomes). Nanotubes (yellow arrows) and GFP-labeled exosomes originating from MSC (white arrows) could be detected between MSC and MCF-7 tumor cells (Fig. 7A). Similar structures were also observed in co-cultures of MSC^{GFP} with NIH:OVCAR-3^{cherry} ovarian adenocarcinoma cells (Supplementary Fig. S4A), SK-OV-3^{cherry} epithelial-like ovarian cancer cells (Supplementary Fig. S4B), and SCCOHT-1^{cherry} small cell hypercalcemic tumor cells of the ovary (Supplementary Fig. S4C), respectively. Furthermore, the release of exosomes and extension of nanotubes was also detectable in MSC monocultures (Supplementary Fig. S4D).

The formation of distinct chimeric/hybrid cells was observed in each of the co-cultures and demonstrated yellow-colored populations by a simultaneous expression of cherry protein and eGFP (Fig. 7B). This observation indicated spontaneous cell fusion between a mesenchymal stem cell and a corresponding tumor cell as previously described for MDA-MB-231 breast cancer cell hybrids [16,26]. Further characterization of such a chimeric/hybrid cell clone revealed CD90 expression by about 90.4% compared with a parental expression of 97.1% in MSC but undetectable levels of less than 0.1% in parental MDA-MB-231 cells (Table 1). The type-1 membrane glycoprotein CD200 (Ox-2) was detectable in 47.9% of MSC and in 69.3% of MDA-MB-231 cells, which was combined to 74.4% in chimeric/hybrid cells. Moreover, cytokeratins were detectable in 99.7% of chimeric/hybrid cells compared with a parental expression of 99.6% in MDA-MB-231 cells but only about 54.1% in parental MSC (Table 1).

To further explore the cellular interactions and the mutual acquisition of membrane proteins, cytochalasin D (cyt D) was applied to the co-cultures to inhibit a potential exchange of membrane proteins between the co-cultured cell populations via exosomes, formation of nanotubes, or exchange of membrane parts by a process termed trogocytosis [33]. Evaluation of a concentration dependency for cyt D in MSC, MCF-7, SK-OV-3, or NIH:OVCAR-3 cells revealed sublethal concentrations of 50 nM in these cell populations (data not shown). MCF-7 cells demonstrated about 66% and

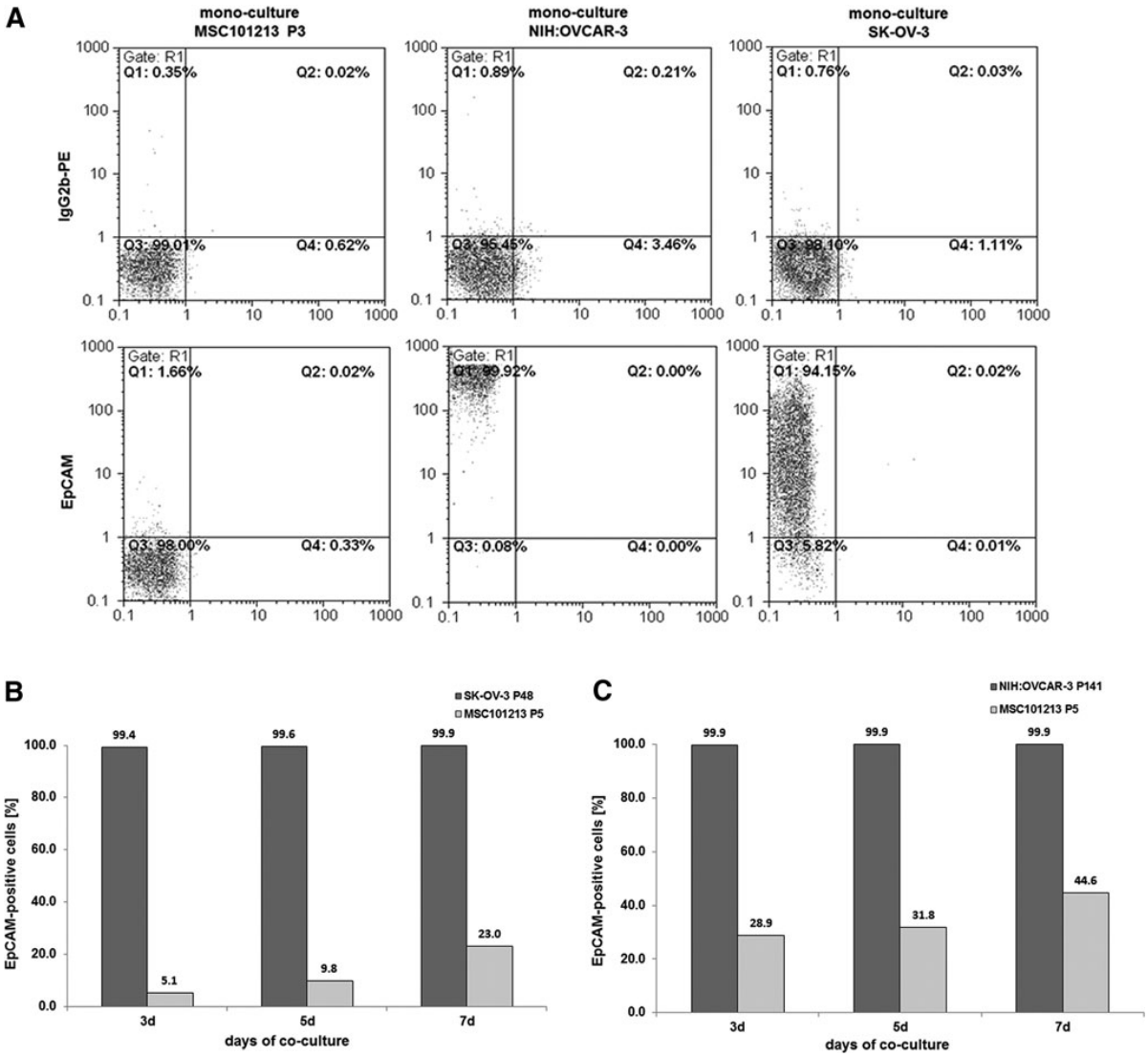

FIG. 6. Co-culture of primary MSC with different human ovarian carcinoma cells (SK-OV-3, NIH:OVCAR-3) at an initial ratio of 40% ovarian carcinoma cells/60% MSC with 2,000 cells/cm^2 till 7 days. **(A)** Detection and analysis of steady-state CD326 (EpCAM) expression in mono-cultures of MSC101213, SK-OV-3, and NIH:OVCAR-3 cells, respectively. **(B)** Quantification of the percentage of EpCAM-positive MSC acquired during a 7 day co-culture with SK-OV-3 cells. **(C)** Quantification of the percentage of EpCAM-positive MSC acquired during a 7 day co-culture with NIH:OVCAR-3 cells. EpCAM, epithelial cell adhesion molecule.

67.7% CD90 expression after 3 and 5 days of co-culture with MSC, respectively, and incubation of this co-culture in the presence of 50 nM cyt D was associated with a marked reduction of the CD90 levels to 36.2% and 32.4% after 3 and 5 days, respectively (Fig. 7C). About 48.4% and 52.6% of SK-OV-3 cells demonstrated CD90 expression after 3 and 5 days of MSC co-culture; however, cyt D treatment significantly reduced these CD90 levels to about 17.8% and 5.4%, respectively. Likewise, CD90 acquisition during co-culture of MSC with NIH:OVCAR-3 cells was markedly reduced in the presence of cyt D (Fig. 7C). A similar effect of cyt D was observed for the acquisition of CD105. Co-culture of SK-OV-3 cells with MSC till 3 days revealed always more than 99% of CD105 in MSC paralleled by progressively increasing CD105 in SK-OV-3 cells from 1.4% at 0 day to 12.6% after 3 days (Fig. 7D, upper panel), whereas co-culture in the presence of 50 nM cytochalasin D was accompanied by markedly reduced CD105 levels of only 2.6% in SK-OV-3 cells after 3 days while CD105 expression was sustained in more than 99% of MSC (Fig. 7D, lower panel). Together, these effects suggested that cyt D predominantly inhibits the acquisition of new membrane proteins such as CD90 and CD105 by the tumor cells, as no effects were observed on the steady-state expression of these membrane proteins by cyt D in MSC mono-cultures (Fig. 7E).

Microarray analysis of MSC co-culture with NIH:OVCAR-3 cells

More detailed functional alterations were observed after microarray analysis of co-cultured cells (Supplementary Table S1–S4). After a 7 days co-culture of MSC^{GFP} and NIH:OVCAR-3^{cherry} cells, the two cell populations were separated into the appropriate mono-cultures by double FACS to yield about 99% of NIH:OVCAR-3 corresponding cherry-positive and MSC corresponding GFP-positive cells, respectively (Fig. 7F, left panel). Selected microarray data of these co-culture-separated MSC compared with steady-state

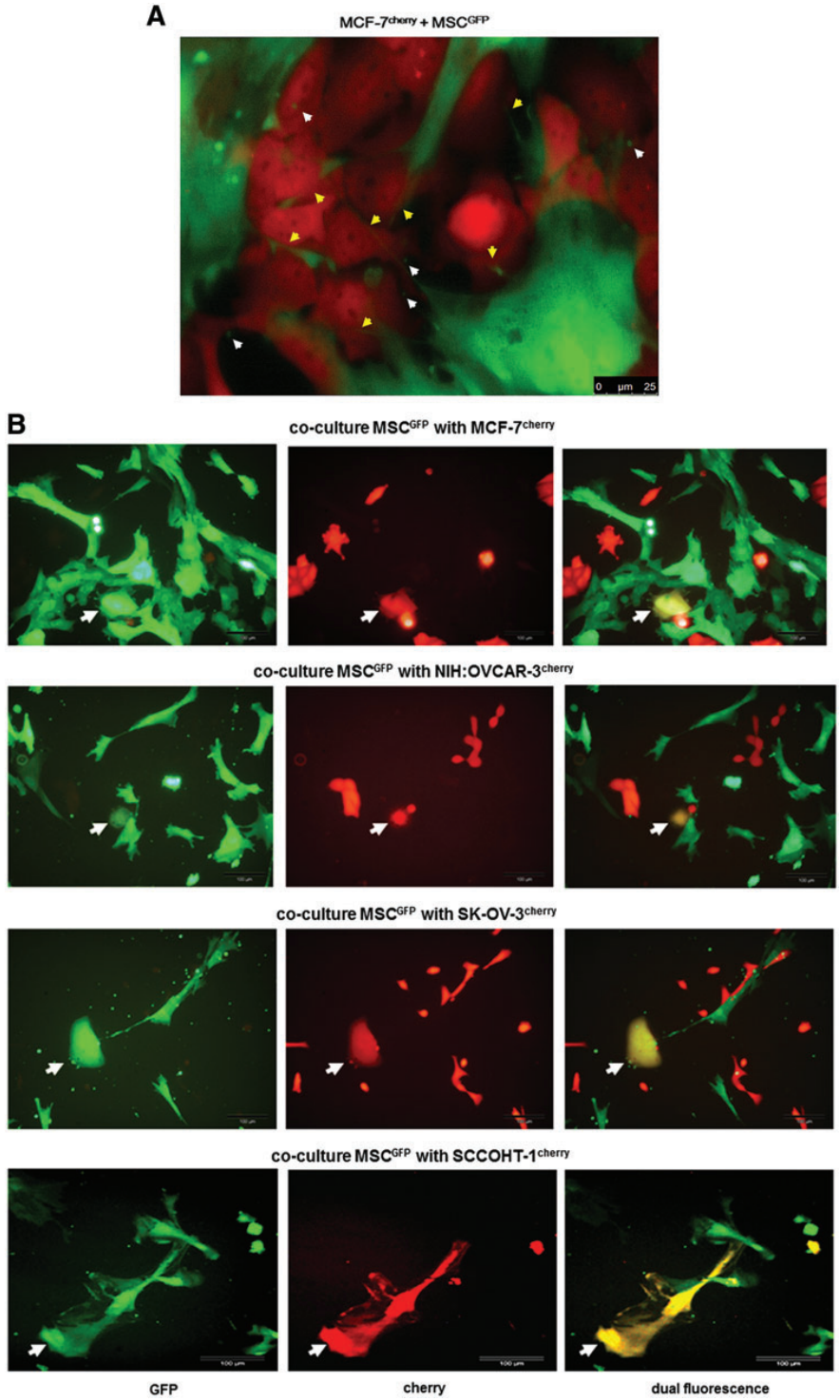

FIG. 7. **(A)** The morphology during co-culture of MSC180314^{GFP} P3 and MCF-7^{cherry} cells demonstrated various cellular interactions with the extension of nanotubes (*yellow arrows*), formation of exosomes (*white arrows*), and overlapping membranes. Scale bars represent 25 µm. **(B)** Co-culture of MSC^{GFP} with different tumor cell lines demonstrated the formation of yellow chimeric/hybrid cells by simultaneous expression of cherry protein and eGPF (*white arrows*). Scale bars represent 100 µm. **(C)** Quantification of acquired CD90 by MCF-7, SK-OV-3, and NIH:OVCAR-3 cells after a 3 and 5 day co-culture with primary MSC180314 P3, respectively, and effect of 50 nM cytochalasin D in these co-cultures. **(D)** Quantification of acquired CD105 by SK-OV-3 cells within 3 days of co-culture with primary MSC100314 P3 (*upper panel*) and effect of 50 nM cytochalasin D in these co-cultures (*lower panel*). **(E)** Effect of cytochalasin D on the constitutive expression of CD90 and CD105 in 3 and 5 days cultured MSC270114 P2. **(F)** Flow cytometric analysis of double FACS-separated cells from a 7 day MSC180314^{GFP} P6 and NIH:OVCAR-3^{cherry} co-culture (*left panels*) and microarray analysis of the separated populations revealed selected prominent changes in gene expression of co-cultured MSC^{GFP} (*upper right panel*) and co-cultured NIH:OVCAR-3^{cherry} cells (*lower right panel*). Color images available online at www.liebertpub.com/scd

(*Figure continued*→)

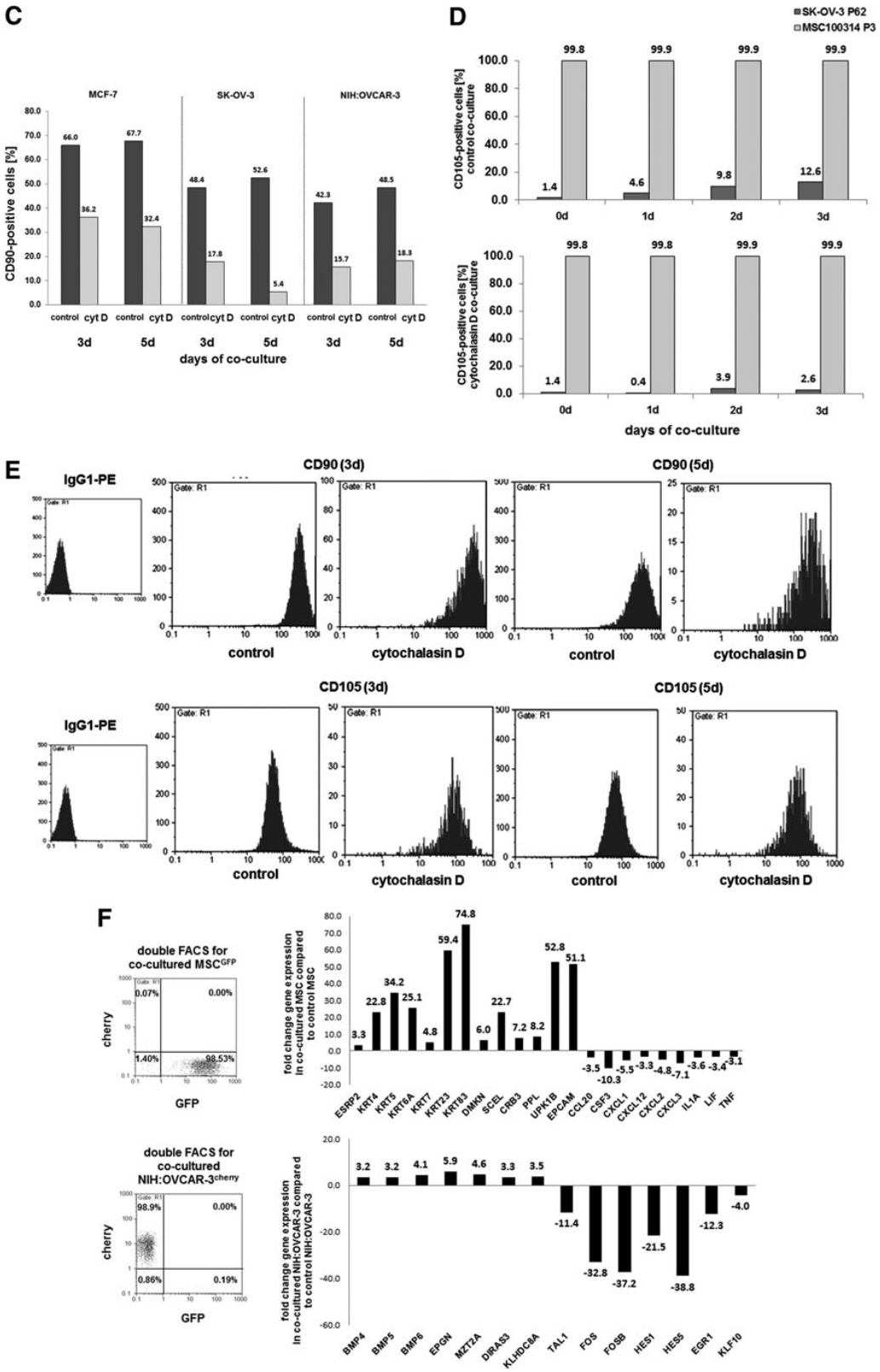

FIG. 7. (Continued).

Table 1. Analysis of Certain Protein Marker Expression by Flow Cytometry

Protein	*MSC (%)*	*MDA-MB-231 (%)*	*Chimeric/hybrid cells (%)*
CD90	97.1	< 0.1	90.4
CD200	47.9	69.3	74.4
Pan-cytokeratin	54.1	99.6	99.7

MSC, mesenchymal stroma/stem cells.

MSC revealed an increase of epithelial cell-specific transcripts, including the *ESPR2* splicing regulator and a variety of cytokeratins (*KRT* genes). Moreover, transcripts of the epithelial-like differentiation factors dermokine and sciellin that contribute to keratinocyte differentiation were up-regulated in co-cultured MSC. Likewise, regulators of cell–cell interactions, including transcripts of the epithelial cell-specific tight junction factor *CRB3*, desmosomal periplakin (*PPL*), and members of the tetraspanin transmembrane components in epithelial cells (*UPK1B*), were significantly elevated in co-cultured MSC. In addition, *EpCAM* mRNAs were markedly enhanced by 51.1-fold in co-cultured MSC, suggesting that MSC acquired a variety of epithelial-like cell functionality during co-culture with NIH:OVCAR-3 cells. Furthermore, a variety of chemokine/cytokine transcripts were down-modulated in co-cultured MSC (Fig. 7F, upper right panel).

Selected genes in co-cultured NIH:OVCAR-3 cells compared with steady-state NIH:OVCAR-3 cells demonstrated an up-regulation of growth factors (*BMPs*), epithelial mitogens (*EPGN*), and mitotic spindle-associated factors (*MZT2A*), which promote proliferative capacity. The protein product of the *DIRAS3* gene can function as a putative tumor suppressor, whereas the induced kelch domain-containing transcript (*KLHDCA8*) is associated with elevated tumor aggressiveness. Down-regulated genes in NIH:OVCAR-3 cells included a variety of transcription factor genes such as *TAL1*, the basic helix-loop-helix family *FOS* and *FOSB*, and also *HES1* and HES5, which are suggested to promote cancerous development on down-modulation. Likewise, genes of zinc finger transcription factors are down-regulated such as *EGR1* and the Kruppel-like factor (*KLF10*) as a repressor of cell growth (Fig. 7F, lower right panel).

Discussion

Invasive tumor growth causes local tissue injuries that are associated with the attraction of MSC to take part in repair mechanisms. This process is also accompanied by interactions between the adjacent neighboring cells, whereby the close vicinity of mesenchymal stem/stroma cells contributes toward altering the proliferative capacity and a certain functionality of the tumor cells.

Co-culture of different cancer cell populations with six individual MSC primary cultures revealed a growth stimulation of the tumor cells, which was also supported by induction of proliferation-promoting genes in NIH:OVCAR-3 cells and down-modulation of certain transcription factor genes with repressor function of tumorigenic development and cell growth. Furthermore, these findings are substantiated by a previous work demonstrating enhanced tumor cell growth by MSC [34–37], although there are also controversial studies suggesting a reduced tumor cell proliferation in the presence of MSC [38,39]. The divergent effects of MSC on tumor cells may be caused, in part, by a different activation status within the heterogeneous MSC population involving interference with the β-catenin pathway such as DKK-1-mediated depression of Wnt signaling [40]. Moreover, secretory pathways within the tumor cell microenvironment such as MSC-mediated release and activation of distinct matrix metalloproteinases interfere with the migratory and invasive potential of tumor cells and reduce their tumorigenicity [41]. Other work postulated bidirectional effects of naïve or innate MSC on tumors with promotion or inhibition of tumor progression, whereas MSC already primed by inflammatory factors within the tumor microenvironment promote tumor progression [42].

MSC that express CD73, CD90, and CD105 surface markers can transfer, exchange, or induce these proteins during their interactions with tumor cells, thereby altering cellular functionality with the consequence of increased tumor heterogeneity. Little, if any, of the GPI-anchored CD90 antigen was expressed in MCF-7, HBCEC 699, NIH:OVACAR-3, and SK-OV-3 cells; however, co-culture of these human cancer cells with different MSC populations was accompanied by a CD90 induction at both the mRNA and protein levels. Moreover, endoglin (CD105) as a part of the TGFβ receptor complex that is predominantly involved in the regulation of angiogenesis in tumors was acquired by SK-OV-3 and SCCOHT-1 cells on MSC interactions. Furthermore, changes in cellular functionality during co-culture with MSC were also observed for acquisition of CD73 transcripts and expression of the active enzyme by SCCOHT-1 cells. This ecto-5′-nucleotidase is associated to the external face of the plasma membrane via a GPI-anchor and catalyzes the dephosphorylation of purine 5′-mononucleotides, particularly AMP, which increases extracellular levels of nucleosides [43]. Therefore, the acquisition of this property by SCCOHT-1 cells in response to interactions with MSC alters the tumor cell functionality and contributes to changes in nucleoside concentrations within the microenvironment on availability of corresponding substrates. Contrary to these functional changes of the tumor cells, the direct intercellular communication processes also affected MSC. The epithelial cell-specific adhesion molecule (CD326/EpCAM), which functions as a transmembrane glycoprotein mediating Ca^{2+}-independent homotypic cell–cell adhesion in epithelia, was undetectable in MSC. However, co-culture of the ovarian cancer cells with MSC was associated with EpCAM mRNA and protein induction, which suggested certain differentiation processes by adding epithelial cell-like properties to the MSC. Such heterogenic functionality was also discussed in vivo with EpCAM-positive subsets of tumor-initiating cells (cancer stem cells) in patient ovarian cancer ascites also carrying markers of cancer-associated fibroblasts [44]. Other in vivo studies demonstrated cross-talk of MSC with tumor cells and promotion of tumor growth in patients with head and neck cancer, whereby MSC isolated from these patient tumors constitutively produced high levels of IL-6, IL-8, and stromal cell-derived factor (SDF)-1α [45]. In addition, co-transplantation of human adipose tissue-derived MSC with MDA-MB-231 breast

cancer cells exhibited partial EMT and was associated with development of tumor xenograft metastases to multiple mouse organs [46].

The alteration in the cellular functionality of tumor cell populations and MSC within the tumor microenvironment contributes to tumor heterogeneity [47] and suggests a process of mutual cellular adaptation whereby MSC acquire tumor cell-specific markers and vice versa. Indeed, enhanced gene expression of epithelial cell-specific markers appeared in MSC after co-culture with ovarian epithelial cancer cells whereas MSC-like properties such as expression of certain chemokine/cytokine genes were down-modulated. These functional alterations can result in MSC differentiation of an altered phenotype, including cancer-associated fibroblasts, perivascular cells, or tumor-associated macrophage-like cells [48]. Moreover, co-culture with injured mesangial cells has demonstrated differentiation of MSC into mesangial cells [49]. In addition, direct co-culture of MSC with human nucleus palposus cells resulted in differentiation of MSC to a nucleus palposus-like phenotype associated with up-regulation of appropriate growth factor and matrix-associated genes [50].

Mutual cellular adaptation was suggested between cells from ductal invasive breast cancer and surrounding MSC [16,51–53], and further studies revealed that disseminated tumor-like cells originating from breast cancer tissue can be long-term hosted in an inactivated (dormant) state in perivascular niches [54], which also provides the stem cell niche for MSC. Therefore, the characterization of a variety of tumor-specific cell types, including cancer-associated fibroblasts or cancer stem cells, may likewise originate from processes of mutual cellular adaptation within the tumor microenvironment. Moreover, altered tumor cell functions during MSC interactions within the tumor microenvironment carry the risk of therapy failure by developing cancer cells displaying certain resistances [55].

According to functional changes by mRNA and/or protein transfer or protein induction via specific communication processes, a previous work confirmed that cellular interactions can promote an MSC-mediated protein expression in MDA-MB-231 breast cancer or natural killer cells, which partially involves GJIC and notch signaling [26,56]. Furthermore, this study demonstrated that the direct interactions include the transfer and exchange of cellular material. This was also substantiated by fluorescence microscopy demonstrating close membrane interactions between MSC and the co-cultured tumor cells together with exosome release and the extension of cytoplasmic protrusions that appear as nanotubes. Exosomes represent the release of extracellular vesicles carrying predominantly proteins, mRNAs, and microRNAs that are exchanged during cellular interactions [57]. Production of exosomes has been described for MSC to transport gene regulatory information to recipient cells that can modulate cell growth and angiogenesis by affecting a variety of cellular pathways [58]. Indeed, the CD73, CD90, and CD105 induction in the different tumor cells was observed at both the protein and mRNA levels, suggesting exchange of proteins and/or transcriptional regulators and/or mRNAs between MSC and co-cultured tumor cells. Moreover, these interactive properties of MSC were also observed in normal cells such as HMEC after MSC co-culture.

Intercellular structures, including membrane channels such as tunneling nanotubes, also enable a direct exchange of biomolecules and small organelles and may also serve as a tool for tumor cell interactions [59]. Thus, a previous work revealed increased regenerative support during nanotubular cross-talk between MSC and damaged cardiomyocytes [60]. Intercellular transport via nanotubes requires actin microfilaments to transmit traction and contraction forces that can be blocked by cytochalasin D for inhibition of actin polymerization. In this context, the transfer between MSC and the different tumor cell populations was significantly reduced in the presence of cytochalasin D. Confirmative studies have demonstrated that formation of nanotubes between MSC and vascular smooth muscle cells enables the exchange of proteins and mitochondria associated with elevated MSC growth that can be abolished by cytochalasin D [61]. These findings suggested that the extent of cellular interactions between MSC and tumor cells is associated with different levels of exchange such as exchange of exosomes or membrane patches or a combination of whole cell membranes by cell fusion. Indeed, all MSC co-cultures revealed a small amount of chimeric/hybrid cells, indicating MSC-tumor cell fusion products. This phenomenon has also been observed in other MSC co-cultures [16,26], and characteristics revealed the acquisition of distinct markers from both parental cell populations. Although most fusion products between MSC and tumor cells are unable to survive due to aberrant signaling by two nuclei, a small amount of chimeric/hybrid cells arrange chromosome/DNA regulation and result in various individual hybrid populations displaying altered expression levels compared with the parental cell types. Fusion of tumor cells with macrophages or bone marrow-derived cells has been discussed in the context of cancer invasion and metastasis [62], whereas the development and progression of chimeric/hybrid populations enhances tumor heterogeneity and complicates therapeutic approaches.

Conclusion

Co-culture of various human cell populations with different individual MSC populations was accompanied by exchange of biological material via different mechanisms, including exosomes and formation of nanotubes. During these cellular interactions, a variety of functional changes were observed, particularly the acquisition of multiple epithelial cell-like properties by MSC after co-culture with ovarian cancer cells and vice versa, an elevated growth of tumor cells. These findings suggested a progressive functional heterogeneity by a process of mutual cellular adaptation.

Acknowledgments

The technical assistance of Juliane von der Ohe and the essential support for the GC/tandem MS analysis by the Metabolomics core unit (Dr. Volkhard Kaever) as well as for the cell separation by the FACS core unit (Dr. Matthias Ballmaier) and the microarray analysis by the research core unit Transcriptomics (Dr. Oliver Dittrich-Breiholz) of Hannover Medical School is acknowledged. Yuanyuan Yang is a visiting research fellow from Tongji University, Shanghai, China.

Author Disclosure Statement

The authors declare no financial, personal, or professional conflicts of interest.

References

1. Caplan AI. (1991). Mesenchymal stem cells. J Orthop Res 9:641–650.
2. Pittenger MF, AM Mackay, SC Beck, RK Jaiswal, R Douglas, JD Mosca, MA Moorman, DW Simonetti, S Craig and DR Marshak. (1999). Multilineage potential of adult human mesenchymal stem cells. Science 284:143–147.
3. Dominici M, K Le Blanc, I Mueller, I Slaper-Cortenbach, F Marini, D Krause, R Deans, A Keating, D Prockop and E Horwitz. (2006). Minimal criteria for defining multipotent mesenchymal stromal cells. The International Society for Cellular Therapy position statement. Cytotherapy 8:315–317.
4. Simmons PJ and B Torok-Storb. (1991). Identification of stromal cell precursors in human bone marrow by a novel monoclonal antibody, STRO-1. Blood 78:55–62.
5. Honczarenko M, Y Le, M Swierkowski, I Ghiran, AM Glodek and LE Silberstein. (2006). Human bone marrow stromal cells express a distinct set of biologically functional chemokine receptors. Stem Cells 24:1030–1041.
6. Kuroda Y, M Kitada, S Wakao, K Nishikawa, Y Tanimura, H Makinoshima, M Goda, H Akashi, A Inutsuka, et al. (2010). Unique multipotent cells in adult human mesenchymal cell populations. Proc Natl Acad Sci U S A 107: 8639–8643.
7. Caplan AI and D Correa. (2011). The MSC: an injury drugstore. Cell Stem Cell 9:11–15.
8. Katsuda T, N Kosaka, F Takeshita and T Ochiya. (2013). The therapeutic potential of mesenchymal stem cell-derived extracellular vesicles. Proteomics 13:1637–1653.
9. Aggarwal S and MF Pittenger. (2005). Human mesenchymal stem cells modulate allogeneic immune cell responses. Blood 105:1815–1822.
10. Hass R, C Kasper, S Bohm and R Jacobs. (2011). Different populations and sources of human mesenchymal stem cells (MSC): A comparison of adult and neonatal tissue-derived MSC. Cell Commun Signal 9:12.
11. De Miguel MP, S Fuentes-Julian, A Blazquez-Martinez, CY Pascual, MA Aller, J Arias and F Arnalich-Montiel. (2012). Immunosuppressive properties of mesenchymal stem cells: advances and applications. Curr Mol Med 12:574–591.
12. Ruster B, S Gottig, RJ Ludwig, R Bistrian, S Muller, E Seifried, J Gille and R Henschler. (2006). Mesenchymal stem cells display coordinated rolling and adhesion behavior on endothelial cells. Blood 108:3938–3944.
13. Nassiri SM and R Rahbarghazi. (2014). Interactions of mesenchymal stem cells with endothelial cells. Stem Cells Dev 23:319–332.
14. Friedl P and S Alexander. (2011). Cancer invasion and the microenvironment: plasticity and reciprocity. Cell 147: 992–1009.
15. Ungefroren H, S Sebens, D Seidl, H Lehnert and R Hass. (2011). Interaction of tumor cells with the microenvironment. Cell Commun Signal 9:18.
16. Hass R and A Otte. (2012). Mesenchymal stem cells as all-round supporters in a normal and neoplastic microenvironment. Cell Commun Signal 10:26.
17. Dubeau L. (2008). The cell of origin of ovarian epithelial tumours. Lancet Oncol 9:1191–1197.
18. Kurman RJ and M Shih Ie. (2010). The origin and pathogenesis of epithelial ovarian cancer: a proposed unifying theory. Am J Surg Pathol 34:433–443.
19. Kim A, Y Ueda, T Naka and T Enomoto. (2012). Therapeutic strategies in epithelial ovarian cancer. J Exp Clin Cancer Res 31:14.
20. Young RH, E Oliva and RE Scully. (1995). Small cell carcinoma of the hypercalcemic type in the ovary. Gynecol Oncol 57:7–8.
21. Hass R and C Bertram. (2009). Characterization of human breast cancer epithelial cells (HBCEC) derived from long term cultured biopsies. J Exp Clin Cancer Res 28:127.
22. Otte A, G Gohring, D Steinemann, B Schlegelberger, S Groos, F Langer, HH Kreipe, A Schambach, T Neumann, et al. (2012). A tumor-derived population (SCCOHT-1) as cellular model for a small cell ovarian carcinoma of the hypercalcemic type. Int J Oncol 41:765–775.
23. Lavrentieva A, I Majore, C Kasper and R Hass. (2010). Effects of hypoxic culture conditions on umbilical cord-derived human mesenchymal stem cells. Cell Commun Signal 8:18.
24. Otte A, V Bucan, K Reimers and R Hass. (2013). Mesenchymal stem cells maintain long-term in vitro stemness during explant culture. Tissue Eng Part C Methods 19:937–948.
25. Bertram C and R Hass. (2008). MMP-7 is involved in the aging of primary human mammary epithelial cells (HMEC). Exp Gerontol 43:209–217.
26. Mandel K, Y Yang, A Schambach, S Glage, A Otte and R Hass. (2013). Mesenchymal stem cells directly interact with breast cancer cells and promote tumor cell growth in vitro and in vivo. Stem Cells Dev 22:3114–3127.
27. Evans BA, C Elford, A Pexa, K Francis, AC Hughes, A Deussen and J Ham. (2006). Human osteoblast precursors produce extracellular adenosine, which modulates their secretion of IL-6 and osteoprotegerin. J Bone Miner Res 21:228–236.
28. Montanucci P, G Basta, T Pescara, I Pennoni, F Di Giovanni and R Calafiore. (2011). New simple and rapid method for purification of mesenchymal stem cells from the human umbilical cord Wharton jelly. Tissue Eng Part A 17:2651–2661.
29. Fonsatti E, AP Jekunen, KJ Kairemo, S Coral, M Snellman, MR Nicotra, PG Natali, M Altomonte and M Maio. (2000). Endoglin is a suitable target for efficient imaging of solid tumors: in vivo evidence in a canine mammary carcinoma model. Clin Cancer Res 6:2037–2043.
30. Gomez-Esquer F, D Agudo, F Martinez-Arribas, MJ Nunez-Villar and J Schneider. (2004). mRNA expression of the angiogenesis markers VEGF and CD105 (endoglin) in human breast cancer. Anticancer Res 24:1581–1585.
31. Bucan V, K Mandel, C Bertram, A Lazaridis, K Reimers, TW Park-Simon, PM Vogt and R Hass. (2012). LEF-1 regulates proliferation and MMP-7 transcription in breast cancer cells. Genes Cells 17:559–567.
32. Mandel K, D Seidl, D Rades, H Lehnert, F Gieseler, R Hass and H Ungefroren. (2013). Characterization of spontaneous and TGF-beta-induced cell motility of primary human normal and neoplastic mammary cells in vitro using novel real-time technology. PLoS One 8:e56591.
33. Joly E and D Hudrisier. (2003). What is trogocytosis and what is its purpose? Nat Immunol 4:815.
34. Karnoub AE, AB Dash, AP Vo, A Sullivan, MW Brooks, GW Bell, AL Richardson, K Polyak, R Tubo and RA Weinberg. (2007). Mesenchymal stem cells within tumour stroma promote breast cancer metastasis. Nature 449:557–563.
35. Muehlberg FL, YH Song, A Krohn, SP Pinilla, LH Droll, X Leng, M Seidensticker, J Ricke, AM Altman, et al. (2009).

Tissue-resident stem cells promote breast cancer growth and metastasis. Carcinogenesis 30:589–597.
36. Roorda BD, A Elst, TG Boer, WA Kamps and ES de Bont. (2010). Mesenchymal stem cells contribute to tumor cell proliferation by direct cell-cell contact interactions. Cancer Invest 28:526–534.
37. Luo J, S Ok Lee, L Liang, CK Huang, L Li, S Wen and C Chang. (2014). Infiltrating bone marrow mesenchymal stem cells increase prostate cancer stem cell population and metastatic ability via secreting cytokines to suppress androgen receptor signaling. Oncogene 33:2768–2778.
38. Chao KC, HT Yang and MW Chen. (2012). Human umbilical cord mesenchymal stem cells suppress breast cancer tumourigenesis through direct cell-cell contact and internalization. J Cell Mol Med 16:1803–1815.
39. Kucerova L, S Skolekova, M Matuskova, M Bohac and Z Kozovska. (2013). Altered features and increased chemosensitivity of human breast cancer cells mediated by adipose tissue-derived mesenchymal stromal cells. BMC Cancer 13:535.
40. Qiao L, ZL Xu, TJ Zhao, LH Ye and XD Zhang. (2008). Dkk-1 secreted by mesenchymal stem cells inhibits growth of breast cancer cells via depression of Wnt signalling. Cancer Lett 269:67–77.
41. Clarke MR, FM Imhoff and SK Baird. (2014). Mesenchymal stem cells inhibit breast cancer cell migration and invasion through secretion of tissue inhibitor of metalloproteinase-1 and -2. Mol Carcinog [Epub ahead of print]; DOI: 10.1002/mc.22178.
42. Sun Z, S Wang and RC Zhao. (2014). The roles of mesenchymal stem cells in tumor inflammatory microenvironment. J Hematol Oncol 7:14.
43. Airas L, J Niemela, M Salmi, T Puurunen, DJ Smith and S Jalkanen. (1997). Differential regulation and function of CD73, a glycosyl-phosphatidylinositol-linked 70-kD adhesion molecule, on lymphocytes and endothelial cells. J Cell Biol 136:421–431.
44. Wintzell M, E Hjerpe, E Avall Lundqvist and M Shoshan. (2012). Protein markers of cancer-associated fibroblasts and tumor-initiating cells reveal subpopulations in freshly isolated ovarian cancer ascites. BMC Cancer 12:359.
45. Kansy BA, PA Dissmann, H Hemeda, K Bruderek, AM Westerkamp, V Jagalski, P Schuler, K Kansy, S Lang, CA Dumitru and S Brandau. (2014). The bidirectional tumor—mesenchymal stromal cell interaction promotes the progression of head and neck cancer. Stem Cell Res Ther 5:95.
46. Rowan BG, JM Gimble, M Sheng, M Anbalagan, RK Jones, TP Frazier, M Asher, EA Lacayo, PL Friedlander, R Kutner and ES Chiu. (2014). Human adipose tissue-derived stromal/stem cells promote migration and early metastasis of triple negative breast cancer xenografts. PLoS One 9:e89595.
47. Li HJ, F Reinhardt, HR Herschman and RA Weinberg. (2012). Cancer-stimulated mesenchymal stem cells create a carcinoma stem cell niche via prostaglandin E2 signaling. Cancer Discov 2:840–855.
48. Barcellos-de-Souza P, V Gori, F Bambi and P Chiarugi. (2013). Tumor microenvironment: bone marrow-mesenchymal stem cells as key players. Biochim Biophys Acta 1836:321–335.
49. Wong CY, EL Tan and SK Cheong. (2014). In vitro differentiation of mesenchymal stem cells into mesangial cells when co-cultured with injured mesangial cells. Cell Biol Int 38:497–501.
50. Strassburg S, SM Richardson, AJ Freemont and JA Hoyland. (2010). Co-culture induces mesenchymal stem cell differentiation and modulation of the degenerate human nucleus pulposus cell phenotype. Regen Med 5:701–711.
51. Mishra PJ, PJ Mishra, R Humeniuk, DJ Medina, G Alexe, JP Mesirov, S Ganesan, JW Glod and D Banerjee. (2008). Carcinoma-associated fibroblast-like differentiation of human mesenchymal stem cells. Cancer Res 68:4331–4339.
52. Chaturvedi S and R Hass. (2011). Extracellular signals in young and aging breast epithelial cells and possible connections to age-associated breast cancer development. Mech Ageing Dev 132:213–219.
53. Kong D, Y Li, Z Wang and FH Sarkar. (2011). Cancer stem cells and epithelial-to-mesenchymal transition (EMT)-phenotypic cells: are they cousins or twins? Cancers (Basel) 3:716–729.
54. Ghajar CM, H Peinado, H Mori, IR Matei, KJ Evason, H Brazier, D Almeida, A Koller, KA Hajjar, et al. (2013). The perivascular niche regulates breast tumour dormancy. Nat Cell Biol 15:807–817.
55. Alexander S and P Friedl. (2012). Cancer invasion and resistance: interconnected processes of disease progression and therapy failure. Trends Mol Med 18:13–26.
56. Chatterjee D, DM Tufa, H Baehre, R Hass, RE Schmidt and R Jacobs. (2014). Natural killer cells acquire CD73 expression upon exposure to mesenchymal stem cells. Blood 123:594–595.
57. Valadi H, K Ekstrom, A Bossios, M Sjostrand, JJ Lee and JO Lotvall. (2007). Exosome-mediated transfer of mRNAs and microRNAs is a novel mechanism of genetic exchange between cells. Nat Cell Biol 9:654–659.
58. Eirin A, SM Riester, XY Zhu, H Tang, JM Evans, D O'Brien, AJ van Wijnen and LO Lerman. (2014). MicroRNA and mRNA cargo of extracellular vesicles from porcine adipose tissue-derived mesenchymal stem cells. Gene 551:55–64.
59. Rustom A, R Saffrich, I Markovic, P Walther and HH Gerdes. (2004). Nanotubular highways for intercellular organelle transport. Science 303:1007–1010.
60. Figeac F, PF Lesault, O Le Coz, T Damy, R Souktani, C Trebeau, A Schmitt, J Ribot, R Mounier, et al. (2014). Nanotubular crosstalk with distressed cardiomyocytes stimulates the paracrine repair function of mesenchymal stem cells. Stem Cells 32:216–230.
61. Vallabhaneni KC, H Haller and I Dumler. (2012). Vascular smooth muscle cells initiate proliferation of mesenchymal stem cells by mitochondrial transfer via tunneling nanotubes. Stem Cells Dev 21:3104–3113.
62. Pawelek JM and AK Chakraborty. (2008). Fusion of tumour cells with bone marrow-derived cells: a unifying explanation for metastasis. Nat Rev Cancer 8:377–386.

Address correspondence to:
Dr. Ralf Hass
Biochemistry and Tumor Biology Lab
Department of Obstetrics and Gynecology
Hannover Medical School
Carl-Neuberg-Str. 1
Hannover D-30625
Germany

E-mail: hass.ralf@mh-hannover.de

Received for publication August 21, 2014
Accepted after revision December 19, 2014
Prepublished on Liebert Instant Online December 19, 2014

2.5 Acquisition of new tumor cell properties by MSC-derived exosomes

Yuanyuan Yang, Vesna Bucan, Heike Baehre, Juliane von der Ohe,
Anna Otte und Ralf Hass

publiziert in
International Journal of Oncology
47 (1), 2015, 244 - 252
doi: 10.3892/ijo.2015.3001

INTERNATIONAL JOURNAL OF ONCOLOGY 47: 244-252, 2015

Acquisition of new tumor cell properties by MSC-derived exosomes

YUANYUAN YANG[1,5], VESNA BUCAN[2], HEIKE BAEHRE[3,4], JULIANE VON DER OHE[1], ANNA OTTE[1] and RALF HASS[1]

[1]Biochemistry and Tumor Biology Laboratory, Department of Obstetrics and Gynecology, [2]Department of Plastic, Hand and Reconstructive Surgery, [3]Institute of Pharmacology, [4]Research Core Unit Metabolomics, Hannover Medical School, Hannover, Germany; [5]Tongji Hospital Affiliated to Tongji University, Shanghai 200065, P.R. China

Received March 6, 2015; Accepted April 9, 2015

DOI: 10.3892/ijo.2015.3001

Abstract. Interaction between multi-functional mesenchymal stroma/stem cells (MSC) and human tumor cells involves the exchange of biological material via extracellular vesicles including exosomes. Protein analysis of MSC-derived exosomes demonstrated the presence of MMP-2 and MSC-specific markers including CD90 and ecto-5'-nucleotidase (CD73). Incubation of tumor cells with these membranous particles revealed a rapid uptake of MSC-released microvesicles whereby breast cancer cells incorporated ~19% and SCCOHT-1 cells representing a rare type of small cell ovarian cancer assimilated ~28% of available exosomes within 24 h. This interaction was accompanied by functional alterations of tumor cell properties during integration of exosomal content from MSC. Indeed, exosome-associated MMP-2 exhibited functional enzyme activity and MCF-7 breast cancer cells with undetectable MMP-2 protein acquired expression of this enzyme and corresponding gelatinase functionality after stimulation with MSC-derived exosomes. Similar effects were observed in SCCOHT-1 cells during culture in the presence of MSC-derived exosomes which enabled new metabolic activities in this tumor cell type. Together, these findings demonstrated that the internalization of MSC-derived exosomes was associated with the acquisition of new tumor cell properties by altering cellular functionalities and providing the capability to re-organize the tumor microenvironment.

Introduction

Multipotent human mesenchymal stroma/stem cells (MSC) are characterized as a heterogeneous cell population which can be found in nearly all vascularized organs and tissues. The stem cell properties include self-renewal and regenerative potential (1). Moreover, MSC display at least a tri-lineage differentiation capacity along the osteogenic, chondrogenic and adipogenic phenotype (2). Certain heterogeneity in morphology and cell fate as demonstrated by isolation of MSC subpopulations (3) may result partially from the cellular microenvironment by neighboring cells, altered trophic factors, pH or hypoxic conditions. Consequently, a broad range of simultaneous properties including the capacity for plastic adherence, paralleled by expression of the CD73, CD90 and CD105 surface molecules with concomitant absence of other cell type-specific markers including CD14, CD31, CD34 CD45 and HLA-DR can be identified for MSC (2,4).

MSC are recruited during tissue damage to support wound repair and tissue regeneration. Likewise, invasive tumor growth also causes tissue injuries and inflammatory processes with the consequence of MSC attraction and cellular crosstalk. MSC can interact with tumor cells via exchange of soluble factors like chemokines, cytokines and further trophic molecules as well as various microvesicles including exosomes. These types of interaction enable multiple pathways for MSC to communicate with neighboring tumor cells whereby release of exosomes can also affect more distant tumor cells. Exosomes represent small membrane particles of endocytic origin which are released into the extracellular compartment (5) and contain a large panel of proteins, mRNAs and regulatory microRNAs (miRs) which can alter the functionality of recipient cells (6). According to the heterogeneity of MSC populations, exosomes from MSC of different tissue origin contain a variety of unique proteins together with some common exosomal marker proteins such as CD29 or CD63 (7,8). Several effects of MSC-derived exosomes on tumor cells have been demonstrated including suppression of angiogenic potential by down-modulation of VEGF in breast cancer cells via exosome-associated miR-16 (9). Moreover, human umbilical cord MSC-derived exosomes can protect against cisplatin-induced nephrotoxicity and promote cell proliferation (10) and other research has demonstrated that human bone marrow MSC-derived exosomes increase tumor growth *in vivo* (11), however, mechanisms for these findings remain unclear.

Correspondence to: Professor Ralf Hass, Biochemistry and Tumor Biology Laboratory, Department of Gynecology and Obstetrics, Medical University Hannover, Carl-Neuberg-Str. 1, D-30625 Hannover, Germany
E-mail: hass.ralf@mh-hannover.de

Key words: mesenchymal stem cells, SCCOHT-1, breast cancer, tumor cell signaling, intercellular communication, exosomes

In the present study, we investigated the effects of MSC-derived exosomes on different tumor types including breast cancer and a rare type of ovarian carcinoma cells. The data demonstrated a variety of functional changes including MMP-2 and ecto-5'-nucleotidase acquisition by different tumor cells following internalization of exosomes.

Materials and methods

Cell culture of mesenchymal stem/stroma cells (MSC). Primary human mesenchymal stem cells were obtained after explant culture of umbilical cord tissue; the procedure was approved by the Ethics Committee of Hannover Medical School, Project no. 443, February 26, 2009, respectively, following informed written consent by the patient.

MSC-like cells were isolated from human umbilical cords as reported previously (12). The cells were obtained from different patients following delivery of full-term (38-40 weeks) infants either spontaneously or by cesarean section. In brief, umbilical cord tissue was washed with PBS to remove blood cells, cut into ~0.5 cm^3 large pieces and incubated in αMEM (Sigma Chemie GmbH, Steinheim, Germany) supplemented with 15% of allogeneic human AB-serum (HS; commercially obtained from blood bank, University Campus Lübeck, Germany), 100 U/ml penicillin, 100 μg/ml streptomycin and 2 mM L-glutamine (Sigma) at 37˚C in a humidified atmosphere with 5% CO_2. After ~14 days of explant culture, the umbilical cord tissue pieces were removed and the adherent cells were harvested by accutase (Sigma) treatment for 3 min at 37˚C. The obtained cell suspension was centrifuged at 320 x g for 5 min and the cells were resuspended in MSC culture medium (αMEM supplemented with 10% HS, 100 U/ml penicillin, 100 μg/ml streptomycin and 2 mM L-glutamine) and subcultured in the appropriate passage. For the experiments, MSC primary cultures from 5 different donors in different passages (P1 to P5) were used (MSC241111 in P3, MSC131113 in P2, MSC101213 in P1 and P3, MSC180314 in P5 and MSC270114 in P1), respectively.

Cell culture of tumor cells. Human MDA-MB-231 and MCF-7 breast carcinoma cell lines were obtained from the American Type Culture Collection (Rockville, MD, USA). MCF-7 cells were grown in Dulbecco's modified Eagle's medium and MDA-MB-231 cells were cultured in Leibovitz medium supplemented with [10% (v/v) fetal calf serum, 2 mM L-glutamine, 100 U/ml penicillin and 100 mg/ml streptomycin] (all from Sigma Chemie GmbH, Steinheim, Germany), respectively. Subculture was performed by trypsin/EDTA (Biochrom GmbH, Berlin, Germany) treatment for 5 min at 37˚C.

SCCOHT-1 cells represent a spontaneously proliferating population derived from a patient with recurrent small cell carcinoma of the ovary hypercalcemic type (SCCOHT) and were maintained in RPMI-1640 with medium supplements as described previously (13).

Cells were cultivated at 37˚C in a humidified atmosphere containing 5% CO_2 and tested for mycoplasma by the luminometric MycoAlert Plus mycoplasma detection kit (Lonza Inc., Rockland, ME, USA) according to the manufacturer's recommendations. Moreover, authentication of the cell lines was performed by short tandem repeat (STR) fragment analysis using the GenomeLab human STR primer set (Beckman Coulter Inc., Fullerton, CA, USA) demonstrating similar STR pattern according to the STR database provided by the Deutsche Sammlung von Mikroorganismen und Zellkulturen (DSMZ, Braunschweig, Germany).

Labeling of MSC by lentiviral transduction. For discrimination of the different tumor cells in co-culture with MSC and for proliferation measurements, all tumor cell populations were transduced with a 3rd generation lentiviral SIN vector containing the mcherry gene. Likewise, the different MSC populations were transduced with a 3rd generation lentiviral SIN vector containing the eGFP gene according to a labeling technique previously described (14).

Analysis of surface markers by flow cytometry. Characterization of the MSC immunophenotype was performed as described previously (15). Briefly, continuously proliferating MSC were harvested and analyzed for cell surface marker expression by flow cytometry. After blocking non-specific binding to Fc-receptors by incubation of 10^6 cells with 2% FCS for 30 min at 4˚C and washing with PBS-BSA, the cells were incubated with the following appropriately-labeled monoclonal anti-human antibodies, respectively: CD73-PE (clone AD2) (BD Bioscience); CD90-PE (clone 5E10, IgG1, BioLegend Inc., San Diego, CA, USA); CD105-PE (clone 43A3, IgG1, BioLegend Inc.); CD31-FITC (Miltenyi Biotec, Bergisch-Gladbach, Germany); CD34-PE and CD45-PE (BD Biosciences). Following antibody staining, all samples were washed twice with PBS-BSA. Positive staining was obtained according to control measurements of the different populations with isotype-matching IgG control antibodies. Flow cytometry analysis and histograms were performed in a Galaxy FACSan (Partec) using FloMax analysis software (Partec).

Preparation of exosomes. Exosomes were isolated using the total exosome isolation kit reagent (Invitrogen, USA). After culture in serum-free conditions for 24 h, cell media were harvested from MSC^{GFP}, MCF-7^{cherry}, and MDA-MB231^{cherry} mono-cultures and from co-cultures of MSC with the two breast cancer cell lines, respectively. Co-culture of MSC and the tumor cells was performed at a cell ratio of 60:40. The cells were cultured at an initial density of 2,000 cells/cm^2 for 7-15 days and following medium exchange with serum-free media, the released exosomes were isolated after subsequent 24 h.

The serum-free cell media samples were centrifuged at 2,000 x g for 30 min to remove cell debris. The supernatant was stored on ice and supplemented with the half volume of the total exosome isolation kit reagent (Invitrogen) according to the manufacturer's instructions. After thorough mixing, the samples were incubated at 4˚C overnight and centrifuged at 100,000 x g/4˚C for 1 h. The supernatant was aspirated and discarded, and the exosome pellet was resuspended for protein and enzymatic analyses.

For incorporation of MSC^{GFP}-derived exosomes into tumor cells, equal aliquots of exosomes were added to 10^4 MCF-7 or SCCOHT-1 cells in a 6-well plate (Nunc). The tumor cell cultures were then incubated for 24 h in the presence of MSC^{GFP}-derived exosomes followed by 5 extensive

washes of the wells with PBS to remove free and loosely cell-attached exosomes. Thereafter, the cells were detached by trypsin/EDTA treatment, homogenized in appropriate buffer and cell homogenates were analyzed by western blot analysis or zymography assay. Alternatively, analysis of exosomes and of the tumor cells with incorporated GFP-labeled exosomes was performed after lysis in 10% (w/v) SDS. Relative fluorescence intensities of the homogenates were quantified for GFP (excitation 485 nm/emission 520 nm) using the Fluoroscan Ascent Fl (Thermo Fisher Scientific).

2D-gel analysis and mass spectrometry identification. The proteins of the different exosome preparations were separated by isoelectric focusing (IEF) followed by SDS-PAGE in the second dimension, respectively. Thus, aliquots of exosomes from each preparation were incubated in reswelling buffer [8 M urea, 1% CHAPS (v/v), 0.5% pharmalytes 3-10 (v/v), 0.002% bromophenol blue (w/v), 0.4% DTT (w/v); according to the GE Healthcare protocol] on an 18-cm IPG Immobiline Dry Strip (pH 3.0-10.0; NL) (Amersham Biosciences GmbH, Freiburg, Germany) and separated for 18 h at 150 V in the first dimension using the IPGphor isoelectric focusing system (Amersham). Thereafter, the IPG strips were incubated in two subsequent equilibration buffers for 15 min, respectively (according to the GE Healthcare protocol), and polymerized on a 10% SDS-PAGE separation gel using 0.5% (w/v) low melting point agarose. Electrophoresis was standardized using appropriate molecular-weight markers (Amersham). Following staining of the gels with Coomassie brilliant blue appropriate protein spots were cut and analyzed by liquid chromatography coupled with tandem mass spectrometry (LC-MS/MS) using the AB5800 TOF/TOF (ABSys GmbH, Darmstadt, Germany).

Western blot analysis. Exosome aliquots from the different cell cultures were homogenized in RIPA buffer containing 0.3 M NaCl, 1% (w/v) sodium desoxycholate, 0.1% (w/v) sodium dodecyl sulfate (SDS), 1% (v/v) Triton X-100, 20 mM Tris-HCl (pH 8.0), 1 mM EDTA supplemented with 1 mM phenylmethylsulfonylfluoride (PMSF). Approximately 15 μg of exosomal protein was separated by electrophoresis on a 15% SDS-polyacrylamide gel and transferred to a PVDF membrane (Millipore Corp., Bedford, MA, USA). Immunoblotting was performed with the following antibodies: polyclonal anti-CD63; polyclonal anti-collagen αI; polyclonal anti-collagen αII, polyclonal anti-CD73 and anti-MMP2 (each 1:500 dilution; all from Abcam, Cambrige, UK); monoclonal anti-CD90 (1:500 dilution; Dianova, Hamburg, Germany). Odyssey 680/800 nm secondary conjugates were used for the quantification of protein expression levels and signals were visualized using the Odyssey Infra-Red Imaging System and software (Li-Cor BioSciences, Lincoln, NE, USA).

Transcript analysis by RT-PCR. Total RNA was isolated from MSC and MSC-derived exosomes using RNeasy Mini kit (Qiagen, Hilden, Germany) according to the manufacturer's instructions. One microgram of RNA was reverse transcribed into cDNA using 500 μM of dNTP (R0193), 5 μM Oligo(dT)18 primer (S0132), 5 μM Random Hexan primer (S0142), 1 U RiboLock™ RNase inhibitor (E00381) and 5 U RevertAid™ M-MuLV reverse transcriptase (EP0441) in the supplied reaction buffer (all reagents from Thermo Scientific, Schwerte, Germany). The cDNA reactions were performed for 10 min/25˚C, 1 h/37˚C and stopped at 72˚C for 10 min. As a template 2.5 μl of cDNA was used with primers specific for: CD73 (forward, 5'-CGCAACAATGGCACAATTAC-3'; reverse, 5'-CTCGACA CTTGGTGCAAAGA-3'; amplification product 241 bp); CD90 (forward, 5'-GGACTGAGATCCCAGAACCA-3'; reverse, 5'-ACGAAGGCTCTGGTCCACTA-3'; amplification product 124 bp); CD105 (forward, 5'-TGTCTCACTTCATGCCTCC AGCT-3'; reverse, 5'-AGGCTGTCCATGTTGAGGCAGT-3'; amplification product 378 bp); MMP-2 (forward, 5'-TTTTCT CGAATCCATGATGG-3'; reverse, 5'-CTGGTGCAGCTCT CATATTT-3'; amplification product 619 bp); fibronectin (forward, 5'-AGCCGCCACGTGCCAGGATTAC-3'; reverse, 5'-CTTATGGGGGTGGCCGTTGTGG-3'; amplification product 439 bp); (all primers customized by Eurofins, MWG GmbH, Ebersberg, Germany). PCR reactions included 0.2 μM of each primer, 200 μM of dNTP (R0193, Thermo Scientific) and 0.03 U One Taq Hot Start DNA polymerase (New England Biolabs GmbH, Frankfurt am Main, Germany) in the supplied reaction buffer. PCR cycling conditions were performed 30 sec at 94˚C, 1 min at 60 and 68˚C for 1 min, respectively, including an initial 30-sec denaturation step at 94˚C and a final 5-min extension step at 68˚C (35 cycles). Aliquots of 25 μl of each RT-PCR product were separated on a 2% agarose gel and visualized by GelRed™ (Biotium Inc., Hayward, CA, USA) staining.

MMP-2 zymography assay. Exosome aliquots from the MSC^{GFP}, MDA-MB-231^{cherry} cells, and from co-cultures of MSC^{GFP}/ MDA-MB-231^{cherry} cells were used in a zymographic assay. Moreover, conditioned media was prepared from 10^6 MSC^{GFP} or MCF-7^{cherry} cells or MCF-7^{cherry} cells with incorporated MSC^{GFP}-derived exosomes after 24-h culture in 0.1% serum and concentrated ~20-fold using Amicon Ultra-4 Centrifugal Filter Devices (10 kDa; Millipore, Carrigtwohill, Ireland) according to the manufacturer's instructions. In the following MMP-2 zymographic assay, aliquots were mixed 2:1 (v/v) with non-reducing sample buffer [10 mM Tris (pH 6.0-8.0), 1% SDS, 10% glycerol and 0.02% bromophenol blue] and subjected to SDS-PAGE containing 2 mg/ml of gelatine (Sigma). Electrophoresis was performed for 30 min at 60 V followed by 120 min at 125 V. The gels were washed twice in 2.5% Triton X-100 on a vertical shaker and five times with H_2O. Thereafter, the gels were incubated with fresh MMP enzyme buffer (50 mM Tris-HCl, pH 7.0, 5 mM $CaCl_2$) overnight at 37˚C. Finally, the gels were stained with 0.4% Coomassie blue whereby the proteolytic activity was detectable by the appearance of light bands.

CD73 activity by analysis of 5'-AMP and adenosine. Exosomes were isolated from steady-state SCCOHT-1 mono-cultures after 7 days, from steady-state MSC101213 P3 mono-cultures after 7 days, and from 7-day co-culture of these MSC with SCCOHT-1 (ratio 60:40; initial seeding of 2,000 cells/cm^2). The appropriate exosomal fractions as well as SCCOHT-1 control cells and SCCOHT-1 cells with 24 h incorporated MSC-derived exosomes were cultivated in PBS with 20 μM 5'-AMP (Sigma, Schnelldorf, Germany) as a substrate for

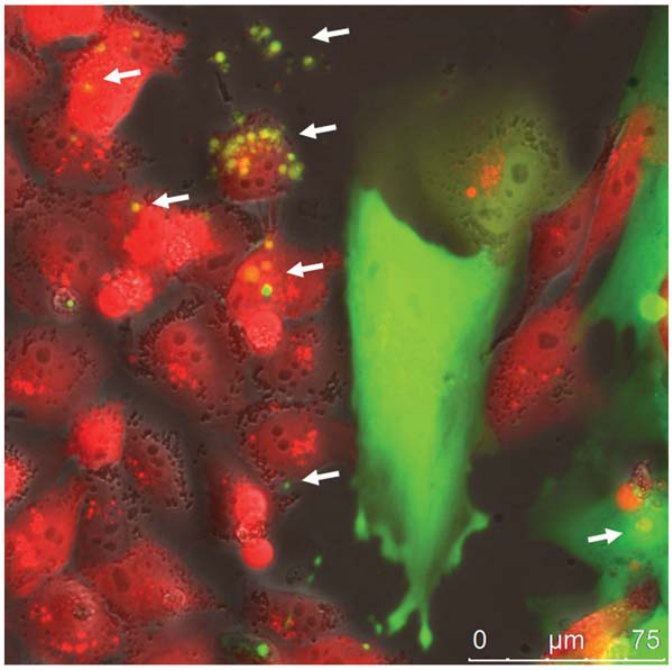

Figure 1. Exchange of extracellular vesicles between MSC and tumor cells. MSC101213^{GFP} P1 and MDA-MB-231^{cherry} breast cancer cells demonstrated the release of green fluorescing exosomes from MSC into the extracellular compartment and a corresponding uptake of these MSC-derived vesicles by various breast cancer cells in 7-day co-culture (white arrows). Bar, 75 μm.

30 min at 37˚C. An exosome-free and a cell-free PBS incubation served as a negative control, respectively. Supernatants were collected and centrifuged (14.000 x g/5 min) to remove debris and supernatants were analyzed by HPLC-MS/MS using a Shimadzu HPLC-system (Shimadzu, Duisburg, Germany) coupled with a QTRAP5500™ triple quadrupole mass spectrometer (ABSCIEX, Foster City, CA, USA) operating in positive ionization mode. Reversed phase chromatographic separation of adenosine and 5'-AMP was performed on a Hypercarb column (30x4.6 mm; 5 μm; Thermo Scientific, Dreieich, Germany) using a linear organic gradient. Data were collected and analyzed with Analyst 1.5.1 software (ABSCIEX).

Results

Direct cellular interaction of MSC^{GFP} with MDA-MB-231^{cherry} breast cancer cells was associated with the exchange of exosome-like micovesicles (Fig. 1). GFP-labeled exosomes derived from MSC241111^{GFP} P3 were detectable within the extracellular space and were incorporated into MDA-MB-231^{cherry} breast cancer cells as indicated by the white arrows (Fig. 1). While these cellular interactions and the exchange of exosomes suggested an intercellular transfer of biological material between MSC and the tumor cells, a 24-h production of exosomes was isolated from the mono-cultures and the co-cultures for further analysis. The protein amount of isolated exosomes from MDA-MB-231^{cherry} mono-cultures was 108 μg, from MSC241111^{GFP} was 90 μg, and the co-culture of MSC^{GFP} with MDA-MB-231^{cherry} yielded 144 μg within 24 h. Comparative protein analysis was performed by 2D-gel separation of 35 μg of the exosomal protein fraction of each preparation (Fig. 2). A variety of common protein spots were detectable in all 3 preparations, however, at least two additional proteins were identified in MSC exosomes (Fig. 2, upper panel) and co-culture exosomes (Fig. 2, lower panel) in contrast to MDA-MB-231 exosomes (Fig. 2, middle panel). Mass spectrometric analysis revealed fibronectin and matrix metalloproteinase-2 (MMP-2) as those protein spots which were undetectable in exosomes from MDA-MB-231 cells (Fig. 2). Western blot analysis of exosomal preparation confirmed these findings (Fig. 3A). Moreover, similar data were also obtained from exosomes after co-culture of MSC with MCF-7 breast cancer cells (Fig. 3B). In addition to the presence of MMP-2 exclusively in exosomes from MSC and the co-culture, the GPI-anchored CD90 antigen was similarly detectable and likewise the ecto-5'-nucleotidase CD73, all of which remain absent in the two breast cancer cell lines (Fig. 3). Whereas fibronectin can associate with certain types of collagen, the isoform collagen α1 was also detectable in exosomes from MSC mono-cultures and was reduced in the co-culture exosomes, however, it was undetectable in the exosome preparation of MDA-MB-231 and MCF-7 cells, respectively (Fig. 3). In contrast, collagen α2 appeared in all exosome preparations and likewise, CD63 as an exosomal marker protein was uniformly present (Fig. 3).

Furthermore, transcripts of the typical MSC marker proteins CD73, CD90, and CD105 were detectable in MSC lysates as well as MMP2 and fibronectin in accordance with the mass spectrometric analysis of the 2D gels (Fig. 4). Likewise, mRNAs of CD73, CD90, and fibronectin also

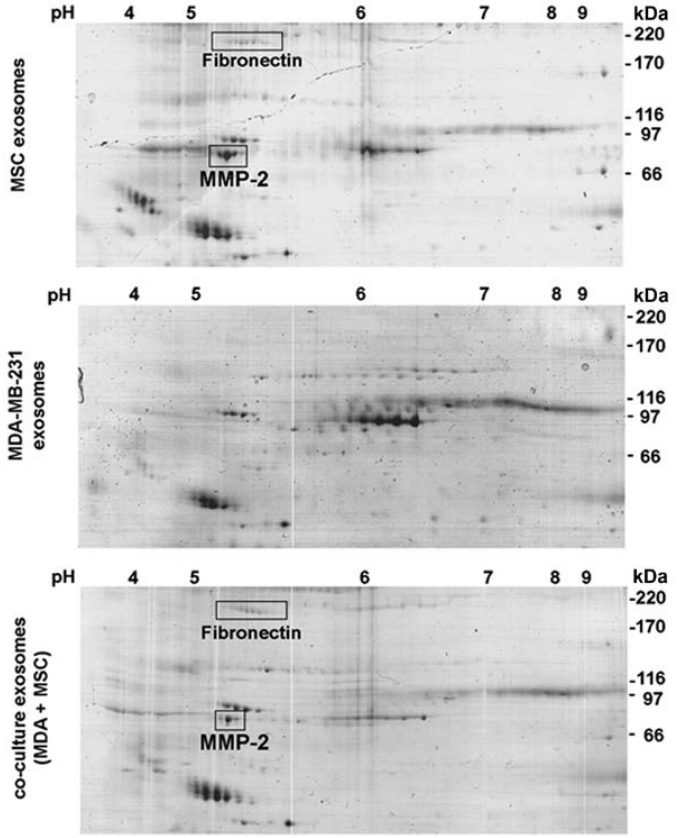

Figure 2. Two dimensional (2D)-gel analysis of exosomal proteins was performed from mono-cultures of MSC241111 P3 (upper panel), MDA-MB-231 cells (middle panel), and during co-culture of MSC241111 P3 with MDA-MB-231 cells (lower panel) by applying 35 μg of exosomal protein to the gels, respectively, whereas exosomes from MSC mono- and co-cultures demonstrated a similar protein pattern, differences compared to proteins derived from the breast cancer cell exosomes were analyzed by liquid chromatography coupled with tandem mass spectrometry and revealed fibronectin and MMP-2 indicated on the upper and lower panel, respectively.

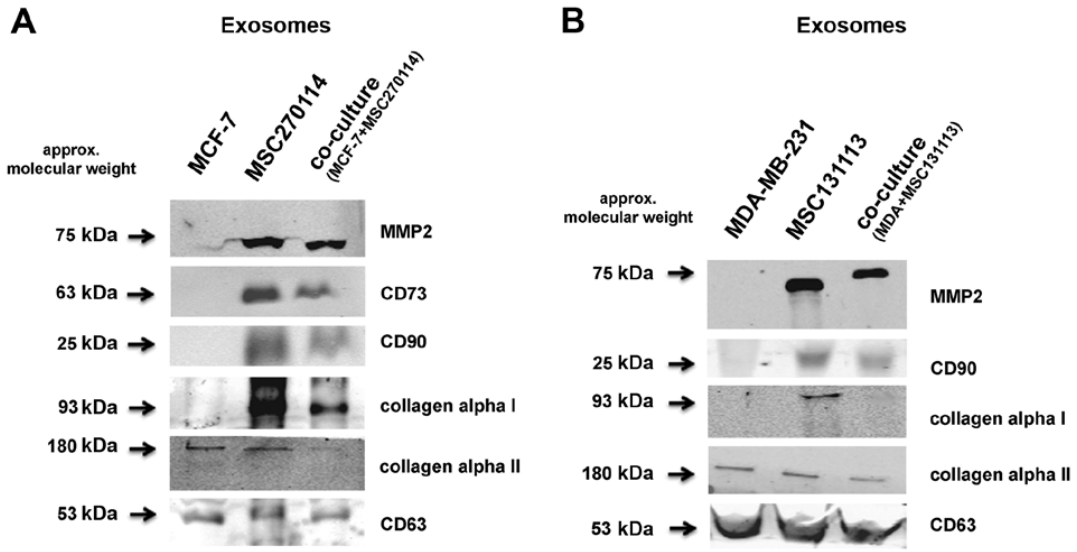

Figure 3. Western blot analysis was performed with 15 μg of exosomal proteins from mono-cultures of MCF-7 cells and MSC270114 P1 as well as their co-culture (A), respectively, and likewise from mono-cultures of MDA-MB-231 cells and MSC131113 P2 with their corresponding co-culture (B), respectively. The unaltered expression of CD63 as exosomal marker protein was used as a control.

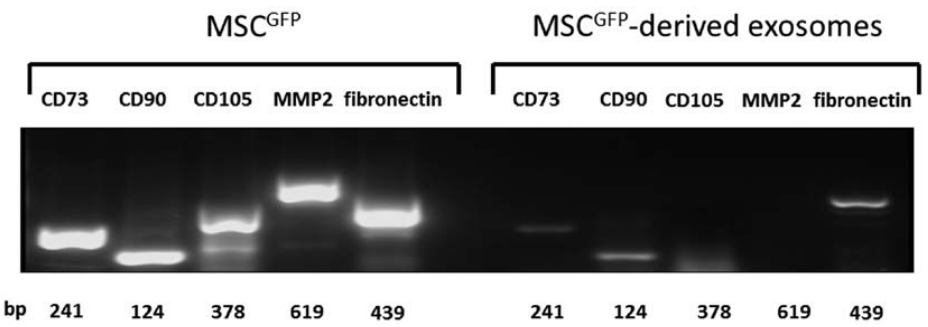

Figure 4. PCR analysis with 62.5 ng/lane of transcripts of the MSC markers CD73, CD90, CD105 and additionally matrix metalloproteinase 2 (MMP-2) and fibronectin was performed in MSC^{GFP} compared to MSC^{GFP}-derived exosomes. The length of the PCR products was indicated in base pairs (bp).

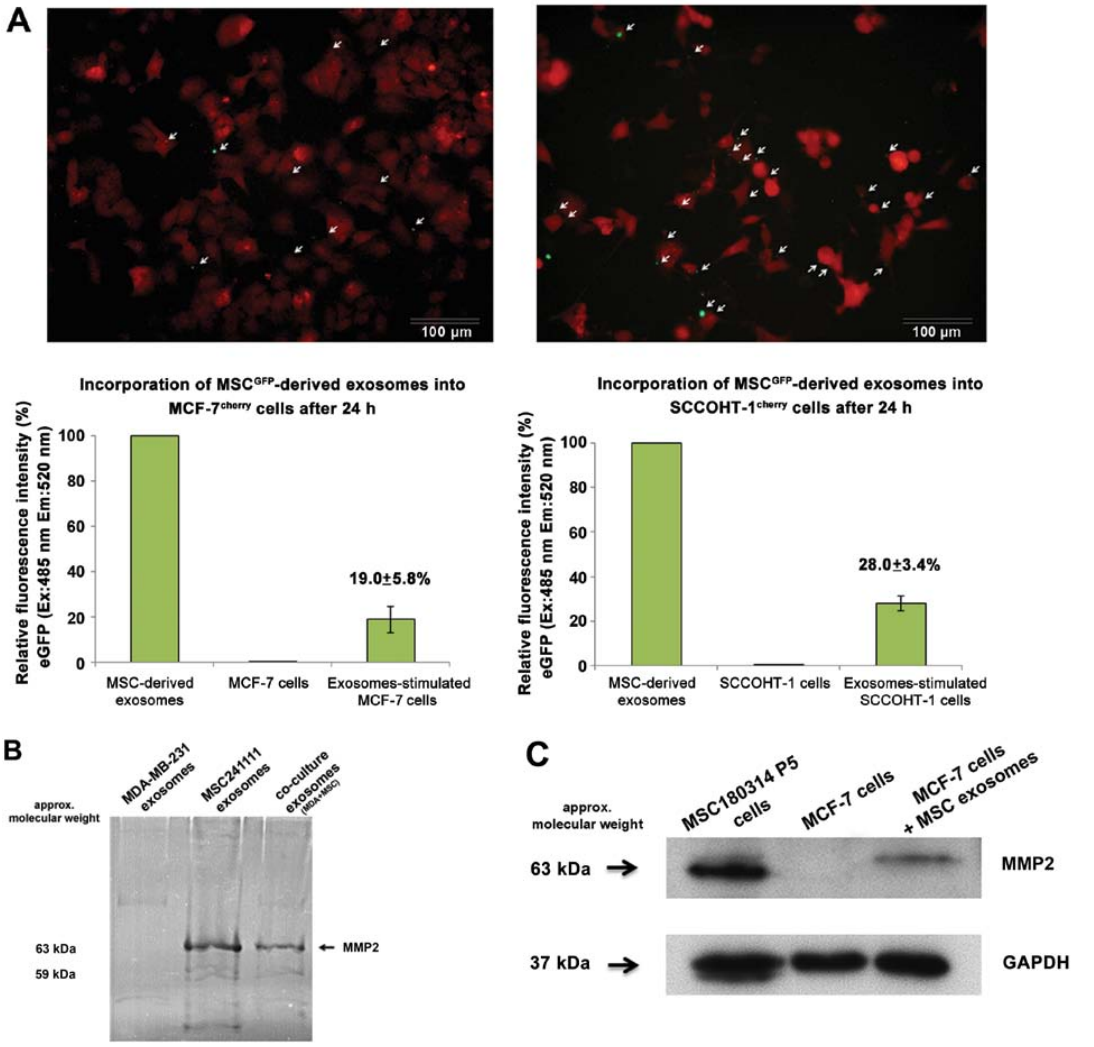

Figure 5. Incorporation and enzymatic analysis of exosomes. (A) Uptake of MSC^{GFP}-derived exosomes by MCF-7^{cherry} breast cancer cells (upper left) or by SCCOHT-1^{cherry} tumor cells (upper right) was performed by incubation of the exosomes with the tumor cultures for 24 h followed by 5 extensive washes with PBS to remove non-incorporated exosomes (bars represent 100 μm). The relative incorporation of MSC^{GFP}-derived exosomes into MCF-7^{cherry} cells (lower left panel) or into SCCOHT-1^{cherry} cells (lower right panel) within 24 h of incubation was quantified by a fluorescence-based assay whereby the fluorescence of GFP-labeled exosomes used for the cell stimulation was calculated as 100%. Data represent the mean ± SD (n=3). (B) Zymography of MMP-2 for gelatinase activity was determined with 5.8 μg of exosomal protein from MDA-MB-231 and MSC mono-cultures and from 8-day co-culture of MSC/breast cancer cells, respectively. (C) MMP-2 western blot analysis of MSC and MCF-7 cell cultures compared to MCF-7 cells after incorporation of MSC-derived exosomes was performed by analysis of 40 μg protein cell lysate/lane. Expression levels of GAPDH were used as a loading control.

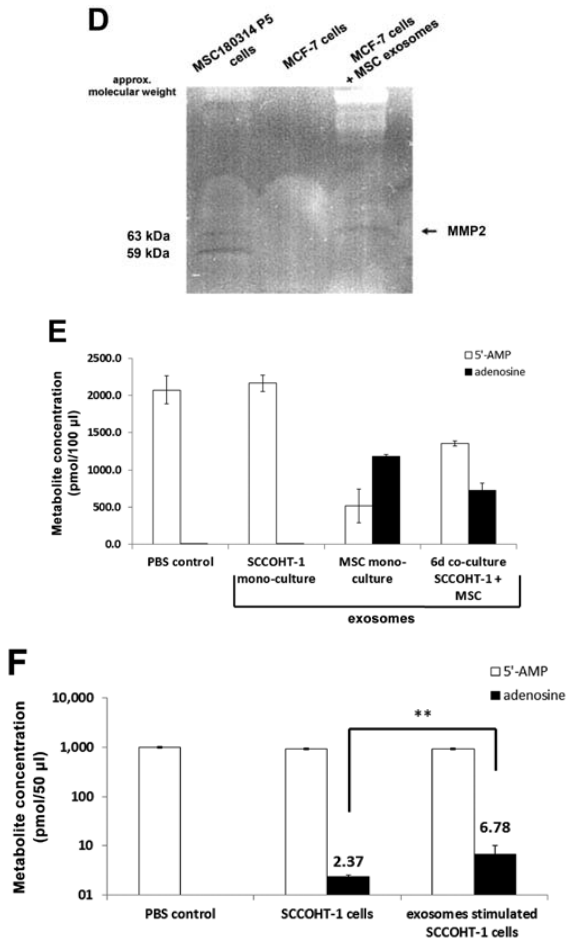

Figure 5. Continued. (D) Detection of MMP-2 gelatinase activity by a zymography assay of MSC and MCF-7 cell cultures compared to MCF-7 cells after incorporation of MSC-derived exosomes. (E) Ecto-5'-nucleotidase (CD73) activity was determined by the capacity of exosomes from equal cell amounts of SCCOHT-1 and MSC mono-cultures and from 6-day co-culture of MSC/SCCOHT-1 cells to metabolize 5'-AMP into adenosine. The metabolites were analyzed by liquid chromatography combined with tandem mass spectrometry. Data represent the mean ± SD of 3 experiments. (F) Ecto-5'-nucleotidase (CD73) activity was determined in SCCOHT-1 cells compared to SCCOHT-1 cells after 24-h incubation in the presence of MSC-derived exosomes. Quantification of 5'-AMP and adenosine was performed by HPLC-MS/MS. Data represent the mean ± SD of 3 experiments.

appeared in MSC-derived exosomes although in reduced quantities as compared to the cells. However, PCR products of CD105 and MMP-2 remained undetectable in these vesicles (Fig. 4) suggesting that only the proteins are carried.

Incubation of MSC^{GFP}-derived exosomes with tumor cells was associated with an uptake of exosomes by $MCF\text{-}7^{cherry}$ cells (Fig. 5A, upper left) and by $SCCOHT\text{-}1^{cherry}$ cells (Fig. 5A, upper right). The tumor cell cultures were incubated with the exosomes for 24 h and analysis of incorporated exosomes was performed after 5 extensive washes with PBS to remove free and loosely cell-attached exosomes. Quantification of incorporated exosomes into the cells was performed by fluorescence measurement of the GFP-labeled vesicles and revealed a relative uptake of 19.0±5.8% (n=3) by MCF-7 cells (Fig. 5A, lower left) and 28.0±3.4 % (n=3) by SCCOHT-1 cells (Fig. 5A, lower right) after 24 h compared to the total amount of available exosomes.

To test, whether the assimilation of MSC-derived exosomes by tumor cells includes transfer of biologically active proteins, gelatinase activity was measured for MMP-2 in an appropriate gelatin zymography assay. In contrast to exosomes from MDA-MB-231, MSC-derived exosomes and exosomes isolated from the MSC/breast cancer cell co-culture exhibited a marked gelatinase activity at ~63 kDa, which corresponded to the active form of MMP-2 (Fig. 5B). A potential MSC-mediated transfer of MMP-2 was also tested for MCF-7 breast cancer cells. MSC cell homogenates demonstrated MMP-2 protein expression in contrast to undetectable MMP-2 levels in MCF-7 cells. However, incubation of MCF-7 cells in the presence of MSC-derived exosomes and subsequent removal of non-incorporated exosomes by extensive washes of the cells was associated with MMP-2 protein expression in the breast cancer cells (Fig. 5C). Moreover, the acquired MMP-2 expression in MCF-7 cells by MSC-derived exosomes was also tested for enzymatic activity. Whereas MSC cell homogenates exhibited MMP-2 gelatinase in-gel activity at ~59 and 63 kDa, there was little if any MMP-2 activity detectable in MCF-7 cell homogenates. In contrast, MMP-2 activity was displayed in MCF-7 cells after incorporation of MSC-derived exosomes in the zymography assay (Fig. 5D).

Further acquisition of enzymatic activity from MSC-derived exosomes was evaluated for the CD73 ecto-5'-nucleotidase which associates to the external face of the plasma membrane via a GPI-anchor. The exosomal transfer of biologically active CD73 was tested by the capability to metabolize 5'-AMP into adenosine using a tumor cell culture model of primary cells from a small cell hypercalcemic ovarian carcinoma (SCCOHT-1). The preparation of exosomes from SCCOHT-1 cells demonstrated no detectable adenosine synthesis similar to PBS control incubation without any cells (Fig. 5E). In contrast, LC/MS-MS analysis of exosomes from MSC mono-culture and from MSC/SCCOHT-1 co-culture revealed a marked reduction of the substrate 5'-AMP paralleled by a significantly increased level of the product adenosine (Fig. 5E) suggesting CD73 activity exclusively in MSC-derived exosomes. Transfer of CD73 became obvious when a markedly elevated ecto-5'-nucleotidase activity was detectable after incorporation of MSC-derived exosomes into SCCOHT-1 cells compared to SCCOHT-1 control cells (Fig. 5F).

Discussion

Previous research has demonstrated that mesenchymal stem/stroma cells contribute to a direct interaction with tumor cells and promote mutual exchange/induction of cellular markers (14,16,17). Alternatively, MSC interaction can be mediated indirectly by the release of soluble biological factors (18) and/or vesicles such as exosomes whereby MSC can affect cellular functionality of distant cell populations in a paracrine manner. These effects can be mediated both, by proteins and RNAs including mRNAs and miRs.

The appearance of the MSC marker proteins CD73, CD90 and CD105 in MSC-derived exosomes has been confirmed by

previous studies (19). In addition, MSC-derived exosomes also contain transcripts for CD73, CD90, and fibronectin, whereas CD105 expression remained undetectable. Likewise, MMP-2 mRNAs were not observed in MSC-derived exosomes, suggesting appropriate protein transport in the microvesicles or regulators that induced expression in the target cells. Previous research has demonstrated that cancer cell-associated fibronectin induces release of matrix metalloproteinase-2 from normal fibroblasts (20). Consequently, MMP-2 protein appearance in MCF-7 and MDA-MB-231 breast cancer cell populations with corresponding enzymatic activity after incorporation of MSC-derived exosomes enables degradation of certain collagens as structural component of basement membranes. Therefore, the acquisition of distinct matrix metalloproteinase activities suggested new properties of the tumor cells with the capability to restructure the tumor microenvironment. Indeed, transfection of MDA-MB-231 human breast cancer cells with pro-matrix metalloproteinase-2 increased growth and metastasis in nude mice (21). Moreover, supportive evidence demonstrated that human adipose MSC-derived exosomes in conditioned medium promote migratory activity of MCF-7 cells accompanied by an upregulation of several cancer-related pathways such as Wnt signaling (22).

The incorporation of MSC-derived exosomes was also associated with acquired ecto-5'-nucleotidase activity by SCCOHT-1 tumor cells whereby this interaction included both, protein and corresponding mRNA assimilation. Previous findings substantiated acquisition of 5'-nucleotidase activity by SCCOHT-1 cells (17) and by normal natural killer cells (23) following direct co-culture with MSC which suggested a transfer by the cells and/or by the exosomes. With this new capability of metabolizing 5'-AMP into adenosine, SCCOHT-1 cells can suppress and modulate pro-inflammatory activities via activation of adenosine receptor signaling present on the surface of most immune cells (24). Indeed, previous reports demonstrated that exosomal conversion of 5'-AMP to adenosine can inhibit T cell activation in a tumor microenvironment (25).

Together, these findings suggested that MSC-derived exosomes can change the cellular functionality of tumor cells by induction of MMP-2 and ecto-5'-nucleotidase activity and thereby contribute to an altered tumor microenvironment and increased tumor heterogeneity (26,27). Further factors including certain microRNAs in MSC-derived exosomes can also hide metastatic breast cancer cells by inducing dormancy (28). Thus, functional changes by MSC-derived exosomes can support a protection of tumor cells against chemotherapeutic approaches and consequently promote tumor cell resistance. Alternatively, MSC-derived exosomes may represent a useful carrier to deliver antitumor cargo.

Acknowledgements

Yuanyuan Yang is a visiting research fellow from Tongji University, Shanghai, China.

References

1. Caplan AI: Mesenchymal stem cells. J Orthop Res 9: 641-650, 1991.
2. Pittenger MF, Mackay AM, Beck SC, Jaiswal RK, Douglas R, Mosca JD, Moorman MA, Simonetti DW, Craig S and Marshak DR: Multilineage potential of adult human mesenchymal stem cells. Science 284: 143-147, 1999.
3. Majore I, Moretti P, Hass R and Kasper C: Identification of subpopulations in mesenchymal stem cell-like cultures from human umbilical cord. Cell Commun Signal 7: 6, 2009.
4. Dominici M, Le Blanc K, Mueller I, Slaper-Cortenbach I, Marini F, Krause D, Deans R, Keating A, Prockop DJ and Horwitz E: Minimal criteria for defining multipotent mesenchymal stromal cells. The International Society for Cellular Therapy position statement. Cytotherapy 8: 315-317, 2006.
5. Théry C, Regnault A, Garin J, Wolfers J, Zitvogel L, Ricciardi-Castagnoli P, Raposo G and Amigorena S: Molecular characterization of dendritic cell-derived exosomes. Selective accumulation of the heat shock protein hsc73. J Cell Biol 147: 599-610, 1999.
6. Valadi H, Ekström K, Bossios A, Sjöstrand M, Lee JJ and Lötvall JO: Exosome-mediated transfer of mRNAs and microRNAs is a novel mechanism of genetic exchange between cells. Nat Cell Biol 9: 654-659, 2007.
7. Lai RC, Tan SS, Teh BJ, Sze SK, Arslan F, de Kleijn DP, Choo A and Lim SK: Proteolytic potential of the MSC exosome proteome: Implications for an exosome-mediated delivery of therapeutic proteasome. Int J Proteomics 2012: 971907, 2012.
8. Yu B, Zhang X and Li X: Exosomes derived from mesenchymal stem cells. Int J Mol Sci 15: 4142-4157, 2014.
9. Lee JK, Park SR, Jung BK, Jeon YK, Lee YS, Kim MK, Kim YG, Jang JY and Kim CW: Exosomes derived from mesenchymal stem cells suppress angiogenesis by down-regulating VEGF expression in breast cancer cells. PLoS One 8: e84256, 2013.
10. Zhou Y, Xu H, Xu W, Wang B, Wu H, Tao Y, Zhang B, Wang M, Mao F, Yan Y, *et al*: Exosomes released by human umbilical cord mesenchymal stem cells protect against cisplatin-induced renal oxidative stress and apoptosis in vivo and in vitro. Stem Cell Res Ther 4: 34, 2013.
11. Zhu W, Huang L, Li Y, Zhang X, Gu J, Yan Y, Xu X, Wang M, Qian H and Xu W: Exosomes derived from human bone marrow mesenchymal stem cells promote tumor growth in vivo. Cancer Lett 315: 28-37, 2012.
12. Lavrentieva A, Majore I, Kasper C and Hass R: Effects of hypoxic culture conditions on umbilical cord-derived human mesenchymal stem cells. Cell Commun Signal 8: 18, 2010.
13. Otte A, Göhring G, Steinemann D, Schlegelberger B, Groos S, Länger F, Kreipe HH, Schambach A, Neumann T, Hillemanns P, *et al*: A tumor-derived population (SCCOHT-1) as cellular model for a small cell ovarian carcinoma of the hypercalcemic type. Int J Oncol 41: 765-775, 2012.
14. Mandel K, Yang Y, Schambach A, Glage S, Otte A and Hass R: Mesenchymal stem cells directly interact with breast cancer cells and promote tumor cell growth in vitro and in vivo. Stem Cells Dev 22: 3114-3127, 2013.
15. Otte A, Bucan V, Reimers K and Hass R: Mesenchymal stem cells maintain long-term in vitro stemness during explant culture. Tissue Eng Part C Methods 19: 937-948, 2013.
16. Hass R and Otte A: Mesenchymal stem cells as all-round supporters in a normal and neoplastic microenvironment. Cell Commun Signal 10: 26, 2012.
17. Yang Y, Otte A and Hass R: Human mesenchymal stroma/stem cells exchange membrane proteins and alter functionality during interaction with different tumor cell lines. Stem Cells Dev: Jan 26, 2015 (Epub ahead of print).
18. Karnoub AE, Dash AB, Vo AP, Sullivan A, Brooks MW, Bell GW, Richardson AL, Polyak K, Tubo R and Weinberg RA: Mesenchymal stem cells within tumour stroma promote breast cancer metastasis. Nature 449: 557-563, 2007.
19. Kim HS, Choi DY, Yun SJ, Choi SM, Kang JW, Jung JW, Hwang D, Kim KP and Kim DW: Proteomic analysis of microvesicles derived from human mesenchymal stem cells. J Proteome Res 11: 839-849, 2012.
20. Saad S, Gottlieb DJ, Bradstock KF, Overall CM and Bendall LJ: Cancer cell-associated fibronectin induces release of matrix metalloproteinase-2 from normal fibroblasts. Cancer Res 62: 283-289, 2002.
21. Tester AM, Waltham M, Oh SJ, Bae SN, Bills MM, Walker EC, Kern FG, Stetler-Stevenson WG, Lippman ME and Thompson EW: Pro-matrix metalloproteinase-2 transfection increases orthotopic primary growth and experimental metastasis of MDA-MB-231 human breast cancer cells in nude mice. Cancer Res 64: 652-658, 2004.

22. Lin R, Wang S and Zhao RC: Exosomes from human adipose-derived mesenchymal stem cells promote migration through Wnt signaling pathway in a breast cancer cell model. Mol Cell Biochem 383: 13-20, 2013.
23. Chatterjee D, Tufa DM, Baehre H, Hass R, Schmidt RE and Jacobs R: Natural killer cells acquire CD73 expression upon exposure to mesenchymal stem cells. Blood 123: 594-595, 2014.
24. Ohta A and Sitkovsky M: Extracellular adenosine-mediated modulation of regulatory T cells. Front Immunol 5: 304, 2014.
25. Clayton A, Al-Taei S, Webber J, Mason MD and Tabi Z: Cancer exosomes express CD39 and CD73, which suppress T cells through adenosine production. J Immunol 187: 676-683, 2011.
26. Ungefroren H, Sebens S, Seidl D, Lehnert H and Hass R: Interaction of tumor cells with the microenvironment. Cell Commun Signal 9: 18, 2011.
27. Friedl P and Alexander S: Cancer invasion and the micro-environment: Plasticity and reciprocity. Cell 147: 992-1009, 2011.
28. Ono M, Kosaka N, Tominaga N, Yoshioka Y, Takeshita F, Takahashi RU, Yoshida M, Tsuda H, Tamura K and Ochiya T: Exosomes from bone marrow mesenchymal stem cells contain a microRNA that promotes dormancy in metastatic breast cancer cells. Sci Signal 7: ra63, 2014.

3 Diskussion

Im Rahmen dieser Dissertation wurde das Augenmerk auf die Charakterisierung einer sehr seltenen und aggressiven Tumorerkrankung, dem kleinzelligen Ovarial Karzinom vom hyperkalzämischen Typ (SCCOHT) gelegt. Hierbei handelt es sich um ein eigenständiges Krankheitsbild eines Ovarialkarzinoms, das erstmals 1979 von Robert Scully dokumentiert wurde [27]. Ein begleitendes typisches Merkmal dieser Erkrankung ist die Entwicklung einer Hyperkalzämie bei ungefähr 2/3 aller Patientinnen [136]. Aufgrund ihrer Seltenheit sind in der Literatur vornehmlich Fallberichte zu finden, die über das Auftreten, den Verlauf und über die Versuche einer Therapie berichten. Bis zum jetzigen Zeitpunkt, sind weltweit in der Literatur nur drei als Zelllinien (SCCOHT-1 [66], BIN-67 [63] und OS-1 [65]) beschriebene Modelle dokumentiert, deren Ursprung das SCCOHT darstellt. Hierbei sind insbesondere die SCCOHT-1 Zellen zu erwähnen, die als erstes Modelsystem für die SCCOHT Erkrankung auch *in vivo* ein tumorigenes Potenzial zeigen [66]. Im Rahmen meiner Diplomarbeit und durch Vorarbeiten der Arbeitsgruppe um Prof. Ralf Hass war es möglich, diese Zellen als Zelllinie zu charakterisieren [66], die anschließend den Grundstein dieser Arbeit legten.

3.1 Exogene Kalziumstimulation und dessen Einfluss auf die Proliferation von Ovarialkarzinomen

Der Begriff „Hyperkalzämie“, der sich im Namen der hier untersuchten Tumorerkrankung, des kleinzelligen Ovarial Karzinoms vom hyperkalzämischen Typ wiederfindet, beschreibt das Phänomen eines erhöhten Serum-Kalziumspiegels. Hierbei unterscheidet man je nach Schweregrad zwischen einer milden (2,5–3,0 mmol/L), moderaten (3,0–3,5 mmol/L) und schweren Hyperkalzämie (> 3,5 mmol/L). In einer Untersuchung aus dem Jahr 2013 stellten Wissenschaftler einen Zusammenhang zwischen der totalen und der ionisierten Serumkalziumkonzentration und der Sterblichkeit von Patientinnen mit einem Ovarialkarzinom fest. Sie postulieren die Hypothese, dass eine Erhöhung der Kalziumkonzentration im Serum einer Patientin als potenzieller Marker zur vorsorglichen Änderung der Behandlungsstrategie eingesetzt werden könnte [52]. Durch das Zufügen von exogenem Kalzium in das Kulturmedium von Zellen der Zelllinien SK-OV-3, NIH:OVCAR-3 (ovariale Adenokarzinome) und SCCOHT-1 war es möglich, die verschiedenen Stufen einer Hyperkalzämie im *in vitro* Versuchsansatz zu simulieren. Hierfür wurden die Zellen in einer Umgebung mit 1,6 mmol/L, 3,2 mmol/L oder 6,4 mmol/L eines

kalziumhaltigen Mediums kultiviert. Es konnte eine wachstumsinhibierende Wirkung bei den Zellen beobachtet werden, die im Kulturmedium mit erhöhter Kalziumkonzentration kultiviert wurden. Um zu überprüfen, ob es sich hierbei um einen kalziumspezifischen Effekt handelt, wurden die Zellen ebenfalls mit den korrespondierenden Magnesiumkonzentrationen inkubiert. Das Vorhandensein einer erhöhten Anzahl von Magnesium-Ionen zeigte dabei keinen signifikanten Einfluss auf die proliferative Kapazität der untersuchten Zellen. Mit Hilfe eines weiteren Tumortyps (Brustkrebszelllinie MDA-MB 231) konnte gezeigt werden, dass diese im Vergleich zu den untersuchten Ovarialkarzinomzellen weniger stark sensitiv auf das Vorhandensein von hohen Kalziumkonzentrationen reagierten. Diese Beobachtung bestätigt ebenfalls das Ergebnis einer Studie von Journé *et al*. [137]. In dieser Studie wurden Brustkrebszellen (MDA-MB 231) mit einer Kalzium- und Magnesiumkonzentration von bis zu 2,0 mmol/L inkubiert, dabei zeigten sich ebenfalls keine signifikanten Änderungen in der Proliferation.

Neben der Tatsache, dass es unter der Verwendung von hohen Kalziumkonzentrationen zu einer Wachstumsinhibition kommt, zeigen diese mit exogenem Kalzium inkubierten Zellen eine deutlich veränderte Morphologie im Vergleich zu den Kontrollzellen, gleichzeitig ist ein deutlicher Anstieg der subG_1-Phase bei Zellzyklusmessungen festzustellen. Daraus lässt sich schließen, dass die Zellen nicht über einen Zellzyklus-Arrest, sondern durch Zellschädigungen/Zelltod aus der Kultur eliminiert werden. Wie bei Trump *et al.* beschrieben, kann es in Folge einer hohen extrazellulären Kalziumkonzentration zu einer Störung der intrazellulären Kalzium-Homöostase kommen, was wiederum zu einer Schädigung der Zellen führt und im Fall eines nicht zu behebenden Schadens den Zelltod initiiert [138]. Eine weitere Erklärung konnte in einer anderen Studie gezeigt werden. Hier wird ein Prozess der programmierten Nekrose („necroptosis“) postuliert, der nach einer zytosolischen Kalziumakkumulation in xenotransplantierten Mäusen mit humanen Neuroblastom auftrat [139].

3.2 Wie wirkt sich die exogene Kalziumstimulation auf die molekularen Prozesse der Zelle aus?

Die Untersuchung einiger kalziumsensibler Proteine zeigte auf molekularer Ebene keinen signifikanten Einfluss, wie beispielsweise das nach exogener Kalziumstimulation auf Kalziumschwankungen im Endoplasmatischen Retikulum der Zelle reagierende Protein STIM-1 (stromal interaction molecule-1). STIM-1 sorgt als sogenannter Kalziumsensor dafür,

dass bei erniedrigtem Kalziumspiegel im Endoplasmatischem Retikulum die ICRAC (Calcium released activated calcium current) Ionenkanäle, die aus dem Protein ORAI1 (Calcium release-activated calcium channel protein 1) aufgebaut werden, an der Plasmamembran aktiviert und damit geöffnet werden. Dadurch kommt es zu einer Einströmung von Kalziumionen ins Zellinnere, so dass die leeren Kalziumspeicher wieder aufgefüllt werden können [140]. Ein weiteres wichtiges Protein der Kalziumregulation in Zellen stellt der IP3-Rezeptor (Inositoltriphosphate receptor) dar. Seine Aufgabe besteht darin, das im Endoplasmatischen Retikulum gespeicherte Kalzium, nach entsprechender Ligandenbindung mit IP3 freizusetzen. Die Generierung der dafür notwendigen Signalmoleküle als „Second-Messenger“, IP3 und DAG (Diaclglycerol), erfolgt durch die hydrolytische Spaltung von vorzugsweise PIP2 (Phosphatidylinositol-4,5-biphosphat) durch Phospholipase C (PLC). Auch bei diesem Protein konnte eine kaum detektierbare Stimulation durch exogenes Kalzium beobachtet werden. Im Gegensatz dazu war eine verstärkte Phosphorylierung und damit Aktivierung des Proteins p44/42 MAPK (ERK1/2) durch die exogene Stimulation mit Kalzium zu beobachten. Das Protein p44/42 MAPK aktiviert darauf das zytosolische Protein PLA2 (Phospholipase A2) [141]. Im nächsten Schritt spaltet PLA2 aus den Phospholipiden der Zellmembran die mehrfach ungesättigte Fettsäure Arachidonsäure ab. Der dadurch ansteigende Spiegel von Arachidonsäure wird durch die Cyklooxygenasen COX-1 und COX-2 zu verschiedenen Prostanoiden, insbesondere PGE2 (Prostglandin E2) metabolisiert [142,143]. Diese durch exogenes Kalzium stimulierte Phosphorylierung von p44/42 MAPK und dessen nachfolgender Signalweiterleitung konnte bei den in dieser Arbeit verwendeten Ovarialkarzinomzellen gezeigt werden. Es konnte ebenfalls nachgewiesen werden, dass dieser Effekt sowohl zeit- als auch konzentrationsabhängig ist. Dies weist auf eine metabolische Modifizierung dieser Zellen während der malignen Transformation und deren weiterer Entwicklung hin. Durch die Bindung von PGE2 an die Prostaglandin E Rezeptoren EP2 und EP4 kommt es zur Weiterleitung suppressiver Effekte, woraufhin eine gesteigerte Produktion von zyklischen AMP (cAMP) zu beobachten ist. Alternativ hat die Bindung von PGE2 an EP3 auch immunstimulierende Eigenschaften, wodurch der cAMP-Spiegel sinkt. Das bedeutet also, dass durch eine PGE2 vermittelte Immunmodulation von Entzündungs- und Immunzellen diese zur Unterstützung der Tumore und einer weiteren Tumorgenese dienen können [144].

Es konnte ebenfalls in dieser Arbeit gezeigt werden, dass eine Stimulation mit PGE2 (1 pg/mL-10 ng/mL) keinen signifikant messbaren Einfluss auf das proliferative Verhalten

der untersuchten Ovarialkarzinomzellen zeigt und der Einsatz eines MAPK Inhibitor (PD98059) die Synthese von PGE2 komplett supprimierte. In der Literatur findet man unterschiedliche Ergebnisse im Bezug auf den Einfluss von PGE2 auf die Proliferation von Zellen. So berichtet zum Beispiel Donnini *et al.* [145], dass PGE2 (1–1000 nM) einen signifikant wachstumssteigernden Einfluss auf die Proliferation bei Zellen des Plattenepithelkarzinom zeigte. Dagegen konnte die Arbeit von Tobey *et al.* [146] keinen wachstumssteigernden Effekt auf das proliferative Verhalten durch exogen stimuliertes PGE2 (5–5000 ng/ml) bei humanen Fibroblasten aus der Lunge feststellen, stattdessen wurde initial ein wachstumsinhibierender Effekt beobachtet.

Zusammenfassend kann festgestellt werden, dass bei SCCOHT-1 und auch anderen Ovarialkarzinomzellen eine erhöhte exogene Kalziumkonzentration die Produktion von PGE2 spezifisch über die p44/42 MAPK Aktivierung stimuliert. Dies führt parallel zu einer Induzierung des Zelltods. Die gezeigten Ergebnisse deuten darauf hin, dass ein erhöhter Kalziumwert eine mögliche physiologische Antitumor-Strategie für das SCCOHT in Unterstützung mit einer kombinierten chemotherapeutischen Behandlung darstellen könnte [147].

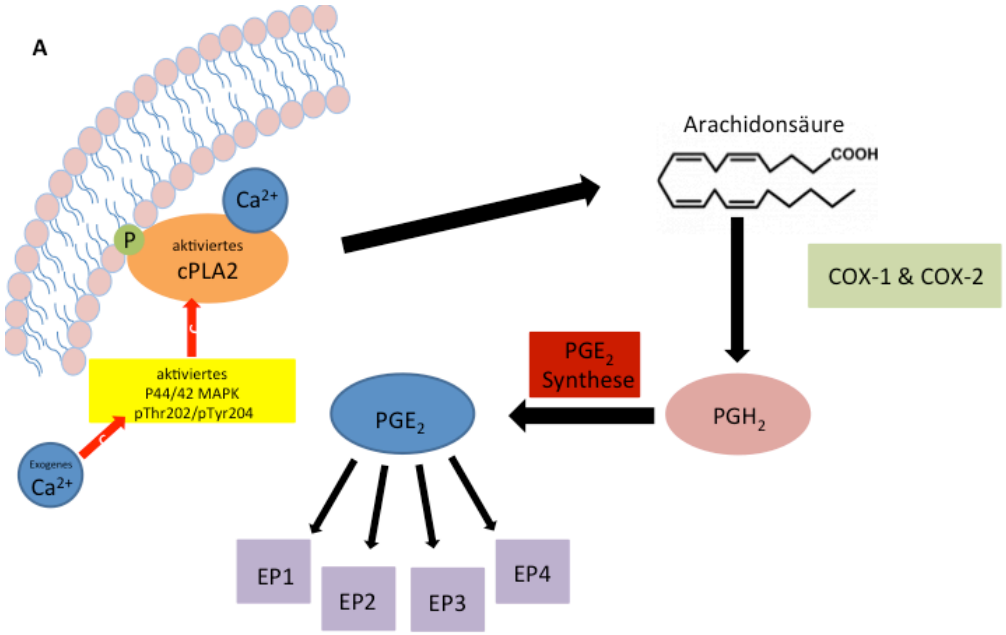

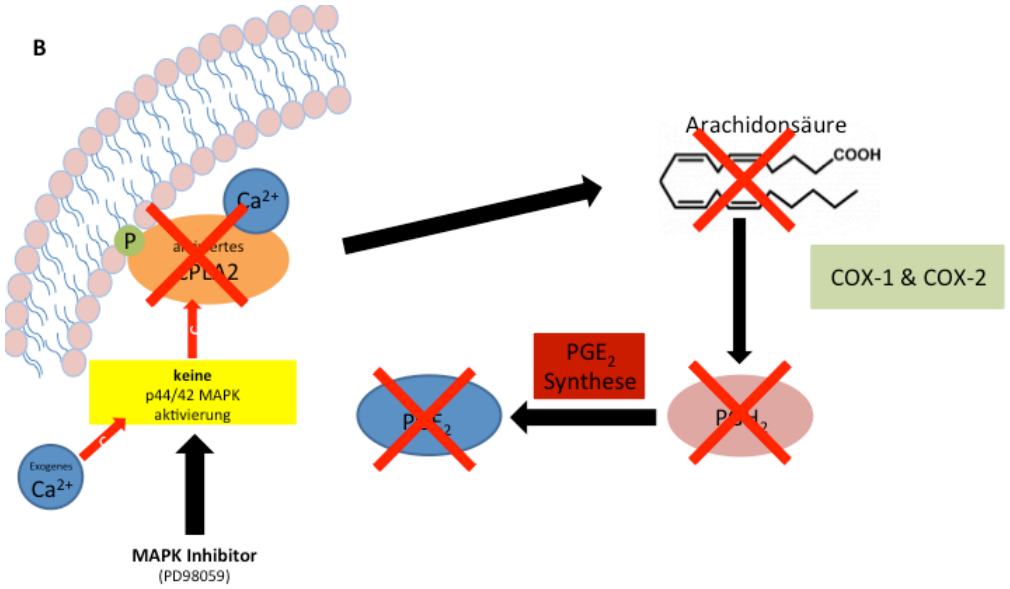

Abbildung 3-1: Schematische Darstellung der durch exogenes Kalzium stimulierten MAPK Kinase Stimulierung der PGE2 Produktion im Ovarialkarzinom (A) und die inhibierende Wirkung des MAPK Inhibitors (B). (adaptiert nach Agard *et al.* [148])

3.3 Medikamentenscreening beim SCCOHT

Betrachtet man die Tatsache, dass die Therapie der Wahl zur chemotherapeutischen Behandlung des SCCOHT zumeist aus der Kombination von Cisplatin und Etoposid oder Carboplatin und Taxan gefolgt von einer Strahlentherapie [43,51] besteht, dabei allerdings die Anzahl der Rezidive äußerst hoch ausfällt und nur ein verschwindend geringer Anteil der Patientinnen diese Erkrankung länger als 5 Jahre überlebt [46,149,150], so verwundert es nicht, dass bis zum jetzigen Zeitpunkt keine „speziell“ auf das SCCOHT abgestimmte Therapieempfehlung in der Fachwelt existiert. Dieses Fehlen einer spezifischen Therapie beruht auf der geringen Anzahl der jährlich auftretenden Fälle und einer zu späten Diagnostik verbunden mit einem häufig hohen FIGO-Stadium, wobei die angesetzte Behandlungsmethode nahezu der tumortherapeutischen Standardbehandlung des gemeinen Ovarialkarzinoms entspricht. Aufgrund der Seltenheit der SCCOHT-Tumorerkrankung, verbunden mit der hohen Sterblichkeit der Patientinnen, ist es sehr schwer, über den im Einzelfall versuchten Heilversuch hin zu einer aussagekräftigen klinischen Studie zu kommen. Eine essenzielle Zwischenstufe stellt dabei unser Zellmodell (SCCOHT-1) und das durch die Gruppe von Gamwell *et al.* etablierte Zellsystem (BIN-67) [63] dar. Mit der Verwendung dieser beiden Zelllinien war es erstmals möglich, diese seltene Erkrankung *in vitro* auf unterschiedliche Wirkstoffklassen hin zu untersuchen, was in diesem Umfang und aus ethischen Gründen am Patienten nicht möglich gewesen wäre. Im Rahmen dieser Arbeit

wurden die *in vitro* Untersuchungen parallel zum Vergleich ebenfalls an zwei ovarialen Adenokarzinom-Zelllinien (SK-OV-3 und NIH:OVCAR-3) durchgeführt. Dabei stellte sich heraus, dass die SCCOHT-1 Zellen gegenüber beiden Platinpräparaten (Cis- und Carboplatin) eine Insensitivität bzw. Resistenz zeigten. Dies konnte ebenfalls bei den Zellen des SK-OV-3 und NIH:OVCAR-3 beobachtet werden und deckt sich mit dafür in der Literatur beschriebenen Ergebnissen [151,152]. Das Vorliegen einer Resistenz gegenüber den Platinpräparaten konnte ebenfalls mit Hilfe von Zellzyklusanalysen bestätigt werden. Dies lässt die Frage aufkommen, ob die Verwendung dieser Chemotherapeutika als Standard Medikation bei Patientinnen mit SCCOHT wirklich einen sinnvollen Therapieansatz darstellt. Auch wenn in einer Metaanalyse von 2011 [44] diskutiert wurde, dass die Verwendung von Platinpräparaten mit einer verbesserten Überlebenschance in Verbindung gebracht werden kann, war zu beobachten, dass die Verwendung dieser Substanzen in der Praxis zu keinem bahnbrechenden Anstieg der Patientinnen mit einer Überlebensrate > 5 Jahre führte, geschweige denn, eine Heilung mit diesen Präparaten bei einem Großteil der Patientinnen eintrat. Daher sollte man das Augenmerk nicht von Reagenzien abwenden, die auf den ersten Blick nicht in das vorherrschende Therapiespektrum passen. Eine solche Stoffklasse könnten unter anderem die Mikrotubuli stabilisierenden Präparate, wie das Taxol oder die Epothilone und im speziellen das Epothilon B darstellen. Hier konnte gezeigt werden, dass Epothilon B einen signifikanten wachstumshemmenden Effekt bei SCCOHT-1 und den ovarialen Adenokarzinom-Zelllinien zeigte. Im Jahr 2004 konnte ebenfalls eine Gruppe am Beispiel der Zelllinie SK-OV-3 zeigen, dass durch den Einsatz von 10 nM Epothilon B ein Zellzyklus-arrest und Apoptose zu beobachten war [153]. Die Pharmafirma Novartis hat von November 2005 bis Februar 2010 eine vergleichende Phase III Studie (NCT00262990) mit Patupilon (Produktname von Epothilon B) bei Patientinnen mit einem Ovarialtumor durchgeführt, die eine Taxan/Platin Resistenz aufweisen. Dieser Therapieansatz wurde verglichen mit einer Behandlung der Tumore mit pegyliertem, liposomalen Doxorubicin. Es stellte sich heraus, das Patupilon keinen signifikant verbesserten Therapieansatz darstellt im Vergleich zu der aktiven Kontrollgruppe, die mit Doxorubicin behandelt wurde [154]. Der wachstumsinhibierende Effekt von Epothilon B ist begleitet von der Aktivierung einer Vielzahl von Proteinen, die eine wichtige Rolle bei der Zell- und DNA-Schadensantwort spielen. Parallel hierzu wurde außerdem eine erhöhte Expression von $HSP27^{(pSer82)}$ und $P53^{(pSer15)}$ detektiert. Dieser Anstieg korrelierte mit dem Anstieg der Apoptoserate/Zelltod in den behandelten Zellen und stellte sich als eine Akkumulierung der SCCOHT-1 Zellen in der subG_1-Phase des Zellzyklus dar. Eine Möglichkeit von Zellen, auf Stress zu reagieren, wie hier durch Epothilon B induziert,

stellt die Phosphorylierung von HSP27 dar, wobei dieser Schutzmechanismus nur eine begrenzte Wirkung hat. Zum Beispiel kann HSP27 die Formation von Apoptosomen inhibieren [155], durch veränderte BID Verteilung an der mitochondrialen Membran der Zellen (BH3 interacting-domain death agonist) und blockiert so die Fas/(CD95) vermittelte Apoptose [156]. In einem Artikel aus dem Jahr 2006 beschreibt Casado *et al.* die Phosphorylierung von HSP27$^{(pSer82)}$ bei Brustkrebszellen nach Inkubation mit Vincristin (einem Vinca-Alkaloid, das ebenfalls über die Mikrotubulistabilisierung wirkt) [157]. Dies scheint ebenso ein Ansatz der Zellen zu sein, sich gegen eine drohende Apoptose zu schützen.

Als Antwort auf eine Schädigung der DNA in der Zelle kommt es auch zu einer Akkumulation des Tumorsuppressorproteins P53 und dessen Phosphorylierung P53$^{(pSer15)}$, was zu einem Zellzyklusarrest führt [158]. Kommt es zu einer vermehrten Anreicherung von P53 in der Zelle, kann dies zur Aktivierung von Proteinen der BAX/BCL2-Familie führen, die über weitere Signalkaskaden Caspasen aktivieren und so die Apoptose initiieren [159]. Interessant ist die Tatsache, dass bei der Behandlung einer humanen Ovarialkarzinom-Zelllinie (A2780) mit Taxol eine Phosphorylierung am Serienrest 20 beobachtet werden konnte [160]. Dies lässt eventuell Rückschlüsse darauf ziehen, dass Taxol und Epothilon die Phosphorylierung unterschiedlicher Serin-Epitope vermitteln. Ioffe *et al.* konnte die Vermutung bestätigen, dass die Zytotoxizität verschiedener Epothilone über unterschiedliche Mechanismen an P53 weitergeleitet wird [161], sodass hier offensichtlich multiple Signalwege über P53 existieren.

Als ein wichtiges Verbindungsglied zwischen den *in vitro* Ergebnissen und der Behandlung am Patienten stehen *in vivo* Versuche. Durch die tumorigene Eigenschaft der SCCOHT-1 Zellen [66] war es uns möglich, das in den *in vitro* Daten vielversprechende Chemo-therapeutikum Epothilon B auch an SCCOHT-1 generierten Tumoren in NODscid Mäusen zu untersuchen. Hierbei konnte ein reduziertes Tumorwachstum der mit Epothilon B behandelten Mäuse im Vergleich zu den unbehandelten Kontroll-Mäusen beobachtet werden. Dabei stellte sich eine unterschiedliche Sensitivität der Zellen *in vitro* und *in vivo* auf das verwendete Epothilon B heraus. Dieses Phänomen hängt möglicherweise davon ab, dass der Tumor nicht isoliert im Körper vorliegt - nur aus Tumorzellen bestehend - sondern im Tumorstroma mit einer Vielzahl von anderen tumorassoziierten Zellpopulationen eingebettet ist. Demnach erfolgt *in vitro* eine direkte Exponierung der Tumorzellen mit dem Chemotherapeutikum, wohingegen *in vivo* die Chemotherapeutika ebenfalls auf die Tumormikroumgebung,

bestehend aus Extrazellularmatrix, eingebetteten endothelialen Zellen, Immunzellen, tumorassoziierten Fibroblasten und mesenchymalen Stammzellen, mitwirken und hieraus der erhöhte Bedarf des Chemotherapeutikums resultiert, um die gewünschte Wirkung *in vivo* erzielen zu können [162,163]. In diesem Kontext war auch ein wichtiges Ergebnis, dass die molekular eng verwandten Reagenzien Ixabepilon und Epothilon B, die sich nur durch den Austausch eines Stickstoffatoms gegen ein Sauerstoffatom voneinander unterscheiden (Abbildung 1-5), in der Praxis *in vitro* bei gleicher Konzentration sehr unterschiedliche Effekte ausbildeten. Ixabepilon zeigte erst bei einem ca. 250-fach höheren Konzentrationsbereich einen ähnlichen wachstumsinhibierenden Effekt wie Epothilon B. Diese Unterschiede können darauf zurückzuführen sein, dass das Ixabepilon-Molekül eine instabilere Bindung mit der Bindungstasche des alpha- und beta-Tubulins eingeht, so dass die stabilisierende Wirkung auf die Mikrotubuli weniger stark ausgeprägt ist und sich damit die geringere Chemosensitivität der Zellen gegenüber Ixabepilon erklären lässt. Ein weiterer Grund könnte sein, dass das Ixabepilon ebenfalls eine geringere Bindungsaffinität zu der in vielen aggressiven und resistenten Tumoren exprimierten Protein-Isoform Tubulin-β3 aufweist [164,165]. Diese Isoform konnte auch bei den Zellen des SCCOHT-1, nicht aber bei den ovarialen Adenokarzinom Zellen (SK-OV-3 und NIH:OVCAR-3) nachgewiesen werden, was wiederum den aggressiven Charakter von SCCOHT-1 Zellen und SCCOHT-1 induzierten Tumoren unterstreicht. Die wachstumshemmende Wirkung von Epothilon B konnte ebenfalls bei *in vitro* rekultivierten Zellen von SCCOHT-1 Xenografttumoren festgestellt werden [147].

3.4 Ist Epothilon B und exogen substituiertes Kalzium eine neue Behandlungsstrategie für das SCCOHT?

Im Rahmen weiterführender Untersuchungen zur Optimierung der Behandlungsstrategie von SCCOHT sollte der Einfluss einer Kombination der einzeln erfolgversprechenden Therapien (unter 3.3 erfolgversprechenden Behandlung der SCCOHT-1 Tumore mit Epothilon B und des unter 3.2 erwähnten wachstumsinhibierenden Effekts von exogener Kalziumsubstitution) getestet werden. Durch die parallele Anwendung von Epothilon B und exogen hinzugefügtem Kalzium konnte eine synergistische Verbesserung des wachstumsinhibierenden Effekts des zuvor einzeln verwendeten Epothilon B *in vitro* und *in vivo* beobachtet werden. Eine ähnliche verbesserte Wirksamkeit eines chemotherapeutischen Präparates durch ein gleichzeitiges Verwenden von exogenem Kalzium konnte in einer Studie von Journé *et al.* gezeigt werden [137]. Hierbei wurde die Vermutung angestellt, dass es durch die Bindung von Ibandronat

und Kalzium zu einer Akkumulation dieses Komplexes in der Zelle kommen könnte, sodass dieser dort seine Wirkung verstärkt entfalten könnte.
Durch den parallelen Einsatz von Epothilon B und Kalzium bei der Behandlung der SCCOHT-1 tumortragenden Mäuse konnte nach Versuchsende eine normale Kalzium-konzentration im Mausserum festgestellt werden, wohingegen bei unbehandelten Kontrollmäusen, sowie bei den ausschließlich mit Kalzium behandelten Mäusen, nach Versuchsende eine persistierende Hyperkalzämie zu beobachten war. Diese Ergebnisse zeigen einen vielversprechenden Ansatz für einen möglichen Therapieansatz (Behandlungsversuch) am Menschen auf. Sie werfen aber auch noch viele Fragen hinsichtlich der hierbei ablaufenden Mechanismen auf, die eine Vielzahl an weiteren Untersuchungen erfordert. Einige dieser Fragen wären: Warum tritt diese, als Hyperkalzämie beschriebene, messbare Kalziumerhöhung im Serum von SCCOHT- und anderer Tumorpatienten auf? Ist die Hyperkalzämie dem Vorhandensein des Tumors geschuldet, der eine erhöhte Kalziumkonzentration vermittelt, oder ist es der Versuch des Körpers, auf diese Tumorerkrankung zu reagieren? Warum wirkt die kombinierte Behandlung der SCCOHT-1 Xenografttumore mit Epothilon B und Kalzium besser als mit Epothilon B allein? Warum zeigt die alleinige Gabe von Kalzium keinen messbaren Einfluss auf das Tumorwachstum?

3.5 Ist der Rezeptor c-Met und sein Ligand ein mögliches Target in der Therapie von SCCOHT-Patientinnen?

Ein Ziel dieser Dissertation war es, neue therapeutische Möglichkeiten zur Behandlung von SCCOHT zu finden. Durch eine gezielte Untersuchung der Zellkulturüberstände von SCCOHT-1 Zellen konnte die konstitutive Sekretion von Zytokin- und Wachstumsfaktoren untersucht werden. Hierbei stellte sich heraus, dass die Zellen eine signifikante Menge des Wachstumsfaktors HGF (Hepatozyten Wachstumsfaktor) produzieren. Daraufhin richtete sich die Fragestellung auf c-Met (Mesenchymal epithelial transition factor), der korrespondierende mit einer intrinsischen Tyrosinkinase assoziierte Rezeptor des Liganden HGF. Durch die Untersuchung der Zellen der ovarialen Adenokarzinome und der SCCOHT-Zellen (SCCOHT-1 und BIN-67) konnte eine starke Expression von c-Met bei SK-OV-3 und NIH:OVCAR-3 und eine geringere Expression bei SCCOHT-1 und BIN-67 beobachtet werden. Diese Beobachtung geht konform mit zahlreichen Veröffentlichungen in der Literatur, die ermittelt haben, dass bei etwa 70 % der humanen Ovarialkarzinome das Protein c-Met exprimiert wird und davon bei etwa 30 % überexprimiert vorliegt (ebenso in Zelllinien) [166-169]. Der ebenfalls als HGF/SF-Rezeptor bekannte membrangebundene Rezeptor c-Met

ist essentiell für die embryonale Entwicklung und spielt eine wichtige Rolle bei der Wundheilung [97]. Eine Überexpression von c-Met bei hyperaktiven Tumoren, auch beim Ovarialkarzinom, korreliert mit einer schlechten Prognose. Hierdurch kann ein verstärktes Tumorwachstum, eine damit gekoppelte Metastasierung und erhöhte Angiogenese beobachtet werden [170-172]. Diese Parameter lassen sich auch bei den Eigenschaften der Zellen des SCCOHT-1 wiederfinden. Die verstärkte Angiogenese *in vivo* korrelierte mit einer im Zytokin/Wachstumsfaktor-Assay registrierten Sekretion von VEGF und VCAM-1 (Vascular cell adhesion molecule 1), da die Freisetzung dieser Wachstumsfaktoren im Mikroumfeld des Tumors eine entsprechende Neovaskularisierung fördert. Das gleichfalls von den SCCOHT-1 Zellen sezernierte IL8 (CXCL8) ist ebenso an der Angiogenese und ferner bei Entzündungsreaktionen beteiligt [173]. Die Tatsache, dass SCCOHT-1 Zellen ein ausgeprägtes Produktionsverhalten von Zytokinen und Wachstumsfaktoren zeigen, legt eine über autokrine Sekretion vermittelte Stimulation der durch c-Met vermittelten Proliferation nahe. Hierzu wurde dieses spezielle Ligand/Rezeptorpaar im Hinblick auf ein potenzielles spezifisches therapeutisches Target genauer untersucht.

Durch exogene HGF Stimulierung konnte die Phosphorylierung von c-Met und durch dessen Signalweiterleitung die Phosphorylierung der p44/42 MAPK Kinase bei den Zellen der ovarialen Adenokarzinome und den SCCOHT-Zellen beobachtet werden. Dabei besitzt c-Met gleich mehrere Bindungsdomänen auf der zytosolischen Seite, die mittels Phosphorylierung der Tyrosin-Reste aktiviert werden, um über weitergeleitete Signale schließlich MAPK/ERK zu aktivieren. Dies wiederum führt zu einer Stimulierung der Proliferation und einer damit verbundenen Zellzyklusprogression bei einer Vielzahl verschiedener Tumortypen (inkl. Ovarialkarzinom) [94,167,174,175].

Um c-Met und HGF als therapeutisches Target nutzen zu können, kommen drei Herangehensweisen in Frage: 1) Störung der Ligand/Rezeptor Interaktion, 2) Inhibierung der katalytischen Tyrosinkinase Aktivität und 3) Blockierung der Interaktionen des aktivierten Rezeptors mit seinen Effektoren. Als initialer Ansatzpunkt wurden zunächst Multi-Target Tyrosinkinase Inhibitoren (TKI) verwendet, im speziellen Crizotinib und Foretinib. Hierbei konnte gezeigt werden, dass Foretinib effizienter als Crizotinib die konstitutive und die durch HGF induzierte Phosphorylierung von c-Met und somit auch die Phosphorylierung der MAP Kinase der getesteten Zellen blockieren konnte. Folglich wurde durch den Einsatz der beiden c-Met Inhibitoren bei allen Zellen ein G_2/M Zellzyklusarrest beobachtet und bestätigte somit

die Ergebnisse von Zillhard *et al*., der dieses Ereignis schon für die Zelllinie SK-OV-3 beschreiben konnte [176]. Aufgrund der höheren Potenz von Foretinib in Bezug auf die wachstumsinhibierende Eigenschaft bei SCCOHT-1 und BIN-67 Zellen und der Tatsache, dass Foretinib bereits erfolgsversprechend bei *in vivo* Studien (Lungenmetastasen [177], Hedgehog Medulloblastom [178] und Nichtkleinzelligen Lungenkarzinom [129]) eingesetzt werden konnte, wurde diese Substanz auch bei *in vivo* Versuchen zum SCCOHT getestet. Bei den IHC-Färbungen von 15 originalen SCCOHT Tumorproben konnte bei ca. 60 % der untersuchten Schnitte eine c-Met Expression und bei ca. 30 % keine c-Met Expression beobachtet werden. Diese Unterschiede in der c-Met Expression konnten ebenfalls in den SCCOHT Zelllinien beobachtet werden (BIN-67 < 6,5 %, SCCOHT-1 ~ 41 %). Im *in vivo* Versuch konnte in beiden Fällen ein substantieller therapeutischer Effekt von Foretinib durch ein vermindertes Wachstum der Tumore im Vergleich zu den Kontrolltumoren beobachtet werden. Es zeigte sich kein Effekt des Foretinib hinsichtlich der Stärke des exprimierten c-Met der injizierten Zellen außer der Auffälligkeit, dass die Tumorentwicklung der BIN-67-Tumore im Vergleich zu den der SCCOHT-1-Tumore deutlich länger dauerte. Dieses Ergebnis lässt vermuten, dass die Verwendung von Foretinib ein weiterer möglicher Therapie-Baustein für diese Tumorart darstellen könnte.

Um den substanziellen Beitrag von c-Met bei der Proliferation von SCCOHT-1 zu untersuchen, wurde das Protein mit der Hilfe eines siRNA Knockdown herunterreguliert. Es konnte gezeigt werden, dass diese Herunterregulation von c-Met sich in einer verlangsamten Proliferation, einem Anstieg der G_0/G_1-Phase und einer erniedrigten S-Phase im Zellzyklus, sowie einer fehlenden Phosphorylierung von MAPK nach HGF Stimulation zeigte. Darüber hinaus wurde in den *in vivo* Versuchsreihen ein reduziertes Tumorwachstum beobachtet. Eine verringerte Proliferationsrate der SCCOHT-1 Zellen war sieben Tage nach Transfektion mit c-Met siRNA wieder auf ein normales Niveau zurückgekehrt und korrelierte mit einer wieder detektierbaren c-Met-Expression im Western Blot.

Neben der Inhibition des c-Met Signalwegs konnte eine negative Regulierung des VEGFR2-Rezeptors im Tumormikromilieu der mit Foretinib behandelten Mäuse beobachtet werden. Dieser Effekt war durch eine verminderte Ausprägung der wachstumsassoziierten Strukturen im Tumormikromilieu begleitet, darunter eine deutlich verringerte Vaskularisierung des Tumors. Unterstützende Evidenz bezüglich der Antitumoraktivität von Foretinib durch die Inhibition der c-Met und VEGFR-2 vermittelten Signalweiterleitung zeigen auch

unterschiedliche Tumormodelle (hepatozelluläres Karzinom [179], Nierenzellkarzinom [180] und Magenkarzinom [93]) und bestätigen die Wirksamkeit. Allerdings zeigt keine dieser Studien das parallele und ebenso wichtige Potenzial von Foretinib zur Blockierung der Neovaskularisierung im Tumormikromilieu, welches eine entscheidende Wirkung bei den SCCOHT Tumoren entfaltet. Zur Tumormikroumgebung konnte gezeigt werden, dass während der Interaktionen von SCCOHT-1 Tumorzellen mit nachbarschaftlichen mesenchymalen Stammzellen ein Transfer von Proteinen, RNA (Exosom) und anderem biologischen Material stattfinden kann. Dies kann zu veränderten Zellfuktionalitäten und zu einem Anstieg der Heterogenität des Tumors beitragen [162,163,181-183].

3.6 Neue Hinweise über die Entität von SCCOHT

Ein Prinzip, auf dem die Wissenschaft beruht, ist die Tatsache, dass sie auf bestehendem Wissen weiter aufbaut und damit auch bereits bekanntes Wissen auf Korrektheit hinterfragt und überprüft. Beispielsweise ist die Ätiologie von SCCOHT bis zum jetzigen Zeitpunkt ungeklärt. Es wurde und wird immer wieder darüber spekuliert, dass die Zellen dieses Tumors epithelialen oder mesenchymalen Ursprungs sind [38,136,184,185], wohingegen andere Arbeitsgruppen auch einen Keimbahn Ursprung [34] postulierten. Seit der Entdeckung einer Mutation von *SMARCA4* bei SCCOHT-Patientinnen wird die Abwesenheit des von *SMARCA4* codierten Protein BRG-1 als potentieller Marker des SCCOHT diskutiert [54-56]. Aufgrund einer Reihe von Ähnlichkeiten zwischen dem SCCOHT-1 und dem malignen rhabdoiden Tumor (u.a. Mutation von SMARCA4) vermuten momentan einige Wissenschaftler einen gemeinsamen Ursprung dieser beiden Tumorarten und fordern eine Umbenennung in „malignant rhabdoid tumor of the ovary“ [62].

Im Rahmen dieser Arbeit konnte gezeigt werden, dass SCCOHT-1 und BIN-67 Zellen im Vergleich zu den ovarialen Adenokarzinom-Zelllinien SK-OV-3 und NIH:OVCAR-3 kein BRG-1 exprimieren. Dieses Resultat konnte somit den Verlust der Expression von BRG-1 bei BIN-67 [55] im Gegensatz zur Präsenz der BRG-1 Expression bei SK-OV-3 Zellen [186] bestätigen. Weiter konnte durch eine Charakterisierung der beiden SCCOHT Zelllinien im Vergleich zu zwei ovarialen Adenokarzinom-Zelllinien gezeigt werden, dass es signifikante Unterschiede in der Expression der Oberflächenmarker [CD90 (+), CD326 (-), Mesothelin (-)] und in der Filament-Expression [Vimentin (+), panCK (+ niedrig)] gibt. Dies lässt die

Schlussfolgerung zu, dass es sich beim SCCOHT tatsächlich um eine separate Tumorentität handelt.

3.7 Ausblick

Die aus dieser Arbeit neugewonnenen Erkenntnisse liefern erstmals spezifische mögliche Therapieansätze auf molekularer Ebene zur gezielten Behandlung der SCCOHT Tumorerkrankung, was die Grundlage für einen translationalen Ansatz von der Grundlagenforschung zur Anwendung in klinischen Studien bietet. Die Ergebnisse dieser Arbeit müssten dabei mit einer größeren Fallzahl multizentrisch in klinischen Studien getestet werden. Ferner sollte berücksichtigt werden, durch breiter angelegte und kombinierte Testreihen mögliche Synergismen von potenten Therapeutika zu identifizieren, um damit die Therapie von SCCOHT-Tumorpatientinnen weiter zu verbessen.

4 Abbildungs- und Tabellenverzeichnis

Abbildungen:

Tabelle:

5 Literatur

1. RKI. *Krebs in Deutschland 2009/2010*. (2013). Robert Koch-Institut (Hrsg) und die Geselschaft der epidemiologischen Krebsregister in Deutschland e.V. (Hrsg), Berlin.
2. Ferlay J, I Soerjomataram, R Dikshit, S Eser, C Mathers, M Rebelo, DM Parkin, D Forman and F Bray. (2015). Cancer incidence and mortality worldwide: sources, methods and major patterns in GLOBOCAN 2012. Int J Cancer 136:E359-86.
3. Bühling KJ and W Friedmann. *Intensivkurs Gynäkologie und Geburtshilfe*. (2009). Elsevier, München.
4. Prat J and FCoG Oncology. (2014). Staging classification for cancer of the ovary, fallopian tube, and peritoneum. Int J Gynaecol Obstet 124:1-5.
5. Mavaddat N, S Peock, D Frost, S Ellis, R Platte, E Fineberg, DG Evans, L Izatt, RA Eeles, J Adlard, R Davidson, D Eccles, T Cole, J Cook, C Brewer, M Tischkowitz, F Douglas, S Hodgson, L Walker, ME Porteous, PJ Morrison, LE Side, MJ Kennedy, C Houghton, A Donaldson, MT Rogers, H Dorkins, Z Miedzybrodzka, H Gregory, J Eason, J Barwell, E McCann, A Murray, AC Antoniou, DF Easton and Embrace. (2013). Cancer risks for BRCA1 and BRCA2 mutation carriers: results from prospective analysis of EMBRACE. J Natl Cancer Inst 105:812-22.
6. King MC, JH Marks, JB Mandell and G New York Breast Cancer Study. (2003). Breast and ovarian cancer risks due to inherited mutations in BRCA1 and BRCA2. Science 302:643-6.
7. Whittemore AS, R Harris and J Itnyre. (1992). Characteristics relating to ovarian cancer risk: collaborative analysis of 12 US case-control studies. II. Invasive epithelial ovarian cancers in white women. Collaborative Ovarian Cancer Group. Am J Epidemiol 136:1184-203.
8. Lukanova A and R Kaaks. (2005). Endogenous hormones and ovarian cancer: epidemiology and current hypotheses. Cancer Epidemiol Biomarkers Prev 14:98-107.
9. del Peso L, M Gonzalez-Garcia, C Page, R Herrera and G Nunez. (1997). Interleukin-3-induced phosphorylation of BAD through the protein kinase Akt. Science 278:687-9.
10. Kaku T, S Ogawa, Y Kawano, Y Ohishi, H Kobayashi, T Hirakawa and H Nakano. (2003). Histological classification of ovarian cancer. Med Electron Microsc 36:9-17.

11. Kurman RJ and M Shih Ie. (2008). Pathogenesis of ovarian cancer: lessons from morphology and molecular biology and their clinical implications. Int J Gynecol Pathol 27:151-60.
12. Kurman RJ and M Shih Ie. (2010). The origin and pathogenesis of epithelial ovarian cancer: a proposed unifying theory. Am J Surg Pathol 34:433-43.
13. Shih Ie M and RJ Kurman. (2004). Ovarian tumorigenesis: a proposed model based on morphological and molecular genetic analysis. Am J Pathol 164:1511-8.
14. Meinhold-Heerlein I, F Zeppernick, A Strauss, N Maass and S Hauptmann. (2011). Die Heterogenität des Ovarialkarzinoms. Der Gynäkologe 44:708-716.
15. Bartel F, J Jung, A Bohnke, E Gradhand, K Zeng, C Thomssen and S Hauptmann. (2008). Both germ line and somatic genetics of the p53 pathway affect ovarian cancer incidence and survival. Clin Cancer Res 14:89-96.
16. Heintz AP, F Odicino, P Maisonneuve, U Beller, JL Benedet, WT Creasman, HY Ngan, M Sideri and S Pecorelli. (2001). Carcinoma of the ovary. J Epidemiol Biostat 6:107-38.
17. Bauerschlag DO, C Schem, MT Weigel, C Von Kaisenberg, A Strauss, T Bauknecht, N Maass and I Meinhold-Heerlein. (2010). The role of p53 as a surrogate marker for chemotherapeutical responsiveness in ovarian cancer. J Cancer Res Clin Oncol 136:79-88.
18. Santillan A, YW Kim, ML Zahurak, GJ Gardner, RL Giuntoli, 2nd, IM Shih and RE Bristow. (2007). Differences of chemoresistance assay between invasive micropapillary/low-grade serous ovarian carcinoma and high-grade serous ovarian carcinoma. Int J Gynecol Cancer 17:601-6.
19. Gershenson DM, CC Sun, D Bodurka, RL Coleman, KH Lu, AK Sood, M Deavers, AL Malpica and JJ Kavanagh. (2009). Recurrent low-grade serous ovarian carcinoma is relatively chemoresistant. Gynecol Oncol 114:48-52.
20. Schmeler KM, CC Sun, DC Bodurka, MT Deavers, A Malpica, RL Coleman, PT Ramirez and DM Gershenson. (2008). Neoadjuvant chemotherapy for low-grade serous carcinoma of the ovary or peritoneum. Gynecol Oncol 108:510-4.
21. Nakayama N, K Nakayama, S Yeasmin, M Ishibashi, A Katagiri, K Iida, M Fukumoto and K Miyazaki. (2008). KRAS or BRAF mutation status is a useful predictor of sensitivity to MEK inhibition in ovarian cancer. Br J Cancer 99:2020-8.

22. Farley J, WE Brady, V Vathipadiekal, HA Lankes, R Coleman, MA Morgan, R Mannel, SD Yamada, D Mutch, WH Rodgers, M Birrer and DM Gershenson. (2013). Selumetinib in women with recurrent low-grade serous carcinoma of the ovary or peritoneum: an open-label, single-arm, phase 2 study. Lancet Oncol 14:134-40.
23. Ledermann JA, A Hackshaw, S Kaye, G Jayson, H Gabra, I McNeish, H Earl, T Perren, M Gore, M Persic, M Adams, L James, G Temple, M Merger and G Rustin. (2011). Randomized phase II placebo-controlled trial of maintenance therapy using the oral triple angiokinase inhibitor BIBF 1120 after chemotherapy for relapsed ovarian cancer. J Clin Oncol 29:3798-804.
24. Gotlieb WH, F Amant, S Advani, C Goswami, H Hirte, D Provencher, N Somani, SD Yamada, JF Tamby and I Vergote. (2012). Intravenous aflibercept for treatment of recurrent symptomatic malignant ascites in patients with advanced ovarian cancer: a phase 2, randomised, double-blind, placebo-controlled study. Lancet Oncol 13:154-62.
25. Gherardi E, W Birchmeier, C Birchmeier and G Vande Woude. (2012). Targeting MET in cancer: rationale and progress. Nat Rev Cancer 12:89-103.
26. Deutsche Krebsgesellschaft, Deutsche Krebshilfe and AWMF. *Leitlinienprogramm Onkologie S3-Leitlinie Diagnostik, Therapie und Nachsorge maligner Ovarialtumoren,*.
27. Scully RE. *Atlas of Tumor Pathology: Tumors of the Ovary and Maldeveloped Gonads*. (1979). Armed Forces Institute of Pathology, Washington,DC,.
28. Reed D, Y Shen, AA Shelat, LA Arnold, AM Ferreira, F Zhu, N Mills, DC Smithson, CA Regni, D Bashford, SA Cicero, BA Schulman, AG Jochemsen, RK Guy and MA Dyer. (2010). Identification and characterization of the first small molecule inhibitor of MDMX. J Biol Chem 285:10786-96.
29. Holtz G, TR Johnson, Jr. and ME Schrock. (1979). Paraneoplastic hypercalcemia in ovarian tumors. Obstet Gynecol 54:483-7.
30. Cannon PM, CR Smart, ML Wilson and CB Edwards. (1975). Hypercalcemia with ovarian granulosa cell carcinoma. Rocky Mt Med J 72:72-4.
31. Bertoni F, B Ferramosca and P Bacchini. (1983). [Small cell ovarian carcinoma with hypercalcemia: the role of the parathyroid hormone]. G Clin Med 64:564-70.
32. Patsner B, MS Piver, SB Lele, Y Tsukada, K Bielat and NB Castillo. (1985). Small cell carcinoma of the ovary: a rapidly lethal tumor occurring in the young. Gynecol Oncol 22:233-9.

33. Senekjian EK, M Hubby, DA Bell, D Anderson and AL Herbst. (1986). Clear cell adenocarcinoma (CCA) of the vagina and cervix in association with pregnancy. Gynecol Oncol 24:207-19.
34. Ulbright TM, LM Roth, FB Stehman, A Talerman and EK Senekjian. (1987). Poorly differentiated (small cell) carcinoma of the ovary in young women: evidence supporting a germ cell origin. Hum Pathol 18:175-84.
35. Abeler V, KE Kjorstad and JM Nesland. (1988). Small cell carcinoma of the ovary. A report of six cases. Int J Gynecol Pathol 7:315-29.
36. McMahon JT and WR Hart. (1988). Ultrastructural analysis of small cell carcinomas of the ovary. Am J Clin Pathol 90:523-9.
37. Senekjian EK, PA Weiser, A Talerman and AL Herbst. (1989). Vinblastine, cisplatin, cyclophosphamide, bleomycin, doxorubicin, and etoposide in the treatment of small cell carcinoma of the ovary. Cancer 64:1183-7.
38. McCluggage WG, E Oliva, LE Connolly, HA McBride and RH Young. (2004). An immunohistochemical analysis of ovarian small cell carcinoma of hypercalcemic type. Int J Gynecol Pathol 23:330-6.
39. Young RH, A Jackson and M Wells. (1994). Ovarian metastasis from thyroid carcinoma 12 years after partial thyroidectomy mimicking struma ovarii: report of a case. Int J Gynecol Pathol 13:181-5.
40. Dickersin GR and RE Scully. (1998). Ovarian small cell tumors: an electron microscopic review. Ultrastruct Pathol 22:199-226.
41. Eichhorn JH, DA Bell, RH Young, CM Swymer, TJ Flotte, RI Preffer and RE Scully. (1992). DNA content and proliferative activity in ovarian small cell carcinomas of the hypercalcemic type. Implications for diagnosis, prognosis, and histogenesis. Am J Clin Pathol 98:579-86.
42. Roth AR and GM Basello. (2003). Approach to the adult patient with fever of unknown origin. Am Fam Physician 68:2223-8.
43. Shrimali RK, PD Correa and NS Reed. (2011). Dose-dense and dose-intense chemotherapy for small cell ovarian cancer: 2 cases and review of literature. Med Oncol 28:766-70.
44. Estel R, A Hackethal, M Kalder and K Munstedt. (2011). Small cell carcinoma of the ovary of the hypercalcaemic type: an analysis of clinical and prognostic aspects of a rare disease on the basis of cases published in the literature. Arch Gynecol Obstet 284:1277-82.

45. Pautier P, V Ribrag, P Duvillard, A Rey, I Elghissassi, I Sillet-Bach, P Kerbrat, F Mayer, A Lesoin, B Brun, H Crouet, JC Barats, P Morice and C Lhomme. (2007). Results of a prospective dose-intensive regimen in 27 patients with small cell carcinoma of the ovary of the hypercalcemic type. Ann Oncol 18:1985-9.

46. Benrubi GI, P Pitel and N Lammert. (1993). Small cell carcinoma of the ovary with hypercalcemia responsive to sequencing chemotherapy. South Med J 86:247-8.

47. Kanwar VS, J Heath, CN Krasner and JM Pearce. (2008). Advanced small cell carcinoma of the ovary in a seventeen-year-old female, successfully treated with surgery and multi-agent chemotherapy. Pediatr Blood Cancer 50:1060-2.

48. Rana S, BK Warren and SD Yamada. (2004). Stage IIIC small cell carcinoma of the ovary: survival with conservative surgery and chemotherapy. Obstet Gynecol 103:1120-3.

49. Sholler GL, F Luks, S Mangray and SJ Meech. (2005). Advanced small cell carcinoma of the ovary in a pediatric patient with long-term survival and review of the literature. J Pediatr Hematol Oncol 27:169-72.

50. Tewari K, C Brewer, F Cappuccini, C Macri, LW Rogers and ML Berman. (1997). Advanced-stage small cell carcinoma of the ovary in pregnancy: long-term survival after surgical debulking and multiagent chemotherapy. Gynecol Oncol 66:531-4.

51. Harrison ML, P Hoskins, A du Bois, M Quinn, GJ Rustin, JA Ledermann, S Baron-Hay and ML Friedlander. (2006). Small cell of the ovary, hypercalcemic type -- analysis of combined experience and recommendation for management. A GCIG study. Gynecol Oncol 100:233-8.

52. Schwartz GG and HG Skinner. (2013). Prospective studies of total and ionized serum calcium in relation to incident and fatal ovarian cancer. Gynecol Oncol 129:169-72.

53. Clement PB. (2005). Selected miscellaneous ovarian lesions: small cell carcinomas, mesothelial lesions, mesenchymal and mixed neoplasms, and non-neoplastic lesions. Mod Pathol 18 Suppl 2:S113-29.

54. Jelinic P, JJ Mueller, N Olvera, F Dao, SN Scott, R Shah, J Gao, N Schultz, M Gonen, RA Soslow, MF Berger and DA Levine. (2014). Recurrent SMARCA4 mutations in small cell carcinoma of the ovary. Nat Genet 46:424-6.

55. Witkowski L, J Carrot-Zhang, S Albrecht, S Fahiminiya, N Hamel, E Tomiak, D Grynspan, E Saloustros, J Nadaf, B Rivera, C Gilpin, E Castellsague, R Silva-Smith, F Plourde, M Wu, A Saskin, M Arseneault, RG Karabakhtsian, EA Reilly, FR Ueland, A Margiolaki, K Pavlakis, SM Castellino, J Lamovec, HJ Mackay, LM Roth, TM

Ulbright, TA Bender, V Georgoulias, M Longy, A Berchuck, M Tischkowitz, I Nagel, R Siebert, CJ Stewart, J Arseneau, WG McCluggage, BA Clarke, Y Riazalhosseini, M Hasselblatt, J Majewski and WD Foulkes. (2014). Germline and somatic SMARCA4 mutations characterize small cell carcinoma of the ovary, hypercalcemic type. Nat Genet 46:438-43.

56. Ramos P, AN Karnezis, DW Craig, A Sekulic, ML Russell, WP Hendricks, JJ Corneveaux, MT Barrett, K Shumansky, Y Yang, SP Shah, LM Prentice, MA Marra, J Kiefer, VL Zismann, TA McEachron, B Salhia, J Prat, E D'Angelo, BA Clarke, JG Pressey, JH Farley, SP Anthony, RB Roden, HE Cunliffe, DG Huntsman and JM Trent. (2014). Small cell carcinoma of the ovary, hypercalcemic type, displays frequent inactivating germline and somatic mutations in SMARCA4. Nat Genet 46:427-9.
57. Wong CY, EL Tan and SK Cheong. (2014). In vitro differentiation of mesenchymal stem cells into mesangial cells when co-cultured with injured mesangial cells. Cell Biol Int 38:497-501.
58. Shain AH and JR Pollack. (2013). The spectrum of SWI/SNF mutations, ubiquitous in human cancers. PLoS One 8:e55119.
59. Karanian-Philippe M, V Velasco, M Longy, A Floquet, L Arnould, JM Coindre, C Le Naoures-Mear, G Averous, F Guyon, G MacGrogan and S Croce. (2015). SMARCA4 (BRG1) Loss of Expression Is a Useful Marker for the Diagnosis of Ovarian Small Cell Carcinoma of the Hypercalcemic Type (Ovarian Rhabdoid Tumor): A Comprehensive Analysis of 116 Rare Gynecologic Tumors, 9 Soft Tissue Tumors, and 9 Melanomas. Am J Surg Pathol.
60. Ramos P, AN Karnezis, WP Hendricks, Y Wang, W Tembe, VL Zismann, C Legendre, WS Liang, ML Russell, DW Craig, JH Farley, BJ Monk, SP Anthony, A Sekulic, HE Cunliffe, DG Huntsman and JM Trent. (2014). Loss of the tumor suppressor SMARCA4 in small cell carcinoma of the ovary, hypercalcemic type (SCCOHT). . Rare Diseases 2:e967148.
61. Brennan B, C Stiller and F Bourdeaut. (2013). Extracranial rhabdoid tumours: what we have learned so far and future directions. Lancet Oncol 14:e329-36.
62. Foulkes WD, BA Clarke, M Hasselblatt, J Majewski, S Albrecht and WG McCluggage. (2014). No small surprise - small cell carcinoma of the ovary, hypercalcaemic type, is a malignant rhabdoid tumour. J Pathol 233:209-14.

63. Gamwell LF, K Gambaro, M Merziotis, C Crane, SL Arcand, V Bourada, C Davis, JA Squire, DG Huntsman, PN Tonin and BC Vanderhyden. (2013). Small cell ovarian carcinoma: genomic stability and responsiveness to therapeutics. Orphanet J Rare Dis 8:33.

64. Upchurch KS, LM Parker, RE Scully and SM Krane. (1986). Differential cyclic AMP responses to calcitonin among human ovarian carcinoma cell lines: a calcitonin-responsive line derived from a rare tumor type. J Bone Miner Res 1:299-304.

65. Ohi S, S Niimi, N Okada, K Yamada, T Tachibana, H Hashimoto, M Nakajima, M Yasuda, T Tanaka, K Sato and H Ishikawa. (2004). Establishment and characterization of a human ovarian small cell carcinoma, hypercalcemic type, cell line (OS-1) secreting PTH, PthrP and ACTH--special reference to the susceptibility of anti-cancer drugs. Hum Cell 17:203-9.

66. Otte A, G Gohring, D Steinemann, B Schlegelberger, S Groos, F Langer, HH Kreipe, A Schambach, T Neumann, P Hillemanns, TW Park-Simon and R Hass. (2012). A tumor-derived population (SCCOHT-1) as cellular model for a small cell ovarian carcinoma of the hypercalcemic type. Int J Oncol 41:765-75.

67. Longley DB, DP Harkin and PG Johnston. (2003). 5-fluorouracil: mechanisms of action and clinical strategies. Nat Rev Cancer 3:330-8.

68. Freireich EJ. (1987). Arabinosyl cytosine: a 20-year update. J Clin Oncol 5:523-4.

69. Rustum YM, C Riva and HD Preisler. (1987). Pharmacokinetic parameters of 1-beta-D-arabinofuranosylcytosine (ara-C) and their relationship to intracellular metabolism of ara-C, toxicity, and response of patients with acute nonlymphocytic leukemia treated with conventional and high-dose ara-C. Semin Oncol 14:141-8.

70. Riva CM, YM Rustum and HD Preisler. (1985). Pharmacokinetics and cellular determinants of response to 1-beta-arabinofuranosylcytosine (ara-C). Semin Oncol 12:1-8.

71. Pharma M. *Methotrexate injection product monograph*. (2003). Montreal, Quebec.

72. Pharma M. *Apo-methotrexate tablet product monograph*. (2003). Montreal, Quebec.

73. Frederick CA, LD Williams, G Ughetto, GA van der Marel, JH van Boom, A Rich and AH Wang. (1990). Structural comparison of anticancer drug-DNA complexes: adriamycin and daunomycin. Biochemistry 29:2538-49.

74. Pommier Y, E Leo, H Zhang and C Marchand. (2010). DNA topoisomerases and their poisoning by anticancer and antibacterial drugs. Chem Biol 17:421-33.

75. Schmidt H. *Pharmakologie und Toxikologie: für Studium und Praxis ; mit 281 Tabellen*. (2007). Schattauer Verlag.
76. Jänicke F. (1997). Topotecen. Internist. Prax. 37:677-678.
77. Brogden RN and LR Wiseman. (1998). Topotecan. A review of its potential in advanced ovarian cancer. Drugs 56:709-23.
78. N.N. (1995). Topotecan hydrochloride. Drugs Fut. 20:483-489.
79. Cersosimo RJ. (1998). Topotecan: a new topoisomerase I inhibiting antineoplastic agent. Ann Pharmacother 32:1334-43.
80. Crom WR, AM Glynn-Barnhart, JH Rodman, ME Teresi, RE Kavanagh, ML Christensen, MV Relling and WE Evans. (1987). Pharmacokinetics of anticancer drugs in children. Clin Pharmacokinet 12:168-213.
81. Martelli L, F Di Mario, P Botti, E Ragazzi, M Martelli and L Kelland. (2007). Accumulation, platinum-DNA adduct formation and cytotoxicity of cisplatin, oxaliplatin and satraplatin in sensitive and resistant human osteosarcoma cell lines, characterized by p53 wild-type status. Biochem Pharmacol 74:20-7.
82. Wani MC, HL Taylor, ME Wall, P Coggon and AT McPhail. (1971). Plant antitumor agents. VI. The isolation and structure of taxol, a novel antileukemic and antitumor agent from Taxus brevifolia. J Am Chem Soc 93:2325-7.
83. Bollag DM, PA McQueney, J Zhu, O Hensens, L Koupal, J Liesch, M Goetz, E Lazarides and CM Woods. (1995). Epothilones, a new class of microtubule-stabilizing agents with a taxol-like mechanism of action. Cancer Res 55:2325-33.
84. Wilson PG. (1999). Special-interest subgroups at the ASCB: gamma-Tubulin: questions outstanding. Trends Cell Biol 9:119-120.
85. Schinzer D and A Limberg. (2000). Epothilone: Neue Wirkstoffe gegen Krebs. Magdeburger Wissenschaftjournal 1:23-29.
86. Hyun H, J Chung, J Kim, JS Lee, BM Kwon, KH Son and K Cho. (2008). Isolation of Sorangium cellulosum carrying epothilone gene clusters. J Microbiol Biotechnol 18:1416-22.
87. Höfle G, N Bedorf, H Steinmetz, D Schomburg, K Gerth and H Reichenbach. (1996). Epothilone A and B—Novel 16-Membered Macrolides with Cytotoxic Activity: Isolation, Crystal Structure, and Conformation in Solution. Angewandte Chemie International Edition in English 35:1567-1569.
88. Reichenbach H and G Hofle. (2008). Discovery and development of the epothilones : a novel class of antineoplastic drugs. Drugs R D 9:1-10.

89. Lipinski CA. (2003). Chris Lipinski discusses life and chemistry after the Rule of Five. Drug Discov Today 8:12-6.
90. Lipinski CA. (2004). Lead- and drug-like compounds: the rule-of-five revolution. Drug Discov Today Technol 1:337-41.
91. Johnson LN. (2009). Protein kinase inhibitors: contributions from structure to clinical compounds. Q Rev Biophys 42:1-40.
92. Müller-Tidow C, U Krug, U Brunnberg, WE Berdel and H Serve. (2007). Tyrosinkinasen als Ziele neuer onkologischer Therapien 104.
93. Shah MA, ZA Wainberg, DV Catenacci, HS Hochster, J Ford, P Kunz, FC Lee, H Kallender, F Cecchi, DC Rabe, H Keer, AM Martin, Y Liu, R Gagnon, P Bonate, L Liu, T Gilmer and DP Bottaro. (2013). Phase II study evaluating 2 dosing schedules of oral foretinib (GSK1363089), cMET/VEGFR2 inhibitor, in patients with metastatic gastric cancer. PLoS One 8:e54014.
94. Organ SL and MS Tsao. (2011). An overview of the c-MET signaling pathway. Ther Adv Med Oncol 3:S7-S19.
95. Comoglio PM, S Giordano and L Trusolino. (2008). Drug development of MET inhibitors: targeting oncogene addiction and expedience. Nat Rev Drug Discov 7:504-16.
96. Trusolino L and PM Comoglio. (2002). Scatter-factor and semaphorin receptors: cell signalling for invasive growth. Nat Rev Cancer 2:289-300.
97. Birchmeier C, W Birchmeier, E Gherardi and GF Vande Woude. (2003). Met, metastasis, motility and more. Nat Rev Mol Cell Biol 4:915-25.
98. Stoker M, E Gherardi, M Perryman and J Gray. (1987). Scatter factor is a fibroblast-derived modulator of epithelial cell mobility. Nature 327:239-42.
99. Nakamura T. (1989). [Molecular characterization of hepatocyte growth factor (HGF)]. Seikagaku 61:1243-7.
100. Weidner KM, N Arakaki, G Hartmann, J Vandekerckhove, S Weingart, H Rieder, C Fonatsch, H Tsubouchi, T Hishida, Y Daikuhara and et al. (1991). Evidence for the identity of human scatter factor and human hepatocyte growth factor. Proc Natl Acad Sci U S A 88:7001-5.
101. Niemann HH. (2011). Structural insights into Met receptor activation. Eur J Cell Biol 90:972-81.

102. Nakamura T, K Sakai, T Nakamura and K Matsumoto. (2011). Hepatocyte growth factor twenty years on: Much more than a growth factor. J Gastroenterol Hepatol 26 Suppl 1:188-202.
103. Rodrigues GA and M Park. (1994). Autophosphorylation modulates the kinase activity and oncogenic potential of the Met receptor tyrosine kinase. Oncogene 9:2019-27.
104. Ponzetto C, Z Zhen, E Audero, F Maina, A Bardelli, ML Basile, S Giordano, R Narsimhan and P Comoglio. (1996). Specific uncoupling of GRB2 from the Met receptor. Differential effects on transformation and motility. J Biol Chem 271:14119-23.
105. Weidner KM, S Di Cesare, M Sachs, V Brinkmann, J Behrens and W Birchmeier. (1996). Interaction between Gab1 and the c-Met receptor tyrosine kinase is responsible for epithelial morphogenesis. Nature 384:173-6.
106. Ponzetto C, A Bardelli, Z Zhen, F Maina, P dalla Zonca, S Giordano, A Graziani, G Panayotou and PM Comoglio. (1994). A multifunctional docking site mediates signaling and transformation by the hepatocyte growth factor/scatter factor receptor family. Cell 77:261-71.
107. Pelicci G, S Giordano, Z Zhen, AE Salcini, L Lanfrancone, A Bardelli, G Panayotou, MD Waterfield, C Ponzetto, PG Pelicci and et al. (1995). The motogenic and mitogenic responses to HGF are amplified by the Shc adaptor protein. Oncogene 10:1631-8.
108. Lock LS, I Royal, MA Naujokas and M Park. (2000). Identification of an atypical Grb2 carboxyl-terminal SH3 domain binding site in Gab docking proteins reveals Grb2-dependent and -independent recruitment of Gab1 to receptor tyrosine kinases. J Biol Chem 275:31536-45.
109. Garcia-Guzman M, F Dolfi, K Zeh and K Vuori. (1999). Met-induced JNK activation is mediated by the adapter protein Crk and correlates with the Gab1 - Crk signaling complex formation. Oncogene 18:7775-86.
110. Sakkab D, M Lewitzky, G Posern, U Schaeper, M Sachs, W Birchmeier and SM Feller. (2000). Signaling of hepatocyte growth factor/scatter factor (HGF) to the small GTPase Rap1 via the large docking protein Gab1 and the adapter protein CRKL. J Biol Chem 275:10772-8.

111. Graziani A, D Gramaglia, P dalla Zonca and PM Comoglio. (1993). Hepatocyte growth factor/scatter factor stimulates the Ras-guanine nucleotide exchanger. J Biol Chem 268:9165-8.

112. Boccaccio C, G Gaudino, G Gambarotta, F Galimi and PM Comoglio. (1994). Hepatocyte growth factor (HGF) receptor expression is inducible and is part of the delayed-early response to HGF. J Biol Chem 269:12846-51.

113. Fixman ED, TM Fournier, DM Kamikura, MA Naujokas and M Park. (1996). Pathways downstream of Shc and Grb2 are required for cell transformation by the tpr-Met oncoprotein. J Biol Chem 271:13116-22.

114. Paumelle R, D Tulasne, Z Kherrouche, S Plaza, C Leroy, S Reveneau, B Vandenbunder and V Fafeur. (2002). Hepatocyte growth factor/scatter factor activates the ETS1 transcription factor by a RAS-RAF-MEK-ERK signaling pathway. Oncogene 21:2309-19.

115. Maroun CR, MA Naujokas and M Park. (2003). Membrane targeting of Grb2-associated binder-1 (Gab1) scaffolding protein through Src myristoylation sequence substitutes for Gab1 pleckstrin homology domain and switches an epidermal growth factor response to an invasive morphogenic program. Mol Biol Cell 14:1691-708.

116. Schaeper U, NH Gehring, KP Fuchs, M Sachs, B Kempkes and W Birchmeier. (2000). Coupling of Gab1 to c-Met, Grb2, and Shp2 mediates biological responses. J Cell Biol 149:1419-32.

117. Rodrigues GA, M Park and J Schlessinger. (1997). Activation of the JNK pathway is essential for transformation by the Met oncogene. EMBO J 16:2634-45.

118. Trusolino L, A Bertotti and PM Comoglio. (2010). MET signalling: principles and functions in development, organ regeneration and cancer. Nat Rev Mol Cell Biol 11:834-48.

119. Vivanco I and CL Sawyers. (2002). The phosphatidylinositol 3-Kinase AKT pathway in human cancer. Nat Rev Cancer 2:489-501.

120. Jeffers M, L Schmidt, N Nakaigawa, CP Webb, G Weirich, T Kishida, B Zbar and GF Vande Woude. (1997). Activating mutations for the met tyrosine kinase receptor in human cancer. Proc Natl Acad Sci U S A 94:11445-50.

121. Peschard P, TM Fournier, L Lamorte, MA Naujokas, H Band, WY Langdon and M Park. (2001). Mutation of the c-Cbl TKB domain binding site on the Met receptor tyrosine kinase converts it into a transforming protein. Mol Cell 8:995-1004.

122. Petrelli A, GF Gilestro, S Lanzardo, PM Comoglio, N Migone and S Giordano. (2002). The endophilin-CIN85-Cbl complex mediates ligand-dependent downregulation of c-Met. Nature 416:187-90.
123. Hammond DE, S Urbe, GF Vande Woude and MJ Clague. (2001). Down-regulation of MET, the receptor for hepatocyte growth factor. Oncogene 20:2761-70.
124. Gandino L, MF Di Renzo, S Giordano, F Bussolino and PM Comoglio. (1990). Protein kinase-c activation inhibits tyrosine phosphorylation of the c-met protein. Oncogene 5:721-5.
125. Gandino L, P Longati, E Medico, M Prat and PM Comoglio. (1994). Phosphorylation of serine 985 negatively regulates the hepatocyte growth factor receptor kinase. J Biol Chem 269:1815-20.
126. Gandino L, L Munaron, L Naldini, R Ferracini, M Magni and PM Comoglio. (1991). Intracellular calcium regulates the tyrosine kinase receptor encoded by the MET oncogene. J Biol Chem 266:16098-104.
127. Bang YJ. (2011). The potential for crizotinib in non-small cell lung cancer: a perspective review. Ther Adv Med Oncol 3:279-91.
128. Cui JJ, M Tran-Dube, H Shen, M Nambu, PP Kung, M Pairish, L Jia, J Meng, L Funk, I Botrous, M McTigue, N Grodsky, K Ryan, E Padrique, G Alton, S Timofeevski, S Yamazaki, Q Li, H Zou, J Christensen, B Mroczkowski, S Bender, RS Kania and MP Edwards. (2011). Structure based drug design of crizotinib (PF-02341066), a potent and selective dual inhibitor of mesenchymal-epithelial transition factor (c-MET) kinase and anaplastic lymphoma kinase (ALK). J Med Chem 54:6342-63.
129. Davare MA, A Saborowski, CA Eide, C Tognon, RL Smith, J Elferich, A Agarwal, JW Tyner, UP Shinde, SW Lowe and BJ Druker. (2013). Foretinib is a potent inhibitor of oncogenic ROS1 fusion proteins. Proc Natl Acad Sci U S A 110:19519-24.
130. Ou SH. (2011). Crizotinib: a novel and first-in-class multitargeted tyrosine kinase inhibitor for the treatment of anaplastic lymphoma kinase rearranged non-small cell lung cancer and beyond. Drug Des Devel Ther 5:471-85.
131. Ou SH. (2012). Crizotinib: a drug that crystallizes a unique molecular subset of non-small-cell lung cancer. Expert Rev Anticancer Ther 12:151-62.

132. Naing A, R Kurzrock, LM Adams, JF Kleha, KH Laubscher, PL Bonate, S Weller, C Fitzgerald, Y Xu and PM LoRusso. (2012). A comparison of the pharmacokinetics of the anticancer MET inhibitor foretinib free base tablet formulation to bisphosphate salt capsule formulation in patients with solid tumors. Invest New Drugs 30:327-34.

133. Eder JP, GI Shapiro, LJ Appleman, AX Zhu, D Miles, H Keer, B Cancilla, F Chu, S Hitchcock-Bryan, L Sherman, S McCallum, EI Heath, SA Boerner and PM LoRusso. (2010). A phase I study of foretinib, a multi-targeted inhibitor of c-Met and vascular endothelial growth factor receptor 2. Clin Cancer Res 16:3507-16.

134. Liu L, Y Liu, A Hong, J Greger, AM Martin and T Gilmer. (2009). Abstract A238: The effects of foretinib on MET phosphorylation, gene expression, cell proliferation and tumor growth in MET-amplified tumor cells in vitro and in vivo. Mol Cancer Ther 8:A238.

135. Bean J, C Brennan, JY Shih, G Riely, A Viale, L Wang, D Chitale, N Motoi, J Szoke, S Broderick, M Balak, WC Chang, CJ Yu, A Gazdar, H Pass, V Rusch, W Gerald, SF Huang, PC Yang, V Miller, M Ladanyi, CH Yang and W Pao. (2007). MET amplification occurs with or without T790M mutations in EGFR mutant lung tumors with acquired resistance to gefitinib or erlotinib. Proc Natl Acad Sci U S A 104:20932-7.

136. Young RH, E Oliva and RE Scully. (1995). Small cell carcinoma of the hypercalcemic type in the ovary. Gynecol Oncol 57:7-8.

137. Journe F, JC Dumon, N Kheddoumi, J Fox, I Laios, G Leclercq and JJ Body. (2004). Extracellular calcium downregulates estrogen receptor alpha and increases its transcriptional activity through calcium-sensing receptor in breast cancer cells. Bone 35:479-88.

138. Trump BF and IK Berezesky. (1995). Calcium-mediated cell injury and cell death. FASEB J 9:219-28.

139. Nomura M, A Ueno, K Saga, M Fukuzawa and Y Kaneda. (2014). Accumulation of cytosolic calcium induces necroptotic cell death in human neuroblastoma. Cancer Res 74:1056-66.

140. Putney JW. (2009). Capacitative calcium entry: from concept to molecules. Immunol Rev 231:10-22.

141. van Rossum GS, R Klooster, H van den Bosch, AJ Verkleij and J Boonstra. (2001). Phosphorylation of p42/44(MAPK) by various signal transduction pathways activates cytosolic phospholipase A(2) to variable degrees. J Biol Chem 276:28976-83.

142. Koehler L, R Hass, DL DeWitt, K Resch and M Goppelt-Struebe. (1990). Glucocorticoid-induced reduction of prostanoid synthesis in TPA-differentiated U937 cells is mainly due to a reduced cyclooxygenase activity. Biochem Pharmacol 40:1307-16.

143. Rehfeldt W, R Hass and M Goppelt-Struebe. (1991). Characterization of phospholipase A2 in monocytic cell lines. Functional and biochemical aspects of membrane association. Biochem J 276 (Pt 3):631-6.

144. Medeiros A, C Peres-Buzalaf, F Fortino Verdan and CH Serezani. (2012). Prostaglandin E2 and the suppression of phagocyte innate immune responses in different organs. Mediators Inflamm 2012:327568.

145. Donnini S, F Finetti, R Solito, E Terzuoli, A Sacchetti, L Morbidelli, P Patrignani and M Ziche. (2007). EP2 prostanoid receptor promotes squamous cell carcinoma growth through epidermal growth factor receptor transactivation and iNOS and ERK1/2 pathways. FASEB J 21:2418-30.

146. Tobey RA, JG Valdez, YE Valdez and BE Lehnert. (1990). Proliferation of rat and human lung fibroblasts following exposure to prostaglandin E2. Exp Lung Res 16:235-55.

147. Otte A, F Rauprich, P Hillemanns, TW Park-Simon, J von der Ohe and R Hass. (2014). In vitro and in vivo therapeutic approach for a small cell carcinoma of the ovary hypercalcaemic type using a SCCOHT-1 cellular model. Orphanet J Rare Dis 9:126.

148. Agard M, S Asakrah and LA Morici. (2013). PGE(2) suppression of innate immunity during mucosal bacterial infection. Front Cell Infect Microbiol 3:45.

149. Reed WC. (1995). Small cell carcinoma of the ovary with hypercalcemia: report of a case of survival without recurrence 5 years after surgery and chemotherapy. Gynecol Oncol 56:452-5.

150. Dykgraaf RH, D de Jong, M van Veen, PC Ewing-Graham, TJ Helmerhorst and ME van der Burg. (2009). Clinical management of ovarian small-cell carcinoma of the hypercalcemic type: a proposal for conservative surgery in an advanced stage of disease. Int J Gynecol Cancer 19:348-53.

151. Hamilton TC, RC Young, WM McKoy, KR Grotzinger, JA Green, EW Chu, J Whang-Peng, AM Rogan, WR Green and RF Ozols. (1983). Characterization of a human ovarian carcinoma cell line (NIH:OVCAR-3) with androgen and estrogen receptors. Cancer Res 43:5379-89.

152. ATCC. Produktbeschreibung HTB-77.

153. Khabele D, M Lopez-Jones, W Yang, D Arango, SJ Gross, LH Augenlicht and GL Goldberg. (2004). Tumor necrosis factor-alpha related gene response to Epothilone B in ovarian cancer. Gynecol Oncol 93:19-26.

154. Colombo N, E Kutarska, M Dimopoulos, DS Bae, I Rzepka-Gorska, M Bidzinski, G Scambia, SA Engelholm, F Joly, D Weber, M El-Hashimy, J Li, F Souami, P Wing, S Engelholm, A Bamias and P Schwartz. (2012). Randomized, open-label, phase III study comparing patupilone (EPO906) with pegylated liposomal doxorubicin in platinum-refractory or -resistant patients with recurrent epithelial ovarian, primary fallopian tube, or primary peritoneal cancer. J Clin Oncol 30:3841-7.

155. Bruey JM, C Ducasse, P Bonniaud, L Ravagnan, SA Susin, C Diaz-Latoud, S Gurbuxani, AP Arrigo, G Kroemer, E Solary and C Garrido. (2000). Hsp27 negatively regulates cell death by interacting with cytochrome c. Nat Cell Biol 2:645-52.

156. Charette SJ and J Landry. (2000). The interaction of HSP27 with Daxx identifies a potential regulatory role of HSP27 in Fas-induced apoptosis. Ann N Y Acad Sci 926:126-31.

157. Casado P, P Zuazua-Villar, E del Valle, C Martinez-Campa, PS Lazo and S Ramos. (2007). Vincristine regulates the phosphorylation of the antiapoptotic protein HSP27 in breast cancer cells. Cancer Lett 247:273-82.

158. Bertram C and R Hass. (2009). Cellular senescence of human mammary epithelial cells (HMEC) is associated with an altered MMP-7/HB-EGF signaling and increased formation of elastin-like structures. Mech Ageing Dev 130:657-69.

159. Vousden KH and X Lu. (2002). Live or let die: the cell's response to p53. Nat Rev Cancer 2:594-604.

160. Damia G, L Filiberti, F Vikhanskaya, L Carrassa, Y Taya, M D'Incalci and M Broggini. (2001). Cisplatinum and taxol induce different patterns of p53 phosphorylation. Neoplasia 3:10-6.

161. Ioffe ML, E White, DA Nelson, D Dvorzhinski and RS DiPaola. (2004). Epothilone induced cytotoxicity is dependent on p53 status in prostate cells. Prostate 61:243-7.

162. Ungefroren H, S Sebens, D Seidl, H Lehnert and R Hass. (2011). Interaction of tumor cells with the microenvironment. Cell Commun Signal 9:18.

163. Hass R and A Otte. (2012). Mesenchymal stem cells as all-round supporters in a normal and neoplastic microenvironment. Cell Commun Signal 10:26.

164. Kavallaris M. (2010). Microtubules and resistance to tubulin-binding agents. Nat Rev Cancer 10:194-204.

165. Seve P and C Dumontet. (2008). Is class III beta-tubulin a predictive factor in patients receiving tubulin-binding agents? Lancet Oncol 9:168-75.

166. Bu R, S Uddin, P Bavi, AR Hussain, F Al-Dayel, S Ghourab, M Ahmed and KS Al-Kuraya. (2011). HGF/c-Met pathway has a prominent role in mediating antiapoptotic signals through AKT in epithelial ovarian carcinoma. Lab Invest 91:124-37.

167. Di Renzo MF, RP Narsimhan, M Olivero, S Bretti, S Giordano, E Medico, P Gaglia, P Zara and PM Comoglio. (1991). Expression of the Met/HGF receptor in normal and neoplastic human tissues. Oncogene 6:1997-2003.

168. Huntsman D, JH Resau, E Klineberg and N Auersperg. (1999). Comparison of c-met expression in ovarian epithelial tumors and normal epithelia of the female reproductive tract by quantitative laser scan microscopy. Am J Pathol 155:343-8.

169. Wong AS, CD Roskelley, S Pelech, D Miller, PC Leung and N Auersperg. (2004). Progressive changes in Met-dependent signaling in a human ovarian surface epithelial model of malignant transformation. Exp Cell Res 299:248-56.

170. Parr C and WG Jiang. (2001). Expression of hepatocyte growth factor/scatter factor, its activator, inhibitors and the c-Met receptor in human cancer cells. Int J Oncol 19:857-63.

171. Yamashita Y, S Akatsuka, K Shinjo, Y Yatabe, H Kobayashi, H Seko, H Kajiyama, F Kikkawa, T Takahashi and S Toyokuni. (2013). Met is the most frequently amplified gene in endometriosis-associated ovarian clear cell adenocarcinoma and correlates with worsened prognosis. PLoS One 8:e57724.

172. Tang C, DL Jardim and D Hong. (2014). MET in ovarian cancer: metastasis and resistance? Cell Cycle 13:1220-1.

173. Brat DJ, AC Bellail and EG Van Meir. (2005). The role of interleukin-8 and its receptors in gliomagenesis and tumoral angiogenesis. Neuro Oncol 7:122-33.

174. Mhawech-Fauceglia P, M Afkhami and T Pejovic. (2012). MET/HGF Signaling Pathway in Ovarian Carcinoma: Clinical Implications and Future Direction. Patholog Res Int 2012:960327.

175. Blumenschein GR, Jr., GB Mills and AM Gonzalez-Angulo. (2012). Targeting the hepatocyte growth factor-cMET axis in cancer therapy. J Clin Oncol 30:3287-96.

176. Zillhardt M, SM Park, IL Romero, K Sawada, A Montag, T Krausz, SD Yamada, ME Peter and E Lengyel. (2011). Foretinib (GSK1363089), an orally available multikinase inhibitor of c-Met and VEGFR-2, blocks proliferation, induces anoikis, and impairs ovarian cancer metastasis. Clin Cancer Res 17:4042-51.

177. Qian F, S Engst, K Yamaguchi, P Yu, KA Won, L Mock, T Lou, J Tan, C Li, D Tam, J Lougheed, FM Yakes, F Bentzien, W Xu, T Zaks, R Wooster, J Greshock and AH Joly. (2009). Inhibition of tumor cell growth, invasion, and metastasis by EXEL-2880 (XL880, GSK1363089), a novel inhibitor of HGF and VEGF receptor tyrosine kinases. Cancer Res 69:8009-16.

178. Faria CC, BJ Golbourn, AM Dubuc, M Remke, RJ Diaz, S Agnihotri, A Luck, N Sabha, S Olsen, X Wu, L Garzia, V Ramaswamy, SC Mack, X Wang, M Leadley, D Reynaud, L Ermini, M Post, PA Northcott, SM Pfister, SE Croul, M Kool, A Korshunov, CA Smith, MD Taylor and JT Rutka. (2015). Foretinib is effective therapy for metastatic sonic hedgehog medulloblastoma. Cancer Res 75:134-46.

179. Huynh H, R Ong and KC Soo. (2012). Foretinib demonstrates anti-tumor activity and improves overall survival in preclinical models of hepatocellular carcinoma. Angiogenesis 15:59-70.

180. Choueiri TK, U Vaishampayan, JE Rosenberg, TF Logan, AL Harzstark, RM Bukowski, BI Rini, S Srinivas, MN Stein, LM Adams, LH Ottesen, KH Laubscher, L Sherman, DF McDermott, NB Haas, KT Flaherty, R Ross, P Eisenberg, PS Meltzer, MJ Merino, DP Bottaro, WM Linehan and R Srinivasan. (2013). Phase II and biomarker study of the dual MET/VEGFR2 inhibitor foretinib in patients with papillary renal cell carcinoma. J Clin Oncol 31:181-6.

181. Mandel K, Y Yang, A Schambach, S Glage, A Otte and R Hass. (2013). Mesenchymal stem cells directly interact with breast cancer cells and promote tumor cell growth in vitro and in vivo. Stem Cells Dev 22:3114-27.

182. Yang Y, V Bucan, H Baehre, J von der Ohe, A Otte and R Hass. (2015). Acquisition of new tumor cell properties by MSC-derived exosomes. Int J Oncol 47:244-52.

183. Yang Y, A Otte and R Hass. (2015). Human mesenchymal stroma/stem cells exchange membrane proteins and alter functionality during interaction with different tumor cell lines. Stem Cells Dev 24:1205-22.

184. Aguirre P, AD Thor and RE Scully. (1989). Ovarian small cell carcinoma. Histogenetic considerations based on immunohistochemical and other findings. Am J Clin Pathol 92:140-9.

185. Walt H, R Hornung, D Fink, D Dobler-Girdziunaite, T Stallmach, MA Spycher, F Maly, U Haller and N Burki. (2001). Hypercalcemic-type of small cell carcinoma of the ovary: characterization of a new tumor line. Anticancer Res 21:3253-9.

186. Havrilesky LJ, CP McMahon, EK Lobenhofer, R Whitaker, JR Marks and A Berchuck. (2001). Relationship between expression of coactivators and corepressors of hormone receptors and resistance of ovarian cancers to growth regulation by steroid hormones. J Soc Gynecol Investig 8:104-13.

6 Schriftenverzeichnis

a) Orginalarbeiten

1. **Otte A**, Mandel K, Reinstrom G, Hass R: Abolished adherence alters signalling pathways in phorbol ester-induced human U937 cells. Cell Commun Signal. 2011, 9:20.

2. **Otte A**, Göhring G, Steinemann D, Schlegelberger B, Groos S, Länger F, Kreipe HH, Schambach A, Neumann T, Hillemanns P, Park-Simon TW, Hass R: A tumor-derived population (SCCOHT-1) as cellular model for a small cell ovarian carcinoma of the hypercalcemic type. Int J Oncol. 2012, 41(2): 765-75

3. Mandel K, **Otte A**, Hass R: Involvement of CD11b integrin in the alteration of metabolic factors after phorbol ester stimulation of human myeloid leukemia cells. Cell Commun Signal. 2012, 10(1):13.

4. Hass R, **Otte A**: Mesenchymal stem cells as all-round supporters in a normal and neoplastic microenviroment. Cell Commun Signal. 2012, 10(1):26.

5. **Otte A**, Bucan V, Reimers K, Hass R: Mesenchymal stem cells maintain long-term in vitro stemness during explant culture. Tissue Eng Part C Methods. 2013, 19(12):937-48.

6. Mandel K, Yang Y, Schambach A, Glage S, **Otte A**, Hass R: Mesenchymal stem cells (MSC) directly interact with breast cancer cells and promote tumor cell growth in vitro and in vivo. Stem Cells Dev. 2013, 22(23): 3114-27.

7. **Otte A**, Rauprich F, von der Ohe J, Hillemanns P, Hass R: Interference of Ca^{2+} with the proliferation of SCCOHT-1 and ovarian adenocarcinoma cells. Int J Oncol. 2014 45(3):1151-8

8. **Otte A**, Rauprich F, Hillemanns P, Park-Simon TW, von der Ohe J, Hass R: *In vitro* and *in vivo* therapeutic approach for a small cell carcinome of the ovary hypercalcaemic type using a SCCOHT-1 cellular model. Orphanet J Rare Dis. 2014 9:126

9. Yang Y, **Otte A**, Hass R: Human Mesenchymal Stroma/Stem Cells Exchange Membrane Proteins and Alter Functionality During Interaction with Different Tumor Cell Lines. Stem Cells Dev. 2015, 24(10): 1205-22.

10. Yang Y, Bucan C, Baehre H, von der Ohe J, **Otte A**, Hass R: Acquisition of new tumor cell properties by MSC-derives exosomes. Int J Oncol. 2015, 47(1): 244-52.

11. **Otte A**, Rauprich F, von der Ohe J, Yang Y, Kommoss F, Feuerhake F, Hillemanns P, Hass R: c-Met inhibitors attenuate tumor growth of small cell hypercalcemic ovarian carcinoma (SCCOHT) populations. Oncotarget. 2015, 6(31): 31640-58.

b) Kongressbeiträge

1. Etablierung von Primärkulturen aus einem kleinzelligen Ovarialkarzinom vom hyperkalzämischen Typ. 127ste Tagung der Norddeutschen Gesellschaft für Gynäkologie und Geburtshilfe (NGGG), Greifswald (2011)

2. Establishment and characterization of primary cells from small cell carcinoma of the ovary hypercalcemic type (SCCOHT). 15th Joint Meeting of the Signal Transduction Society (STS), Weimar (2011).

3. Characterization of a Xenograft Model of a Small Cell Carcinoma of the Ovary, hypercalcemic type (SCCOHT-1) in Mice. 16th Joint Meeting of the Signal Transduction Society (STS), (Weimar 2012).

4. *In vitro* and *in vivo* chemotherapeutic treatment of Small Cell Carcinoma of the Ovary, hypercalcemic type (SCCOHT). 17th Joint Meeting of the Signal Transduction Society (STS), (Weimar 2013).

5. Different molecluar effects of extracellular calcium on human ovarian cancer cells. 17th Joint Meeting of the Signal Transduction Society (STS), (Weimar 2013).

6. Exogenous calcium stimulation regulates phosphorylation of MAP kinase and stimulates prostaglandin E2 production in small cell carcinoma oft he ovary, hypercalcemic type and human ovarian cancer cells. 18th Joint Meeting of the Signal Transduction Society (STS), Weimar (2014).

7. Foretinib, a c-Met inhibitor, reduce tumor growth of ovarian small cell carcinoma of hypercalcemic type. 19th Joint Meeting of the Signal Transduction Society (STS), Weimar (2015).

7 Danksagung

Fragte man mich vor circa 30 Jahren, was mein Berufswunsch sei, so kam prompt freudestrahlend die Antwort: „Putzfrau“. Es kam wie so häufig im Leben etwas anders, als man es sich vorgestellt hat und ich fing nach dem Abitur an, Biochemie zu studieren. Dafür, dass sie mich bei all meinen Ideen unterstützt haben und auch stolz auf Ihre „Putzfrau“ gewesen wären, möchte ich meinen Eltern von Herzen danken.

Durch meine Entscheidung für das Biochemiestudium in Hannover habe ich meinen Doktorvater Prof. Dr. rer. nat. Ralf Hass kennengelernt. Während der Doktorarbeit konnte ich dank seines umfangreichen Wissen und seiner Erfahrung sehr viel von Ihm lernen, wofür ich mich hiermit herzlich bei ihm bedanken möchte. Ein besonderer Dank gilt ebenfalls der verstorbenen Patientin, durch deren Tumorgewebespende der Grundstein meiner wissenschaftlichen Arbeit überhaupt erst gelegt werden konnte.

Für die Übernahme des Korreferats möchte ich an dieser Stelle Herrn Prof. Dr. rer. nat. Walter Müller und Herrn Prof. Dr. rer. nat. Frank Entschladen danken. Und für die Übernahme des Prüfungsvorsitz danke ich Herrn Prof. Dr. rer. nat. Bernhard Huchzermeyer.

Rückblickend sind die 1766 Tage meiner Doktorarbeit wie im Fluge vergangen. Aus Kollegen wurde meine „Arbeits-Familie“. Es gab viel zu lachen und zu feiern, es floss aber auch die eine oder andere Träne. Für diese einmalige Zeit gilt mein besonderer Dank Jutta Beu und Juliane von der Ohe, den guten Seelen der AG Biochemie und Tumorbiologie. Ferner möchte ich mich bei meinen Kollegen Yuanyuan (alias Kate) Yang, Catharina Melzer, Finn Rauprich, Katharina Mandel, Ricarda Lehmann (geb. Niendorf), Catharina Bertram, Elisabeth Stelling, Bruni Köpsel, Marianne Thren, Marion Haidukiewicz, Eva Kiene-Stengel, Britta Wieland, Peter Schürmann, Bianca Schröder-Heurich, Sonja Helbig, Kathy Neuhäuser, Lea Völkening, Natallia Darashonak, Natallia Bogdanova, Tessa Spethmann, Kristine Bousset, Katja Borns, Thilo Dörk-Bousset, Anne Rohrbach und Frauke von Versen-Höynck für das gute Arbeitsklima und die fachlichen aber teils auch privaten Diskussionen bedanken. Und allen, die ich hier nicht mehr namentlich erwähnen konnte, vor allem meiner Praktikanten-Schar, sei ebenfalls versichert, mein Dank gilt auch Euch.

Auch wenn während der Doktorarbeit das Privatleben zeitweise etwas kurz kam, möchte ich mich bei meinen Freunden und meiner Familie, im speziellen Arinc & Hacer Kayaçelebi, Vera Meyer & Jens Mattiza, Piotr Wagner, Susi & Marcus Zeckert, Susi Wiederholz, Andrea Zachrau & Sebastian Fischer, Birgit Sevecke & Rudi Paasch, Gabi & Bernd Isensee, Michaela, Mathilda & Daniel Isensee und Bärbel Biese bedanken, dass ihr für mich da wart, wenn ich Euch brauchte.

Und dafür, dass er mein Leben so sehr bereichert, möchte ich mich bei Eric bedanken. Ich hoffe dass wir auch weiterhin unser gemeinsames Leben meistern werden.

8 Lebenslauf

Persönliche Daten:

Name:	Anna-Kathrin Otte
Geburtsdatum:	02.12.1982
Geburtsort:	Bremen

Schulbildung:

1988 - 1993	Grundschule an der Uphuser Straße, Bremen
1993 - 1999	Gesamtschule Ost, Bremen
1999 - 2002	Gymnasium an der Hamburger Straße, Bremen
13.06.2002	Zuerkennung der Allgemeinen Hochschulreife

Studium:

Studienrichtung:	Diplom Biochemie
10/2003 - 01/2011	Grund- und Hauptstudium an der Gottfried Wilhelm Leibniz Universität Hannover
07/2010 - 01/2011	Diplomarbeit in der Klinik für Frauenheilkunde und Geburtshilfe, AG Biochemie und Tumorbiologie, Medizinische Hochschule Hannover (MHH). Thema der Diplomarbeit: „Charakterisierung von Zellpopulationen aus einem humanen kleinzelligen Ovarialkarzinom“
01.02.2011	Abschluss mit dem Hochschulgrad Diplom-Biochemikerin an der Gottfried Wilhelm Leibniz Universität Hannover

Dissertation:

03/2011 - 12/2015	Promotionsstudentin an der Gottfried Wilhelm Leibniz Universität Hannover, Klinik für Frauenheilkunde und Geburtshilfe AG Biochemie und Tumorbiologie, Medizinische Hochschule Hannover (MHH). Thema der Dissertation: „*In vitro* und *in vivo* Tumoreigenschaften eines kleinzelligen Ovarialkarzinoms vom hyperkalzämischen Typ und mögliche therapeutische Ansätze“